DOC.20070917.0006

QA: QA

MDL-WIS-AC-000001 REV 00

September 2007

Mechanical Assessment of Degraded Waste Packages and Drip Shields Subject to Vibratory Ground Motion

Prepared for:
U.S. Department of Energy
Office of Civilian Radioactive Waste Management
Office of Repository Development
1551 Hillshire Drive
Las Vegas, Nevada 89134-6321

Prepared by:
Sandia National Laboratories
OCRWM Lead Laboratory for Repository Systems
1180 Town Center Drive
Las Vegas, Nevada 89144

Under Contract Number
DE-AC04-94AL85000

DISCLAIMER

This report was prepared as an account of work sponsored by an agency of the United States Government. Neither the United States Government nor any agency thereof, nor any of their employees, nor any of their contractors, subcontractors or their employees, makes any warranty, express or implied, or assumes any legal liability or responsibility for the accuracy, completeness, or any third party's use or the results of such use of any information, apparatus, product, or process disclosed, or represents that its use would not infringe privately owned rights. Reference herein to any specific commercial product, process, or service by trade name, trademark, manufacturer, or otherwise, does not necessarily constitute or imply its endorsement, recommendation, or favoring by the United States Government or any agency thereof or its contractors or subcontractors. The views and opinions of authors expressed herein do not necessarily state or reflect those of the United States Government or any agency thereof.

QA: QA

Mechanical Assessment of Degraded Waste Packages and Drip Shields Subject to Vibratory Ground Motion

MDL-WIS-AC-000001 REV 00

September 2007

Model Signature Page/Change History

Complete only applicable items.

1. Total Pages: 488

2 Type of Mathematical Model

☒ Process Model ☐ Abstraction Model ☐ System Model

Describe Intended Use of Model

The intended use of this model is to provide input to the *Seismic Consequence Abstraction* model report. The results from this model are needed to incorporate into the total system performance assessment (TSPA) the response of the Engineered Barrier System (EBS) to vibratory ground motion that may occur over the regulatory time frame. Results from this model are also used to respond to an Additional Information Need (AIN) from the U.S. Nuclear Regulatory Commission (NRC).

3 Title

Mechanical Assessment of Degraded Waste Packages and Drip Shields Subject to Vibratory Ground Motion

4. DI (including Revision No. and Addendum No.):

MDL-WIS-AC-000001 REV 00

		Printed Name	Signature	Date
5	Originator	Stephen C. Blair		9/7/07
6	Independent Technical Reviewer for	Jean Younker		9/10/07
7	Checker	Steven Carlson		9/7/07
8	OCS/Lead Lab QA Reviewer	Brian Mitchelltree		9/10/07
9	Responsible Manager/Lead	Mike Gross		9/12/07
10	Responsible Manager	Cliff Howard		9/12/07

11 Remarks

Change History

12. Revision No. and Addendum No.	13. Description of Change
00	Initial Issue Addresses the following portions of CR 9202 Action Number 9202-002: See Section 4.2 and 8.3 Action Number 9202-003: See Section 5 Action Number 9202-007: See Section 3.2 Action Number 9202-009: See Section 6.3 Action Number 9202-011: See Sections 6.4.3 and 6.4.4 Action Number 9202-012: See Sections 6.4.3, 6.4.4, and 6.4.7 Responds to Additional Information Need from the NRC (Key Technical Issue Agreement Total System Performance Assessment and Integration 2.02, Comment J-2, AIN: See Section 6.4.6)

INTENTIONALLY LEFT BLANK

CONTENTS

Page

CONTENTS (Continued)

Page

CONTENTS (Continued)

Page

CONTENTS (Continued)

Page

FIGURES

Page

FIGURES (Continued)

Page

FIGURES (Continued)

Page

FIGURES (Continued)

Page

FIGURES (Continued)

Page

FIGURES (Continued)

Page

FIGURES (Continued)

Page

FIGURES (Continued)

Page

TABLES

Page

TABLES (Continued)

TABLES (Continued)

TABLES (Continued)

TABLES (Continued)

TABLES (Continued)

TABLES (Continued)

TABLES (Continued)

TABLES (Continued)

TABLES (Continued)

TABLES (Continued)

INTENTIONALLY LEFT BLANK

ACRONYMS

AIN	Additional Information Need
ASCE	American Society of Civil Engineers
ASME	American Society of Mechanical Engineers
ASTM	American Society for Testing and Materials
BWR	boiling water reactor
CDSP	alternate designation for codisposal (waste package)
CRWMS	Civilian Radioactive Waste Management System
DHLW	defense high-level (radioactive) waste
DNA	Defense Nuclear Agency
DOE	U.S. Department of Energy
DTN	data tracking number
EBS	Engineered Barrier System
FEPs	features, events, or processes
LLNL	Lawrence Livermore National Laboratory
NL/TAD	alternate designation for TAD-bearing (waste package)
NRC	Nuclear Regulatory Commission
NUREG	Nuclear Regulatory Commission technical report designation
OCB	outer corrosion barrier
PGA	peak ground acceleration
PGV	peak ground velocity (refers to H1 horizontal component in each analysis)
PSHA	Probabilistic Seismic Hazard Analysis
PWR	pressurized water reactor
SCC	stress corrosion cracking
SNF	spent nuclear fuel
TAD	transportation, aging, and disposal (canister)
TSPA	total system performance assessment
TSPA-LA	total system performance assessment for the license application
TSw2	Topopah Spring welded hydrogeologic 2 (unit)
TWP	technical work plan

INTENTIONALLY LEFT BLANK

1. PURPOSE

The purpose of this model report is to document simulations of waste package and drip shield damage that may occur in response to vibratory ground motion. These damage calculations, which are referred to as damage models in this report, are needed in order to incorporate into the total system performance assessment (TSPA) the response of the Engineered Barrier System (EBS) to vibratory ground motion that may occur over the regulatory time frame. These damage models also respond to an Additional Information Need (AIN) from the U.S. Nuclear Regulatory Commission (NRC). The specific AIN is provided in Key Technical Issue Agreement Total System Performance Assessment and Integration 2.02, Comment J-2, AIN (Kokajko 2005 [DIRS 177025], pp. 5 to 6 of enclosure).

This report provides input to *Seismic Consequence Abstraction* (SNL 2007 [DIRS 176828]). It was prepared under procedure SCI-PRO-006, *Models*, and provides validation of the seismic damage models and associated numerical calculations.

The analyses reported here include both two-dimensional and three-dimensional kinematic simulations of the response of the EBS components to seismically induced vibratory ground motion. The output of these structural analyses includes estimates of damage to the waste packages and the drip shield as a function of seismic ground motion and of the physical condition of the EBS components, which are recognized to change as a function of time due to corrosion or prior seismic events. Additional analyses are presented that assess the effect of vibratory ground motion on the EBS components after the drip shield has failed, and quasi-static analysis to determine drip shield fragility. Outputs from this report include the probability of rupture and estimated damaged area of the waste package and drip shield due to vibratory ground motion. The requirements for development of the models presented here are defined in *Technical Work Plan for: Calculation of Waste Package and Drip Shield Response to Vibratory Ground Motion and Revision of the Seismic Consequence Abstraction* (SNL 2007 [DIRS 179869]).

1.1 DESCRIPTION OF EBS COMPONENTS THAT MAY BE AFFECTED BY VIBRATORY GROUND MOTION

The concept of drift emplacement of waste packages at Yucca Mountain is illustrated in Figure 1-1. The cylindrical waste packages are to be emplaced in horizontal drifts with the axes of the cylinders aligned parallel with the axis of the drift. The waste packages will be closely spaced, and waste packages of different sizes may be placed adjacent to each other. During seismic shaking, end-to-end impacts between waste packages, impacts between waste packages and pallets, and possibly impacts between waste packages and the drip shield may damage the waste packages or other components of the EBS. Moreover, during the postclosure period, significant changes in the drift environment are expected to occur. These include changes in temperature and seepage rates in the drift, degradation of the drift ground control system and the EBS components, and rockfall from the host rock surrounding the drift.

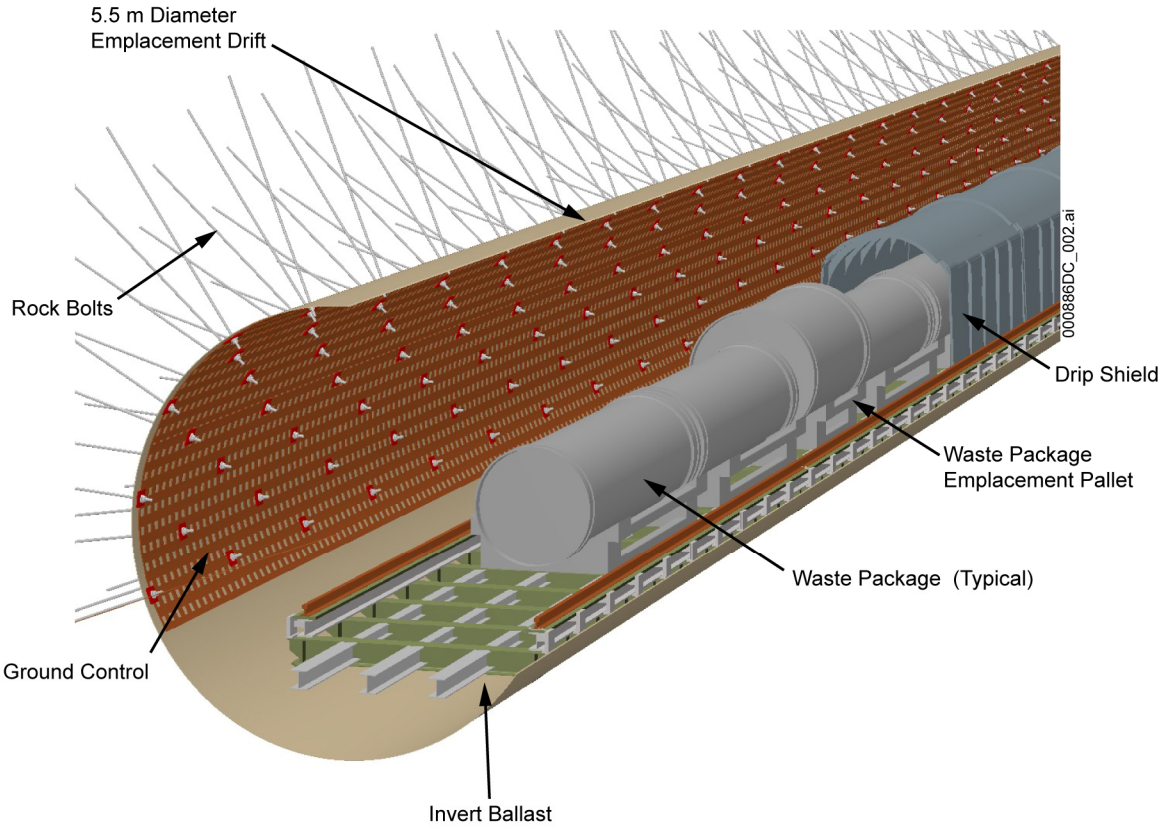

Source: Created for illustrative purposes only.

Figure 1-1. Schematic Illustration of the EBS Emplacement Geometry

Vibratory ground motion from a remote earthquake may affect several of the primary EBS components. These components are shown in Figure 1-2 and include: (a) the waste package; (b) the waste package internals, which in this document are defined to include all components and materials contained inside the Alloy 22 outer containment barrier (OCB); (c) the invert, which is composed of a steel framework filled with engineered ballast composed of crushed tuff; (d) the emplacement pallet, a platform constructed of Alloy 22 (UNS N06022) end piers and Stainless Steel Type 316 connector tubes, which rests on the invert and supports the waste package; and (e) the drip shield, a structure constructed of Titanium Grade 7 plates and Titanium Grade 29 framework that protects the waste package from seepage water and rockfall (SNL 2007 [DIRS 179354], Section 4.1).

The waste form packaging design for commercial spent nuclear fuel (SNF) calls for the use of a standardized transportation, aging, and disposable (TAD) canister system (SNL 2007 [DIRS 179394]), which will be used for packaging pressurized water reactor (PWR) and boiling water reactor (BWR) waste forms at the reactor sites. Moreover, each TAD canister will be inserted into a waste package, consisting of an outer corrosion barrier (OCB) and a structural inner vessel, prior to emplacement in Yucca Mountain. The TAD canister and waste package are referred to as the TAD-bearing waste package throughout this document. The weight, length, and center of gravity for the TAD canister and waste package are incorporated into the seismic damage models documented in this report. In addition, calculations for codisposal waste

packages are also documented. This type (configuration) of waste package is used for defense high-level (radioactive) waste (DHLW) and U.S. Department of Energy (DOE) SNF. This second type of waste package is referred to throughout this document as the codisposal waste package and will contain vitrified high-level waste forms and spent fuel assemblies (SNL 2007 [DIRS 179567], Tables 4-2 and 4-3).

The major EBS components are free-standing structures. The drip shield and the emplacement pallet rest on top of the invert, while the waste package rests on top of the emplacement pallet. Because the EBS components are unconstrained, impacts can occur between waste packages, drip shields, emplacement pallets, the invert (or the invert ballast), and the drift walls in response to significant ground motions. The drift invert, the waste package internals, and the mass of the waste form are also considered in structural response simulations presented in this report.

These components are important because their failure has the potential to directly influence release of radionuclides or to form diffusive or advective transport pathways. The effectiveness of these barriers is potentially compromised by the direct effects of an earthquake, which include vibratory ground motion, fault displacement, and rockfall induced by ground motion. The effectiveness of these barriers is also potentially compromised by indirect effects after an earthquake, including in-drift changes in seepage, temperature, and relative humidity.

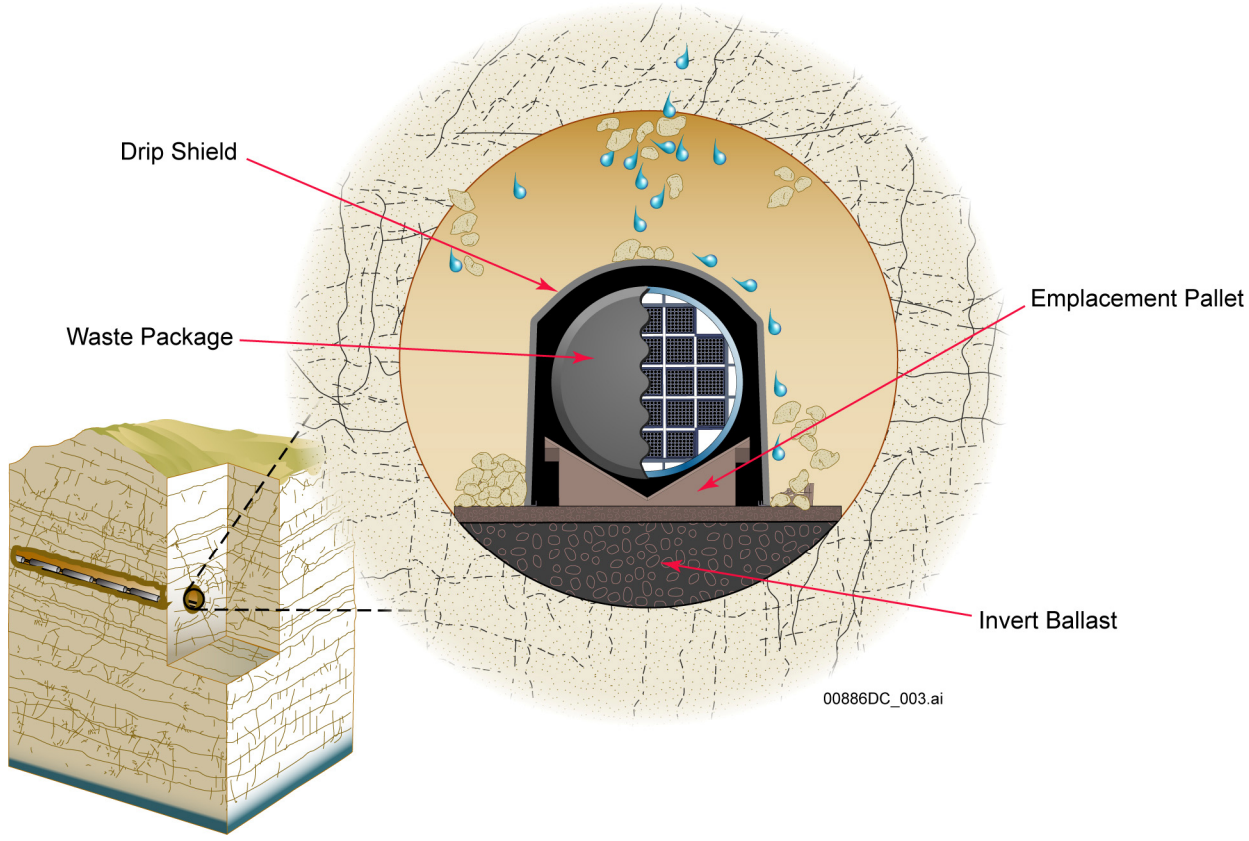

Source: Created for illustrative purposes only.

Figure 1-2. Diagram of the Engineered Barrier System Components in a Typical Emplacement Drift

1.2 LONG-TERM EVOLUTION OF THE EBS ENVIRONMENT

Shaking of the EBS components due to vibratory ground motion associated with earthquakes may occur at any time during the lifetime of the repository. Moreover, the consequences of seismic shaking on the EBS components may be highly dependent on the condition of the components and the "in-drift" environment. For example, a seismic event occurring a few hundred years after repository closure that causes moderate vibratory ground motion in the emplacement drifts may not cause damage to the EBS components, but the same ground motion occurring 100,000 years after closure may cause significant damage to EBS components that have been weakened by corrosion. Similarly, shaking of the EBS components arranged in the geometry shown in Figure 1-2 may yield a damage estimate much different than the estimate produced by shaking EBS components when the drip shield is covered by rockfall and pinned in place.

The radioactive wastes contained in the waste packages will generate heat for several thousand years after emplacement, causing drift temperatures to increase early in the postclosure period, and then later to decrease. Figure 1-3 shows how drift wall temperature is expected to vary over the postclosure period for a range of thermal loads for the repository. Prior to repository closure, the drifts will be ventilated, which removes decay heat prior to closure. The sudden rise in temperature at 50 years reflects closure of the repository and the end of ventilation.

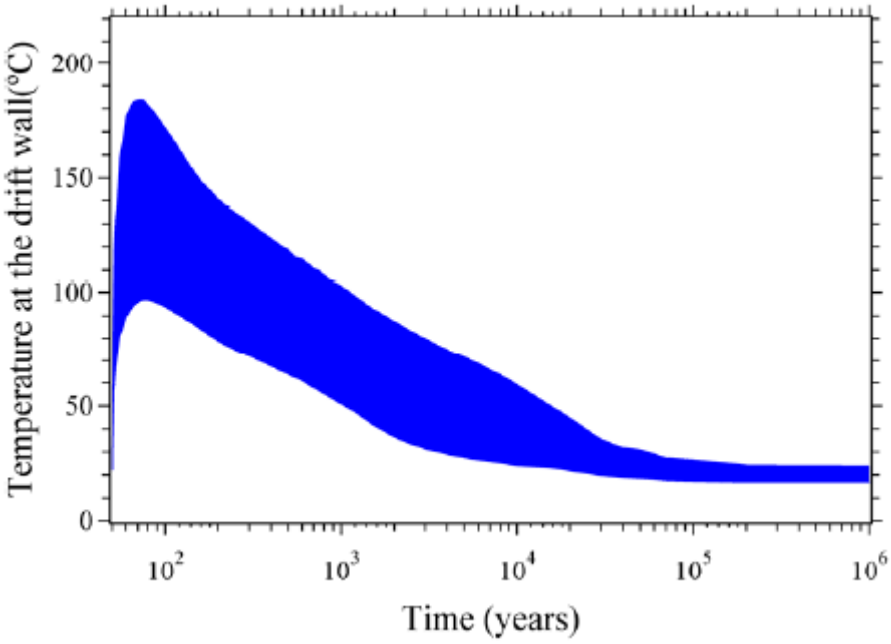

Source: SNL 2007 [DIRS 181383], Figure 6.3-76[a].

Figure 1-3. Predicted Temperature at the Drift Wall vs. Time for a Range of Thermal Loads

The repository is to be constructed in the Topopah Spring welded hydrogeologic 2 (TSw2) unit of the Topopah Spring member of the Paintbrush Tuff, which is a densely welded, partially saturated, fractured rock mass consisting of both lithophysal and nonlithophysal rock. Over the long duration of the postclosure period, it is anticipated that rockfall will occur from the surrounding drift walls, and some water will enter the tunnels.

The evolution of the EBS components is represented in Figure 1-4 by three idealized configurations. Figure 1-4 also presents a summary of the analyses presented in this report that address each of these configurations. Figure 1-4(a) represents an early EBS configuration, with an intact drip shield and minimal rockfall in the drifts. Over time, rockfall will begin to accumulate from multiple seismic events, partly restricting the motion of the drip shields. However, the waste packages will continue to move freely beneath the drip shields. The kinematic damage calculations for the waste package in this configuration are discussed in Section 6.3.

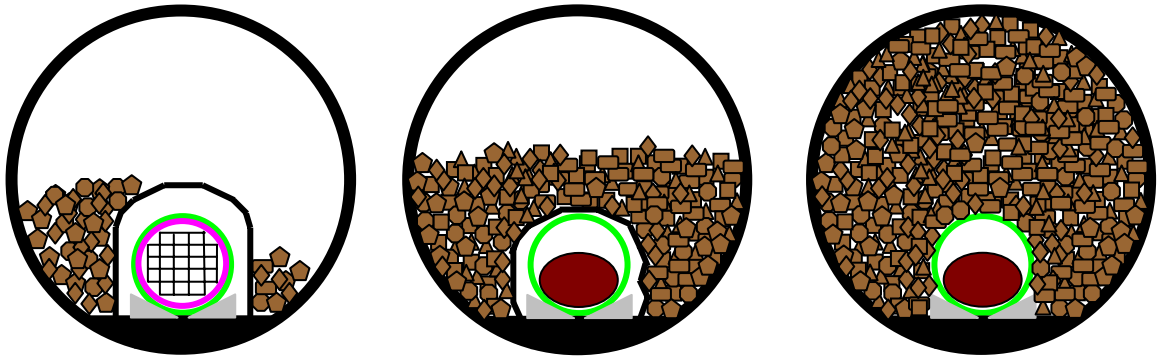

(a) Initial Configuration

- Kinematic damage simulations for TAD-bearing waste package (Section 6.3)
- Kinematic damage simulations for codisposal waste package (Section 6.3)
- Drip shield damage simulations in lithophysal units (Section 6.4)
- Drip shield damage simulations for large rock blocks in nonlithophysal units (Section 6.4)

(b) After Drip Shield Collapse

- Fragility of drip shield framework (Section 6.4)
- Damage for a waste package loaded by a collapsed drip shield (Section 6.5.2)
- Drip shield damage abstraction in lithophysal units (Section 6.4)

(c) After Drip Shield Plates Fail

- Fragility of drip shield plates (Section 6.4)
- Damage simulations for TAD-bearing waste package surrounded by rubble (Section 6.5.1)

Source: Created for illustrative purposes only.

NOTE: Section numbers shown in parentheses indicate where detailed discussions may be found.

Figure 1-4. Seismic Damage Simulations Representing the Future EBS Configurations

Figure 1-4(b) represents an intermediate state of the system, in which the legs of the drip shield have buckled under combined rockfall/seismic load, but the drip shield plates remain intact. In this configuration, the drip shield may collapse onto the waste package, inhibiting free movement of the waste package and emplacement pallet during the seismic event. Figure 1-4(c) represents a late stage of the system, after the drip shields have failed from general corrosion but

the OCB is still intact. In this late stage, rubble surrounds the waste package and pallet after failure of the drip shield plates.

The late-time configuration represented in Figure 1-4(c) is reasonable because the general corrosion rate for titanium alloys, although small, is significantly greater than the general corrosion rate for Alloy 22. In this situation, the titanium drip shield will degrade rapidly relative to the Alloy 22 OCB of the waste package and pallet structure, and significant rockfall volume will probably be present in the drifts. The waste package internals in Figure 1-4(c) are degraded because seismic damage from previous events allows moisture to enter the waste package through cracks in the OCB, leading to long-term corrosion that degrades the internals as structural components. The damage estimates for the drip shield surrounded by rubble are discussed in Section 6.4, and damage estimates for a waste package surrounded by rubble are discussed in Section 6.5.

Drip shield failure determines the transition between the three states in Figure 1-4. Drip shield failure can result from general corrosion of the drip shield, static rockfall load on top of the drip shield, and the dynamic acceleration that occurs during a seismic event. The probability of drip shield failure is represented by fragility curves for two failure models of the drip shield: (1) buckling of the sidewalls of the drip shield, and (2) rupture of the drip shield plates. Buckling of the sidewalls determines the transition from the first to the second state in Figure 1-4, and plate rupture determines the transition from the second to the third state in Figure 1-4. This order is appropriate because the probability that the sidewalls will buckle is greater than the probability that the drip shield plate will rupture for the cases considered, if all other factors (drip shield thicknesses, rockfall load, and intensity of the seismic event) are equal. Fragility analysis of the drip shield is documented in Section 6.4.3.

The timing of these transitions cannot be predicted as a deterministic value because of the uncertainties in the timing and intensity of individual seismic events, in the corrosion rates for titanium and Alloy 22, and in the accumulation of rockfall within the emplacement drifts. Drip shield failures from sidewall buckling or plate rupture are anticipated to occur over a broad range of times. While the timing of the transitions has a range of values, the individual states in Figure 1-4 are consistent with the long-term evolution of the EBS components:

- The as-emplaced configuration in Figure 1-4(a) is expected to be applicable during the first 10,000 years after repository closure because there will be minimal degradation of EBS components from general corrosion during that period and because a very high-intensity earthquake is a low-probability event during a 10,000-year period. In fact, this configuration may persist over a period of several tens of thousands of years.

- The third configuration (Figure 1-4(c)) represents the late-time system configuration, after the drip shield has failed, the drifts have collapsed, and the waste package internals have failed as structural elements. This final state is consistent with the observations that: (1) the drip shield will degrade more rapidly than the Alloy 22 OCB of the waste package and pallet structure, (2) significant rockfall volume will accumulate in the drifts from multiple seismic events, (3) waste package internals will begin corroding after first breach of the OCB that allows moisture in the form of water vapor or liquid water to enter the waste package.

It follows that the long-term evolution of EBS components illustrated in Figure 1-4 is consistent with the initial as-emplaced configuration and with the final late-time configuration for EBS components. Since the starting and ending states of the system have been defined, the remaining issue is to define reasonable intermediate state(s) of the system. The second configuration (Figure 1-4(b)) is an intermediate state that is based on the observations that the titanium drip shield will corrode more rapidly than the Alloy 22 OCB and pallet structure, and that sidewall buckling is more probable than rupture of the drip shield plates. In effect, the drip shield is the weakest element in the system and its response determines the preferred pathway between the starting and ending states of the system.

This intermediate state has several branches that are not illustrated in the simple schematic in Figure 1-4(b). These branches relate to waste package internals and to the potential for rupture or puncture of the OCB. Waste package internals are assumed to degrade as load-bearing elements after the OCB is first damaged by a seismic event. More exactly, the internals degrade as a structural component by the time of the next seismic event after the first seismic event that breaches the waste package. The timing of the first seismic event that breaches the waste package is a strong function of waste package type. The TAD-bearing waste package has two independent stainless steel vessels, the inner vessel and its lids and the TAD canister itself. The codisposal waste package has only the inner vessel and its lids. With intact internals, the TAD-bearing waste package is demonstrably more robust than the codisposal waste package (Section 6.3). In this situation, a TAD-bearing waste package is likely to have intact (i.e., undamaged) internals when the sidewalls of the drip shield buckle, while the codisposal waste package is likely to have degraded internals from damage during a prior seismic event when the sidewalls buckle.

The potential for rupture or puncture of the OCB is not illustrated in Figure 1-4 but is considered in the seismic damage calculations. The failure mechanism leading to rupture is postulated to be the accumulation of damage from high-velocity impacts. This is a postulated mechanism because the strain in the Alloy 22 OCB is always below the effective strain limit from individual waste package-pallet impacts. However, the potential for more rapid general corrosion in localized regions of the OCB may produce weakened regions where damage could accumulate from several seismic events with severe deformation of the waste package. The failure mechanism leading to puncture is postulated to be collapse of the OCB around the degraded waste package internals. Although the waste package internals are assumed to degrade as structural elements after the OCB is first breached, large fragments of the stainless steel inner vessel and parts of the Zircaloy cladding are likely to persist for long periods of time. The sharp edges or corners on these fragments may puncture a severely deformed OCB when it is loaded down by rockfall in the final state illustrated in Figure 1-4(c).

The simulations presented in this report are designed to provide input into the seismic damage abstractions in *Seismic Consequence Abstraction* (SNL 2007 [DIRS 176828], Figure 6-3) that represent the mechanical response for each of the three states in Figure 1-4. The state of the internals and the occurrence of rupture or puncture are integral with the damage abstractions (SNL 2007 [DIRS 176828]) and are not identified separately.

1.3 VIBRATORY GROUND MOTION

In order to simulate the effects of vibratory ground motion on the EBS during the postclosure period, numerical models have been developed that incorporate many details of the EBS and emplacement drift. These models are then excited using time histories of vibratory ground motion that represent seismic motions that may be experienced in the emplacement drifts.

The site-specific time histories used in this report are based on actual recordings of strong ground motion from earthquakes in the western United States and around the world (McGuire et al. 2001 [DIRS 157510], Appendix B).

Suites of three-component time histories were developed for the following peak ground velocities (PGVs): 0.4 m/s, 1.05 m/s, 2.44 m/s, and 4.07 m/s. These PGVs adequately represent the variability of seismic hazard at Yucca Mountain, as is explained in *Seismic Consequence Abstraction* (SNL 2007 [DIRS 176828], Section 6.4.3). Each of these time histories included one vertical and two horizontal components, and the records were scaled to the site-specific PGV using only one horizontal component as a reference in order to preserve the intercomponent variability of the original records. Consequently, for a given time history, other components may have a higher PGV.

Seventeen sets of time histories have been developed for each of the PGV levels. Each set of time histories consists of acceleration, velocity, and displacement. These ground motions cover the range of required frequency of occurrence (exceedance frequencies) for earthquakes of various magnitudes and represent the variability in amplitude and response spectrum expected for the ground motion hazard at Yucca Mountain. Examples of the time histories can be found in Section 6.3.2.1.2 of this report.

1.4 SCOPE

The scope of this report includes major activities necessary to provide input to damage abstractions associated with postclosure vibratory ground motion for the TAD-bearing waste package, for the codisposal waste package, and for the drip shield. In addition, information is provided in Appendix F for use in a cladding damage abstraction to support sensitivity studies for the license application.

A complete discussion of the technical basis for the seismic scenario class in TSPA for the license application (TSPA-LA) can be found in *Seismic Consequence Abstraction* (SNL 2007 [DIRS 176828]).

The simulations for the EBS components mentioned above are based on the design data that were available when the calculations were started. Section 2 provides information on the quality assurance procedures used to govern this work, and Section 3 provides the list of computer software used to accomplish the analyses. Section 4 documents the data inputs used in the analyses, and Section 5 presents assumptions used. Section 6.1 provides a general overview of each of the analyses presented in this report and the models used to perform these analyses. The remainder of Section 6 provides detailed descriptions of the technical approach and scope for each analysis, as follows:

- *Failure Mechanisms*. Section 6.2 discusses failure mechanisms associated with mechanical processes that may occur during seismic ground motion and presents the basis for failure criteria used in the analysis. In particular, discussion is focused on development of a criterion for initiation of stress corrosion cracking (SCC) and a rupture criterion based on tensile elongation.
- *Kinematic Analysis with Multiple Wastes Packages Subject to Vibratory Ground Motion*. The three-part analysis presented in Section 6.3 consists of three-dimensional rigid-body numerical calculations for the kinematics of waste package movement associated with (postclosure) vibratory ground motion. These rigid body kinematic calculations are used in combination with three-dimensional finite-element calculations for the damage from individual impacts between waste packages and between waste packages and pallets, to determine the probability of rupture and the magnitude of damaged areas[1] in response to vibratory ground motion for multiple waste packages in an emplacement drift. The probability of rupture and extent of the damaged areas are passed to *Seismic Consequence Abstraction* (SNL 2007 [DIRS 176828]) as the basis for new seismic damage abstractions for the TAD-bearing and codisposal waste packages.
- *Drip Shield Damage Mechanisms*. The damage mechanisms of the drip shield are evaluated in Sections 6.4.2 through 6.4.4 with numerical calculations to determine the seismic event that changes the EBS configuration. The change in EBS configuration causes the damage abstractions to switch from the kinematic representation to the representation for a waste package surrounded by rubble or another appropriate configuration in TSPA. Evaluation of the failure mechanisms includes consideration of rupture of the drip shield plates and the potential for collapse of the drip shield framework. These mechanisms also consider the potential for drip shield failure from impacts between the lip of the waste package and the internal bulkheads of the drip shield. In this report, these damage mechanisms are represented as a set of fragility curves that are functions of drip shield thickness, seismic intensity, and the static rockfall load on the drip shield.
- *Drip Shield Damaged Area*. The damaged areas on the drip shield resulting from vibratory ground motion and rockfall induced by vibratory ground motion must be calculated for use as the basis of seismic damage abstractions for the drip shield for TSPA. This discussion is located in Sections 6.4.3 and 6.4.5.
- *Uneven Settlement of the Invert*. Section 6.4.6 evaluates the potential for uneven settlement of the invert and the effect of such settlement on EBS response to seismic events. The effect of uneven settlement of the drip shield is analyzed for two loading conditions: a static rubble load and dynamic impact by large blocks. Work in this area responds to an AIN from the NRC (Key Technical Issue Agreement Total System Performance Assessment and Integration 2.02, Comment J-2, AIN) (Kokajko 2005 [DIRS 177025], pp. 5 to 6 of enclosure).

[1] Throughout this document, "damaged area" refers to a deformed region where the residual stress exceeds the (tensile) threshold for initiation of SCC. "Rupture" refers to complete mechanical failure, when a material exceeds its ultimate tensile strain.

- *Analysis of Drip Shield Damage due to Impact of Large Blocks*. Section 6.4.7 considers the effect of large rock blocks impacting the drip shield during rockfall events in the nonlithophysal rock mass. This analysis provides lookup tables for damage area and strain in the drip shield as functions of block energy and time-dependent corrosion of the drip shield.
- *Waste Package Analysis after Drip Shield Failure*. This analysis, found in Section 6.5, consists of numerical calculations for the damaged areas on a single waste package surrounded by rubble in response to vibratory ground motion, and analysis of the waste package structural integrity, stability, and damage that may occur if the drip shield collapses onto the waste package and transfers the weight of the rubble load and collapsed drip shield onto the waste package. These calculations represent the response of the EBS after the drift has collapsed. The calculations for the waste package surrounded by rubble are performed for the TAD-bearing waste package only. These calculations determine the probability of rupture and the magnitude of the damaged areas that will be used as the basis for new seismic damage abstractions for TSPA.

The above analyses have been designed to incorporate several aspects of the EBS. First, two different types of waste packages, the TAD-bearing waste package and the codisposal waste package, are included. Then, degraded states of the EBS are considered. In particular, this report develops fragility analyses, represented by numerically defined curves, for potential failure of the drip shield plates. These curves represent the case where failure of the drip shield plates results in a waste package being surrounded by rubble that restrains the motion of the waste package.

The potential for degradation of the inner vessel and waste form is incorporated into the seismic damage models documented in this report. This is necessary because failure of the waste package outer barrier may initiate corrosion of the inner vessel and waste form, decreasing their capacity to support a structural load.

Section 6.6 provides a list of features, events, and processes (FEPs) addressed in this report. Sections 6.7 and 6.8 discuss uncertainty and limitations on the work presented in this report, respectively. Section 7 presents validation activities performed for each of the models used in the analysis, and Section 8 presents outputs to *Seismic Consequence Abstraction* (SNL 2007 [DIRS 176828]). References for and inputs to this document are found in Section 9.

1.5 DEVIATION FROM THE TECHNICAL WORK PLAN

The approach for this model report follows the technical work plan (TWP) (SNL 2007 [DIRS 179869]). However, the work scope of this report has been revised from that cited in the TWP to include:

- Analysis of the waste package loaded by the drip shield (Section 6.5.2)
- Summary of accelerations of waste package internals due to impacts and maximum velocities of impact (Appendix F).

Some acceptance criteria cited in the TWP (SNL 2007 [DIRS 179869]) were excluded from this report. Justification for their exclusion is presented in Section 4.2.

FEP 2.1.03.10.0B, Advection of Liquids and Solids Through Cracks in the Drip Shield, is screened out of TSPA; and FEP 1.2.03.02.0B, Seismic-Induced Rockfall Damages EBS Components, remains excluded from TSPA, as discussed in Section 6.6.

Validation activities for the Model for Deformation and Damage of Drip Shield under Static and Dynamic Conditions were modified from those presented in Table 2-1 of the TWP in that "corroboration of the technical approach with analog studies" was not used. Instead, FLAC3D results are compared to dynamic LS-DYNA predictions of drip shield response to block impact. Postdevelopment model validation review criteria for this validation activity are the same as the validation review criteria listed in Table 2-1 of TWP for "corroboration of the technical approach with analog studies."

INTENTIONALLY LEFT BLANK

2. QUALITY ASSURANCE

Preparation of this model report and its supporting technical activities has been performed in accordance with the appropriate requirements of the Yucca Mountain Project quality assurance program. Analysis and modeling activities performed under this TWP (SNL 2007 [DIRS 179869]) are subject to the requirements of *Quality Assurance Requirements and Description* (DOE 2007 [DIRS 182051]) because they are associated with the characterization of the waste form and waste package in support of performance assessment (SNL 2007 [DIRS 179869], Section 8). The TWP was prepared in accordance with SCI-PRO-002, *Planning for Science Activities*.

This document is prepared in accordance with SCI-PRO-006, *Models*, and reviewed in accordance with SCI-PRO-003, *Document Review*, as directed in the TWP (SNL 2007 [DIRS 179869]). Input information for this model report is identified and tracked in accordance with SCI-PRO-004, *Managing Technical Product Inputs*. The methods used to control the electronic management of data, as required by IM-PRO-002, *Control of the Electronic Management of Information*, are identified in Section 8 of the TWP (SNL 2007 [DIRS 179869]). The software used was controlled as required by IM-PRO-003, *Software Management*.

Planning and preparation of the report were initiated under the Bechtel SAIC Company Quality Assurance Program. Therefore, forms and associated documentation (primarily the TWP (SNL 2007 [DIRS 179869])) prepared prior to October 2, 2006, the date this work transitioned to the Lead Laboratory, were completed in accordance with Bechtel SAIC Company procedures.

INTENTIONALLY LEFT BLANK

3. USE OF SOFTWARE

3.1 QUALIFIED SOFTWARE

All controlled and baselined software used in the development of the kinematic analyses and waste package–drip shield interaction results is identified in Table 3-1. The table gives the software tracking number, version, operating environment, and range of use for each software item. Table 3-1 also includes a discussion of why the software was selected and describes any limitations on outputs from the software. The software items documented in this section are appropriate for the applications used in this model report, and the implementation of each item is consistent with its intended use. Each software item was obtained from Software Configuration Management in accordance with established procedures (e.g., IM-PRO-003, *Software Management*). Each software item was used only within the range of its validation, as specified in the software qualification documentation in accordance with IM-PRO-003.

Table 3-1. Computer Software

Software Title/Version	Software Tracking Number	Operating Environment (Platform/Operating System)	Brief Description of Software (Range of Use/Selection/Limitations)
UDEC (V. 3.1 [DIRS 161949])	10173-3.1-00	PC/Windows 2000	UDEC was used to analyze the drip shield failure (Section 6.4) and the waste package surrounded by rubble (Section 6.5). UDEC was selected for its capability to model solid body interactions with a computationally efficient algorithm. UDEC was used only within the range of its validation, as specified in the software qualification report (BSC 2002 [DIRS 172041]). There are no known limitations on outputs.
FLAC (V. 4.0 [DIRS 161953])	10167-4.0-00	PC/Windows 2000	FLAC was used to simulate the invert material during seismic shaking (Sections 6.4 through 6.5). FLAC was selected for its capability to model dynamic loading for the continuum with a computationally efficient algorithm. FLAC was used only within the range of its validation, as specified in the software qualification report (BSC 2002 [DIRS 168820]). There are no known limitations on outputs.

Table 3-1. Computer Software (Continued)

Software Title/Version	Software Tracking Number	Operating Environment (Platform/Operating System)	Brief Description of Software (Range of Use/Selection/Limitations)
FLAC3D (V. 2.1 [DIRS 161947])	10502-2.1-00	PC/Windows 2000	FLAC3D V. 2.1 was used to simulate the drip shield and invert during quasi-static loading (Section 6.4.6). FLAC3D V. 2.1 was selected for its capability to model dynamic loading for the continuum with a computationally efficient algorithm. FLAC3D V. 2.1 simulates the behavior of three-dimensional structures built of soil, rock, or other materials that are subject to various loading conditions. FLAC3D V. 2.1 was used only within the range of its validation, as specified in the software qualification report (BSC 2002 [DIRS 168821]) which states that it will be used for drift degradation, stability modeling, and analyses of the EBS (BSC 2002 [DIRS 168821], Section 1.1). The code is applicable for modeling elastoplastic materials, including metals associated with the drip shield and waste package, which are components of the engineered barrier system. For example, test cases 1, 2, and 3 in *Software Implementation Report for FLAC3D Version 2.1* (BSC 2002 [DIRS 168821]) justify use of the software for this application. The Tresca constitutive relation, which is used for representation of mechanical behavior of metals, is a special case of the Mohr-Coulomb constitutive relation (when the friction angle is set to zero) included in test case 1 (BSC 2002 [DIRS 168821]). There are no known limitations on outputs.

Table 3-1. Computer Software (Continued)

Software Title/Version	Software Tracking Number	Operating Environment (Platform/Operating System)	Brief Description of Software (Range of Use/Selection/Limitations)
FLAC3D (V. 2.14 [DIRS 172323])	10502-2.14-00	PC/Windows 2000	FLAC3D V. 2.14 was used to simulate the drip shield during quasi-static and dynamic loading (Sections 6.4.3 and 6.4.7), and to simulate the waste package loaded by the drip shield (Section 6.5.2). FLAC3D V. 2.14 was selected for its capability to model dynamic loading for the continuum with a computationally efficient algorithm. FLAC3D was used only within the range of its validation. Note that FLAC3D V. 2.14 and FLAC3D V. 2.1 are identical codes (DOE 2004 [DIRS 181350], Section 1). The description of FLAC3D V. 2.1 provided in this table is also applicable to FLAC3D V. 2.14. For example, test cases 1, 2, and 3 in *Software Implementation Report for FLAC3D Version 2.1* (BSC 2002 [DIRS 168821]) justify use of the software for this application. The Tresca constitutive relation, which is used for representation of mechanical behavior of metals, is a special case of the Mohr-Coulomb constitutive relation (when the friction angle is set to zero) included in test case 1 (BSC 2002 [DIRS 168821]). There are no known limitations on outputs.
LS-DYNA SMP D (V. 970.3858 [DIRS 172925])	10300-970.3858-02	DEC ALPHA/OSF1 V. 5.1	LS-DYNA SMP D V. 970.3858 DEC ALPHA was used to analyze the kinematic impacts between the waste packages and between waste packages and pallets (Section 6.3). LS-DYNA was selected for its capability to model solid mechanics in dynamic loading conditions. LS-DYNA was used only within the range of its validation, as specified in the software qualification report (DOE 2005 [DIRS 174541]). There are no known limitations on outputs.
LS-DYNA (V. 971.7600.398 [DIRS 178801])	10300-971.7600.398-00	AMD Opteron 64 /Redhat Linux Chaos 3.0	LS-DYNA V. 971.7600.398-00 AMD Opteron 64/Redhat Linux Chaos 3.0 was used to analyze the kinematic impacts between the waste packages and between waste packages and pallets (Section 6.3). LS-DYNA was selected for its capability to model solid mechanics in dynamic loading conditions. LS-DYNA was used only within the range of its validation, as specified in the software validation report (DOE 2007 [DIRS 178853]). There are no known limitations on outputs.

Table 3-1. Computer Software (Continued)

Software Title/Version	Software Tracking Number	Operating Environment (Platform/Operating System)	Brief Description of Software (Range of Use/Selection/Limitations)
LS-DYNA (V. 971.7600.398 [DIRS 178801])	10300-971.7600.398-00	Intel Itanium/Redhat Linux Chaos 3.0	LS-DYNA V. 971.7600.398-00 Intel Itanium /Redhat Linux Chaos 3.0 was used to analyze the kinematic impacts between the waste packages and between waste packages and pallets (Section 6.3). LS-DYNA was selected for its capability to model solid mechanics in dynamic loading conditions. LS-DYNA was used only within the range of its validation, as specified in the software validation report (DOE 2007 [DIRS 178852]). There are no known limitations on outputs.
km_impacts_pp (V. 1.0 [DIRS 178489])	11235-1.0-00	AMD Opteron Redhat Linux 4	km_impacts_pp V. 1.0 was used on an AMD Opteron Redhat Linux 4 system to postprocess output from LS-DYNA. km_impacts_pp is used to produce estimates of damaged areas for the waste packages along with estimates of the number of ruptured waste packages. km_impacts_pp was selected for its capability to process the output of LS-DYNA and directly produce data for the seismic abstraction. km_impacts_pp was used only within the range of its validation as specified in the software validation report (DOE 2007 [DIRS 178854]). There are no known limitations on outputs.
km_impacts_pp (V. 1.0 [DIRS 178489])	11235-1.0-00	Intel Itanium2 Redhat Linux 4	km_impacts_pp was used on an Intel Itanium2 Redhat Linux 4 system to postprocess output from LS-DYNA. km_impacts_pp is used to produce estimates of damaged areas for the waste packages along with estimates of the number of ruptured waste packages. km_impacts_pp was selected for its capability to process the output of LS-DYNA and directly produce data for the seismic abstraction. km_impacts_pp was used only within the range of its validation as specified in the software validation report (DOE 2007 [DIRS 178855]). There are no known limitations on outputs.
GoldSim (V. 8.02.500 [DIRS 174650])	10344-8.02-05	PC/Windows 2000	GoldSim was used to sample the rock block pattern, rock strength, and ground motion number. GoldSim is widely used for probabilistic and decision analyses and provides capability for Latin Hypercube analysis used to sample the parameters listed above. GoldSim was only used within the range of its validation as specified in the software validation report (DOE 2005 [DIRS 174693]). There are no known limitations on outputs.

NOTE: PC = personal computer.

3.2 OTHER SOFTWARE

Commercial off-the-shelf software was used in the creation of tables and figures shown in this document, as well as for simple analyses such as computing basic statistics for selected data sets. This software includes Microsoft Word and Excel and was run on Microsoft Windows XP 2002. Use of this software is exempt from the requirements for software qualification, as allowed under IM-PRO-003, Section 2.0.

LS-PREPOST V. 1.0 and V. 2.0 were used to produce some of the plots in Section 6.3 and were used in the postprocessing of the output of a few LS-DYNA simulations for which the possibility of rupture was evaluated. This software was used solely for visual display or graphical representation of data in this report. Information generated by this software was checked and approved in accordance with applicable procedures and was found to meet stated acceptance criteria. This software was run on the AMD Opteron Redhat Linux 4, Intel Itanium2 Redhat Linux 4, and DEC ALPHA/OSF1 V. 5.1 systems. This software is exempt from the requirements for software qualification, as allowed under IM-PRO-003, Section 2.0.

TrueGrid V. 2.2.0, V. 2.2.6, and V. 2.3.0 were used to preprocess data and generate model geometry for input to LS-DYNA. TrueGrid is an off-the-shelf software program and analysis package that was used to support this report. All calculations done with TrueGrid used the standard functions available in TrueGrid, and the results are not dependent upon this software (i.e., the same result would be obtained whether TrueGrid or another gridding program was used). This software was used in accordance with SCI-PRO-006 and was run on the AMD Opteron Redhat Linux 4 and DEC ALPHA/OSF1 V. 5.1 systems. Use of this software is exempt from the requirements for software qualification, as allowed under IM-PRO-003, Section 2.0.

Mathcad® V. 7.0 is a commercial off-the-shelf software program used in this report to postprocess data from UDEC and to solve non-linear equations for stress profiles in Appendix B. Mathcad V. 7.0 was installed on personal computers equipped with the Windows 2000 operating system. Mathcad is appropriate for this application because it offers the mathematical and graphical functionality necessary to perform and document the numerical manipulations used in this report. The Mathcad computations performed in this report use only standard built-in functions and are documented in sufficient detail in Appendix B to allow an independent technical reviewer to reproduce or verify the results by visual inspection or hand calculation without recourse to the originator. The calculation results are not dependent upon the use of this particular software. Therefore, use of this software is exempt from the requirements for software qualification, as allowed under IM-PRO-003, Section 2.0.

Numerical results from the use of commercial off-the-shelf software in this report are not dependent on the software used. The documentation of each such use includes sufficient detail to allow an independent reviewer to reproduce or verify the results by visual inspection or hand calculation.

INTENTIONALLY LEFT BLANK

4. INPUTS

4.1 DIRECT INPUT

The input parameters used for this analysis include:

- Design inputs for EBS components (Section 4.1.1)
- Material properties for EBS components (Section 4.1.2)
- Material properties for rock rubble (Section 4.1.3)
- Seismic ground motions (Section 4.1.4)
- Information accepted by the scientific and engineering community as Established Fact.

The direct inputs used to develop the models are not used to validate the models. Established fact used in this document includes information from sources that scientists and engineers would use in standard work practice such as density tables; gravitational laws; equations of state established in engineering and scientific textbooks; professional society monographs; professional society/industry codes, criteria, and/or standards; numerical data from federal, state, or local government organizations such as the Naval Reactor Program, the National Weather Service, Census Bureau, or Department of Agriculture; numerical data from a primary source for the specific type of data (e.g., commercial nuclear facilities, supplier of proprietary products or materials); and other definitive, recognized authoritative sources (e.g., DOE Orders, codes, and regulations).

The results and conclusions presented in this report are based on the current design information contained in the four design information TSPA data input packages (SNL 2007 [DIRS 179394]; SNL 2007 [DIRS 179567]; SNL 2007 [DIRS 179354]; SNL 2007 [DIRS 179466]). Therefore, design information TSPA data input packages provide direct inputs to this report. However, it is important to note that analyses presented in this report required several months to complete, and, while they were underway, a few of the design parameter values used as input underwent minor revision. Consequently, some of the analyses use design values that are now superseded. These preliminary values are designated as indirect inputs in this report.

Section 4.1.5 provides an impact assessment that confirms that the mechanical assessment results and conclusions accurately (within the context of other model uncertainties and margins) represent the response of the Engineered Barrier System to vibratory ground motion.

4.1.1 Component Design Specification

The representations of drip shields, waste packages, emplacement pallets, the invert, and the drift configuration are based on the current design configuration (SNL 2007 [DIRS 179394]; SNL 2007 [DIRS 179567]; SNL 2007 [DIRS 179354]). Figure 4-1 (SNL 2007 [DIRS 179354], Figure 4-1, “In-Drift Configuration”) presents a cross section of the emplacement drift. The input parameters are provided in Table 4-1.

The emplacement drift has a nominal diameter of 18 ft (5,500 mm). Within the drift, steel support beams and associated ballast form a level invert whose top surface is 52 in (1,320 mm) above the lowest part of the drift (SNL 2007 [DIRS 179354], Figure 4-1, "In-Drift Configuration"). The waste package sits on an emplacement pallet that raises the bottom of the waste package above the invert.

The drip shield is a freestanding structure that sits on the invert and covers the waste package. The drip shield has an external height of 113.62 in (2,886 mm) (SNL 2007 [DIRS 179354], Section 4.1.2, Table 4-2, item 07-01). The internal height of the drip shield, defined as the distance from the invert floor to the lowest point on the underside of the top of the drip shield, is 106.93 in (2,716 mm) (SNL 2007 [DIRS 179354], Section 4.1.2, Table 4-2, item 07-01). There is a clearance of 50.37 in (1,279 mm) between the crown (top) of the drip shield and the drift roof (SNL 2007 [DIRS 179354], Section 4.1.2, Table 4-2, item 07-01).

Two waste package configurations, TAD-bearing and codisposal, are considered in this analysis. The basic dimensions of these waste packages are provided in Table 4-2. The actual dimensions and masses used for the numerical representation of the waste packages, drip shields, emplacement pallets, drift, and invert for detailed analysis are located in Sections 6.3.2 and 6.4.6, respectively.

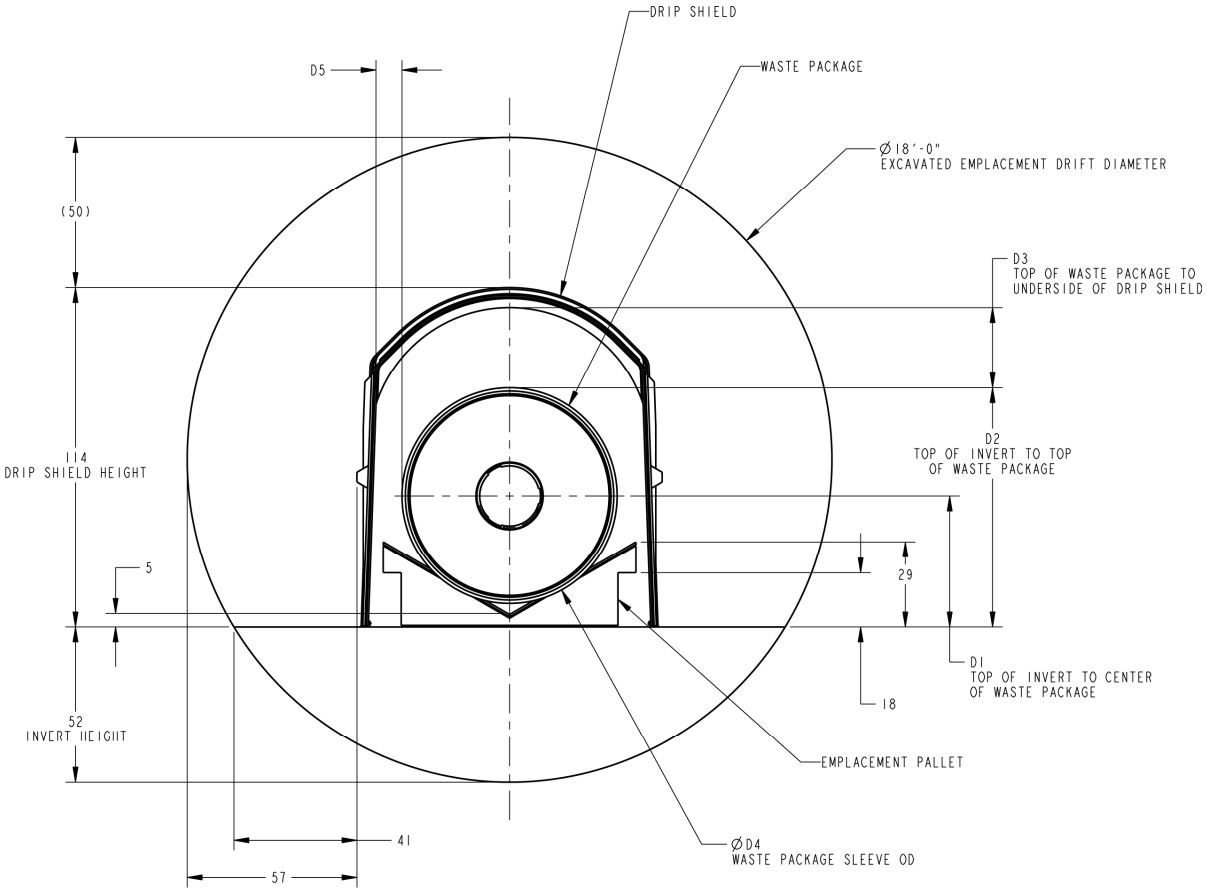

Source: SNL 2007 [DIRS 179354], Figure 4-1.

NOTE: Dimensions are rounded to the nearest inch. For dimensions of D1 through D5, see the source document.

Figure 4-1. Emplacement Drift Cross Section Showing EBS Components

Table 4-1. Design Inputs for EBS Components

Input Parameters	Value	Source	Application
Drift			
Emplacement drift diameter	18 ft (5,500 mm)	SNL 2007 [DIRS 179354], Section 4.1.1, Table 4-1, item 01-10	Sections 6.4, 6.5
Waste package skirt-to-skirt spacing	3.937 in (100 mm)	SNL 2007 [DIRS 179354], Section 4.1.4, Table 4-4, item 05-02	Section 6.3
Height of the invert	52 in (1,320 mm)	SNL 2007 [DIRS 179354], Figure 4-1	Sections 6.4, 6.5
Emplacement drift steel invert structure transverse support beam spacing	5 ft (1524 mm)	SNL 2007 [DIRS 179354], Section 4.1.1, Table 4-1, item 02-07	Section 6.4
Clearance from crown of drip shield to roof of drift	50.37 in (1,279 mm)	SNL 2007 [DIRS 179354], Section 4.1.2, Table 4-2, item 07-01	Sections 6.3, 6.4

Table 4-1. Design Inputs for EBS Components (Continued)

Input Parameters	Value	Source	Application
Drip Shield			
Drip shield height – Exterior overlap section – Framework interior	113.62 in (2,886 mm) 106.93 in (2,716 mm)	SNL 2007 [DIRS 179354], Section 4.1.2, Table 4-2, item 07-01	Sections 6.3, 6.4
Drip shield radius – Top of plate – Inside of framework	51.2 in (1,300 mm) 47.05 in (1,195 mm)	SNL 2007 [DIRS 179354], Section 4.1.2, Table 4-2, item 07-01	Sections 6.3, 6.4, Appendix B
Drip shield plate thickness	0.59 in (15 mm)	SNL 2007 [DIRS 179354], Section 4.1.2, Table 4-2, item 07-04A	Section 6.4, Appendix B
Bulkhead spacing	42.19 in (1,071.6 mm)	SNL 2007 [DIRS 179354], Section 4.1.2, Table 4-2, item 07-08	Section 6.4, Appendix B
Longitudinal stiffener spacing	8.85 in (224.7 mm)	SNL 2007 [DIRS 179354], Section 4.1.2, Table 4-2, item 07-08	Section 6.4
Bulkhead thickness	3.54 in (90 mm)	SNL 2007 [DIRS 179354], Section 4.1.2, Table 4-2, item 07-08 (outer radius – inner radius)	Appendix B
Bulkhead width	1.5 in (38 mm)	SNL 2007 [DIRS 179354], Section 4.1.2, Table 4-2, item 07-08	Appendix B
Bulkhead flange thickness	0.78 in (20 mm)	SNL 2007 [DIRS 179354], Section 4.1.2, Table 4-2, item 07-08 (outer radius – inner radius)	Appendix B
Bulkhead flange width	1.97 in (50 mm)	SNL 2007 [DIRS 179354], Section 4.1.2, Table 4-2, item 07-08	Appendix B
Support beam (large) thickness at bottom	1.09 in (28 mm)	SNL 2007 [DIRS 179354], Section 4.1.2, Table 4-2, item 07-08	Appendix B
Support beam (large) thickness at top	3.40 in (86 mm)	SNL 2007 [DIRS 179354], Section 4.1.2, Table 4-2, item 07-08	Appendix B
Support beam (large) width	3.0 in (76 mm)	SNL 2007 [DIRS 179354], Section 4.1.2, Table 4-2, item 07-08	Appendix B
Mass of drip shield segment	5,000 kg	SNL 2007 [DIRS 179354], Section 4.1.2, Table 4-2, item 07-01	Section 6.5
Balance of drip shield dimensions	See Source	SNL 2007 [DIRS 179354], Section 4.1.2	Sections 6.3, 6.4, Appendix B

Table 4-1. Design Inputs for EBS Components (Continued)

Input Parameters	Value	Source	Application
Emplacement Pallet			
Total long pallet length	163.3 in (4,148 mm)	SNL 2007 [DIRS 179354], Section 4.1.3, Table 4-3, item 08-01A	Sections 6.3, 6.5
Support pad length	21.37 in (542.9 mm)	SNL 2007 [DIRS 179354], Section 4.1.3, Table 4-3, item 08-01C	Sections 6.3, 6.5
Width	84.65 in (2,150 mm)	SNL 2007 [DIRS 179354], Section 4.1.3, Table 4-3, item 08-01A	Sections 6.3, 6.4, 6.5
Height	28.59 in (726.3 mm)	SNL 2007 [DIRS 179354], Section 4.1.3, Table 4-3, item 08-01A	Section 6.3
Support pad angle	30 degrees	SNL 2007 [DIRS 179354], Section 4.1.3	Sections 6.3, 6.5
Mass	4,340 lbs (1,970 kg)	SNL 2007 [DIRS 179354], Section 4.1.3, Table 4-3, item 08-01B	Sections 6.3, 6.5
Plate thickness of bottom	0.38 in (9.5 mm)	SNL 2007 [DIRS 179354], Section 4.1.3, Table 4-3, item 08-01A	Section 6.3
Plate thickness of sides	0.69 in (17.5 mm)	SNL 2007 [DIRS 179354], Section 4.1.3, Table 4-3, item 08-01A	Section 6.3
Plate thickness of top	0.88 in (22.2 mm)	SNL 2007 [DIRS 179354], Section 4.1.3, Table 4-3, item 08-01A	Section 6.3
Area, 6 × 6 × 3/8-in tube	8.08 in^2 (5,212.9 mm^2)	AISC 1995 [DIRS 114107], p. 1-95	Section 6.3
Rectangular moment of inertia, 6 × 6 × 3/8-in tube	41.6 in^4 (1.73 x $10^7 mm^4$)	AISC 1995 [DIRS 114107], p. 1-95	Section 6.3
Polar moment of inertia, 6 × 6 × 3/8-in tube	68.5 in^4 (2.85 x $10^7 mm^4$)	AISC 1995 [DIRS 114107], p. 1-95	Section 6.3
Waste Package			
Waste package dimensions	See Table 4-2	See Table 4-2	Sections 6.3, 6.5
Nominal loaded mass for TAD-bearing waste package	162,055 lbm (73.5 mT)	SNL 2007 [DIRS 179394], Table 4-3	Sections 6.3, 6.5
Nominal Alloy 22 mass for TAD-bearing waste package	21,878 lbm (9.9 mT)	SNL 2007 [DIRS 179394], Table 4-3	Section 6.5
Nominal mass of 21-PWR assemblies	35,300 lbm (16.0 mT)	SNL 2007 [DIRS 179394], Section 4.1.1.3	Section 6.5
Nominal mass of TAD canister basket	35,000 lbm (15.9 mT)	SNL 2007 [DIRS 179394], Section 4.1.1.3	Section 6.5
Nominal loaded mass for codisposal waste package	127,870 lbm (58 mT)	SNL 2007 [DIRS 179567], Table 4-9	Sections 6.3, 6.5

Table 4-2. Waste Package Dimensions and Clearance between Drip Shield and Waste Package

Waste Package Type	Outside Diameter[a]	Inside Diameter of OCB	Length[b]	Waste Package Clearance to Drip Shield[c]
TAD-bearing	77.28 in (1,962.8 mm)[d]	72.08 in (1,830.7 mm)[d]	230.32 in (5,850.1 mm)[d]	21 in (530 mm)
Codisposal	83.70 in (2,126.0 mm)[e]	N/A	208.82 in (5,303.9 mm)[e]	14 in (360 mm)

[a] Includes upper and lower sleeves which add 3.2 in (81 mm) to the diameter of the outer corrosion barrier (OCB) of each waste package.
[b] Nominal length includes 31.8 mm (1.25 inch) OCB lid-lifting feature.

Sources: [c] SNL 2007 [DIRS 179354], Figure 4-1, *In-Drift Configuration*.
[d] SNL 2007 [DIRS 179394], Table 4-3.
[e] SNL 2007 [DIRS 179567], Table 4-9.

4.1.2 Material Properties

Material properties used in the numerical analyses include those for (1) EBS components, (2) contact friction for metal-to-metal and metal-to-rock interfaces, and (3) host rock and caved lithophysal rock surrounding the drip shield. A description for each category is provided below.

4.1.2.1 Material Properties for EBS Components

Material properties for EBS components are given in Table 4-3 and include input parameters for the waste package and waste package internals, drip shield, and pallet. The drip shield framework is modeled as Titanium Grade 24 as opposed to Titanium Grade 29 (see Section 4.1.5 and Assumption 5.23, Section 5 for further explanation).

Table 4-3. Material Properties for Engineered Barrier System Components

Parameter	Value	Source	Application
Material Properties for the Drip Shield Plates (Titanium Grade 7, SB-265 R52400)			
Drip shield plate material	Titanium Grade 7	SNL 2007 [DIRS 179354], Table 4-2, item 07-04A	Sections 6.4, 6.5
Average density (at 20°C)	4,520 kg/m^3	DTN: MO0003RIB00073.000 [DIRS 152926], Table S04197_001, p. 2, indicates a range of 4,500 to 4,540 kg/m^3	Sections 6.4, 6.5
Average yield strength (at room temperature)	363 MPa	DTN: MO0003RIB00073.000 [DIRS 152926], Table S04197_001, p. 2, indicates a range of 275 to 450 MPa	Appendix A
Yield strength (at 60°C)	316 MPa	DTN: MO0003RIB00073.000 [DIRS 152926], Table S04197_001, p. 2, by interpolation in Appendix A	Sections 6.4, 6.5
Yield strength (at 150°C)	176 MPa	BSC 2005 [DIRS 174715], Table 5.2-1	Section 6.4.6
Average yield strength (at 204°C)	145 MPa	DTN: MO0003RIB00073.000 [DIRS 152926], Table S04197_001, p. 2, indicates a range of 138 to 152 MPa	Appendix A

Table 4-3. Material Properties for Engineered Barrier System Components (Continued)

Parameter	Value	Source	Application
Material Properties for the Drip Shield Plates (Titanium Grade 7, SB-265 R52400) (Continued)			
Ultimate tensile strength (at room temperature)	345 MPa	DTN: MO0003RIB00073.000 [DIRS 152926], Table S04197_001, p. 2	Appendix A
Ultimate tensile strength (at 60°C)	318 MPa	DTN: MO0003RIB00073.000 [DIRS 152926], p. 2, by interpolation in Appendix A	Sections 6.4, 6.5
Average ultimate tensile strength (at 204°C)	218 MPa	DTN: MO0003RIB00073.000 [DIRS 152926], Table S04197_001, p. 2, indicates a range of 207 to 228 MPa	Appendix A
Poisson's ratio (at room temperature)	0.32	DTN: MO0003RIB00073.000 [DIRS 152926], Table S04197_001, p. 3	Sections 6.4, 6.5
Modulus of elasticity (Young's modulus) (at 21°C)	107 GPa	DTN: MO0003RIB00073.000 [DIRS 152926], Table S04197_001, p. 3	Appendix A
Modulus of elasticity (Young's modulus) (at 60°C)	105 GPa	DTN: MO0003RIB00073.000 [DIRS 152926], Table S04197_001, p. 3, by interpolation in Appendix A	Sections 6.4, 6.5
Modulus of elasticity (Young's modulus) (at 93°C)	103 GPa	DTN: MO0003RIB00073.000 [DIRS 152926], Table S04197_001 p. 3	Appendix A
Modulus of elasticity (Young's modulus) (at 150°C)	101 GPa	BSC 2005 DIRS 174715], Table 5.2-1	Section 6.4.6
Modulus of elasticity (Young's modulus) (at 204°C)	97 GPa	DTN: MO0003RIB00073.000 [DIRS 152926], Table S04197_001, p. 3	Appendix A
Material Properties for Drip Shield Framework (Titanium Grade 29, SB-265 R56404)			
Drip shield framework material	Titanium Grade 29	SNL 2007 [DIRS 179354], Table 4-2, item 07-04B	Table 4-6
Density (at room temperature)	4,430 kg/m^3	ASM International 1990 [DIRS 141615], p. 620	Sections 6.4, 6.5
Yield strength (at room temperature)	759 MPa (110 ksi)	ASTM 2002 [DIRS 162726], Table 1	Sections 6.4, 6.5
Ultimate tensile strength (at room temperature)	828 MPa (120 ksi)	ASTM 2002 [DIRS 162726], Table 1	Sections 6.4, 6.5
Poisson's ratio (at 20°C)	0.31	TIMET 2000 [DIRS 160688], Table 2	Sections 6.4, 6.5
Modulus of elasticity (at 20°C)	107-122 GPa	TIMET 2000 [DIRS 160688], Table 2	Sections 6.4, 6.5
Modulus of elasticity (at 230°C)	95-111 GPa	TIMET 2000 [DIRS 160688], Table 2	Sections 6.4, 6.5
Material Properties for Waste Package and Pallet Plates (Alloy 22) (UNS N06022)			
Waste package material	Alloy 22	SNL 2007 [DIRS 179394], Table 4-1, item 03-03	Section 6.3, 6.4, 6.5
Pallet plate material	Alloy 22	SNL 2007 [DIRS 179354], Table 4-3, item 08-03	Section 6.3, 6.4, 6.5
Density (at room temperature)	8,690 kg/m^3	DTN: MO0003RIB00071.000 [DIRS 148850], Table S04196_001, p. 2	Sections 6.3, 6.5
Yield strength (at room temperature)	372 MPa	DTN: MO0003RIB00071.000 [DIRS 148850], Table S04196_001, p. 6, Plate ¼ - ¾ in thick	Appendix A

Table 4-3. Material Properties for Engineered Barrier System Components (Continued)

Parameter	Value	Source	Application
Material Properties for Waste Package and Pallet Plates (Alloy 22) (UNS N06022) (Continued)			
Yield strength (at 60°C)	350 MPa	DTN: MO0003RIB00071.000 [DIRS 148850], Table S04196_001, p. 6, by interpolation in Appendix A	Sections 6.3, 6.5
Yield strength (at 93°C)	338 MPa	DTN: MO0003RIB00071.000 [DIRS 148850], Table S04196_001, p. 6, Plate ¼ - ¾ in thick	Appendix A
Ultimate tensile strength (at room temperature)	786 MPa	DTN: MO0003RIB00071.000 [DIRS 148850], Table S04196_001, p. 6, Plate ¼ - ¾ in thick	Appendix A
Ultimate tensile strength (at 60°C)	758 MPa	DTN: MO0003RIB00071.000 [DIRS 148850], Table S04196_001, p. 6, by interpolation in Appendix A	Sections 6.3, 6.5
Ultimate tensile strength (at 93°C)	738 MPa	DTN: MO0003RIB00071.000, [DIRS 148850], Table S04196_001 p. 6, Plate ¼ - ¾ in thick	Appendix A
Poisson's ratio (at 21°C)	0.278	DTN: MO0003RIB00071.000 [DIRS 148850], Table S04196_001, p. 5	Sections 6.3, 6.5
Modulus of elasticity (Young's modulus) (at room temperature)	206 GPa	DTN: MO0003RIB00071.000 [DIRS 148850], Table S04196_001, p. 5	Appendix A
Modulus of elasticity (Young's modulus) (at 60°C)	204 GPa	DTN: MO0003RIB00071.000 [DIRS 148850], Table S04196_001, p. 5, by interpolation in Appendix A	Sections 6.3, 6.5
Modulus of elasticity (Young's modulus) (at 93°C)	203 GPa	DTN: MO0003RIB00071.000 [DIRS 148850], Table S04196_001, p. 5	Appendix A
Residual stress threshold for initiation of SCC on a smooth surface of Alloy 22	Distribution between 90% and 105% of the yield strength of Alloy 22	DTN: MO0702PASTRESS.002 [DIRS 180514], *Model Output DTN.doc*, Table 8-3	Sections 6.3, 6.5
Material Properties for Stainless Steel Type 316 (SA-240 S31600)			
Density (at room temperature)	7,980 kg/m^3	ASTM G 1-90 1999 [DIRS 103515], Table X1.1, p. 7	Sections 6.3, 6.5
Yield strength (−20 to 100°F) assumed at 38°C	30 ksi (207 MPa)	ASME 2005 [DIRS 176967], Table Y-1, Row 603	Appendix A
Yield strength (at 60°C)	193 MPa	ASME 2005 [DIRS 176967], Table Y-1, Row 603, by interpolation in Appendix A	Sections 6.3, 6.5
Yield strength (≤150°F) assumed at 66°C	27.4 ksi (189 MPa)	ASME 2005 [DIRS 176967], Table Y-1, Row 603	Appendix A
Ultimate tensile strength (−20 to 100°F) assumed at 38°C	75 ksi (517 MPa)	ASME 2005 [DIRS 176967], Table U, Row 588	Appendix A
Ultimate tensile strength (at 60°C)	517 MPa	ASME 2005 [DIRS 176967], Table U, Row 588, by interpolation in Appendix A	Sections 6.3, 6.5
Ultimate tensile strength (<200°F) assumed at 93 °C	75 ksi (517 MPa)	ASME 2005 [DIRS 176967], Table U, Row 588	Appendix A
Poisson's ratio (at room temperature)	0.30	ASM 1980 [DIRS 104317], Figure 15, p. 755	Sections 6.3, 6.5

Table 4-3. Material Properties for Engineered Barrier System Components (Continued)

Parameter	Value	Source	Application
Material Properties for Stainless Steel Type 316 (SA-240 S31600) (Continued)			
Modulus of elasticity (70°F or 21°C)	28.3×10^6 psi 195 GPa	ASME 2005 [DIRS 176967], Table TM-1, Material Group G	Appendix A
Modulus of elasticity (at 60°C)	192 GPa	ASME 2005 [DIRS 176967], Table TM-1, Material Group G, by interpolation in Appendix A	Sections 6.3, 6
Modulus of elasticity (200°F or 93°C)	27.5×10^6 psi 190 GPa	ASME 2005 [DIRS 176967], Table TM-1, Material Group G	Appendix A
Contact Friction			
Metal-to-metal	see Table 4-3a	BSC 2005 [DIRS 173172], Table X-1; DTN: MO0508SPAMECHA.000 [DIRS 181067], *AttachmentX.zip*, file *All_3_Sampling_Groups.txt*	Sections 6.3, 6.4, 6.5
Metal-to-rock	see Table 4-3b	BSC 2005 [DIRS 173172], Table X-2; DTN: MO0508SPAMECHA.000 [DIRS 181067], *AttachmentX.zip*, file *All_3_Sampling_Groups.txt*	Sections 6.3, 6.4, 6.5

Table 4-3a. Metal-to-Metal Coefficients of Friction

Rlz #	A	B	C	D	E	F	G	H	I	J
1	0.65366	0.32093	0.41049	0.59397	0.62892	0.60661	0.75327	0.57638	0.76666	0.51524
2	0.29918	0.57656	0.22729	0.29634	0.37167	0.42698	0.58001	0.74702	0.71202	0.45004
3	0.2101	0.2978	0.4157	0.42111	0.21613	0.39713	0.64045	0.68395	0.38015	0.74051
4	0.24688	0.76289	0.77047	0.72159	0.46025	0.73011	0.6898	0.77928	0.59089	0.69082
5	0.75363	0.40389	0.70558	0.5344	0.26819	0.37264	0.25901	0.59054	0.5031	0.25947
6	0.71345	0.76851	0.54769	0.46224	0.27656	0.54725	0.35055	0.21888	0.63054	0.61473
7	0.4989	0.5181	0.24096	0.58065	0.30793	0.50815	0.39718	0.26039	0.46047	0.39442
8	0.5422	0.34158	0.29694	0.67685	0.55815	0.33421	0.54781	0.35253	0.3539	0.56025
9	0.3427	0.43203	0.68965	0.77302	0.59291	0.64669	0.22696	0.63342	0.25203	0.62505
10	0.55884	0.47415	0.44808	0.21811	0.4267	0.22592	0.61641	0.38865	0.67503	0.70393
11	0.39109	0.61478	0.73592	0.31189	0.48914	0.71904	0.27611	0.27828	0.5235	0.30831
12	0.77613	0.70504	0.32481	0.24897	0.74443	0.77381	0.44932	0.50972	0.28727	0.44546
13	0.41564	0.21201	0.51689	0.36124	0.67096	0.67343	0.7712	0.33653	0.75305	0.28574
14	0.66831	0.67482	0.61252	0.76417	0.38496	0.29131	0.32614	0.53427	0.21966	0.37392
15	0.46891	0.64929	0.3414	0.65683	0.71042	0.58101	0.48249	0.69819	0.43675	0.77906
16	0.32215	0.25919	0.57013	0.40938	0.54539	0.25453	0.44579	0.46026	0.57408	0.2031
17	0.61847	0.48698	0.65764	0.50213	0.7805	0.4677	0.72451	0.44673	0.31337	0.52999

Table 4-3a. Metal-to-Metal Coefficients of Friction (Continued)

Rlz #	K	L	M	N	O	P	Q	R	S
1	0.75102	0.5157	0.35643	0.69366	0.73239	0.32978	0.45509	0.47652	0.33038
2	0.6042	0.54777	0.79724	0.4289	0.60267	0.66686	0.5569	0.53298	0.58714
3	0.30566	0.39408	0.72101	0.47896	0.62874	0.49866	0.39225	0.3118	0.76816
4	0.50778	0.63458	0.58404	0.56918	0.48607	0.75819	0.35277	0.41628	0.61648
5	0.25645	0.24232	0.2559	0.77613	0.7796	0.47424	0.7833	0.40907	0.2673
6	0.22337	0.67929	0.53094	0.33738	0.38909	0.63465	0.66789	0.36621	0.36401
7	0.47226	0.34823	0.20738	0.50467	0.20838	0.25892	0.28686	0.2363	0.29154
8	0.42133	0.33122	0.68088	0.20348	0.46616	0.54976	0.74678	0.51548	0.44214
9	0.56144	0.46093	0.44477	0.521	0.26916	0.41464	0.52274	0.76424	0.76228
10	0.31181	0.77204	0.76396	0.30025	0.36628	0.21822	0.2544	0.21257	0.52024
11	0.64231	0.30564	0.51383	0.26906	0.28635	0.77079	0.30623	0.64481	0.47137
12	0.53103	0.43039	0.29137	0.70908	0.71439	0.71873	0.6035	0.77892	0.68733
13	0.39125	0.55866	0.63641	0.38089	0.30884	0.59673	0.50447	0.58825	0.50157
14	0.69048	0.21786	0.6201	0.74224	0.44618	0.34999	0.44056	0.27381	0.6299
15	0.37143	0.59041	0.33604	0.63661	0.56526	0.55725	0.63521	0.71355	0.2114
16	0.79285	0.73881	0.38888	0.34412	0.68342	0.28076	0.20709	0.66586	0.6973
17	0.72249	0.70122	0.45875	0.61745	0.53808	0.38202	0.70639	0.58018	0.38288

Sources: BSC 2005 [DIRS 173172], Table X-1; DTN: MO0508SPAMECHA.000 [DIRS 181067], *AttachmentX.zip*, file *All_3_Sampling_Groups.txt*.

NOTE: Rlz # = Realization number; column headings A-S refer to waste packages as shown in Figure 6-10 in Section 6 of this report.

Table 4-3b. Metal-to-Rock Coefficients of Friction

Rlz #	A	B	C	D	E	F	G	H	I	J
1	0.42599	0.75925	0.49458	0.53287	0.31878	0.35173	0.74103	0.45704	0.69753	0.54255
2	0.30763	0.21838	0.26419	0.25372	0.21881	0.47556	0.62115	0.30541	0.78146	0.72809
3	0.70431	0.32817	0.52106	0.71835	0.46306	0.23268	0.54727	0.66563	0.47206	0.28081
4	0.29588	0.53062	0.7556	0.60512	0.70412	0.26512	0.50095	0.75224	0.31661	0.51729
5	0.25515	0.71205	0.67405	0.63946	0.51949	0.31998	0.21052	0.4118	0.54475	0.25932
6	0.60713	0.39082	0.21636	0.51602	0.59847	0.65986	0.58546	0.78554	0.63455	0.77163
7	0.46305	0.42466	0.30311	0.55353	0.36894	0.48884	0.37835	0.69816	0.57661	0.38194
8	0.49958	0.2369	0.63152	0.37594	0.68582	0.76938	0.64869	0.6382	0.24013	0.42889
9	0.76426	0.49614	0.57289	0.28445	0.40191	0.76276	0.34456	0.37726	0.30423	0.67262
10	0.66982	0.29126	0.72884	0.7718	0.64684	0.57507	0.33072	0.3751	0.60203	0.61763
11	0.53046	0.59736	0.44766	0.75096	0.73761	0.61313	0.2599	0.22524	0.74656	0.73279
12	0.23096	0.69271	0.6006	0.45188	0.27697	0.54717	0.69196	0.50715	0.40301	0.45438
13	0.6353	0.78792	0.3432	0.30981	0.2418	0.6487	0.79918	0.56208	0.49327	0.58555
14	0.39148	0.36413	0.76763	0.66907	0.5721	0.41082	0.72599	0.60736	0.22821	0.32038
15	0.36656	0.62453	0.39484	0.41988	0.42366	0.4285	0.4673	0.54813	0.35977	0.36674
16	0.77983	0.46813	0.44287	0.39528	0.50229	0.30264	0.4403	0.2652	0.44273	0.65572
17	0.55932	0.57103	0.31062	0.21597	0.7717	0.70299	0.29046	0.3228	0.66081	0.21857

Table 4-3b. Metal-to-Rock Coefficients of Friction (Continued)

Rlz #	K	L	M	N	O	P	Q	R	S
1	0.38877	0.57453	0.79893	0.56298	0.34316	0.54326	0.52918	0.20182	0.51192
2	0.75214	0.32463	0.20062	0.60189	0.27448	0.6097	0.72886	0.76432	0.68681
3	0.60163	0.61272	0.25471	0.64311	0.72375	0.27107	0.78317	0.29239	0.78193
4	0.35038	0.43717	0.46407	0.26659	0.77564	0.34663	0.73924	0.36955	0.7167
5	0.69165	0.54699	0.35103	0.67948	0.50768	0.46019	0.24674	0.77885	0.21525
6	0.31924	0.72421	0.61791	0.79615	0.45665	0.41425	0.36236	0.60087	0.37303
7	0.48086	0.22705	0.73956	0.34598	0.3188	0.586	0.44123	0.72705	0.2458
8	0.72895	0.6255	0.28395	0.2151	0.57393	0.22714	0.60287	0.32736	0.43934
9	0.64526	0.23701	0.38195	0.44947	0.3943	0.26013	0.33219	0.66914	0.59323
10	0.27976	0.73971	0.72279	0.33801	0.68688	0.64201	0.48012	0.56923	0.28825
11	0.76485	0.39674	0.6633	0.51543	0.25447	0.72468	0.22319	0.43012	0.56685
12	0.41936	0.27781	0.52803	0.27384	0.21461	0.7963	0.50208	0.46139	0.32037
13	0.55591	0.7672	0.42402	0.53312	0.64854	0.68441	0.57084	0.54066	0.53606
14	0.53052	0.46441	0.64702	0.44138	0.6173	0.38265	0.68507	0.39297	0.63893
15	0.24573	0.51169	0.49723	0.72925	0.73842	0.50685	0.64582	0.51668	0.40874
16	0.21804	0.66316	0.31832	0.38214	0.52296	0.31738	0.39991	0.64781	0.75924
17	0.4937	0.37117	0.56647	0.73483	0.41704	0.75098	0.2781	0.24537	0.46195

Sources: BSC 2005 [DIRS 173172], Table X-2; DTN: MO0508SPAMECHA.000 [DIRS 181067], *AttachmentX.zip*, file *All_3_Sampling_Groups.txt*.

NOTE: Rlz # = Realization number; column headings A-S refer to waste packages as shown in Figure 6-10 in Section 6 of this report.

A bilinear elastoplastic constitutive model was used to obtain damage estimates for waste package-to-waste package impacts, waste package-to-pallet impacts (Section 6.3), and waste package-to-drip shield interactions (Section 6.4.5), as well as for analyses of a waste package surrounded by rubble (Section 6.5.1). This material model utilizes a tangent (hardening) modulus, as defined in Figure 4-2, and the material properties are evaluated for 60°C (Assumption 5.7, Section 5). Certain temperature-dependent material properties are not available at elevated temperatures for materials such as Alloy 22, Stainless Steel Type 316, Titanium Grade 7, and Titanium Grade 24 that are used in the EBS components. Therefore, room temperature values for density and Poisson's ratio are used for Alloy 22, Stainless Steel Type 316, Titanium Grade 7, and Titanium Grade 24 (see Assumption 5.5, Section 5). The calculation of the material properties for Alloy 22 and Stainless Steel Type 316 at 60°C is described in Appendix A.

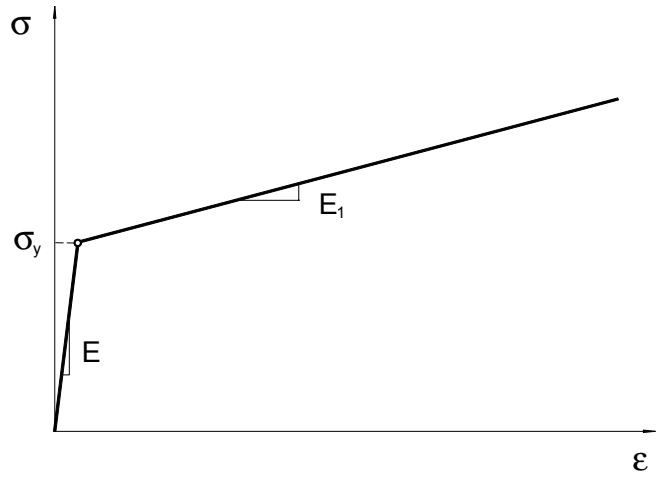

Source: For illustrative purposes only.

NOTE: σ_y = yield strength, E = modulus of elasticity, E_1 = tangent modulus.

Figure 4-2. Bilinear Elastoplastic Constitutive Representation

4.1.2.2 Contact Friction

Contact friction is an essential factor in the transfer of seismic ground motion from the invert to the waste package and thus is important in the analysis of the effect of vibratory ground motion on EBS components (Sections 6.3 through 6.5). The friction coefficients for all contacts are randomly sampled from a uniform distribution between 0.2 and 0.8, as described in Assumption 5.4 (Section 5) and Section 6.3.2.1.3. This is due to the absence of more specific data on the coefficient of contact friction for metal-to-metal and metal-to-rock contacts over the wide range of surface conditions expected over time in the repository. The static and dynamic friction coefficients are defined to be equal (Assumption 5.6, Section 5).

4.1.3 Material Properties for Rock Mass at Emplacement Level

In the analysis of the drip shield failure modes and the waste package surrounded by rubble (Sections 6.4 and 6.5.1), the simulations not only include the motion of the objects inside the emplacement drift, but also the response of the rock mass and the overall stability of the emplacement drift during strong seismic ground motion. The lithophysal rock mass is selected in the analysis since approximately 85% of the emplacement volume is located in the lithophysal rock (BSC 2007 [DIRS 178693], Section 6.1.3). The material model representation of the lithophysal rock mass is described in detail in *Drift Degradation Analysis* (BSC 2004 [DIRS 166107], Section 6.4). The material properties for lithophysal rock mass are provided in Table 4-4 and include the micro-mechanical properties of bonded polygonal blocks and the contacts between the blocks (Sections 6.4 and 6.5).

In the LS-DYNA analyses for waste package-drip shield interaction (Section 6.4.5), the TSw2 rock is used to represent the rigid invert, and the material properties are necessary only for the contact definitions.

4.1.3.1 Material Properties for Caved Lithophysal Rock

An estimate of deformability of the caved rock mass covering the drip shield is required for the analysis of the interaction between the waste package, the drip shield, and the surrounding rock mass. The estimate is based on the numerical simulation of load testing on caved rock with corroborative empirical results (Duncan et al. 1980 [DIRS 161776]; Marachi et al. 1972 [DIRS 157883]).

A typical form of deviatoric (or shear) yield function with three constants, a_0, a_1, and a_2, was used for this estimate. This is expressed in Equation 4-1 as:

$$\phi = J_2 - \left(a_0 + a_1 p + a_2 p^2\right) \quad \text{(Eq. 4-1)}$$

where p is the mean stress or pressure, and J_2 is the second stress invariant defined in terms of principal stresses. The material properties of caved lithophysal rock are provided in Table 4-4.

Table 4-4. Material Properties for Rock Mass

Parameter	Value	Source	Application
Material Properties for Host Rock—Category 1			
Category 1 lithophysal rock mass, unconfined compressive strength	10 MPa	DTN: MO0408MWDDDMIO.002 [DIRS 171483], file Calculation Files\Material property*rock mass strength v2.xls*, Category 1	Appendix C
Category 1 lithophysal rock mass, Young's modulus	1.9 GPa	DTN: MO0408MWDDDMIO.002 [DIRS 171483], file Calculation Files\Material property*rock mass strength v2.xls*, Category 1	Appendix C
Category 1 lithophysal rock mass, bonded joint friction angle	35°	DTN: MO0408MWDDDMIO.002 [DIRS 171483], file UDEC Inputs and Outputs\Lithophysal*properties.fis*, Category 1	Appendix C
Category 1 lithophysal rock mass, bonded joint residual friction angle	15°	DTN: MO0408MWDDDMIO.002 [DIRS 171483], file UDEC Inputs and Outputs\Lithophysal*properties.fis*, Category 1	Appendix C
Category 1 lithophysal rock mass, bonded joint cohesion	3.83 MPa	DTN: MO0408MWDDDMIO.002 [DIRS 171483], file UDEC Inputs and Outputs\Lithophysal*properties.fis*, Category 1	Appendix C
Category 1 lithophysal rock mass, bonded joint tensile strength	1.53 MPa	DTN: MO0408MWDDDMIO.002 [DIRS 171483], file UDEC Inputs and Outputs\Lithophysal*properties.fis*, Category 1	Appendix C
Category 1 lithophysal rock mass, bonded joint normal stiffness	9.34 GPa/m	DTN: MO0408MWDDDMIO.002 [DIRS 171483], file UDEC Inputs and Outputs\Lithophysal*properties.fis*, Category 1	Appendix C

Table 4-4. Material Properties for Rock Mass (Continued)

Parameter	Value	Source	Application
Material Properties for Host Rock—Category 1 (Continued)			
Category 1 lithophysal rock mass, bonded joint shear stiffness	4.67 GPa/m	DTN: MO0408MWDDDMIO.002 [DIRS 171483], file UDEC Inputs and Outputs\Lithophysal*properties.fis*, Category 1	Appendix C
Category 1 lithophysal rock mass, Voronoi block bulk modulus	9.03 GPa	DTN: MO0408MWDDDMIO.002 [DIRS 171483], file UDEC Inputs and Outputs\Lithophysal*properties.fis*, Category 1	Appendix C
Category 1 lithophysal rock mass, Voronoi block shear modulus	6.80 GPa	DTN: MO0408MWDDDMIO.002 [DIRS 171483], file UDEC Inputs and Outputs\Lithophysal*properties.fis*, Category 1	Appendix C
Material Properties for Host Rock—Category 2			
Category 2 lithophysal rock mass, unconfined compressive strength	15 MPa	DTN: MO0408MWDDDMIO.002 [DIRS 171483], file Calculation Files\Material property*rock mass strength v2.xls*, Category 2	Appendix C
Category 2 lithophysal rock mass, Young's modulus	6.4 GPa	DTN: MO0408MWDDDMIO.002 [DIRS 171483], file Calculation Files\Material property*rock mass strength v2.xls*, Category 2	Appendix C
Category 2 lithophysal rock mass, bonded joint friction angle	35°	DTN: MO0408MWDDDMIO.002 [DIRS 171483], file UDEC Inputs and Outputs\Lithophysal*properties.fis*, Category 2	Appendix C
Category 2 lithophysal rock mass, bonded joint residual friction angle	15°	DTN: MO0408MWDDDMIO.002 [DIRS 171483], file UDEC Inputs and Outputs\Lithophysal*properties.fis*, Category 2	Appendix C
Category 2 lithophysal rock mass, bonded joint cohesion	5.85 MPa	DTN: MO0408MWDDDMIO.002 [DIRS 171483], file UDEC Inputs and Outputs\Lithophysal*properties.fis*, Category 2	Appendix C
Category 2 lithophysal rock mass, bonded joint tensile strength	2.34 MPa	DTN: MO0408MWDDDMIO.002 [DIRS 171483], file UDEC Inputs and Outputs\Lithophysal*properties.fis*, Category 2	Appendix C
Category 2 lithophysal rock mass, bonded joint normal stiffness	31.48 GPa/m	DTN: MO0408MWDDDMIO.002 [DIRS 171483], file UDEC Inputs and Outputs\Lithophysal*properties.fis*, Category 2	Appendix C
Category 2 lithophysal rock mass, bonded joint shear stiffness	15.72 GPa/m	DTN: MO0408MWDDDMIO.002 [DIRS 171483], file UDEC Inputs and Outputs\Lithophysal*properties.fis*, Category 2	Appendix C
Category 2 lithophysal rock mass, Voronoi block bulk modulus	30.44 GPa	DTN: MO0408MWDDDMIO.002 [DIRS 171483], file UDEC Inputs and Outputs\Lithophysal*properties.fis*, Category 2	Appendix C

Table 4-4. Material Properties for Rock Mass (Continued)

Parameter	Value	Source	Application
Material Properties for Host Rock—Category 2 (Continued)			
Category 2 lithophysal rock mass, Voronoi block shear modulus	22.88 GPa	DTN: MO0408MWDDDMIO.002 [DIRS 171483], file UDEC Inputs and Outputs\Lithophysal*properties.fis*, Category 2	Appendix C
Material Properties for Host Rock—Category 3			
Category 3 lithophysal rock mass, unconfined compressive strength	20 MPa	DTN: MO0408MWDDDMIO.002 [DIRS 171483], file Calculation Files\Material property*rock mass strength v2.xls*, Category 3	Sections 6.4, 6.5, and Appendix C
Category 3 lithophysal rock mass, Young's modulus	10.8 GPa	DTN: MO0408MWDDDMIO.002 [DIRS 171483], file Calculation Files\Material property*rock mass strength v2.xls*, Category 3	Sections 6.4, 6.5, and Appendix C
Category 3 lithophysal rock mass, bonded joint friction angle	35°	DTN: MO0408MWDDDMIO.002 [DIRS 171483], file UDEC Inputs and Outputs\Lithophysal*properties.fis*, Category 3	Sections 6.4, 6.5, and Appendix C
Category 3 lithophysal rock mass, bonded joint residual friction angle	15°	DTN: MO0408MWDDDMIO.002 [DIRS 171483], file UDEC Inputs and Outputs\Lithophysal*properties.fis*, Category 3	Sections 6.4, 6.5, and Appendix C
Category 3 lithophysal rock mass, bonded joint cohesion	7.94 MPa	DTN: MO0408MWDDDMIO.002 [DIRS 171483], file UDEC Inputs and Outputs\Lithophysal*properties.fis*, Category 3	Sections 6.4, 6.5, and Appendix C
Category 3 lithophysal rock mass, bonded joint tensile strength	3.18 MPa	DTN: MO0408MWDDDMIO.002 [DIRS 171483], file UDEC Inputs and Outputs\Lithophysal*properties.fis*, Category 3	Sections 6.4, 6.5, and Appendix C
Category 3 lithophysal rock mass, bonded joint normal stiffness	53.08 GPa/m	DTN: MO0408MWDDDMIO.002 [DIRS 171483], file UDEC Inputs and Outputs\Lithophysal*properties.fis*, Category 3	Sections 6.4, 6.5, and Appendix C
Category 3 lithophysal rock mass, bonded joint shear stiffness	26.57 GPa/m	DTN: MO0408MWDDDMIO.002 [DIRS 171483], file UDEC Inputs and Outputs\Lithophysal*properties.fis*, Category 3	Sections 6.4, 6.5, and Appendix C
Category 3 lithophysal rock mass, Voronoi block bulk modulus	51.37 GPa	DTN: MO0408MWDDDMIO.002 [DIRS 171483], file UDEC Inputs and Outputs\Lithophysal*properties.fis*, Category 3	Sections 6.4, 6.5, and Appendix C
Category 3 lithophysal rock mass, Voronoi block shear modulus	38.60 GPa	DTN: MO0408MWDDDMIO.002 [DIRS 171483], file UDEC Inputs and Outputs\Lithophysal*properties.fis*, Category 3	Sections 6.4, 6.5, and Appendix C

Table 4-4. Material Properties for Rock Mass (Continued)

Parameter	Value	Source	Application
Material Properties for Host Rock—Category 4			
Category 4 lithophysal rock mass, unconfined compressive strength	25 MPa	DTN: MO0408MWDDDMIO.002 [DIRS 171483], file Calculation Files\Material property*rock mass strength v2.xls*, Category 4	Appendix C
Category 4 lithophysal rock mass, Young's modulus	15.3 GPa	DTN: MO0408MWDDDMIO.002 [DIRS 171483], file Calculation Files\Material property*rock mass strength v2.xls*, Category 4	Appendix C
Category 4 lithophysal rock mass, bonded joint friction angle	35°	DTN: MO0408MWDDDMIO.002 [DIRS 171483], file UDEC Inputs and Outputs\Lithophysal*properties.fis*, Category 4	Appendix C
Category 4 lithophysal rock mass, bonded joint residual friction angle	15°	DTN: MO0408MWDDDMIO.002 [DIRS 171483], file UDEC Inputs and Outputs\Lithophysal*properties.fis*, Category 4	Appendix C
Category 4 lithophysal rock mass, bonded joint cohesion	10.09 MPa	DTN: MO0408MWDDDMIO.002 [DIRS 171483], file UDEC Inputs and Outputs\Lithophysal*properties.fis*, Category 4	Appendix C
Category 4 lithophysal rock mass, bonded joint tensile strength	4.03 MPa	DTN: MO0408MWDDDMIO.002 [DIRS 171483], file UDEC Inputs and Outputs\Lithophysal*properties.fis*, Category 4	Appendix C
Category 4 lithophysal rock mass, bonded joint normal stiffness	74.90 GPa/m	DTN: MO0408MWDDDMIO.002 [DIRS 171483], file UDEC Inputs and Outputs\Lithophysal*properties.fis*, Category 4	Appendix C
Category 4 lithophysal rock mass, bonded joint shear stiffness	37.60 GPa/m	DTN: MO0408MWDDDMIO.002 [DIRS 171483], file UDEC Inputs and Outputs\Lithophysal*properties.fis*, Category 4	Appendix C
Category 4 lithophysal rock mass, Voronoi block bulk modulus	72.80 GPa	DTN: MO0408MWDDDMIO.002 [DIRS 171483], file UDEC Inputs and Outputs\Lithophysal*properties.fis*, Category 4	Appendix C
Category 4 lithophysal rock mass, Voronoi block shear modulus	54.70 GPa	DTN: MO0408MWDDDMIO.002 [DIRS 171483], file UDEC Inputs and Outputs\Lithophysal*properties.fis*, Category 4	Appendix C
Material Properties for Host Rock—Category 5			
Category 5 lithophysal rock mass, unconfined compressive strength	30 MPa	DTN: MO0408MWDDDMIO.002 [DIRS 171483], file Calculation Files\Material property*rock mass strength v2.xls*, Category 5	Appendix C
Category 5 lithophysal rock mass, Young's modulus	19.7 GPa	DTN: MO0408MWDDDMIO.002 [DIRS 171483], file Calculation Files\Material property*rock mass strength v2.xls*, Category 5	Appendix C

Table 4-4. Material Properties for Rock Mass (Continued)

Parameter	Value	Source	Application
Material Properties for Host Rock—Category 5 (Continued)			
Category 5 lithophysal rock mass, bonded joint friction angle	35°	DTN: MO0408MWDDDMIO.002 [DIRS 171483], file UDEC Inputs and Outputs\Lithophysal*properties.fis*, Category 5	Appendix C
Category 5 lithophysal rock mass, bonded joint residual friction angle	15°	DTN: MO0408MWDDDMIO.002 [DIRS 171483], file UDEC Inputs and Outputs\Lithophysal*properties.fis*, Category 5	Appendix C
Category 5 lithophysal rock mass, bonded joint cohesion	12.30 MPa	DTN: MO0408MWDDDMIO.002 [DIRS 171483], file UDEC Inputs and Outputs\Lithophysal*properties.fis*, Category 5	Appendix C
Category 5 lithophysal rock mass, bonded joint tensile strength	4.92 MPa	DTN: MO0408MWDDDMIO.002 [DIRS 171483], file UDEC Inputs and Outputs\Lithophysal*properties.fis*, Category 5	Appendix C
Category 5 lithophysal rock mass, bonded joint normal stiffness	97.00 GPa/m	DTN: MO0408MWDDDMIO.002 [DIRS 171483], file UDEC Inputs and Outputs\Lithophysal*properties.fis*, Category 5	Appendix C
Category 5 lithophysal rock mass, bonded joint shear stiffness	48.40 GPa/m	DTN: MO0408MWDDDMIO.002 [DIRS 171483], file UDEC Inputs and Outputs\Lithophysal*properties.fis*, Category 5	Appendix C
Category 5 lithophysal rock mass, Voronoi block bulk modulus	93.60 GPa	DTN: MO0408MWDDDMIO.002 [DIRS 171483], file UDEC Inputs and Outputs\Lithophysal*properties.fis*, Category 5	Appendix C
Category 5 lithophysal rock mass, Voronoi block shear modulus	70.50 GPa	DTN: MO0408MWDDDMIO.002 [DIRS 171483], file UDEC Inputs and Outputs\Lithophysal*properties.fis*, Category 5	Appendix C
TSw2 Unit Material Properties			
Nonlithophysal rock mass, density	2,410 kg/m^3	BSC 2004 [DIRS 166107] Appendix E, Section E1 and Table E-2	Section 6.4
TSw2 unit, Poisson's ratio	0.19	BSC 2007 [DIRS 178693], Table 6-19, Tptpmn lithostratigraphic zone, mean value	Section 6.4
TSw2 unit, modulus of elasticity	33 GPa	BSC 2007 [DIRS 178693], Table 6-15, Tptpmn lithostratigraphic zone, mean value	Section 6.4
TSw2 unit, compressive strength	290 MPa	BSC 2007 [DIRS 178693], Table 6-9, Tptpmn lithostratigraphic zone, maximum value	Section 6.4

Table 4-4. Material Properties for Rock Mass (Continued)

Parameter	Value	Source	Application
Material Properties for Caved Lithophysal Rock			
Block size	0.2 m	BSC 2004 [DIRS 166107], Section 6.4.1.1, and DTN: MO0408MWDDDMIO.002 [DIRS 171483], file: *nonlith rockfall characteristics in emplacement drifts with 1e-4gm.xls*	Section 6.4.3.2, Table 4-9
Bulk modulus	335 MPa	BSC 2005 [DIRS 173172], Attachment IX, p. IX-15; DTN: MO0508SPAMECHA.000 [DIRS 181067], *AttachmentIX.zip*, file *uni window1.xls*, sheet "summary"	Sections 6.4, 6.5
Shear modulus	201 MPa	BSC 2005 [DIRS 173172], Attachment IX, p. IX-15; DTN: MO0508SPAMECHA.000 [DIRS 181067], *AttachmentIX.zip*, file *uni window1.xls*, sheet "summary"	Sections 6.4, 6.5
Yield function constant a_0	0	BSC 2005 [DIRS 173172], Attachment IX, p. IX-14; DTN: MO0508SPAMECHA.000 [DIRS 181067], *AttachmentIX.zip*, file *uni window1.xls*, sheet "readme"	Sections 6.4, 6.5
Yield function constant a_1	0	BSC 2005 [DIRS 173172], Attachment IX, p. IX-14; DTN: MO0508SPAMECHA.000 [DIRS 181067], *AttachmentIX.zip*, file *uni window1.xls*, sheet "readme"	Sections 6.4, 6.5
Yield function constant a_2	0.305	BSC 2005 [DIRS 173172], Attachment IX, pp. IX-14, IX-15, Table IX-2; DTN: MO0508SPAMECHA.000 [DIRS 181067], *AttachmentIX.zip*, file *uni window1.xls*, sheet "summary"	Sections 6.4, 6.5

NOTES: The above properties for Category 1 to Category 5 host rock can also be found in BSC 2004 [DIRS 166107], Tables 6-41 and 6-43.

The average dry density of Tptpln rock mass is 2,211 kg/m^3 (BSC 2004 [DIRS 166107], Table E-1; DTN: MO0408MWDDDMIO.002 [DIRS 171483], *Calculation Files\Material property\thermal properties TM units v2.xls*, worksheet "Conductivity and Density"). The average saturated density for the same unit is 2,411 kg/m^3 (BSC 2004 [DIRS 166107], Table E-2). The saturated density is approximately 10% greater than the dry density. Because the average dry density of the lithophysal units (both Tptpul and Tptpll) ranges from 1,834 to 1,979 kg/m^3 (BSC 2004 [DIRS 166107], Table E-1; DTN: MO0408MWDDDMIO.002 [DIRS 171483], *Calculation Files\Material property\thermal properties TM units v2.xls*, worksheet "Conductivity and Density") the average saturated density of lithophysal units is taken to be 2,140 kg/m^3.

4.1.4 Seismic Ground Motions

The development of the ground motion time histories is based on the results of a probabilistic seismic hazard analysis and a Yucca Mountain site response model as described in *Development of Earthquake Ground Motion Input for Preclosure Seismic Design and Postclosure Performance Assessment of a Geologic Repository at Yucca Mountain, NV* (BSC 2004 [DIRS 170027], Section 6.3.2). The number of ground motion time histories (17) for postclosure

performance assessment is obtained from the documents listed by data tracking numbers (DTNs) in Table 4-5. In these documents, 17 sets of three-component time histories were developed for each annual probability of exceedance considered for postclosure analyses. The selected time histories were based on strong motion records chosen to represent the range of earthquake magnitudes and distances indicated by the PGV hazard analysis (BSC 2004 [DIRS 170027], Section 6.3.1.4). As explained in that document, 15 sets of input ground motions are recommended by NUREG/CR-6728 (McGuire et al. 2001 [DIRS 157510], p. 3-3) when using a suite of time histories to perform a soil-structure interaction analysis that is consistent with a probabilistically defined seismic hazard. Two extra sets were developed to allow for substitutions if necessary. For the analyses, the full suite of 17 three-component ground motions is retained to provide the broadest range of variability in the kinematic response. The PGV levels shown in Table 4-5 are for the H1 component of the time histories; maximum PGV levels for other components may be higher.

Table 4-5. Source Information for Seismic Time Histories

Seismic Time Histories	Description	Source	Application
PGV 1.05 m/s level (1×10^{-5} per year)	All ASCII files contained in *Time Histories-Acceleration.zip*	DTN: MO0610AVDTM105.002 [DIRS 178664]	Sections 6.3, 6.4, 6.5
PGV 2.44 m/s level (1×10^{-6} per year)	All ASCII files contained in *ats.zip*	DTN: MO0403AVDSC106.001 [DIRS 168891]	Sections 6.3, 6.4, 6.5
PGV 5.35 m/s level (1×10^{-7} per year)	All ASCII files contained in *ats.zip*	DTN: MO0403AVTMH107.003 [DIRS 168892]	Sections 6.3, 6.4, 6.5

4.1.5 Input Parameters Used in Numerical Representation

The development of the numerical representation for the analysis was completed based on preliminary design concepts for the EBS components (see Assumption 5.23). These values are compared to the design values in Table 4-6, Table 4-7, and Table 4-8. Impact assessments are provided in Table 4-6. Table 4-7 and Table 4-8 provide supporting comparisons of design values with simulation values for the TAD-bearing and codisposal waste packages, respectively.

Table 4-6. Parameter Values Used in Numerical Simulations Compared with Design Values

Input Parameter	Design Value[a]	Value Used in Simulations[b]	Impact Assessment
Drift			
The height of invert	52 in (1,320 mm)	34 in (860 mm)	Analysis for amplification of seismic waves passing through the invert shows that the invert height has a minor effect (BSC 2005 [DIRS 173172], Section 5.8). Thus, a taller invert is not expected to result in a significant change.

Table 4-6. Parameter Values Used in Numerical Simulations Compared with Design Values (Continued)

Input Parameter	Design Value[a]	Value Used in Simulations[b]	Impact Assessment
Drift (Continued)			
TSw2 unit, Poisson's ratio	0.19	0.21	The value used in the simulations is well within one standard deviation of the mean value. Furthermore, this difference of 9.5% is not significant because a change of this magnitude in Poisson's ratio does not have a significant effect on the structural behavior.
Waste Package			
TAD-bearing waste package dimensions	See Table 4-7	See Table 4-7	Minor differences in dimensions and removal of the middle lid do not affect numerical simulations significantly. The removed middle lid has little significance because of its very small mass relative to the entire waste package and its close proximity to the outer lid. The additional gap between the outer lid and the inner vessel has little significance because it is small relative to the overall length and diameter of the components, and friction between the outer shell and the inner vessel are also important in limiting sliding.
Codisposal waste package dimensions	See Table 4-8	See Table 4-8	Minor differences in dimensions do not affect numerical simulations significantly.
Nominal loaded weight for TAD-bearing waste package	162,055 lbs (73.5 mT)	163,000 lbs (73.9 mT)	The 0.5% difference has an insignificant impact on the numerical simulations.
Nominal loaded weight for codisposal waste package. Upper weight (53.1 mT) was used for 11-waste package kinematic analyses; lower weight (59.7 mT) was used for the 13-waste package kinematic analyses and detailed impact analyses	127,870 lbs (58 mT)	117,000 lbs (53.1 mT)	The weight in the simulations is 9.2% lower than the design value. In these analyses, the focus was on the TAD-bearing waste packages, so the difference does not affect the numerical simulations significantly.
		131,600 lbs (59.7 mT)	The weight in the simulations is 2.8% higher than the design value. This small difference does not affect the numerical simulations significantly.

Table 4-6. Parameter Values Used in Numerical Simulations Compared with Design Values (Continued)

Input Parameter	Design Value[a]	Value Used in Simulations[b]	Impact Assessment
Drip Shield (Titanium Grade 29 = Design Value, Titanium Grade 24 = Value Used in Simulations)			
Yield strength	759 MPa (minimum value at room temperature)	862 MPa (typical value at 60°C) 683 MPa (typical value at 150°C)[c]	60°C—While a typical value was used in the simulations, the minimum value for Titanium Grade 24 is 828 MPa (at room temperature). This is 8.3% larger than the minimum room temperature value for Titanium Grade 29. See text in Section 4.1.5 for impact assessment. The value at 150°C was used in evaluation of uneven settlement of the invert (Section 6.4.6) and the difference in yield strength does not have a significant effect.
Ultimate strength	828 MPa (minimum value at room temperature)	951 MPa (typical value at 60°C)	While a typical value was used in the simulations, the minimum value for Titanium Grade 24 is 895 MPa (at room temperature). This is 7.5% larger than the minimum room temperature value for Titanium Grade 29. See text in Section 4.1.5 for impact assessment.
Poisson's ratio (at room temperature)	0.31	0.34	This difference of 8.8% is not significant because a change of this magnitude in Poisson's ratio does not have a significant effect on the structural behavior.
Modulus of elasticity	107-122 GPa (at 20°C) 95-111 GPa (at 230°C)	112 GPa (at 60°C) 108 GPa (at 150°C)[c]	The values used are consistent with the design range.

Sources: [a] Tables 4-1, 4-2, 4-3, and 4-4.
[b] See Assumption 5.23, Section 5.
[c] From BSC 2005 [DIRS 174715], Table 5.2-1.

Table 4-7. TAD-Bearing Waste Package Parameter Comparison

Parameter	Design Values[a]	Values Used in Simulations[c]
Outer Corrosion Barrier		
Length (less lid-lifting feature)	229.07 in	229.312 in
Lid-lifting feature	1.25 in	1.0 in
Overall length	230.32 in	230.312 in
Outer shell diameter/thickness	74.08 in/1.0 in	74.075 in/1.0 in
Upper sleeve	77.28 in (outer diameter) 12 in long	77.275 in (outer diameter) 12 in long
Lower sleeve	77.28 in (outer diameter) 12 in long with 4-in overhang	77.275 in (outer diameter) 12 in long with 4-in overhang

Table 4-7. TAD-Bearing Waste Package Parameter Comparison (Continued)

Parameter	Design Values[a]	Values Used in Simulations[c]
Outer Corrosion Barrier (Continued)		
Middle lid thickness	N/A	0.5 in
Gap between outer and middle lids	N/A	1.1875 in
Middle lid weight	N/A	649 lbs
Nominal Alloy 22 weight	21,878 lbs	21,750 lbs
Inner Vessel		
Inner vessel length (less lid-lifting feature)	218.50 in	217.94 in (used in Section 6.5.2)
Inner vessel diameter/thickness	71.70 in/2.0 in	71.70 in/2.0 in
Outer Corrosion Barrier and Inner Vessel		
Unloaded weight	53,555 lbs	53,700 lbs
TAD Canister		
Canister length	212 in (+0.0 in/−0.5 in)	212 in (+0.0 in/−0.5 in) 212.94 in (used in Section 6.5.2)
Canister outer diameter	66.5 in (+0.0 in/−0.5 in)	66.5 in (+0.0 in/−0.5 in)
Canister thickness	1.0 in	1.0 in
Canister shield plug thickness	15.0 in[b]	15.0 in
Canister bottom lid thickness	3.5 in[b]	3.5 in
Canister basket weight	35,000 lbs (approximate 4,500-lb increase due to neutron absorber on all four sides of a fuel assembly)	30,571 lbs
Canister loaded weight	108,500 lbs	109,000 lbs

Sources: [a] SNL 2007 [DIRS 179394], Table 4-3.
[b] SNL 2007 [DIRS 179394], Table A-3.
[c] See Assumption 5.23, Section 5.

Table 4-8. Codisposal Waste Package Parameter Comparison

Parameter	Design Values[a]	Values Used in Simulations[b]	Values Used in Simulations[c]
Outer Corrosion Barrier			
Length (less lid-lifting feature)	207.57 in	198.19 in	207.57 in
Lid-lifting feature	1.25 in	1.00 in	1.25 in
Overall length	208.82 in	199.19 in	208.82 in
Outer shell diameter/ thickness	80.50 in/1.0 in	80.50 in/1.0 in	80.50 in/1.0 in
Upper sleeve	83.70 in (outer diameter) 12 in long	83.70 in (outer diameter) 12 in long	83.70 in (outer diameter) 12 in long
Lower sleeve	83.70 in (outer diameter) 12 in long with 4-in overhang	83.70 in (outer diameter) 12 in long with 4-in overhang	83.70 in (outer diameter) 12 in long with 4-in overhang

Table 4-8. Codisposal Waste Package Parameter Comparison (Continued)

Parameter	Design Values[a]	Values Used in Simulations[b]	Values Used in Simulations[c]
Inner Vessel			
Inner vessel length (less lid-lifting feature)	194.38 in	187.39 in	194.57 in
Inner vessel diameter/thickness	78.13 in/2.00 in	78.13 in/2.00 in	78.13 in/2.00 in
Outer Corrosion Barrier and Inner Vessel			
Unloaded weight	75,570 lbs	65,500 lbs	75,500 lbs

Sources: [a] SNL 2007 [DIRS 179567], Table 4-9.
[b] 11-waste package kinematic analyses: see Assumption 5.23, Section 5.
[c] 13-waste package kinematic analyses and detailed impact analyses: see Assumption 5.23, Section 5.

The impact assessment for the differences in yield and ultimate strengths between Titanium Grade 29 and Titanium Grade 24 (as shown in Table 4-6) is provided below:

> Calculations for drip shield fragility were done using material properties for Titanium Grade 24 to characterize the drip shield frame-work, but subsequent to these calculations being performed, the structural material comprising the drip shield frame-work was changed to Titanium Grade 29. The mechanical strength properties for Titanium Grade 24 are less than 10% higher than those of Titanium Grade 29; thus estimates of the rubble load-bearing capacity of the drip shields would be overestimated with respect to this single input to the calculations. But uncertainties in several other inputs to this estimate of load-bearing capacity, and the prediction of whether or not the drip shield will collapse are sufficiently large to essentially subsume this overestimate of material strength input, as explained below.
>
> A prediction of the limit load of the drip shield frame can be evaluated as a function of two primary inputs: (1) the physical size of the structural member of the drip shield (which is a function of how much corrosion has been assumed to occur at the time represented by the calculation), and (2) the mechanical strength of the frame members.
>
> The limit load for the drip shield is not only a function of the magnitude of the load—it is also a function of its distribution. The limit load at which the framework fails was determined using the load distributions based on two load distributions to capture uncertainty in this input as discussed in Section 6.4.3.2. These were (a) rock-load realization 3, which was selected as the most severe load realization among the six generated cases in the previous study, and (b) an average of the six loads used in the previous study. A comparison of the magnitude difference in these two loading schemes is provided in Table 4-9. The result of this load difference is evaluated in Section 6.4.3.2.3 and can be seen in Figure 6-57.

Table 4-9. Average Pressure Values on the Drip Shield for Quasi-Static Drift Degradation (Rock Block Size 0.2 m)

Realization	Pressure (kPa)		
	Left Leg	Top (Crown)	Right Leg
1	41.54	108.91	58.76
2	19.15	147.07	19.33
3	31.35	154.81	6.69
4	57.23	129.75	128.81
5	69.69	112.73	105.43
6	32.97	113.87	52.19
Average	41.99	127.86	61.87

Source: DTN: MO0407MWDDSLCR.000 [DIRS 170873], file *final drip shield quasi-static pressure.xls*.

NOTE: The source DTN provides pressures only for the average of the loading realizations. The other averages are calculated from the segment pressures provided in the DTN.

The physical size of the structural member is assumed to be a function of the corrosion rate of Titanium Grade 29 and time. The corrosion rate for Titanium Grade 29 is calculated as a multiplier on the corrosion rate of Titanium Grade 7 as discussed in DTN: SN0704PADSGCMT.002 [DIRS 182188], *Ti29Multiplier.xls*. The multiplier ranges between 1 and more than 6.6 times; thus the uncertainty of the size reduction from initial conditions of the Titanium Grade 29 structural supports in the drip shield is significant.

In combination, the loading uncertainties on the drip shield and the corrosion rate of Titanium Grade 29 are sufficiently broad to encompass the less-than-10% overestimate of strength in the drip shield structural supports. The calculations for drip shield fragility due to failure of the drip shield frame discussed in Section 6.4 reasonably estimate the expected behavior of drip shield collapse.

The above impact assessments also account for any cumulative effect of using the above values in the analyses presented in this report.

4.1.6 In-Situ State of Stress in Rock Mass

The vertical component of in situ stress is approximated as 7 MPa considering an overburden depth of 300 m (BSC 2003 [DIRS 166183], Section 4.2.1) and an overburden density of 2.41 g/cm^3 (BSC 2004 [DIRS 166107], Section 4.1.3) (i.e., vertical stress = 300 m × 9.81 m/sec^2 × 2.41 g/cm^3 ≈ 7 MPa). The horizontal components of in situ stress (the minor and intermediate principal stresses) are estimated to be 3.5 MPa based on an average horizontal-to-vertical stress ratio of 0.5 (i.e., the average of 0.617 and 0.361 as described in Section 6.3.1.1 of *Drift Degradation Analysis* (BSC 2004 [DIRS 166107])).

4.1.7 Established Fact References

The following references used in this report are classified as "Established Fact" in the DIRS:

AISC (American Institute of Steel Construction) 1995. *Manual of Steel Construction, Allowable Stress Design.* 9th Edition, 2nd Revision. Chicago, Illinois: American Institute of Steel Construction [DIRS 114107] is considered established fact because it is a professional society/industry code, criteria, and/or standard.

ASM (American Society for Metals) 1980. *Properties and Selection: Stainless Steels, Tool Materials and Special-Purpose Metals.* Volume 3 of *Metals Handbook.* 9th Edition. Benjamin, D., ed. Metals Park, Ohio: American Society for Metals [DIRS 104317] is considered established fact because it is a professional society/industry code, criteria, and/or standard.

ASM International 1990. *Properties and Selection: Nonferrous Alloys and Special-Purpose Materials.* Volume 2 of *ASM Handbook.* Formerly Tenth Edition, Metals Handbook. 5th Printing 1998. Materials Park, Ohio: ASM International [DIRS 141615] is considered established fact because it is a professional society/industry code, criteria, and/or standard.

ASME (American Society of Mechanical Engineers) 2005. "Materials." Section II of *2004 ASME Boiler and Pressure Vessel Code (includes 2005 Addenda).* New York, New York: American Society of Mechanical Engineers [DIRS 176967] is considered established fact because it is a professional society/industry code, criteria, and/or standard.

ASTM B 265-02 2002. *Standard Specification for Titanium and Titanium Alloy Strip, Sheet, and Plate.* West Conshohocken, Pennsylvania: American Society for Testing and Materials [DIRS 162726] is considered established fact because it is a professional society/industry code, criteria, and/or standard.

ASTM G 1-90 (Reapproved 1999) 1999. *Standard Practice for Preparing, Cleaning, and Evaluating Corrosion Test Specimens.* West Conshohocken, Pennsylvania: American Society for Testing and Materials [DIRS 103515] is considered established fact because it is a professional society/industry code, criteria, and/or standard.

TIMET 2000. "Timetal 6-4, 6-4 ELI, 6-4-.1Ru Medium to High Strength General-Purpose Alloys." Denver, Colorado: Titanium Metals Corporation [DIRS 160688] is considered established fact because it is a professional society/industry code, criteria, and/or standard.

4.2 CRITERIA

Section 2.2.1.3.2.3, Mechanical Disruption of Engineered Barriers, from *Yucca Mountain Review Plan, Final Report* (NRC 2003 [DIRS 163274]), provides guidance regarding the acceptance criteria that may be used by the NRC staff to determine whether the technical requirements have been met by the mechanical assessment analyses for the seismic scenario. Section 2.2.1.3.2.3

lists five general acceptance criteria; acceptance criteria 1 through 4 are listed below, along with the subcriteria specifically addressed by this report. Acceptance criterion 5 is not listed, since it is not applicable to this report. Section 8.3 provides a detailed discussion of how the results presented in this report address the applicable acceptance criteria presented below.

Acceptance Criterion 1: System Description and Model Integration Are Adequate.

(1) Total system performance assessment adequately incorporates important design features, physical phenomena, and couplings, and uses consistent and appropriate assumptions throughout the mechanical disruption of engineered barrier abstraction process.

(2) The description of geological and engineering aspects of design features, physical phenomena, and couplings that may affect mechanical disruption of engineered barriers is adequate. For example, the description may include materials used in the construction of engineered barrier components, environmental effects (e.g., temperature, water chemistry, humidity, radiation, etc.) on these materials, and mechanical-failure processes and concomitant failure criteria used to assess the performance capabilities of these materials. Conditions and assumptions in the abstraction of mechanical disruption of engineered barriers are readily identified and consistent with the body of data presented in the description.

(4) Boundary and initial conditions used in the total system performance assessment abstraction of mechanical disruption of engineered barriers are propagated throughout its abstraction approaches.

Several subcriteria are beyond the scope of this report. Subcriterion (3) is not discussed here, as it relates directly to the abstraction of the results in this report. Subcriterion (5) is not discussed because it relates to FEPs analyses. Subcriterion (6) is not discussed because it is related to transient criticality. Subcriterion (7) is not discussed here because no activities related to peer review or qualification of existing data are discussed in this report.

Acceptance Criterion 2: Data Are Sufficient for Model Justification.

(1) Geological and engineering values, used in the license application to evaluate mechanical disruption of engineered barriers, are adequately justified. Adequate descriptions of how the data were used, interpreted, and appropriately synthesized into the parameters are provided.

(3) Data on geology of the natural system, engineering materials, and initial manufacturing defects, used in the total system performance assessment abstraction, are based on appropriate techniques. These techniques may include laboratory experiments, site-specific field measurements, natural analog research, and process-level modeling studies. As appropriate, sensitivity or uncertainty analyses used to support the U.S. Department of Energy total system performance assessment abstraction are adequate to determine the possible need for additional data.

(4) Engineered barrier mechanical failure models for disruptive events are adequate. For example, these models may consider effects of prolonged exposure to the expected emplacement drift environment, material test results not specifically designed or performed for the Yucca Mountain site, and engineered barrier component fabrication flaws.

Subcriterion (2) is not discussed here because data collection activities related to the geology of the natural system engineering materials and initial manufacturing defects are beyond the scope of this report.

Acceptance Criterion 3: Data Uncertainty Is Characterized and Propagated Through the Model Abstraction.

(1) Models use parameter values, assumed ranges, probability distributions, and bounding assumptions that are technically defensible, reasonably account for uncertainties and variabilities, and do not result in an under-representation of the risk estimate.

(2) Process-level models used to represent mechanically disruptive events, within the emplacement drifts at the proposed Yucca Mountain repository, are adequate. Parameter values are adequately constrained by Yucca Mountain site data, such that the effects of mechanically disruptive events on engineered barrier integrity are not underestimated. Parameters within conceptual models for mechanically disruptive events are consistent with the range of characteristics observed at Yucca Mountain.

(3) Uncertainty is adequately represented in parameter development for conceptual models, process-level models, and alternative conceptual models considered in developing the assessment abstraction of mechanical disruption of engineered barriers. This may be done either through sensitivity analyses or use of conservative limits.

Subcriterion (4) is not discussed here because an expert elicitation was not performed during the development of the seismic damage abstractions.

Acceptance Criterion 4: Model Uncertainty Is Characterized and Propagated Through the Model Abstraction.

(2) Consideration of conceptual model uncertainty is consistent with available site characterization data, laboratory experiments, field measurements, natural analog information and process-level modeling studies; and the treatment of conceptual model uncertainty does not result in an under-representation of the risk estimate.

(3) Appropriate alternative modeling approaches are investigated that are consistent with available data and current scientific knowledge, and appropriately consider their results and limitations using tests and analyses that are sensitive to the processes modeled.

Subcriterion (1) is not discussed here because alternate modeling approaches for FEPs are beyond the scope of this report.

Acceptance Criterion 5: Model Abstraction Output is Supported by Objective Comparisons.

(3) Well-documented procedures, that have been accepted by the scientific community to construct and test the mathematical and numerical models, are used to simulate mechanical disruption of engineered barriers.

Subcriteria (1), (2), and (4) are not discussed here because they pertain to the model abstractions for seismic damage. These abstractions are presented in *Seismic Consequence Abstraction* (SNL 2007 [DIRS 176828]).

4.3 CODES, STANDARDS, AND REGULATIONS

No engineering codes or engineering standards are applicable to the simulation of damage to EBS components due to seismic ground motion. The regulation that is applicable to these simulations is 10 CFR Part 63, Energy: Disposal of High-Level Radioactive Wastes in a Geologic Repository at Yucca Mountain, Nevada [DIRS 180319], specifically 10 CFR 63.114, Requirements for Performance Assessment, which requires providing the technical basis for the data, models, parameter uncertainties, and alternative conceptual models that are included in TSPA, and 10 CFR 63.115, Requirements for Multiple Barriers, which requires providing the technical basis for the barriers that are important to waste isolation.

INTENTIONALLY LEFT BLANK

5. ASSUMPTIONS

This section includes a description of the assumptions used, in the absence of direct confirming data or evidence, to perform the model activity. As necessary, other model assumptions are provided throughout Section 6 of this report. The assumptions listed below do not require verification, and there are no assumptions that require verification for this document.

5.1 REPRESENTATION OF DRIP SHIELD

Assumption: The drip shield is represented by a boundary above the waste package that moves synchronously with the free field for the kinematic analyses and waste package-drip shield interaction analysis.

Rationale: Justification for this assumption is found in two documents: *Drift Degradation Analysis* (BSC 2004 [DIRS 166107]) and *Mechanical Assessment of the Drip Shield Subject to Vibratory Motion and Dynamic and Static Rock Loading* (BSC 2004 [DIRS 169753], Section 5.4). *Drift Degradation Analysis* (BSC 2004 [DIRS 166107], Sections 6.3 and 6.4) shows that, for ground motions with annual exceedance frequencies of 10^{-6} (2.44 m/s PGV) and 10^{-7} (5.35 m/s PGV), emplacement drifts are expected to undergo substantial rockfall in the nonlithophysal rock and complete collapse in the lithophysal rock within seconds of the arrival of an incoming earthquake wave and prior to substantial movement of the waste package and emplacement pallet. The rockfall pins the drip shield in place via both the frictional resistance of the rubble against the drip shield outer surface (which develops forces that oppose the ground motion) and the weight of the rubble bearing on the drip shield. This is confirmed by the cross-drift analysis results reported in *Mechanical Assessment of the Drip Shield Subject to Vibratory Motion and Dynamic and Static Rock Loading* (BSC 2004 [DIRS 169753], Section 5.4). These forces result in synchronous motion of the drip shield and invert with the surrounding rock mass free field (BSC 2004 [DIRS 169753], Section 5.3.3.1).

Where Used: Sections 6.3, 6.4.5.

5.2 REPRESENTATION OF INVERT

Assumption: The invert is assumed to be rigid and to move synchronously with the free field. The carbon steel structural elements in the invert are not modeled for the postclosure analyses.

Rationale: It has been demonstrated that amplification of the seismic waves as they pass through the crushed rock in the invert of the drift is negligible (BSC 2005 [DIRS 173172], Section 5.8). The results presented in Section 5.8 and Attachment VIII of *Mechanical Assessment of the Waste Package Subject to Vibratory Ground Motion* (BSC 2005 [DIRS 173172]) show that the resultant impacts from the rigid invert are higher than those for the deformable invert. In addition, analyses with the invert represented by discontinuum blocks show that the invert does not lose integrity with the EBS components at the end of the simulation (BSC 2005 [DIRS 173172], Section 5.8 and Attachment VIII). The structural elements in the invert are assumed to be completely degraded, because carbon steel is not corrosion resistant. Thus, the invert steel will corrode very early in the postclosure period.

Where Used: Sections 6.3, 6.4.5, 6.4.7.

5.3 USE OF APPROXIMATE REPRESENTATIONS

Assumption: The waste packages, drip shield, emplacement pallets, invert, and drift are approximate representations with appropriate dimensions and mass in the finite element or distinct element representations. While the finite element representations for the detailed impact calculations model the multiple components of the waste package, the kinematic representations characterize the waste package as a hollow cylinder with end caps.

Rationale: Simplification of the geometry and material property representations is used in the numerical analyses to account for the important features and overall configuration of the problem. Detailed geometry in areas not directly relevant to the problem is simplified for numerical efficiency. This is consistent with engineering practice for numerical analysis. Modeling the waste package as a single hollow cylinder in the kinematic analyses has an insignificant effect on the overall kinematic behavior of the system, because friction and the relatively small gaps between the components of the waste package would limit the impact that differential movements of the components can have on the motion. Furthermore, any effect would be expected to decrease the overall energy in the system, because multiple components in the waste package representation moving independently would tend to interfere and dissipate energy. The effects of multiple components of the waste package are accounted for when determining damaged area and the potential for rupture of a waste package through the detailed impact calculations.

Where Used: Sections 6.3, 6.4, 6.5.

5.4 FRICTION COEFFICIENTS

Assumption: The friction coefficients for the metal-to-metal and metal-to-rock contacts are considered random parameters with a uniform distribution in the kinematic analyses. The range of values for both of these friction coefficients is 0.2 to 0.8. A friction coefficient of 0.4 is assumed for the calculations of damage to the drip shield due to large-block impacts.

Rationale: Coefficients of static and dynamic friction for various metals and other materials are provided in various handbooks (e.g., Avallone and Baumeister 1987 [DIRS 103508], Table 3.2.1, p. 3-26). However, the coefficients of friction for the specific materials in this analysis are not defined in this handbook. In addition, the potential for long-term corrosion to modify the dynamic friction should also be considered in defining the friction coefficient. In this situation, the appropriate coefficients of friction for the repository components are expected to have high uncertainty and high spatial variability due to variations in long-term corrosion and surface conditions for the waste packages.

It is thus appropriate to pick a distribution of friction coefficients that encompasses a range of materials and mechanical responses, from little or no sliding to substantial sliding between components. It is also appropriate to represent the potential spatial variability between individual waste packages by multiple sampling of the friction coefficient distribution. A distribution of friction coefficients has been prepared, ranging between 0.2 and 0.8 to achieve these goals (BSC 2005 [DIRS 173172], Attachment X; DTN: MO0508SPAMECHA.000 [DIRS 181067], *AttachmentX.zip*, files *All_3_Sampling_Groups.txt* and *Definition of Stochastic*

Parameters.doc). Moreover, this distribution is broad enough to encompass typical values of the dry dynamic friction coefficients for a wide variety of metals and other materials (Avallone and Baumeister 1987 [DIRS 103508], Table 3.2.1, p. 3-26). The appropriateness of this range is independently confirmed by seismic analyses for spent fuel storage racks (DeGrassi 1992 [DIRS 161539]). This distribution is also broad enough to represent a range of mechanical responses for the waste package, emplacement pallet, and drip shield. A friction coefficient near 0.2 maximizes sliding of the waste package on the emplacement pallet, sliding of the emplacement pallet on the invert, and sliding of the drip shield on the invert. Similarly, a friction coefficient near 0.8 minimizes sliding among the various components.

Where Used: Sections 6.3, 6.4, 6.5.

5.5 ROOM TEMPERATURE DENSITY VALUES AND POISSON'S RATIO

Assumption: Room temperature values for density and Poisson's ratio are assumed for Titanium Grade 7 (SB-265 R52400), Titanium Grade 24 (SB-265 R56405), Stainless Steel Type 316, and Alloy 22. Titanium Grade 24 has the same mechanical properties as Titanium Grade 5.

Rationale: The rationale for assuming the room temperature values is that the material properties in question do not have a significant impact on the results of this analysis. The impact of using room temperature values for density and Poisson's ratio is anticipated to be negligible. Mechanical properties of Titanium Grade 24 are currently unavailable, and since the compositions of Titanium Grades 5 and 24 are almost identical (ASME 2001 [DIRS 158115], Section II, Part B, SB-265, Table 2) it is assumed that Titanium Grade 24 has the same mechanical properties as Titanium Grade 5.

Where Used: Sections 6.3, 6.4, 6.5.

5.6 STATIC AND DYNAMIC FRICTION COEFFICIENTS

Assumption: The dynamic friction coefficient and static friction coefficient are assumed to be equal. The effect of relative velocity of the surfaces in contact is not considered in the analyses.

Rationale: Assumption 5.4 (above) explains the range of friction coefficients used in the analyses. Once a value is assigned for the dynamic friction coefficient, then using the identical value for the static friction coefficient maximizes the relative motion of the system components.

Where Used: Sections 6.3, 6.4, 6.5.

5.7 TEMPERATURE OF 60°C FOR EVALUATION OF MATERIAL PROPERTIES

Assumption: A temperature of 60°C is appropriate and reasonable for evaluation of material properties of EBS components during the entire post-closure period.

Rationale: The temperature in the drift drops below 60°C in the first 10,000 years after repository closure (Figure 1-3). Thus, the repository is at temperatures above 60°C for only the first 1% of the evaluated time frame of the repository. The relevant material properties, in

general, show lower strength at elevated temperatures than at room temperature conditions, so 60°C is an upper bound on temperature for most of the repository life. Furthermore, sensitivity analyses with material properties at elevated temperatures (Section 6.3.2.2.2) demonstrate that damaged area of the OCB is relatively insensitive to elevated temperature. Thus, 60°C is a reasonable temperature for determining material properties for the entire life of the repository.

Where Used: Sections 6.3, 6.4, 6.5, 8.2, 8.3.

5.8 REPRESENTATION OF EMPLACEMENT PALLET CONNECTING BEAMS

Assumption: Emplacement pallets in the LS-DYNA kinematic analyses for multiple waste packages are represented using beam elements connecting the two support structures. The beam elements are not permitted to interact with the waste packages (i.e., no contact is defined).

Rationale: The focus of the kinematic analyses is on waste package-to-waste package and waste package-to-emplacement pallet structure interactions, and any potential interaction between waste packages and the emplacement pallet beam connectors is of secondary importance.

Where Used: Sections 6.3, 6.4.5.

5.9 USE OF ELASTIC PROPERTIES

Assumption: The waste packages and emplacement pallets are characterized with elastic properties in the LS-DYNA kinematic analysis for multiple waste packages. The elastic properties are assumed to be isotropic and homogeneous.

Rationale: The use of elastic properties allows the kinematic analysis to be conservative and computationally efficient. Energy dissipation during contact is accounted for through contact damping in order to obtain physically reasonable impact behavior between components of the system, which is related to a coefficient of restitution. However, this assessment is qualitative because no single coefficient of restitution can be defined for impacts between components since energy dissipation during an impact is a nonlinear process and depends on several factors specific to an impact scenario.

Where Used: Sections 6.3, 6.4.5.

5.10 POROSITY OF DEGRADED INTERNALS

Assumption: Porosity of degraded internals inside the OCB of waste packages is assumed to be 0.50.

Rationale: *EBS Radionuclide Transport Abstraction* (BSC 2005 [DIRS 173433], Table 6.3-9) estimates the initial porosity of waste package internals as 0.584, based on the Westinghouse 17 × 17-unit fuel assembly. Porosity will change as the internals degrade. Because smaller porosity results in greater OCB deformation and damage, the assumed value of 0.5 is a reasonable, conservative assumption.

Where Used: Sections 6.3, 6.5.

5.11 MODULUS OF ELASTICITY AND POISSON'S RATIO

Assumption: The modulus of elasticity and Poisson's ratio are the same for all waste package and pallet components in the LS-DYNA kinematic analyses. The modulus of elasticity is 200 GPa, and Poisson's ratio is 0.29.

Rationale: The focus of the analysis is the kinematic response of the waste packages. The material deformation and damage to the components are not in the scope of the analyses. Therefore, typical mechanical properties are adequate for this purpose.

Where Used: Sections 6.3, 6.4.5.

5.12 EDGE IMPACT INTO THE DRIP SHIELD

Assumption: Rock block/drip shield impacts occur along a rock block edge with the center of gravity aligned with the block trajectory.

Rationale: The rock blocks that may be dislodged in the nonlithophysal rock mass around the emplacement drifts will impact the drip shield at a wide range of angles. Also, the shape of the rock block impact surface could be very variable, from almost planar surfaces to relatively sharp corners, and direct impact of the rock block corner aligned with the block trajectory into the drip shield is highly unlikely. (Direct impact is an impact in which point of impact and block center are aligned with impact velocity.) Consideration of such an impact would lead to significant overestimation of damage in the drip shield. Therefore, the analyses were carried out for an edge impact that represents a reasonable bounding scenario of block impact into the drip shield.

Where Used: Section 6.4.7.

5.13 UNIFORM THINNING OF COMPONENT DIMENSIONS

Assumption: The weakening of components due to corrosion during postclosure can be approximated by uniform thinning of the component dimensions in simulations.

Rationale: While surface imperfections, residual stresses from welding, and local chemical environments may result in variable corrosion rates, spatially averaged thickness is most relevant to overall structural response. The analyses model the occurrence of multiple events that are spatially distributed, so spatially averaged thickness provides an appropriate measure of structural deformation and damaged area. For example, the damaged area from the kinematic response of the waste package is dominated by waste package-to-pallet impacts. These impacts involve contact of the pallet with a significant area on the surface of the waste package, thereby averaging the impact loads across regions with multiple OCB thicknesses due to nonuniform corrosion. If rubble surrounds the waste package, then the seismic loads are spread over the whole surface of the waste package, again providing a mechanism to average the loads over the surface of the waste package.

Where Used: Sections 6.3, 6.4, 6.5.

5.14 DEGRADATION OF OCB INTERNALS

Assumption: At later times during the period that the drip shield is still intact, and at even later times when drip shield plates have failed and the waste package is covered with rubble, OCB internals (including the inner vessel/canister shell, baskets and guides, and SNF) will have degraded completely.

Rationale: Corrosion processes occurring over long times and in the presence of moisture (after drip shield failure) will degrade the internals.

Where Used: Sections 6.3, 6.5.

5.15 REPRESENTATION OF DEGRADED INTERNALS

Assumption: The degraded metallic components of the internals can be represented in the analyses as a relatively soft and weak, elastic-perfectly plastic Tresca material.

Rationale: The input parameters used to represent the mechanical behavior of degraded internals are listed in Table 5-1. The internals will degrade mechanically with time. The mechanical properties listed in Table 5-1 underestimate the strength and stiffness of internals irrespective of the level of their degradation. For example, the bulk modulus of 10 MPa is representative of loose sand (Das 1990 [DIRS 172418], Table 8.5), as is the Poisson's ratio of 0.3 (Das 1990 [DIRS 172418], Table 8.6). The shear modulus is determined using the bulk modulus and Poisson's ratio. A cohesion of 50 kPa is typical of medium-to-stiff clays (Das 1990 [DIRS 172418], Table 9.4). Although it is expected intuitively that the internals will degrade into a state equivalent to a granular, frictional material, they are approximated in the analysis as a cohesive, frictionless material (friction angle of zero).

Where Used: Sections 6.3, 6.5.

Table 5-1. Material Properties Used to Represent the Mechanical Behavior of Degraded Internals

Property	Value
Bulk modulus (K)	10 MPa
Poisson's ratio (ν)	0.3
Shear modulus (G)	4.62 MPa
Cohesion (c)	50 kPa
Friction angle (ϕ)	0

Source: Das 1990 [DIRS 172418].

5.16 LINEAR SCALING OF PEAK GROUND VELOCITY

Assumption: Linear scaling of PGV and amplification of the vertical static load proportional to vertical peak ground acceleration (PGA) plus the acceleration of gravity provide adequate seismic input for these analyses.

Rationale: Linear scaling of the ground motion to different PGV levels is reasonable to obtain ground motions that are of the same order. Deaggregation of the PSHA results for Yucca Mountain shows that earthquakes controlling the ground motion hazard do not vary rapidly as a function of annual frequency of exceedance (BSC 2004 [DIRS 170027], Figures 6.2-17 through 6.2-28). The change in frequency content should not be significant for ground motions that have similar amplitudes. Scaling of the vertical static load proportional to vertical PGA+g (where g is the acceleration of gravity) is reasonable for analyses in which the maximum vertical acceleration is the dominant factor.

Where Used: Sections 6.3, 6.4, 6.5.

5.17 SIMULATION OF GROUND-MOTION TIME HISTORIES

Assumption: The portions of ground-motion time histories bracketed by the 15% and 85% points in energy buildup measured by Arias intensity were simulated as an adequate representation of the ground motion input.

Rationale: Arias intensity is defined as the sum of all the squared acceleration values from seismic strong motion records for an earthquake. The truncated time histories between the 15% and 85% points in energy buildup measured by Arias intensity always include the PGV, the PGA, and the interval of most intense shaking. Because drift collapse occurs in an interval of a few seconds, the simulated duration of the time histories is sufficient to allow accumulation of rubble around the waste package or the drip shield. Consequently, the neglected intervals of ground-motion time histories, before the 15% and after the 85% points in energy buildup, do not have significant effect on damage, deformation, and stresses in the waste package or drip shield.

Where Used: Sections 6.4.4, 6.5.1.

5.18 DEGRADATION OF STRUCTURAL ELEMENTS IN INVERT

Assumption: The potential for invert settlement due to corrosion of carbon steel under-girding was estimated by assuming total degradation of the steel structural elements.

Rationale: The structural elements of the invert are to be fabricated from carbon steel. Corrosion processes occurring over long times and in the presence of moisture will degrade these components. In assessment of the potential for uneven invert settlement, the assumption that the under-girding will have completely degraded will result in an upper bound on invert inclination.

Where Used: Section 6.4.6.

5.19 SHAPE OF ROCK BLOCKS IMPACTING THE DRIP SHIELD

Assumption: Large blocks that impact the drip shield are assumed to have a cubic shape.

Rationale: Rock blocks that form as a result of drift collapse in the nonlithophysal rock mass can have variable shapes. If a block impacts the drip shield edge first (Assumption 5.12, above) only a small surface of the block around the edge comes in the contact with the drip shield. The shape of the rest of the block does not have an effect on the interaction between the drip shield

and the rock block. The most important factors affecting drip shield deformation and damage are the rock block mass and impact velocity (i.e., impact energy).

Where Used: Section 6.4.7.

5.20 FAILURE CRITERION FOR STRESS CORROSION CRACKING

Assumption: The waste package is assumed to fail immediately by SCC once the residual tensile stress threshold is exceeded, providing a potential pathway for transport through the areas exceeding the residual tensile stress threshold.

Rationale: The time of failure is assumed to be immediate (i.e., the same time as when the seismic shaking occurs). However, in reality, any cracks that form would take time to develop after the shaking event causes a change in loading. This overestimates the rate of crack growth and material failure. A more-detailed discussion is presented in Section 6.2.1.

Where Used: Section 6.2.1.

5.21 PALLET STIFFNESS

Assumption: The emplacement pallet is represented in UDEC simulations (waste package surrounded by rubble) as an elastic solid body with stiffness such that its deformability is negligible. (Note: This assumption does not apply for the kinematic analyses in Section 6.3.)

Rationale: In the analyses of the waste package (Section 6.5.1) and the drip shield (Section 6.4.4) surrounded by rubble, the correct geometry of the emplacement pallet in the cross section is represented. However, because of two-dimensional numerical approximation, the actual structure of the emplacement pallet is ignored, and the pallet is represented as a very stiff elastic solid block. The pallet structure has finite strength and stiffness that will further decay with time. The assumption of having the elastic and very stiff emplacement pallet in contact with the deformable and plastic waste package will result in overestimation of deformation and damage in the waste package.

Where Used: Sections 6.4.4, 6.5.1.

5.22 SYMMETRY OF THE WASTE PACKAGE

Assumption: Deformation analysis of the waste package loaded by the collapsed drip shield assumes the cross-sectional mid-plane of the waste package to be bilaterally symmetrical, and representative of damage along the length of the package.

Rationale: Details of geometry at two ends of waste packages are different, and strict symmetry does not exist. Deformation and damage of the waste package close to the lids (on both ends), both of which are affected by details of lid geometry, are negligible compared to deformation of the waste package near the center. The lids act as rigid supports to lateral deformation of the OCB on both ends, and the difference in the geometrical details at the ends will have insignificant effect on the result of interest (i.e., deformation and damage of the waste package away from the ends), where damage is expected to be the greatest.

Where Used: Section 6.5.2.

5.23 USE OF REPRESENTATIVE VALUES FOR DESIGN INPUT PARAMETERS

Assumption: Based on preliminary concepts for the EBS components, representative values for the necessary design parameters were assumed to perform the simulations discussed in this report.

Rationale: Many of the simulations were started before the direct confirming data were available in the design interface documents, so it was necessary to utilize preliminary values for the design of the EBS components. These values are compared to the direct confirming data values in Table 4-6, Table 4-7, and Table 4-8. Impact assessments are provided in Section 4.1.5 and Table 4-6. The assessments indicate that the use of the assumed representative values has a negligible impact on the results presented in this report.

Where Used: Sections 6.3, 6.4, 6.5.

INTENTIONALLY LEFT BLANK

6. MODEL DISCUSSION

6.1 INTRODUCTION

The objective of this model report is to present postclosure seismic analyses of engineered barriers and to provide estimates of damage to the Engineered Barrier System (EBS) components as a function of vibratory ground motion. The intended use of this output is to provide input to abstractions developed for the seismic scenario class for the (postclosure) compliance case for the license application. In particular, this includes inputs to:

- Abstractions for the kinematic response of the transportation, aging, and disposal (TAD)-bearing waste package with a 23-mm-thick outer corrosion barrier (OCB) and intact internals (accounts for an initial amount of general corrosion), with a 23-mm-thick outer corrosion barrier and degraded internals, and with a 17-mm-thick OCB and degraded internals in response to vibratory ground motion (Section 6.3)

- Abstractions for the kinematic response of the codisposal waste package with a 23-mm-thick OCB and intact internals, with a 23-mm-thick OCB and degraded internals, and with a 17-mm-thick OCB and degraded internals in response to vibratory ground motion (Section 6.3)

- Fragility curves for the drip shield plates in response to the combined loads from vibratory ground motion and rockfall that accumulate on the drip shield (Section 6.4)

- Fragility curves for the drip shield framework in response to the combined loads from vibratory ground motion and rockfall that accumulate on the drip shield (Section 6.4)

- Abstraction for drip shield damage due to impact from large rock blocks induced by vibratory ground motion (an abstraction appropriate for drifts that are unfilled or partly filled and lie in nonlithophysal units) (Section 6.4)

- Abstraction for the drip shield partly or completely surrounded by lithophysal rubble in response to vibratory ground motion (Section 6.4)

- Abstractions for the TAD-bearing waste package surrounded by rubble for the 23-mm-thick and 17-mm-thick OCBs with degraded internals in response to vibratory ground motion (Section 6.5).

A series of damage models is used to develop waste package and drip shield damaged areas resulting from vibratory ground motion and from rockfall induced by vibratory ground motion. Specifically, these estimates are for the TAD-bearing and the codisposal waste packages. Additionally, the results from the damage models can be used to address an NRC issue raised in *Integrated Issue Resolution Status Report* (NRC 2002 [DIRS 159538]). As described in Section 1, the emplacement drift EBS consists of several primary components that will be affected by vibratory ground motion from a remote earthquake. These components, presented earlier in Figures 1-1 and 1-2, are: (a) the waste package, (b) the waste package internals, (c) the emplacement pallet, (d) the drip shield, and (e) the invert.

The analysis of damage to engineered barriers resulting from seismic shaking is a complex problem that may involve large displacements of free bodies and potential collisions and localized failure mechanisms of the waste packages and drip shields. Additionally, intense ground motions from low-probability earthquakes may result in substantial rockfall or collapse of emplacement drifts (BSC 2004 [DIRS 166107], Section 6.4). It is assumed that the drip shields, when confined by rubble, will subsequently move in synchronous motion with the free field rock mass (Assumption 5.1, Section 5) until the drip shield collapses. Thus, one problem analyzed in this model report considers behavior of a string of many waste packages aligned end-to-end beneath a series of interlocked drip shields within a collapsed emplacement drift (see Figure 1-4(a)).

Other analyses presented in this report concern damage to the waste package when the drip shield has collapsed onto the waste package, and when the waste package is surrounded by rubble after the drip shield has lost all integrity due to corrosion. The effect of uneven settlement of the invert on the behavior of the drip shield is also analyzed.

During seismic-induced vibratory motion, the waste packages will move synchronously with the invert and/or the surrounding rubble in the emplacement drift (or free-field rock mass) unless the inertial forces acting on the waste package are sufficient to: (a) cause sliding of the waste package relative to the emplacement pallet (or sliding of both the emplacement pallet and the waste package relative to the invert and the surrounding rubble); or (b) throw the waste package into free flight after the waste package separates from the emplacement pallet. As long as the waste packages move synchronously with the free field, they will not interact with each other, or with any other object inside the emplacement drift except the emplacement pallet on which the waste packages rest.

When the peak acceleration of the ground motion exceeds a critical value, resulting in sliding and separation of the waste package relative to the emplacement pallet and the invert or surrounding rubble, interaction and impacts between the waste package and other objects inside the emplacement drift become possible. The horizontal acceleration normal to the axis of the emplacement drift could cause lateral impacts between the waste package and the drip shield. The vertical acceleration could be the cause of impacts between the waste package and the emplacement pallet and between the waste package and the inner surfaces of the top of the drip shield. In the case of the waste package surrounded by rubble, the rubble will exert dynamic loads on the waste package during episodes of vibratory ground motion. The horizontal acceleration along the axis of the emplacement drift could cause interaction and impacts between the neighboring waste packages.

The approach taken is to partition the analysis into five parts which include:

- *Kinematic Analyses with Multiple Waste Packages*—This analysis includes: (a) three-dimensional rigid body kinematic calculations of waste packages, pallets, and drip shields subjected to postclosure ground motions[1], and (b) detailed numerical

[1] The postclosure ground motions consist of 17 sets of time histories at four hazard levels (i.e., annual exceedance probabilities): 1×10^{-4} per year (PGV level of 0.4019 m/sec), 1×10^{-5} (PGV level of 1.05 m/sec), 4.5×10^{-7} (PGV level of 2.44 m/sec), and 1×10^{-8} (PGV level of 4.07 m/sec) (SNL 2007 [DIRS 176828], Section 6.4).

calculations for the damage from individual impacts. The detailed damage calculations for individual impacts include several outer barrier thicknesses and the potential for the waste package internals to be either intact or degraded. In particular, kinematic calculations have evaluated seismic-induced damage for three future states of the waste package:

- 23-mm-thick OCB with intact internals
- 23-mm-thick OCB with degraded internals
- 17-mm-thick OCB with degraded internals.

- *Drip Shield Failure Mechanisms due to Vibratory Ground Motion*—This analysis involves three-dimensional numerical calculations of the plastic load capacity of the drip shield plates and framework.

- *Drip Shield Damaged Areas*—This analysis involves finite-element numerical calculations for the damaged areas on the drip shield from vibratory ground motion and from rockfall induced by vibratory ground motion. Several plate thicknesses are considered to incorporate long-term degradation of the drip shield. This analysis also includes kinematic calculations for the interaction of the waste package and drip shield in collapsed emplacement drifts. The failure of the drip shield from rupture or buckling is also based on future states of the EBS. For these calculations, the ultimate plastic load capacity of the drip shield is determined as a function of plate thickness, the static load from rubble in the drift, and the vertical peak ground acceleration. The plastic load capacity is determined using a quasi-static approach, avoiding the need to evaluate 17 sets of ground motions at multiple peak ground velocity (PGV) levels. Finite-element calculations have also been performed to define the damaged areas on the drip shield as a function of vibratory ground motion and of rockfall induced by vibratory ground motion. The residual stress threshold for determining damaged area in titanium is 80% of the yield strength of Titanium Grade 7 (DTN: MO0702PASTRESS.002 [DIRS 180514]).

- *Uneven Settlement of the Invert*—This analysis involves a study of the potential for uneven settlement of the invert and its effect on the orientation of emplaced drip shields, their rockfall load carrying capacity, and potential interactions with a waste package.

- *Waste Package Analysis After Drip Shield Failure*—This analysis includes two-dimensional numerical calculations to determine the response of a waste package surrounded by rubble in the lithophysal zone and analysis of the OCB structural integrity, stability, and damage that may occur if the drip shield collapses onto the OCB and transfers the weight of the rubble load and collapsed drip shield onto the OCB. The presence of rubble around the waste package is a function of the fragility of the drip shield and a function of the accumulation of rubble from multiple seismic events. Several outer barrier thicknesses and the potential for waste package internals to be intact or degraded represent the long-term degradation of the waste package and its internals. The waste package/rubble damage calculations are performed with a fully coupled two-dimensional representation of the lithophysal rubble, the OCB, and

degraded internals. Seismic-induced damage is evaluated for two future states of the waste package:

- 23-mm-thick OCB with degraded internals
- 17-mm-thick OCB with degraded internals.

The finite-element and distinct-element calculations are based on four levels of horizontal PGV: 0.4 m/s, 1.05 m/s, 2.44 m/s, and 4.07 m/s. Each level is represented by 17 sets of three-component ground motions. The calculations for kinematic response and for a waste package surrounded by rubble use 17 sets of ground motions at each level.

Figure 6-1 presents an overview of the individual analyses and the sections within this document where they are found. The basic input data required for these analyses include the postclosure ground motion time histories and material property estimates for the waste package, drip shield, invert materials, and caved rock mass. These inputs are described in Section 4.1 of this document. Additionally, an analysis of drip shield stability under possible impact from the waste package during large amplitude ground motions assumes that the drift will already have collapsed, resulting in a drip shield surrounded by rock rubble.

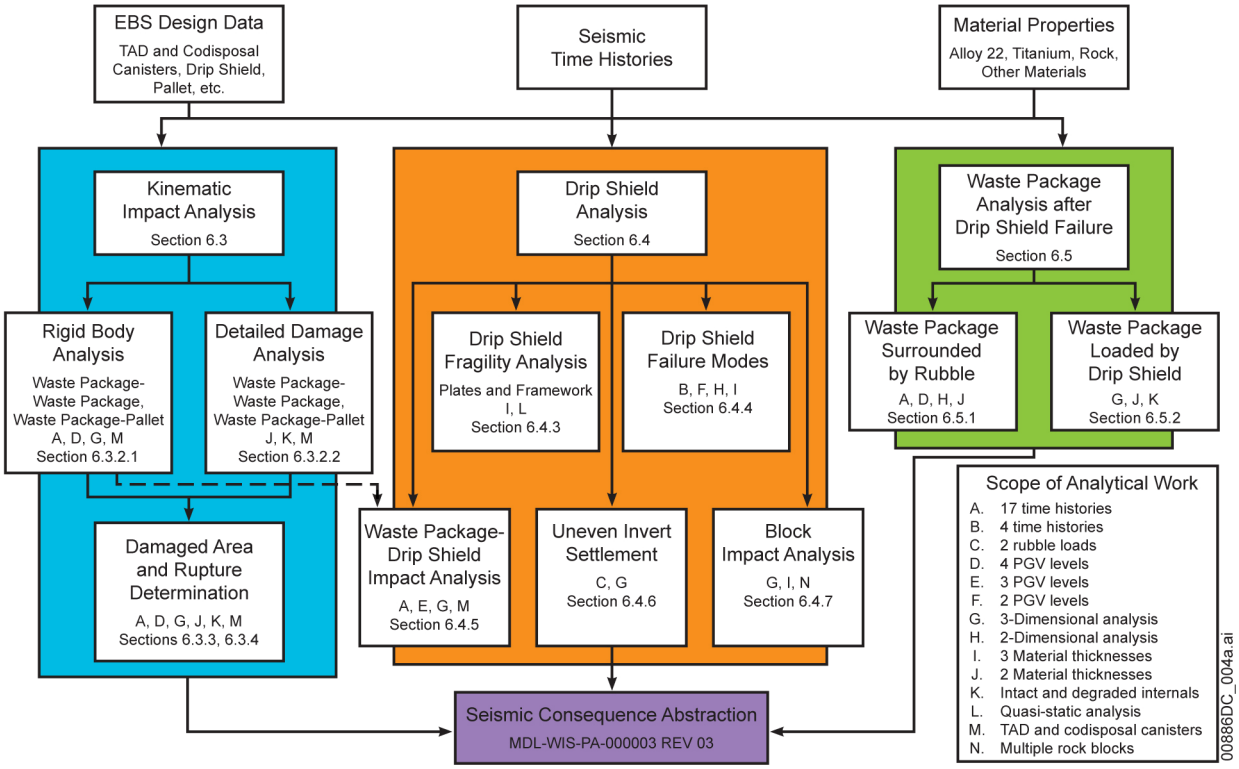

Source: Created for illustrative purposes.

NOTES: Boxes give the section where each analysis is discussed and the types of analysis performed. Chart shows outputs to *Seismic Consequence Abstraction* (SNL 2007 [DIRS 176828]).

Figure 6-1. General Document Organization and Outputs to *Seismic Consequence Abstraction*

Section 6.2 presents a discussion of failure mechanisms that are considered for the EBS when subjected to vibratory ground motion, and Sections 6.3 to 6.5 present detailed analyses and results. Section 6.6 presents features, events, and processes (FEPs) associated with this analysis.

6.2 FAILURE MECHANISMS

Mechanical processes that occur during a significant seismic event (i.e., an event with the capacity to deform or rupture the waste package) have the potential to compromise the functionality of the waste packages and drip shields as barriers to radionuclide release. These mechanical processes include impacts between components caused by vibratory ground motion and impacts caused by rock blocks and rockfall induced by vibratory ground motions.

Vibratory ground motions can cause impacts to occur between adjacent waste packages and between the waste package and its emplacement pallet, the surrounding drip shield or rubble, and the invert. Impacts can also occur between the drip shield and the emplacement pallet, the invert, and even the drift wall. Rockfall induced by vibratory ground motions can result in impacts on the drip shield when the drip shield is intact and impacts on the waste packages after drip shield failure. Rockfall induced by vibratory ground motion may collapse the drifts, resulting in static loads from the mass of rubblized rock surrounding the drip shield or the waste package if the drip shield has collapsed.

These mechanical processes are associated with a number of potential failure mechanisms for the waste package resulting from vibratory ground motions.[2] These failure mechanisms are discussed below:

- Dynamic loads have the potential to result in rupture (ductile tearing) or puncture of a waste package if the local strain exceeds the ultimate tensile strain. A waste package that has been ruptured or punctured provides a potential pathway for seepage to flow into, and for radionuclides to be transported out of, the waste package.

- Impact-related dynamic loads may dent the waste package, resulting in permanent structural deformation with residual stress. High levels of residual tensile stress may lead to local degradation from accelerated corrosion processes. Areas that are breached from corrosion processes provide a potential pathway for seepage to flow into, and for radionuclides to be transported out of, the waste package.

- The static load from rockfall combined with the dynamic load during a seismic event may buckle the drip shield or rupture the drip shield plates. Buckling or rupture compromises the capacity of the drip shield to deflect seepage and rockfall away from the waste package.

[2] Impacts between adjacent waste packages, and other impacts involving the waste packages, impose dynamic loads on waste package internals and may also result in deformed fuel rods and perforated cladding. Failure of cladding provides a potential pathway for release of radionuclides from fuel rods. However, analysis of the cladding is beyond the scope of this report.

- The static load from rockfall combined with the dynamic load during a seismic event may deform the plates on the crown of the drip shield. High levels of residual tensile stress may lead to local degradation from accelerated corrosion processes. Areas that are breached from corrosion processes provide a potential pathway for seepage through the drip shield.

- Impacts by large rock blocks in unfilled or partly filled drifts in nonlithophysal units may deform the drip shield or fail the plates and axial stiffeners on the crown of the drip shield. Failed plates provide a potential pathway for seepage through the drip shield. Areas that are breached from accelerated corrosion processes provide a potential pathway for seepage through the drip shield.

- Vibratory ground motion may cause adjacent drip shields to separate if there is large vertical displacement between them or if the welds holding the drip shield connector guides tear loose from the drip shield plates during the dynamic response. Separation compromises the capacity of the drip shield to deflect seepage and rockfall away from the waste package.

- Vibratory ground motion may cause waste package-to-drip shield impacts that could compromise the structural stability of the drip shield or tear the interior support bulkhead beneath the crown of the drip shield. A failed drip shield could provide a potential pathway for seepage through the drip shield.

6.2.1 Formation of Stress Corrosion Cracks

The high residual tensile stress, discussed above, may cause accelerated SCC. This is a combined mechanical-corrosion process and is expected to be the most likely cause of failure for the waste package and drip shield from impact processes caused by vibratory ground motions. The areas that exceed the residual tensile stress threshold are referred to throughout this document as the damaged area. The effective area for transport through the damaged areas will be substantially less than the damaged area because the cross-sectional area of the stress corrosion cracks is much less than the total surface area that exceeds the residual stress threshold (BSC 2005 [DIRS 173247], Section 6.3.5).

The damaged or deformed area that exceeds a residual stress threshold is conceptualized to result in a tightly spaced network of stress corrosion cracks. Application of a residual tensile stress threshold for seismic failures in this analysis is nonmechanistic in the sense that detailed analyses with accelerated corrosion rates or crack propagation are not used to determine the actual failure time after a seismic event. Rather, a network of stress corrosion cracks is considered to immediately form once the residual tensile stress threshold is exceeded, providing potential pathways for transport through the areas exceeding the residual tensile stress threshold (Assumption 5.20, Section 5). The residual tensile stress threshold is often referred to as the residual stress threshold or more simply the stress threshold, with the understanding that the principal residual stress must always be tensile to initiate an accelerated corrosion process.

Figure 6-2 is a simplified illustration of how residual stress is generated by permanent (plastic) deformation in a simple uniaxial strain model. The loading path in Figure 6-2 has three phases: (1) elastic loading until reaching the elastic yield limit, (2) plastic loading above the elastic yield limit, and (3) elastic unloading when the external load reduces the local stress. Figure 6-2 also shows that plastic deformation does not always generate a damaged area because the final residual stress state may be compressive or, if tensile, may be below the threshold to initiate accelerated localized corrosion or SCC. It should be recognized that propagation of a stress corrosion crack can be arrested if the crack tip encounters an unfavorable residual stress field.

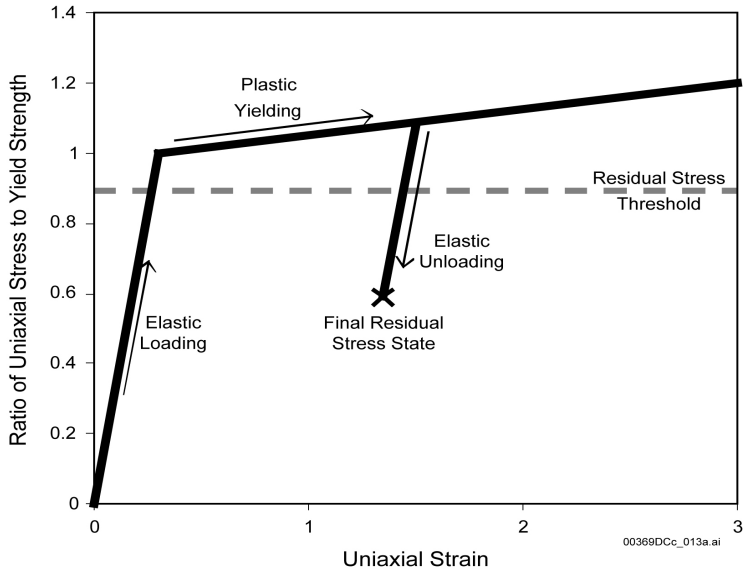

Source: Created for illustrative purposes only.

Figure 6-2. Idealized Elastic-Plastic Model

Accelerated SCC from high residual stress is expected to be the most likely cause of failure for the waste package from impact processes under vibratory ground motion. A criterion for initiation of SCC of Alloy 22 based on residual stress thresholds is utilized (SNL 2007 [DIRS 177417], Section 6.2.2). The use of an SCC initiation criterion is appropriate for seismic analysis because regions where the residual stress from mechanical damage exceeds the residual stress threshold are expected to be severely cold-worked and, hence, potentially subject to enhanced SCC.

A residual stress threshold is a bounding failure criterion because detailed corrosion models will have a delay time until failure. This approach is appropriate because the residual stress failure criterion is transparent and because it is easily applied to the output from structural response calculations. The residual stress threshold for failure of the waste package is represented by a distribution with a lower bound of 90% of the yield strength of Alloy 22 and an upper bound of 105% of the yield strength of Alloy 22 (SNL 2007 [DIRS 176828], Section 6.1.4; DTN: MO0702PASTRESS.002 [DIRS 180514], *Model Output DTN.doc*, Table 8-3).

The damage to the waste package has been evaluated at the extremes of the distribution and at one intermediate value. The results from each structural response analysis are postprocessed to determine the elements in the outer corrosion barrier (OCB) of the waste package whose residual stress exceeds 90% of the yield strength of Alloy 22, to determine the elements in the OCB of the waste package whose residual stress exceeds 100% of the yield strength of Alloy 22, and to determine the elements in the OCB of the waste package whose residual stress exceeds 105% of the yield strength of Alloy 22. The areas at intermediate values of the residual stress threshold can then be determined by linear interpolation between the 90%, 100%, and 105% values. The elements that exceed 105% of the yield strength are always a subset of the elements that exceed 100% of the yield strength, which are a subset of the elements that exceed 90% of the yield strength. In other words, the damaged area for the 105% residual stress threshold is always less than the damaged area for the 100% residual stress threshold, which is always less than the damaged area for the 90% residual stress threshold.

6.2.2 Ultimate Tensile Failure

Ultimate tensile failure (rupture) of the waste package occurs when the effective strain exceeds a threshold value that is dependent on the state of stress at the location of interest. Analysis presented in Appendix A shows that for stress states likely to occur in the waste package under impact conditions, failure occurs when effective strain reaches one-half the tensile elongation. This follows work by Manjoine (1983 [DIRS 178496]). It is important to note that the tensile elongation due to impact events occurs at relatively high strain rates that are on the order of 150 s^{-1}. Moreover, tensile elongation is dependent on strain rate, and Zabotkin et al. (2003 [DIRS 178494]) have indicated that the tensile elongation of Alloy 22 decreases 11% as strain rate increases from 10^{-4} s^{-1} to 200 s^{-1}. This indicates that the tensile elongation at failure measured in standard tests (0.64) should be reduced by 11% to a value of 0.57. Then following the relation between effective strain and tensile elongation stated above, a value of 0.285 is determined for the effective strain threshold for Alloy 22. A more detailed analysis is presented in Appendix A. This method provides a conservative threshold for the effective strain to determine whether rupture has occurred. Alternatively, effective plastic strain can be used in place of effective strain as the metric. As is explained in Appendix A, using the effective plastic strain is conservative compared to the effective strain.

6.3 KINEMATIC ANALYSES WITH MULTIPLE WASTE PACKAGES

6.3.1 Purpose of Kinematic Analyses

Three-dimensional kinematic calculations are used to examine the motion and impact of multiple waste packages, pallets, and drip shields in an emplacement drift. The objectives of these analyses are to define the history of impact parameters for collisions of the waste packages, pallets, and drip shields as a function of the applied ground motion time histories, and to determine the associated probability of rupture and damaged areas on the waste package. Seventeen separate ground motion time histories are used, and each is used at four different PGV levels. Separate kinematic calculations are performed for each PGV level of each ground motion time history. The kinematic calculations are appropriate to define the damage to the waste package when the drip shield is intact and the waste package can move freely beneath the drip shield.

The kinematic calculations consider a "string" of multiple waste packages in a section of an emplacement drift. The "string" will be composed of a combination of TAD-bearing waste packages and codisposal (specifically the 5-DHLW/DOE SNF-Long codisposal) waste packages. The appropriate mix of waste packages and the number of waste packages is chosen to make the number of waste packages representative of the package inventory and to make the response of the string representative of the middle of an emplacement drift, independent of the end conditions. That is, the string must have enough waste packages to make the response of the central waste packages independent of the free boundaries at either end of the string.

For computational efficiency, the kinematic calculations use relatively coarse finite-element representations of the waste package and pallet as elastic bodies that preserve the mass and dimensions of the components (Assumptions 5.3 and 5.9, Section 5). The kinematic calculations are too coarse to directly determine the structural deformation or damage from multiple impacts. Instead, the damage induced by these impacts is calculated from the kinematic impact parameters for end-to-end impacts and for waste package-pallet impacts by using lookup tables. A direct correlation is made between damaged surface area and impact velocity, angle of impact, force of impact, and/or impact location, allowing the kinematic calculations to represent the damage to multiple waste packages without the penalty of running very detailed finite-element models. The final damaged area from multiple impacts is determined by summing the damaged areas from individual impacts, based on the lookup table and the impact parameters. These final damaged areas form the basis of the seismic damage abstractions for TSPA.

The kinematic calculations represent an emplacement drift that has partially or completely collapsed, with the result that the drip shield is pinned in place and moves synchronously with the free field (Assumption 5.1, Section 5). *Drift Degradation Analysis* (BSC 2004 [DIRS 166107], Section 6.4.2.2.2.1) showed that complete collapse of the emplacement drifts in the lithophysal rock occurs at a PGV of approximately 2 m/sec and that substantial rock blocks are dislodged at this level in the nonlithophysal unit as well. Even relatively small amounts of rockfall tend to prevent drip shield separation, as demonstrated in *Mechanical Assessment of the Drip Shield Subject to Vibratory Motion and Dynamic and Static Rock Loading* (BSC 2004 [DIRS 169753], Section 5.3.3.1). Therefore, the drip shield is represented as a boundary that moves synchronously with the free field for the kinematic calculations.

The input data for the kinematic calculations include the following:

- Seventeen ground motion time histories for each of the 0.4m/sec, 1.05 m/sec, 2.44 m/sec, and 4.07 m/sec PGV levels. (The same kinematic model is used at all PGV levels, and is valid and appropriate for these levels.)
- Friction coefficient for metal-to-metal (waste package-to-pallet and waste package-to-waste package) contacts.
- Friction coefficient for metal-to-crushed tuff (invert) contact.
- Elastic material properties of the waste package and pallet.
- Dimensions and masses of EBS components (drip shield, waste package, pallet).

The uncertainty in the ground motions and in the friction coefficients is propagated into the kinematic calculations through sampled values for these input parameters. To this end, Latin Hypercube sampling of the metal-to-metal friction coefficient, the metal-to-invert friction coefficient, and the ground motion number has been performed (BSC 2005 [DIRS 173172], Attachment X; DTN: MO0508SPAMECHA.000 [DIRS 181067], *AttachmentX.zip*, files *All_3_Sampling_Groups.txt* and *Definition of Stochastic Parameters.doc*). Each friction coefficient is independently sampled from a uniform distribution with a range of 0.2 to 0.8. The ground motion number is sampled from a discrete distribution from 1 to 17, with equal probability for each number. This sampling provides a list of input data in which a given time history (numbered from 1 to 17) is randomly paired with metal-to-metal and metal-to-invert friction coefficients for each waste package and pallet. This listing provides part of the basis for the input data for the kinematic calculations at the 0.4 m/s, 1.05 m/sec, 2.44 m/sec, and 4.07 m/sec PGV levels.

The kinematic calculations are designed to represent the rigid body motions of multiple waste packages, not the structural deformation of each waste package. Each waste package is therefore represented as an elastic body with Young's modulus and Poisson's ratio defined at room temperature. While elastic properties vary with temperature, the use of room-temperature values is a reasonable approximation for the rigid body interactions of the waste packages.

The output data from the kinematic calculations are a set of impact parameters, including:

- Impact location and time of impact
- Relative velocity of the impacting bodies
- Relative angle of impact of the impacting bodies
- Force between the impacting bodies.

For every impact between adjacent waste packages or between a waste package and an emplacement pallet, the time, location, relative velocity, relative angle, and force of the collision is recorded. The corresponding damage from multiple impacts during a given ground motion is determined from a series of lookup tables that relate the relevant impact parameter(s) to surface area that has overcome a residual tensile stress criterion. The lookup tables for end-to-end impacts are generated from detailed finite-element calculations for the horizontal impact of a moving waste package onto an initially stationary (but not fixed) waste package. The lookup tables for waste package-pallet impacts are generated from detailed finite-element analyses of side-on impacts of a waste package on an emplacement pallet. The potential for rupture will also be determined, in part, from the lookup tables, based on the ultimate tensile strain of Alloy 22 and a "knockdown" factor that accounts for the potential effects of a biaxial stress field on the ultimate strength of a material. This knockdown factor provides an initial basis for screening cases with the potential for rupture. Once a case exceeds the knockdown factor, the detailed stress state is considered to determine if rupture occurs. The basis for the knockdown factor is documented in Appendix A. The occurrence of multiple large impacts is also considered in determining the potential for rupture.

The input data for the lookup table calculations include the temperature for material properties and the residual stress threshold for initiation of SCC in deformed areas. Elastic and plastic material properties are set to constant values at 60°C based on data from handbooks or

manufacturers' catalogs (see Appendix A). This temperature provides bounding values for material properties over the long time scale for the seismic scenario class after 10,000 years (Assumption 5.7, Section 5). A sensitivity study (Section 6.3.2.2.2) shows that the damaged area is relatively insensitive to elevated temperatures, so the elevated temperatures during the first 10,000 years are of negligible significance.

The residual stress threshold for initiation of SCC on the Alloy 22 outer barrier is defined as a range from 90% to 105% of the yield strength of Alloy 22 (see technical studies for *Technical Work Plan for Postclosure Waste Package Modeling and Testing* (BSC 2006 [DIRS 177536], Section 2.3.1.1)). The uncertainty associated with this range is propagated into TSPA in *Seismic Consequence Abstraction* (SNL 2007 [DIRS 176828]) by defining abstractions that are a function of the residual stress threshold and by interpolating between the damaged areas at the 90%, 100%, and 105% residual stress thresholds to capture this uncertainty in TSPA.

Multiple lookup tables are defined to represent a range of future states of the TAD-bearing waste package or the codisposal waste package. For end-to-end impacts of adjacent waste packages, the future states are: 23-mm-thick outer barrier with intact internals, 23-mm-thick outer barrier with degraded internals, and 17-mm-thick outer barrier with degraded internals. These thicknesses are the spatially averaged thickness of the outer barrier, because average thickness is anticipated to be the key parameter for structural response (Assumption 5.13, Section 5). The outer barrier thicknesses have been reduced to represent the potential for general corrosion to reduce the thickness of the outer barrier. The first state, 23 mm with intact internals, approximates the relatively early behavior of the waste package under an intact drip shield with minimal corrosion; the third state, 17 mm with degraded internals, approximates relatively late behavior of the waste packages under an intact drip shield; and the second state, 23 mm with degraded internals, approximates a period between the other two states. For the states with degraded internals, credit is not taken for the stainless steel inner vessel, for the TAD canister, or for the fuel baskets as structural elements (Assumption 5.14, Section 5). This approach maximizes structural deformation and damaged area if the stainless steel elements do not degrade quickly in a dilute chemical environment. Each end-to-end lookup table has multiple entries for impact velocity, impact angle, and impact location. The impact configurations are described in Section 6.3.2.2.3.

The lookup tables for waste package-to-pallet impacts are structured in a manner similar to those for end-to-end impacts. The future states are 23-mm-thick outer barrier with intact internals, 23-mm-thick outer barrier with degraded internals, and 17-mm-thick outer barrier with degraded internals. Each waste package-to-pallet lookup table has multiple entries for impact velocity, impact angle, and impact location. The impact configurations are described in Section 6.3.2.2.3.

The output from the damage calculations provides the basis for new seismic damage abstractions that are documented in *Seismic Consequence Abstraction* (SNL 2007 [DIRS 176828]). These calculations have been performed with qualified versions of the finite-element software LS-DYNA currently under Software Configuration Management and listed in the Software Baseline Report. Specific versions of LS-DYNA are listed in Table 3-1.

The summation of damaged areas from individual impacts was performed as a postprocessing step. The postprocessing software is written in FORTRAN and executed on the YANA cluster at Lawrence Livermore National Laboratory (LLNL). The input for this software is the kinematic impact parameters, the end-to-end damage lookup tables, and the waste package–to-pallet damage lookup tables generated by LS-DYNA. The output from this software is the summation of the damaged areas on the waste package and the potential for rupture of the waste package. This software, called km_impacts_pp (V. 1.0. STN: 11235-1.0-00 [DIRS 178489]), was qualified in accordance with IM-PRO-003.

6.3.2 Three-Dimensional Kinematic Model of EBS Damage Due to Vibratory Ground Motion

6.3.2.1 Rigid Body Kinematic Analysis

The kinematic analyses were performed using a finite-element representation of a series of waste packages emplaced in a drift (Figure 6-3 and Figure 6-4). This representation includes waste packages, emplacement pallets, and a rigid representation of the invert and drip shield (Assumptions 5.1 and 5.2, Section 5). The waste packages were characterized as hollow cylinders with end caps (Figure 6-5, Figure 6-6, and Assumption 5.3, Section 5). The dimensions of the waste packages approximate the actual waste packages and produce material densities similar to the density of other components in the finite-element representation, with the intent of maintaining reasonable analytic time steps.

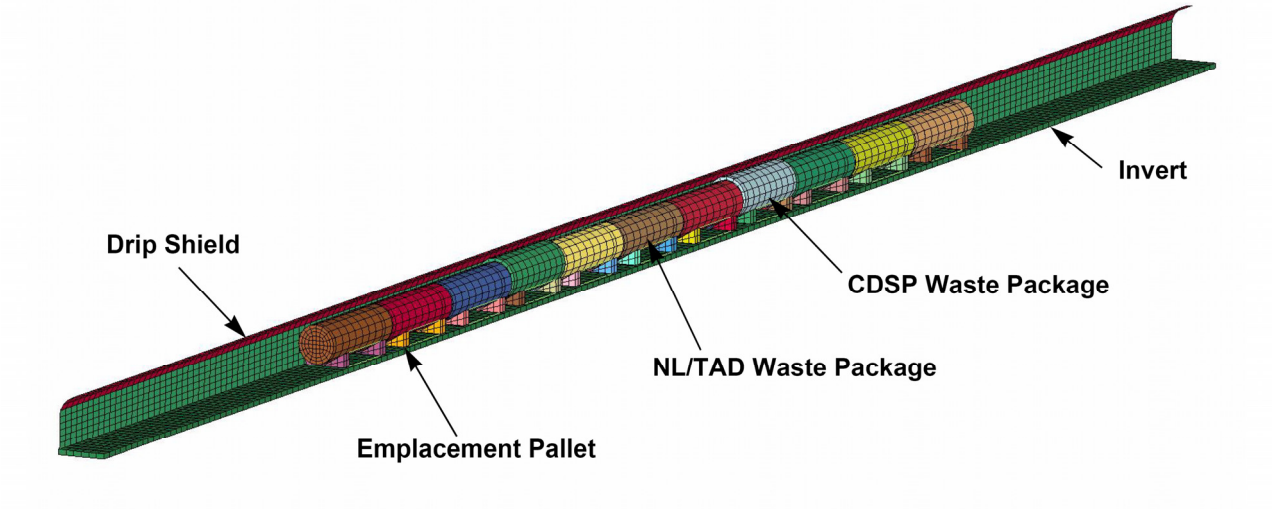

Output DTN: LL0704PA051SPC.026, file *Figures_Mech_Assessment_AMR.tar.gz*.

NOTES: The configuration consists of nine TAD-bearing (NL/TAD) packages and two codisposal (CDSP) waste packages. Impacts to the center three packages are considered representative of those to a typical repository TAD-bearing waste package. One side of the drip shield is removed for clarity.

Figure 6-3. Eleven-Waste-Package Configuration Showing Focus on Central Three TAD-Bearing Waste Packages

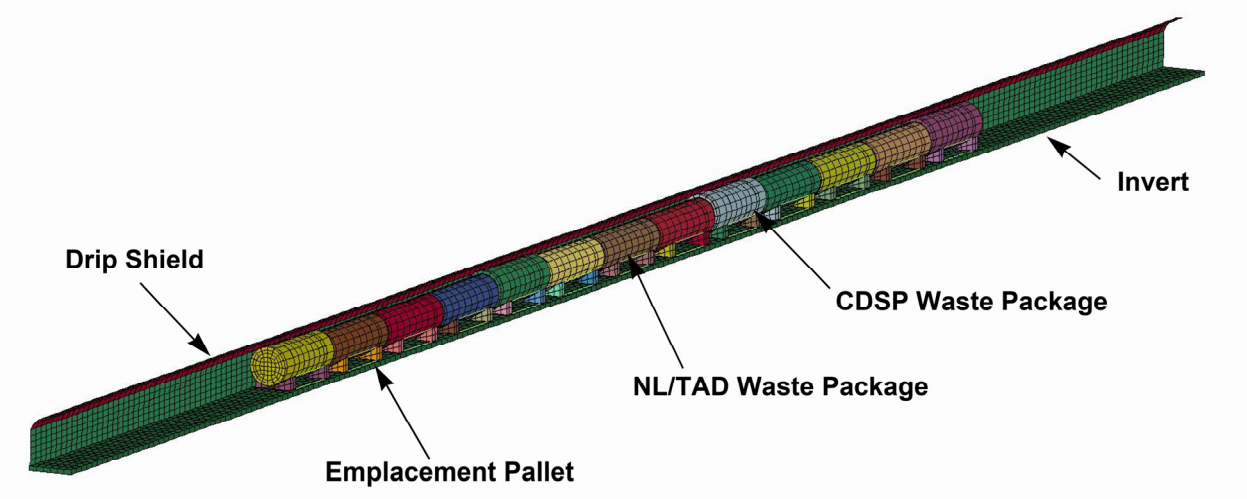

Output DTN: LL0704PA051SPC.026, file *Figures_Mech_Assessment_AMR.tar.gz*.

NOTES: The configuration consists of nine TAD-bearing (NL/TAD) packages and four codisposal (CDSP) waste packages. Impacts to the two central codisposal waste packages are considered representative of those to a typical repository codisposal waste package. One side of the drip shield is removed for clarity.

Figure 6-4. Thirteen-Waste-Package Configuration for Focus on Central Two Codisposal Waste Packages

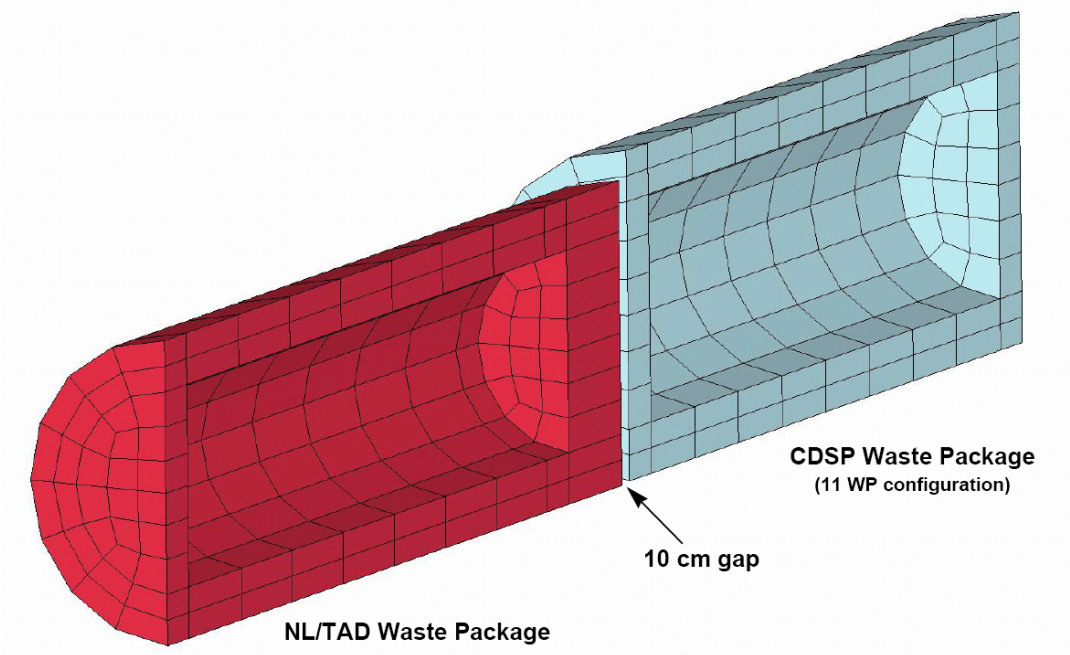

Output DTN: LL0704PA051SPC.026, file *Figures_Mech_Assessment_AMR.tar.gz.*

NOTES: Adjacent waste packages are positioned 10 cm apart.
Waste packages are shown in a cut-away view to show the interior.
NL/TAD = TAD-bearing; CDSP = codisposal; WP = waste package.

Figure 6-5. Geometry of TAD-Bearing and Codisposal Waste Packages for the 11-Waste-Package Configuration (TAD-bearing waste package analyses)

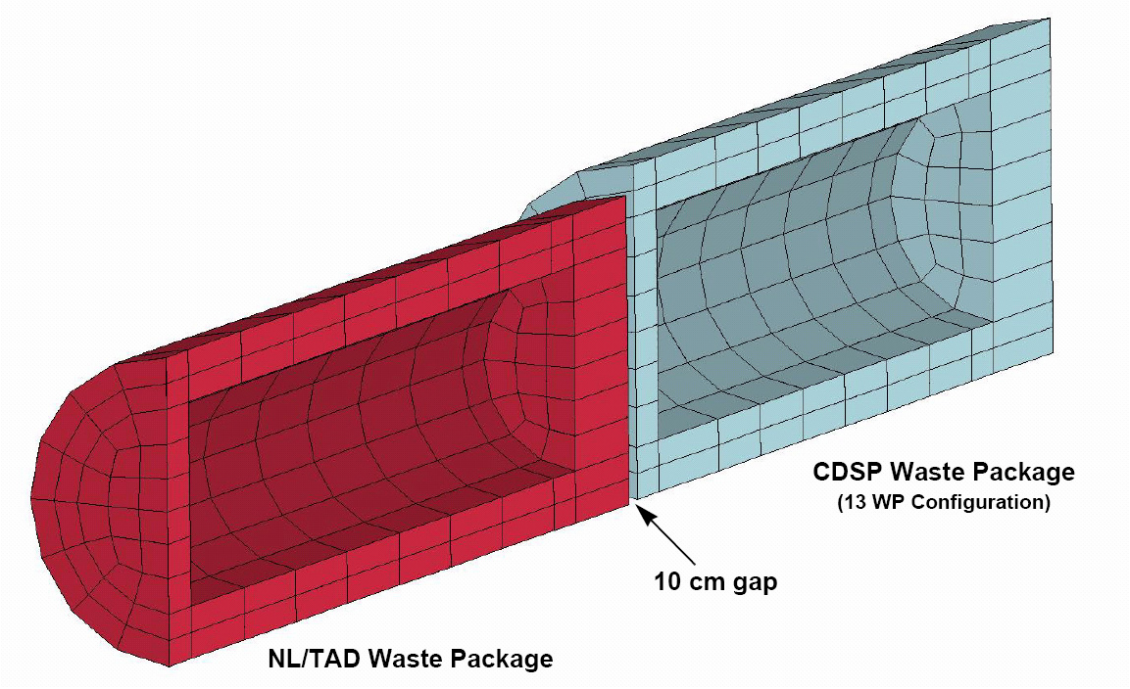

Output DTN: LL0704PA051SPC.026, file *Figures_Mech_Assessment_AMR.tar.gz.*

NOTES: Adjacent waste packages are positioned 10 cm apart.
Waste packages are shown in a cut-away view to show the interior.
NL/TAD = TAD-bearing; CDSP = codisposal; WP = waste package.

Figure 6-6. Geometry of TAD-Bearing and Codisposal Waste Packages for the 13-Waste Package Configuration (codisposal waste package analyses)

The kinematic analyses presented here use a limited series of waste packages to reasonably represent the mechanical response of waste packages in a complete emplacement drift. A typical waste emplacement drift, 600 m in length, will contain roughly 100 waste packages of various types. It is desirable to reduce the analysis complexity and run time by representing the mechanical response of the emplacement drift using the minimum number of waste packages necessary without sacrificing the validity of the analysis. To this end, several configurations of waste packages were studied to determine a representative series of waste packages (BSC 2005 [DIRS 173172], Section I-3.3.2). In these studies, the number of waste packages and the mix of package geometries in the series were varied, and results show that 11 waste packages was a reasonable configuration for analysis of waste package damage due to vibratory ground motion. The selected configuration focused on the central three waste packages, as if they were in the center of a very long string of waste packages. This condition was simulated by bounding the central three waste packages on each side by a larger-diameter codisposal waste package and three additional waste packages. This configuration is shown for the TAD-bearing waste packages in Figure 6-3.

For the current analyses, two waste package representations were created, one approximating a TAD-bearing waste package and the other a codisposal waste package. In order to expand the focus to include the two central codisposal waste packages, the 11-waste-package configuration was extended to 13 waste packages by including additional codisposal waste packages at each

end of the series, maintaining the bounding of the waste packages of interest by four waste packages. The invert and drip shield were extended beyond the waste packages (by the length of four waste packages) to accommodate relative horizontal motion of the waste packages. The 13-waste-package configuration is shown in Figure 6-4. Note that, while the 11-waste-package finite-element analyses were performed with one version of the commercially available LS-DYNA finite-element code (LS-DYNA SMP D V. 970.3858. STN: 10300-970.3858-02 [DIRS 172925]), the 13-waste-package finite-element analyses were performed with a slightly newer version of the same commercially available LS-DYNA finite-element code (V. 971.7600.398. STN: 10300-971.7600.398-00 [DIRS 178801]).

The inner diameter and end cap thickness of the waste packages were selected to approximate the inner cavity of the waste packages, to approximate any appropriate axial shift of the center of gravity, and to produce material densities on the same order as the density of other components in the finite-element representation, with the intent of maintaining reasonable analytic time steps. The geometry and mass of these waste packages are listed in Table 6-1. Adjacent waste packages are spaced 10 cm apart (Table 4-1). The TAD-bearing waste package analyses (the 11-waste-package configuration) were performed with a preliminary representation of the codisposal waste packages (Figure 6-5)). The codisposal waste package representation was updated for the codisposal waste package analyses (the 13-waste-package configuration), reflecting changes in dimensions, mass, and an axial shift of the center of gravity (Figure 6-6).

Table 6-1. Geometry and Mass of Waste Package Representations

Waste Package	TAD-Bearing Waste Package	Codisposal Waste Package (11-Waste Package Configuration)	Codisposal Waste Package (13-Waste-Package Configuration)
Outer Diameter (mm/in)	1,962.8/77.275[b]	2,126.0/83.70[c]	2,126.0/83.70[c]
Inner Diameter (mm/in)[a]	1,302.4/51.275	1,465.6/57.70	1,465.6/57.70
Length (mm/in)	5,824.5/229.312[b]	5,034.0/198.19[c]	5,272.3/207.57[c]
Bottom End Cap Thickness (mm/in)[a]	279.4/11.0	279.4/11.0	279.4/11.0
Top End Cap Thickness (mm/in)[a]	673.1/26.5	279.4/11.0	754.4/29.7
Mass (kg/lb)	73,900/163,000[d]	53,100/117,000[d]	59,700/131,600[d]

[a] Selected as convenient dimensions to approximate the inner cavity of the waste packages and to produce material densities on the same order as the density of other components in the finite-element representation (Assumption 5.3, Section 5).

Sources: [b] Table 4-7.
[c] Table 4-8.
[d] Table 4-6.

The emplacement pallets were represented as two hollow shell structures connected with beams (Assumption 5.3, Section 5). The pallet model is shown in Figure 6-7. The shell thickness of the sides and ends are 17.5 mm (0.69 in), the shell thickness of the top surface is 22.2 mm (0.875 in), and the shell thickness of the bottom surface is 9.5 mm (0.375 in). The connecting beams are $6 \times 6 \times 3/8$-inch-square tubes and were represented using the LS-DYNA Belytschko-Schwer resultant beam element (Assumption 5.8, Section 5). The emplacement pallet tubes remain intact for the kinematic analyses. The emplacement pallet geometry, mass, and properties are listed in Table 6-2. The shear area is calculated as the width of the tube (6 in) times the total thickness of

the walls in the direction in question (3/8 in + 3/8 in = 3/4 in). Thus, the shear area is 6 in × 3/4 in or 4.5 in^2. This applies in both directions because the tubes are square.

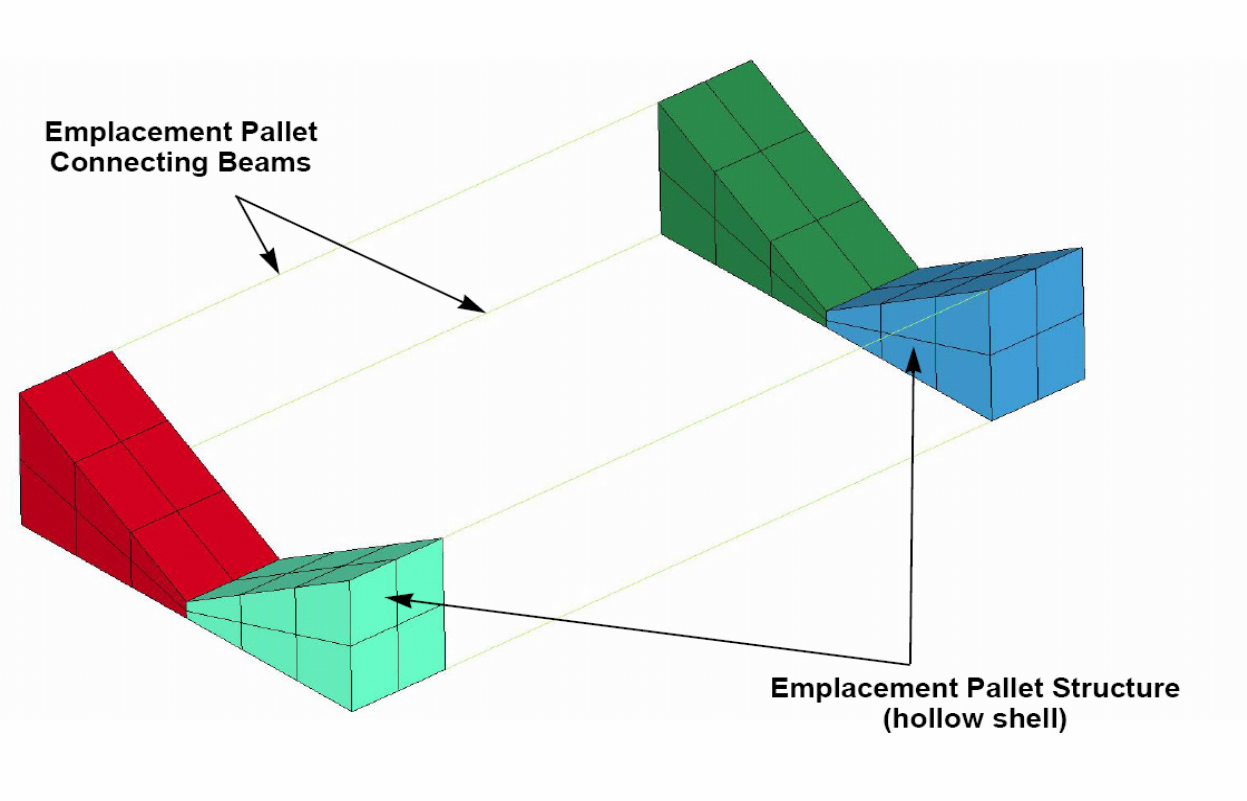

Output DTN: LL0704PA051SPC.026, file *Figures_Mech_Assessment_AMR.tar.gz.*

Figure 6-7. Finite-Element Model of a Waste Package Emplacement Pallet

Table 6-2. Emplacement Pallet Geometry, Mass and Properties

Dimensions and Mass	
Total Length (mm/in)[b]	4,148/163.3
Support Pad Length (mm/in)[b]	542.9/21.375
Width (mm/in)[b]	2,150/84.65
Height (mm/in)[b]	726.3/28.59
Support Pad Angle (degrees)[b]	30
Mass (kg/lb)[b]	1,970/4340
Shell Thicknesses	
Sides and Ends (mm/in)[b]	17.5/0.69
Top (mm/in)[b]	22.2/0.875
Bottom (mm/in)[b]	9.5/0.375
Connecting Beam Properties (6 x 6 x 3/8-inch tube)	
Area (mm^2/in^2)[c]	5,212.9/8.08
Rectangular Moment of Inertia (mm^4/in^4)[c]	1.73×10^7/41.6
Polar Moment of Inertia (mm^4/in^4)[c]	2.85×10^7/68.5
Shear Area (mm^2/in^2)[a]	2,903.2/4.5

[a] Calculated as the width of the tube (6 in) times the total wall thickness of the walls in the direction in question (3/8 in + 3/8 in = 3/4 in). Thus, the shear area is 6 in × 3/4 in or 4.5 in^2.

Sources: [b] Table 4-1.

[c] AISC 1995 [DIRS 114107], p. 1-95.

The invert is represented by a 254-mm (10-in)-thick block, slightly wider than the emplacement pallet, and extended by the length of four waste packages (about 23,400 mm/920 in). The drip shield is represented with a shell structure that approximates the drip shield dimensions (BSC 2004 [DIRS 170791], Attachment I). The lower surface of the crown of the drip shield is 2,736.3 mm (107.728 in) above the invert, which represents the approximate height from the invert to the longitudinal stiffeners of the drip shield. The sides of the drip shield are tilted inward at an angle of 2 degrees from vertical.

6.3.2.1.1 Boundary Conditions and Gravity Initialization

There is a 0.5-second period for gravity initialization before ground motion time histories are applied. The force of gravity is ramped up to full strength over the first 0.2 seconds. During gravity initialization, every node of the invert and the drip shield is held fixed in the vertical direction, and the waste packages and emplacement pallets are free to settle. Global damping with a damping constant of 200.0 is applied over the first 0.4 seconds of the gravity initialization and then ramped down to 0.01 at 0.5 seconds. The global damping factor of 200 was selected as sufficient to allow the dynamic gravity initialization to be applied in 0.4 seconds, simulating a static solution. At 0.5 seconds, the vertical restraint is removed, and every node of the invert and the drip shield is prescribed to move with the input ground acceleration (Assumptions 5.1 and 5.2, Section 5).

Ground motion is applied simultaneously in three orthogonal directions as follows; the H2 component of the ground motion is applied in the horizontal direction across the emplacement drift (X), the V component is applied in the vertical direction (Y), and the H1 component is applied in the horizontal direction along the axis of the emplacement drift (Z), as illustrated in Figure 6-8.

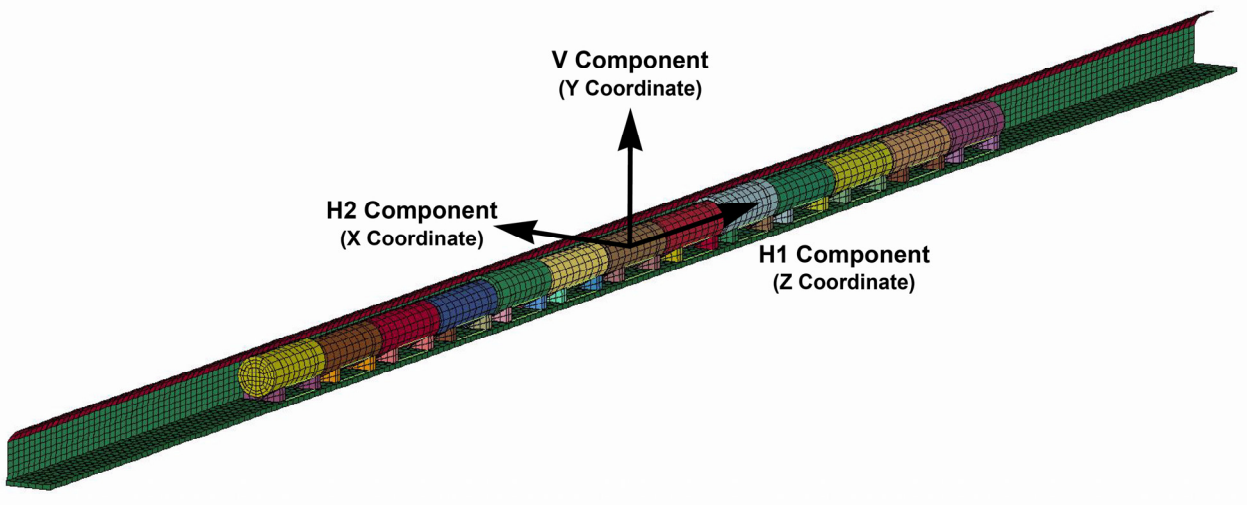

Output DTN: LL0704PA051SPC.026, file *Figures_Mech_Assessment_AMR.tar.gz*.

Figure 6-8. Ground Motion Components and Corresponding Model Coordinate Directions

6.3.2.1.2 Ground Motions

Seventeen sets of three-component ground motion acceleration time histories for four different levels of horizontal PGV are used as input. The PGV of each three-component ground motion is based on the H1 component. The four PGV values are 0.40 m/s, 1.05 m/s, 2.44 m/s, and 4.07 m/s. The 0.40 m/s PGV level ground motion time histories were scaled from 1.05 m/s PGV level ground motions by applying a scale factor of 0.380952 (0.40/1.05). The 4.07 m/s PGV level ground motion time histories were scaled from 5.35 m/s PGV level ground motions by applying a scale factor of 0.760748 (4.07/5.35) (Assumption 5.16, Section 5). While linear scaling is an approximation, the difference between linearly scaled values and values produced by more sophisticated scaling methods is negligible relative to other uncertainties in the calculations. The 17 realizations referred to in this section correspond to the ground motions as shown in Table 6-3. Typical ground motion time histories are shown in Figure 6-9. Ground motion time histories are located in the following data tracking numbers (DTNs): for 1.05 m/s, MO0610AVDTM105.002 [DIRS 178664], file *Time Histories-Acceleration.zip*; for 2.44 m/s, MO0403AVDSC106.001 [DIRS 168891], file *ats.zip*; and for 5.35 m/s, MO0403AVTMH107.003 [DIRS 168892], file *ats.zip*.

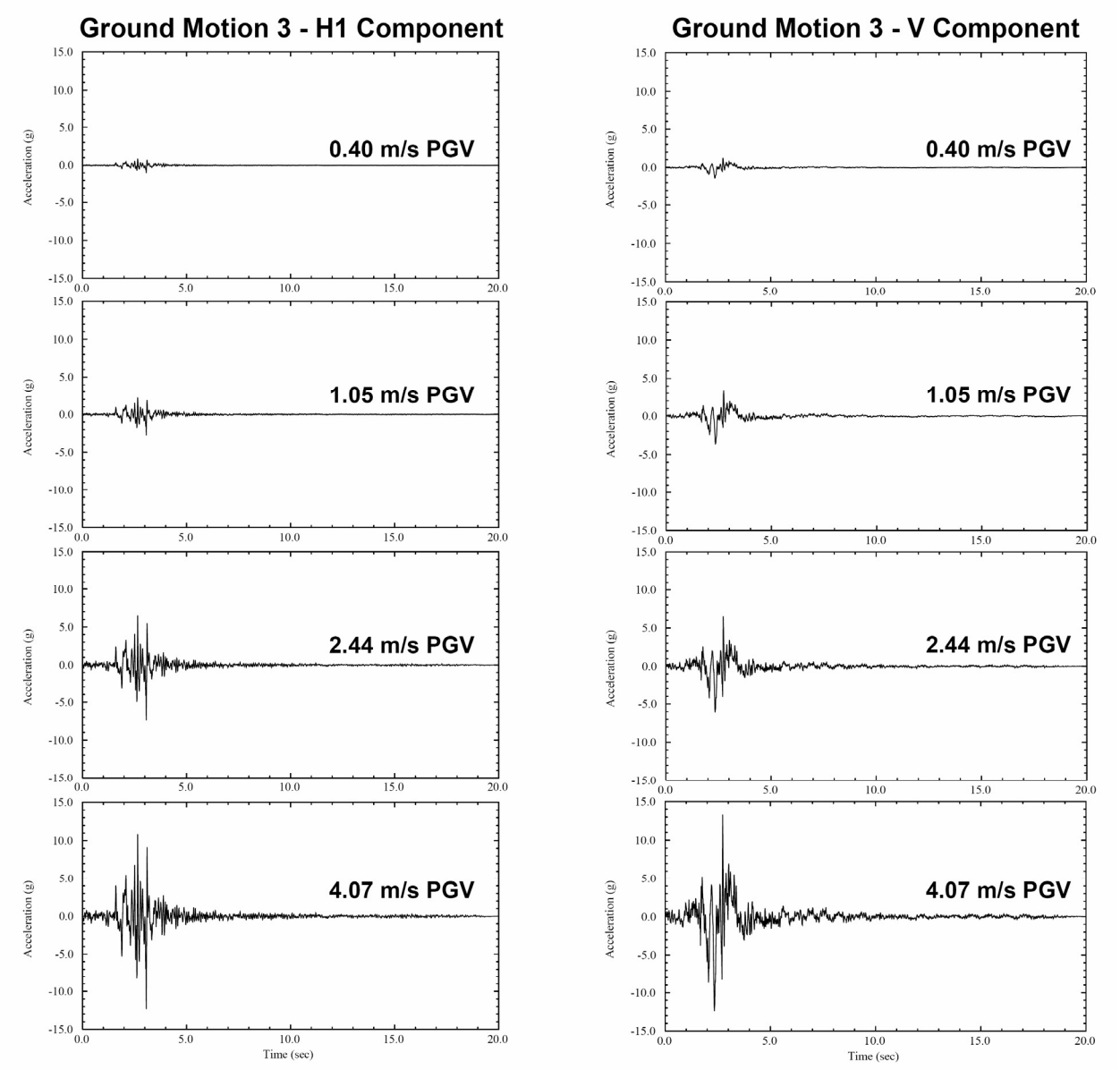

Sources: PGV 1.05 – DTN: MO0610AVDTM105.002 [DIRS 178664], file *Time Histories-Acceleration.zip*; PGV 2.44 – DTN: MO0403AVDSC106.001 [DIRS 168891], file *ats.zip*; PGV 5.35 – DTN: MO0403AVTMH107.003 [DIRS 168892], file *ats.zip*.

NOTES: The H1 and V components for Ground Motion 3 are shown for each PGV level. The 0.40 m/s PGV level is scaled from 1.05 m/s PGV, and the 4.07 m/s PGV level is scaled from 5.35 m/s PGV (not shown).

Figure 6-9. Typical Acceleration Time Histories

Table 6-3. Relationship between Realization Number and Ground Motion Number

Realization Number	Ground Motion Number
1	17
2	16
3	3
4	2
5	11
6	4
7	12
8	5
9	15
10	9
11	8
12	6
13	10
14	1
15	7
16	14
17	13

Source: BSC 2005 [DIRS 173172], Attachment X, Table X-1;
DTN: MO0508SPAMECHA.000 [DIRS 181067],
AttachmentX.zip, file *All_3_Sampling_Groups.txt*.

6.3.2.1.3 Material Properties

The representations of the TAD-bearing and codisposal waste packages are hollow cylinders with the density chosen so that they have the correct mass of the actual package. The waste packages and emplacement pallets are characterized with elastic properties (Assumption 5.9, Section 5). The weight of the TAD-bearing waste package is taken to be 73.9 mT (163,000 lbs) (Table 4-6). In the 11-waste-package configuration, the weight of the codisposal waste package is 53.1 mT (117,000 lbs) (Table 4-6), and in the 13-waste-package configuration, the weight of the codisposal waste package is 59.7 mT (131,600 lbs) (Table 4-6). The density of the emplacement pallets is also chosen to give the correct emplacement pallet mass. The emplacement pallet weight is 1.97 mT (4,340 lbs) (SNL 2007 [DIRS 179354], Table 4-3). The modulus of elasticity and Poisson's ratio are the same for all components (Assumption 5.11, Section 5). The unit weight and linear elastic material properties for each component are summarized in Table 6-4.

Table 6-4. Material Properties for the Waste Packages and Emplacement Pallets in the Kinematic Analyses

	TAD-Bearing Waste Package	Codisposal Waste Package (11-Waste Package Config.)	Codisposal Waste Package (13-Waste Package Config.)	Emplacement Pallet Shells	Emplacement Pallet Beams
Unit weight (Mass density)[a]	6,810 kg/m^3 (0.2461 lbs/in^3)	5,280 kg/m^3 (0.1906 lbs/in^3)	5,300 kg/m^3 (0.1913 lbs/in^3)	7,890 kg/m^3 (0.2852 lbs/in^3)	7,830 kg/m^3 (0.283 lbs/in^3)
Modulus of elasticity[b]	200 GPa (29.0 × 10^6 psi)	200 GPa (29.0 × 10^6 psi)	200 GPa (29.0 × 10^6 psi)	200 GPa (29.0 × 10^6 psi)	200 GPa (29.0 × 10^6 psi)
Poisson's ratio[b]	0.29	0.29	0.29	0.29	0.29

Sources: [a] The densities were calculated as the waste package weight divided by the waste package volume.
[b] Assumption 5.11, Section 5.

The coefficients of friction for metal-to-metal and metal-to-rock contact are random parameters that differ for each waste package and emplacement pallet set. The static and dynamic friction coefficients are taken to be the same, and the values range between 0.2 and 0.8 (Assumptions 5.4 and 5.6, Section 5). The waste packages and emplacement pallets are named A to S, as shown in Figure 6-10. The coefficients of friction for 19 waste packages for each of the 17 realizations for metal-to-metal and metal-to-rock contact are presented in Table 6-5 and Table 6-6, respectively. The coefficients of friction for the 19 waste packages are a subset of values for 21 waste packages (BSC 2005 [DIRS 173172], Attachment X; DTN: MO0508SPAMECHA.000 [DIRS 181067], *AttachmentX.zip*, file *All_3_Sampling_Groups.txt*), from which the middle 19 packages are utilized. Metal-to-metal contact includes waste package to emplacement pallet, waste package to drip shield, waste package to waste package, emplacement pallet to emplacement pallet and emplacement pallet to drip shield. Metal-to-rock contact includes emplacement pallet to invert and waste package to invert.

The coefficients of friction are defined such that if two waste packages are in contact, then the governing metal-to-metal coefficient of friction is the value associated with the waste package closer to the central waste package, which is waste package J. For example, if packages I and J are in contact, then the coefficient of friction for J governs; and if packages K and L are in contact, then the coefficient of friction for K governs. The same is true for two emplacement pallets in contact, and a waste package and an emplacement pallet in contact. The metal-to-metal friction coefficient associated with the part closer to the center always governs (Figure 6-11). The friction tables addressed contact between a waste package and its associated pallet. Because the tables did not address contact between adjacent waste packages and pallets, this method was selected to apply the friction table values to adjacent contact as a straightforward and systematic approach.

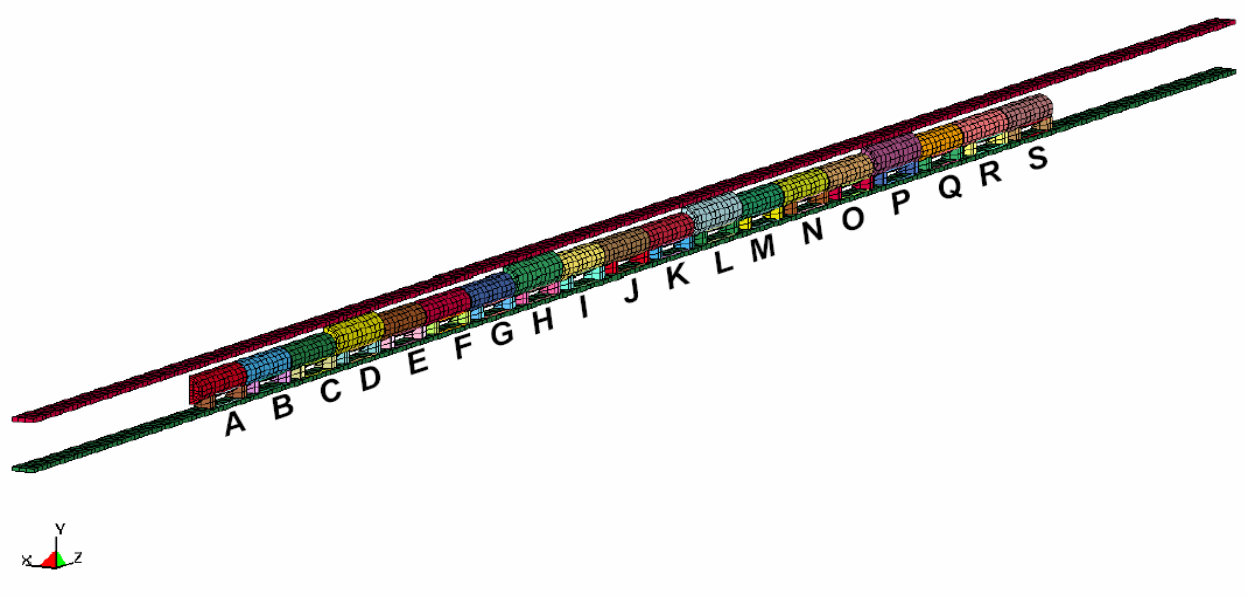

Output DTN: LL0704PA051SPC.026, file *Figures_Mech_Assessment_AMR.tar.gz.*

NOTE: The letters A to S represent the naming convention, with J being the center waste package. The 11-waste-package configuration includes waste packages E to O, and the 13-waste-package configuration includes waste packages D to P.

Figure 6-10. Naming Convention Used for Assigning Friction Values to a Series of 19 Waste Packages

Table 6-5. Metal-to-Metal Coefficients of Friction

Rlz #	A	B	C	D	E	F	G	H	I	J
1	0.65366	0.32093	0.41049	0.59397	0.62892	0.60661	0.75327	0.57638	0.76666	0.51524
2	0.29918	0.57656	0.22729	0.29634	0.37167	0.42698	0.58001	0.74702	0.71202	0.45004
3	0.2101	0.2978	0.4157	0.42111	0.21613	0.39713	0.64045	0.68395	0.38015	0.74051
4	0.24688	0.76289	0.77047	0.72159	0.46025	0.73011	0.6898	0.77928	0.59089	0.69082
5	0.75363	0.40389	0.70558	0.5344	0.26819	0.37264	0.25901	0.59054	0.5031	0.25947
6	0.71345	0.76851	0.54769	0.46224	0.27656	0.54725	0.35055	0.21888	0.63054	0.61473
7	0.4989	0.5181	0.24096	0.58065	0.30793	0.50815	0.39718	0.26039	0.46047	0.39442
8	0.5422	0.34158	0.29694	0.67685	0.55815	0.33421	0.54781	0.35253	0.3539	0.56025
9	0.3427	0.43203	0.68965	0.77302	0.59291	0.64669	0.22696	0.63342	0.25203	0.62505
10	0.55884	0.47415	0.44808	0.21811	0.4267	0.22592	0.61641	0.38865	0.67503	0.70393
11	0.39109	0.61478	0.73592	0.31189	0.48914	0.71904	0.27611	0.27828	0.5235	0.30831
12	0.77613	0.70504	0.32481	0.24897	0.74443	0.77381	0.44932	0.50972	0.28727	0.44546
13	0.41564	0.21201	0.51689	0.36124	0.67096	0.67343	0.7712	0.33653	0.75305	0.28574
14	0.66831	0.67482	0.61252	0.76417	0.38496	0.29131	0.32614	0.53427	0.21966	0.37392
15	0.46891	0.64929	0.3414	0.65683	0.71042	0.58101	0.48249	0.69819	0.43675	0.77906
16	0.32215	0.25919	0.57013	0.40938	0.54539	0.25453	0.44579	0.46026	0.57408	0.2031
17	0.61847	0.48698	0.65764	0.50213	0.7805	0.4677	0.72451	0.44673	0.31337	0.52999

Table 6-5. Metal-to-Metal Coefficients of Friction (Continued)

Rlz #	K	L	M	N	O	P	Q	R	S
1	0.75102	0.5157	0.35643	0.69366	0.73239	0.32978	0.45509	0.47652	0.33038
2	0.6042	0.54777	0.79724	0.4289	0.60267	0.66686	0.5569	0.53298	0.58714
3	0.30566	0.39408	0.72101	0.47896	0.62874	0.49866	0.39225	0.3118	0.76816
4	0.50778	0.63458	0.58404	0.56918	0.48607	0.75819	0.35277	0.41628	0.61648
5	0.25645	0.24232	0.2559	0.77613	0.7796	0.47424	0.7833	0.40907	0.2673
6	0.22337	0.67929	0.53094	0.33738	0.38909	0.63465	0.66789	0.36621	0.36401
7	0.47226	0.34823	0.20738	0.50467	0.20838	0.25892	0.28686	0.2363	0.29154
8	0.42133	0.33122	0.68088	0.20348	0.46616	0.54976	0.74678	0.51548	0.44214
9	0.56144	0.46093	0.44477	0.521	0.26916	0.41464	0.52274	0.76424	0.76228
10	0.31181	0.77204	0.76396	0.30025	0.36628	0.21822	0.2544	0.21257	0.52024
11	0.64231	0.30564	0.51383	0.26906	0.28635	0.77079	0.30623	0.64481	0.47137
12	0.53103	0.43039	0.29137	0.70908	0.71439	0.71873	0.6035	0.77892	0.68733
13	0.39125	0.55866	0.63641	0.38089	0.30884	0.59673	0.50447	0.58825	0.50157
14	0.69048	0.21786	0.6201	0.74224	0.44618	0.34999	0.44056	0.27381	0.6299
15	0.37143	0.59041	0.33604	0.63661	0.56526	0.55725	0.63521	0.71355	0.2114
16	0.79285	0.73881	0.38888	0.34412	0.68342	0.28076	0.20709	0.66586	0.6973
17	0.72249	0.70122	0.45875	0.61745	0.53808	0.38202	0.70639	0.58018	0.38288

Sources: BSC 2005 [DIRS 173172], Table X-1; DTN: MO0508SPAMECHA.000 [DIRS 181067], *AttachmentX.zip*, file *All_3_Sampling_Groups.txt*.

NOTE: Rlz # = Realization number.

Table 6-6. Metal-to-Rock Coefficients of Friction

Rlz #	A	B	C	D	E	F	G	H	I	J
1	0.42599	0.75925	0.49458	0.53287	0.31878	0.35173	0.74103	0.45704	0.69753	0.54255
2	0.30763	0.21838	0.26419	0.25372	0.21881	0.47556	0.62115	0.30541	0.78146	0.72809
3	0.70431	0.32817	0.52106	0.71835	0.46306	0.23268	0.54727	0.66563	0.47206	0.28081
4	0.29588	0.53062	0.7556	0.60512	0.70412	0.26512	0.50095	0.75224	0.31661	0.51729
5	0.25515	0.71205	0.67405	0.63946	0.51949	0.31998	0.21052	0.4118	0.54475	0.25932
6	0.60713	0.39082	0.21636	0.51602	0.59847	0.65986	0.58546	0.78554	0.63455	0.77163
7	0.46305	0.42466	0.30311	0.55353	0.36894	0.48884	0.37835	0.69816	0.57661	0.38194
8	0.49958	0.2369	0.63152	0.37594	0.68582	0.76938	0.64869	0.6382	0.24013	0.42889
9	0.76426	0.49614	0.57289	0.28445	0.40191	0.76276	0.34456	0.37726	0.30423	0.67262
10	0.66982	0.29126	0.72884	0.7718	0.64684	0.57507	0.33072	0.3751	0.60203	0.61763
11	0.53046	0.59736	0.44766	0.75096	0.73761	0.61313	0.2599	0.22524	0.74656	0.73279
12	0.23096	0.69271	0.6006	0.45188	0.27697	0.54717	0.69196	0.50715	0.40301	0.45438
13	0.6353	0.78792	0.3432	0.30981	0.2418	0.6487	0.79918	0.56208	0.49327	0.58555
14	0.39148	0.36413	0.76763	0.66907	0.5721	0.41082	0.72599	0.60736	0.22821	0.32038
15	0.36656	0.62453	0.39484	0.41988	0.42366	0.4285	0.4673	0.54813	0.35977	0.36674
16	0.77983	0.46813	0.44287	0.39528	0.50229	0.30264	0.4403	0.2652	0.44273	0.65572
17	0.55932	0.57103	0.31062	0.21597	0.7717	0.70299	0.29046	0.3228	0.66081	0.21857

Table 6-6. Metal-to-Rock Coefficients of Friction (Continued)

Rlz #	K	L	M	N	O	P	Q	R	S
1	0.38877	0.57453	0.79893	0.56298	0.34316	0.54326	0.52918	0.20182	0.51192
2	0.75214	0.32463	0.20062	0.60189	0.27448	0.6097	0.72886	0.76432	0.68681
3	0.60163	0.61272	0.25471	0.64311	0.72375	0.27107	0.78317	0.29239	0.78193
4	0.35038	0.43717	0.46407	0.26659	0.77564	0.34663	0.73924	0.36955	0.7167
5	0.69165	0.54699	0.35103	0.67948	0.50768	0.46019	0.24674	0.77885	0.21525
6	0.31924	0.72421	0.61791	0.79615	0.45665	0.41425	0.36236	0.60087	0.37303
7	0.48086	0.22705	0.73956	0.34598	0.3188	0.586	0.44123	0.72705	0.2458
8	0.72895	0.6255	0.28395	0.2151	0.57393	0.22714	0.60287	0.32736	0.43934
9	0.64526	0.23701	0.38195	0.44947	0.3943	0.26013	0.33219	0.66914	0.59323
10	0.27976	0.73971	0.72279	0.33801	0.68688	0.64201	0.48012	0.56923	0.28825
11	0.76485	0.39674	0.6633	0.51543	0.25447	0.72468	0.22319	0.43012	0.56685
12	0.41936	0.27781	0.52803	0.27384	0.21461	0.7963	0.50208	0.46139	0.32037
13	0.55591	0.7672	0.42402	0.53312	0.64854	0.68441	0.57084	0.54066	0.53606
14	0.53052	0.46441	0.64702	0.44138	0.6173	0.38265	0.68507	0.39297	0.63893
15	0.24573	0.51169	0.49723	0.72925	0.73842	0.50685	0.64582	0.51668	0.40874
16	0.21804	0.66316	0.31832	0.38214	0.52296	0.31738	0.39991	0.64781	0.75924
17	0.4937	0.37117	0.56647	0.73483	0.41704	0.75098	0.2781	0.24537	0.46195

Sources: BSC 2005 [DIRS 173172], Table X-2; DTN: MO0508SPAMECHA.000 [DIRS 181067], *AttachmentX.zip*, file *All_3_Sampling_Groups.txt*.

NOTE: Rlz # = Realization number.

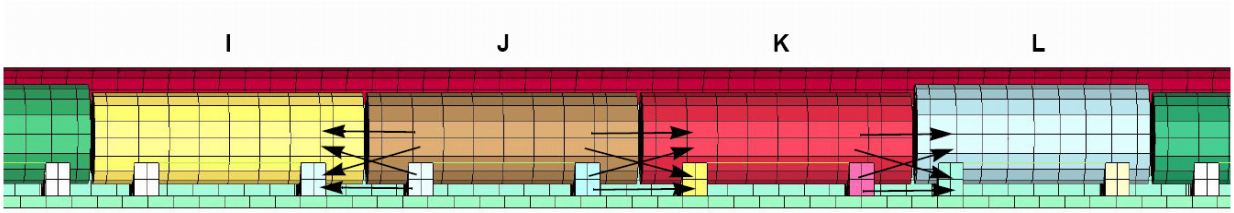

Output DTN: LL0704PA051SPC.026, file *Figures_Mech_Assessment_AMR.tar.gz*.

NOTE: Arrows indicate which friction coefficients are used when units interact horizontally. The friction coefficients associated with the J waste package and emplacement pallet are used for interactions with I and K waste packages and emplacement pallets. The friction coefficients associated with the K waste package are used for interactions with the L waste package and emplacement pallet.

Figure 6-11. Convention for Friction Coefficients between Waste Packages

All interactions between components in the finite-element model are defined using surface-to-surface contact. The contact interfaces for interaction between adjacent waste packages are defined based on segment sets. This reduced the computational intensity of these contact interfaces by limiting the scope of the contact search algorithm. All other contact interfaces are defined using part-to-part contact, where the contact surfaces are determined by LS-DYNA based on all surfaces of the parts. Interface contact definitions and parameters are discussed in Hallquist (1998 [DIRS 155373], Section 23) and *LS-DYNA Keyword User's Manual* (Livermore Software Technology Corporation 2003 [DIRS 166841], Section 6).

6.3.2.2 Detailed Damage Analyses

This section describes the detailed analyses of a single waste package impacting another waste package or an emplacement pallet. These analyses were conducted to provide more precise estimates of damage induced to the waste package as a function of impact parameters such as location-, angle-, and velocity-determined rigid body analyses described in the previous section. These detailed analyses are used to produce lookup tables of damage values as a function of impact parameters. Lookup tables are produced for both waste package-to-waste package and waste package-to-pallet impacts at each PGV level.

6.3.2.2.1 Description of Finite-Element Models for Detailed Damage Analyses

Detailed analyses were conducted for both the TAD-bearing and the codisposal waste packages. Each waste package was analyzed with intact and degraded internal structure and an OCB thickness of 23 mm. In addition, the degraded case was also analyzed with a thinned OCB of 17 mm. The TAD-bearing waste package with intact internals includes a 50.8-mm-thick inner vessel, 25.4-mm-thick TAD canister, and contents. The codisposal waste package with intact internals includes a 50.8-mm-thick inner vessel and contents. The different representations of the waste packages used in the detailed analyses are shown in Figure 6-12 to Figure 6-15. Figure 6-16 shows the finite element representation of the pallet structure.

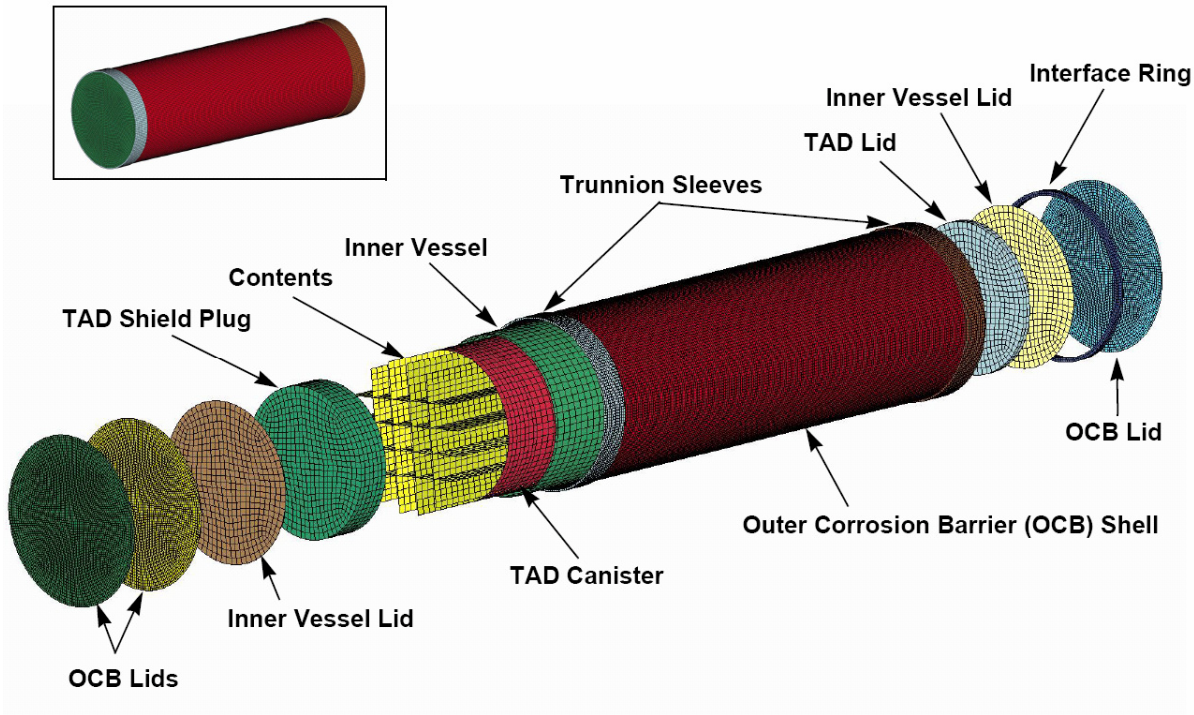

Output DTN: LL0704PA051SPC.026, file *Figures_Mech_Assessment_AMR.tar.gz.*

Figure 6-12. Detailed Representation of the TAD-Bearing Waste Package with Intact Internals Used for Waste Package Damage Lookup Table Analyses

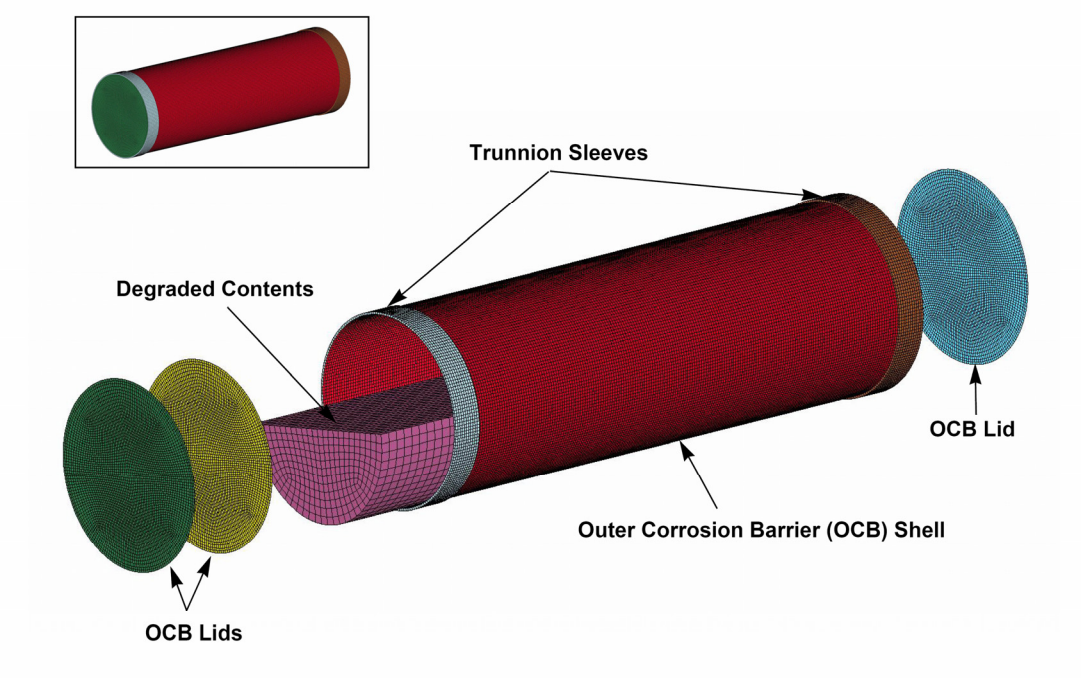

Output DTN: LL0704PA051SPC.026, file *Figures_Mech_Assessment_AMR.tar.gz.*

Figure 6-13. Detailed Representation of the TAD-Bearing Waste Package with Degraded Internals Used for Waste Package Damage Lookup Table Analyses

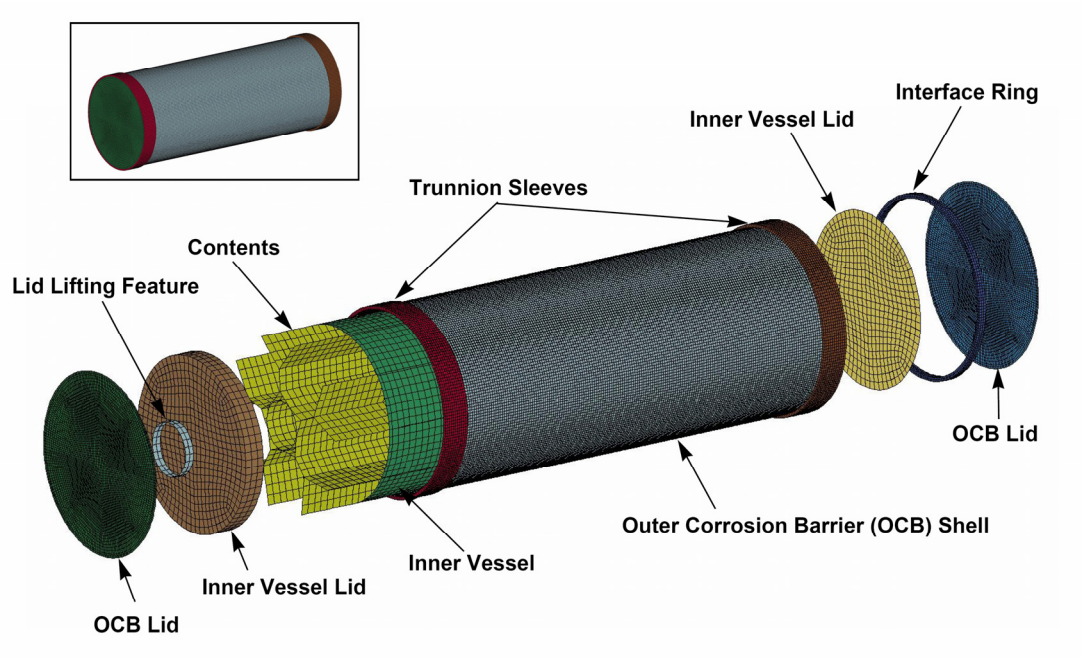

Output DTN: LL0704PA051SPC.026, file *Figures_Mech_Assessment_AMR.tar.gz.*

Figure 6-14. Detailed Representation of the Codisposal Waste Package with Intact Internals Used for Waste Package Damage Lookup Table Analyses

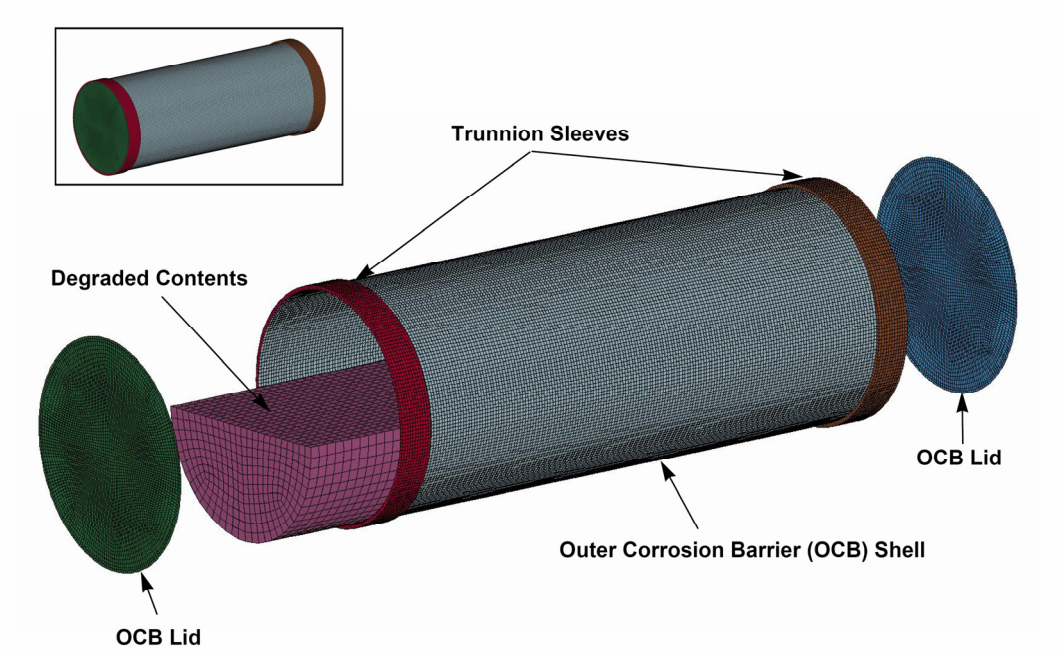

Output DTN: LL0704PA051SPC.026, file *Figures_Mech_Assessment_AMR.tar.gz.*

Figure 6-15. Detailed Representation of the Codisposal Waste Package with Degraded Internals Used for Waste Package Damage Lookup Table Analyses

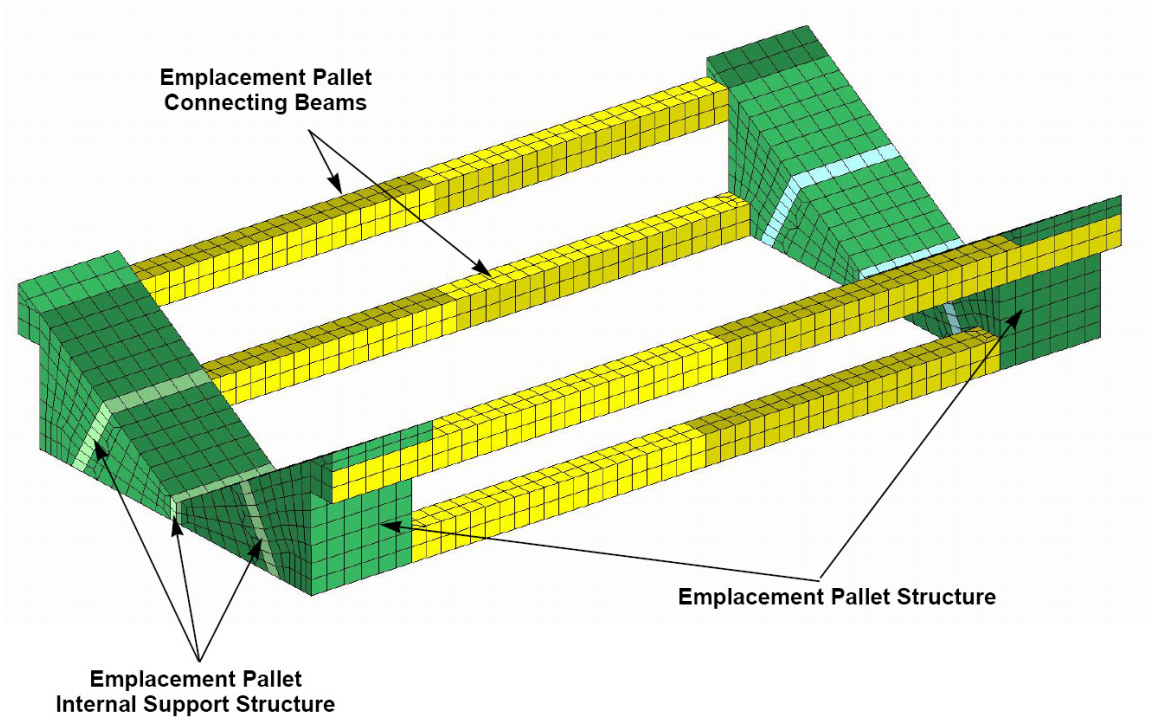

Output DTN: LL0704PA051SPC.026, file *Figures_Mech_Assessment_AMR.tar.gz.*

NOTE: The connecting beams are removed for analyses with degraded internals.

Figure 6-16. Detailed Representation of the Emplacement Pallet Used for Waste Package Damage Lookup Table Analyses

The model of the TAD-bearing waste package with intact internals is an approximate representation based on (a) the Naval Long waste package OCB and inner vessel, and (b) an approximate representation of a TAD canister and fuel basket (Figure 6-12 and Assumption 5.23, Section 5). The model of the codisposal waste package with intact internals is an approximate representation based on the 5-DHLW/DOE SNF-Long codisposal waste package OCB, inner vessel, and fuel basket (Figure 6-14 and Assumption 5.23, Section 5).

Because the behavior of the Alloy 22 OCB is the focus of the analyses for the waste package models, the material properties of the inner vessel and other components of intact internals are modeled using the properties of Stainless Steel Type 316 as an approximation, and the fuel basket representations do not explicitly include all components of the baskets. Both the Alloy 22 and Stainless Steel Type 316 components are modeled as bilinear elastic-plastic with kinematic hardening. Material densities are scaled to obtain the correct mass for each component.

The degraded internals (Figure 6-13 and Figure 6-15) are modeled as a Tresca material with a 0° friction angle, cohesion of 50 kPa (7.25 psi), and a bulk modulus of 10 MPa (1,450 psi) (Assumption 5.15, Section 5). The internals have a porosity of 50% (Assumption 5.10, Section 5). The density of the degraded internals is chosen so that the mass of the degraded internals is equal to the mass of the intact internals. The emplacement pallet model is an approximate representation (Assumption 5.3, Section 5). The connecting beams are modeled with Stainless Steel Type 316 properties, and the rest of the pallet structure is modeled with Alloy 22 properties. A thickness reduction equal to the OCB thickness reduction is also applied to the Alloy 22 plates of the pallet for each analysis.

6.3.2.2.2 Temperature-Dependent Material Properties

A temperature of 60°C (Assumption 5.7, Section 5) is used for the mechanical properties of Alloy 22 and Stainless Steel Type 316 in the detailed analyses of waste package-to-waste package and waste package-to-pallet impacts. The temperature-dependent mechanical properties are provided in Appendix A. A sensitivity study was performed with a model of the TAD-bearing waste package for waste package-to-pallet impacts to determine the significance of Assumption 5.7 in the period before the temperature drops below 60°C. The mechanical properties for 90°C and 150°C were determined in a manner similar to properties for 60°C, as described in Appendix A. The temperature-dependent mechanical properties (modulus of elasticity, yield strength, and tangent modulus) are summarized in Table 6-7.

Table 6-7. Mechanical Properties of Alloy 22 and Stainless Steel Type 316 at 60°C, 90°C, and 150°C

Property	Alloy 22			Stainless Steel Type 316		
	60°C	90°C	150°C	60°C	90°C	150°C
Modulus of Elasticity (GPa)	204	203	199	192	190	186
Yield Strength (MPa)	350	340	310	193	180	161
Tangent Modulus (GPa)	1.94	1.89	1.78	1.58	1.61	1.61

Source: Appendix A.

A single waste package-to-pallet impact analysis was performed for each of the temperatures. Analyses were performed for models with a 23-mm-thick OCB, for both intact internals and degraded internals. For the analyses with intact internals, the impact velocity was 5 m/s, the impact angle was +6 degrees, and the impact location was the 1/4-point. For the analyses with degraded internals, the impact velocity was 3 m/s, the impact angle was −6 degrees, and the impact location was the 3/4-point. The resulting damaged areas for each analysis are summarized in Table 6-8 and Table 6-9. As can be seen from the tables, the damaged area is relatively insensitive to changes in mechanical properties for temperature. Thus, the significance of using 60°C in the period of time before the temperature drops below 60°C is small. This was an independent sensitivity analysis, and the damage values given in Table 6-8 and Table 6-9 are for comparison only and are not used in the analyses presented in subsequent sections of this report. Input and output files for these analyses can be found in output DTN: LL0703PA031SPC.015, files *NavalLong_TAD_WPP_temperature_analyses.tar.gz* and *NavalLong_TAD_WPP_temperature _crvfiles.tar.gz*.

Table 6-8. Damaged Area for a Waste Package-to-Pallet Impact Analysis at 5 m/s, +6 Degrees, and1/4-Point for 23-mm-Thick OCB with Intact Internals at 60°C, 90°C, and 150°C

Temperature	Damaged Area at 90% Yield Strength (m^2)	Damaged Area at 100% Yield Strength (m^2)	Damaged Area at 105% Yield Strength (m^2)
60°C	0.0000	0.0000	0.0000
90°C	0.0000	0.0000	0.0000
150°C	0.0000	0.0000	0.0000

Output DTN: LL0703PA031SPC.015, file *NavalLongTAD_WPP_temperature_analyses_DA.xls,* sheet "i23."

Table 6-9. Damaged Area for a Waste Package-to-Pallet Impact Analysis at 3 m/s, −6 Degrees, and 3/4-Point for 23-mm-Thick OCB with Degraded Internals at 60°C, 90°C, and 150°C

Temperature	Damaged Area at 90% Yield Strength (m^2)	Damaged Area at 100% Yield Strength (m^2)	Damaged Area at 105% Yield Strength (m^2)
60°C	0.4486	0.2191	0.1289
90°C	0.4494	0.2226	0.1289
150°C	0.4451	0.2157	0.1160

Output DTN: LL0703PA031SPC.015, file *NavalLongTAD_WPP_temperature_analyses_DA.xls,* sheet "d23."

6.3.2.2.3 Analysis Configurations

The impact configurations for the waste package-to-waste package and the waste package-to-pallet damage lookup table analyses were determined by considering the range of impact configurations calculated from the kinematic analyses. Also, in order to reduce the total number of analyses to the minimum necessary number, choices for impact angles and impact locations were made based on conservatism and on the relative significance of the damaged areas computed for the two types of impact events. While there is a 10-cm gap between waste packages, each package rests on its pallet under gravity. Thus, there are significantly fewer waste package-to-waste package impacts than waste package-to-pallet impacts in the kinematic analyses. Furthermore, the damaged area computed from waste package-to-waste package impacts is generally far less than the damaged area computed from waste package-to-pallet impacts (see Sections 6.3.2.2.6 and 6.3.2.2.7). Therefore, it is not necessary to consider multiple

impact angles for the waste package-to-waste package damage lookup table analyses, but multiple angles are considered for the waste package-to-pallet analyses. Multiple impact locations are considered for both types of analyses.

The impact velocities, angles, and locations for TAD-bearing waste package-to-TAD-bearing waste package impacts and the impact forces, angles, and locations for TAD-bearing waste package-to-pallet impacts in the kinematic analyses are available in output DTN: LL0704PA048SPC.023, file *NavalLong_TAD_kinematic_analyses.tar.gz*. The impact velocities, angles, and locations for codisposal waste package-to-TAD-bearing waste package impacts and the impact forces, angles, and locations for codisposal waste package-to-pallet impacts in the kinematic analyses are available in output DTN: LL0704PA049SPC.024, file *CDSP_kinematic_analyses.tar.gz*.

For waste package-to-waste package impacts, the impact velocity is defined as the relative velocity between the packages in the direction along the axis of the drift (Figure 6-8). The impact angle is defined as the angle between the planes of the lids of the two waste packages. The impact location is defined as the normalized distance between the impact point and the outer circumference of the waste package that is being impacted on the lid by the other package. The distance is normalized by the outer diameter of the waste package that is being impacted on the lid by the other package.

For both the TAD-bearing waste package-to-TAD-bearing waste package and codisposal waste package-to-TAD-bearing waste package analyses, an impact angle of 1.5 degrees was chosen. While impacts with larger angles occur in the kinematic analyses, most of the impacts have angles on the order of 1.5 degrees or less. Five impact locations were used for the waste package-to-waste package analyses. Results of the kinematic analyses show no impact for TAD-bearing waste package-to-TAD-bearing waste package and codisposal waste package-to-TAD-bearing waste package has an impact location magnitude greater than 0.30. Thus, the five impact locations utilized for both types of waste package-to-waste package analyses are −0.30, −0.15, 0.00, 0.15, and 0.30, which are shown in Figure 6-17 for TAD-bearing-to-TAD-bearing waste packages and Figure 6-18 for codisposal-to-TAD-bearing waste packages. For all analyses, the waste packages are oriented in the same direction. For TAD-bearing-to-TAD-bearing impacts, damaged area is recorded for both the left and right waste packages (WP1 and WP2, respectively). For codisposal waste package-to-TAD-bearing waste package impacts, the damaged area is only recorded for the codisposal package. Notice from Figure 6-18 that the codisposal waste package is always the package on the left. The sleeve (or trunnion sleeve) overhangs the waste packages on the left side. When the codisposal waste package is on the left, it is the right side of the codisposal package that is involved in the impact. Thus, this is the more severe configuration in terms of damage to the codisposal package, since the overhanging sleeve would tend to protect the outer corrosion barrier of the waste package. Analyses for the other configuration with the codisposal package on the right were not performed.

The ranges of impact velocities for the TAD-bearing waste package-to-TAD-bearing waste package and codisposal waste package-to-TAD-bearing waste package analyses were chosen to encompass the maximum impact velocities observed in the corresponding kinematic analyses.

The lower limit for impact velocities was a velocity that yields zero damaged area. The impact velocities utilized for both sets of analyses are given in Section 6.3.2.2.6.

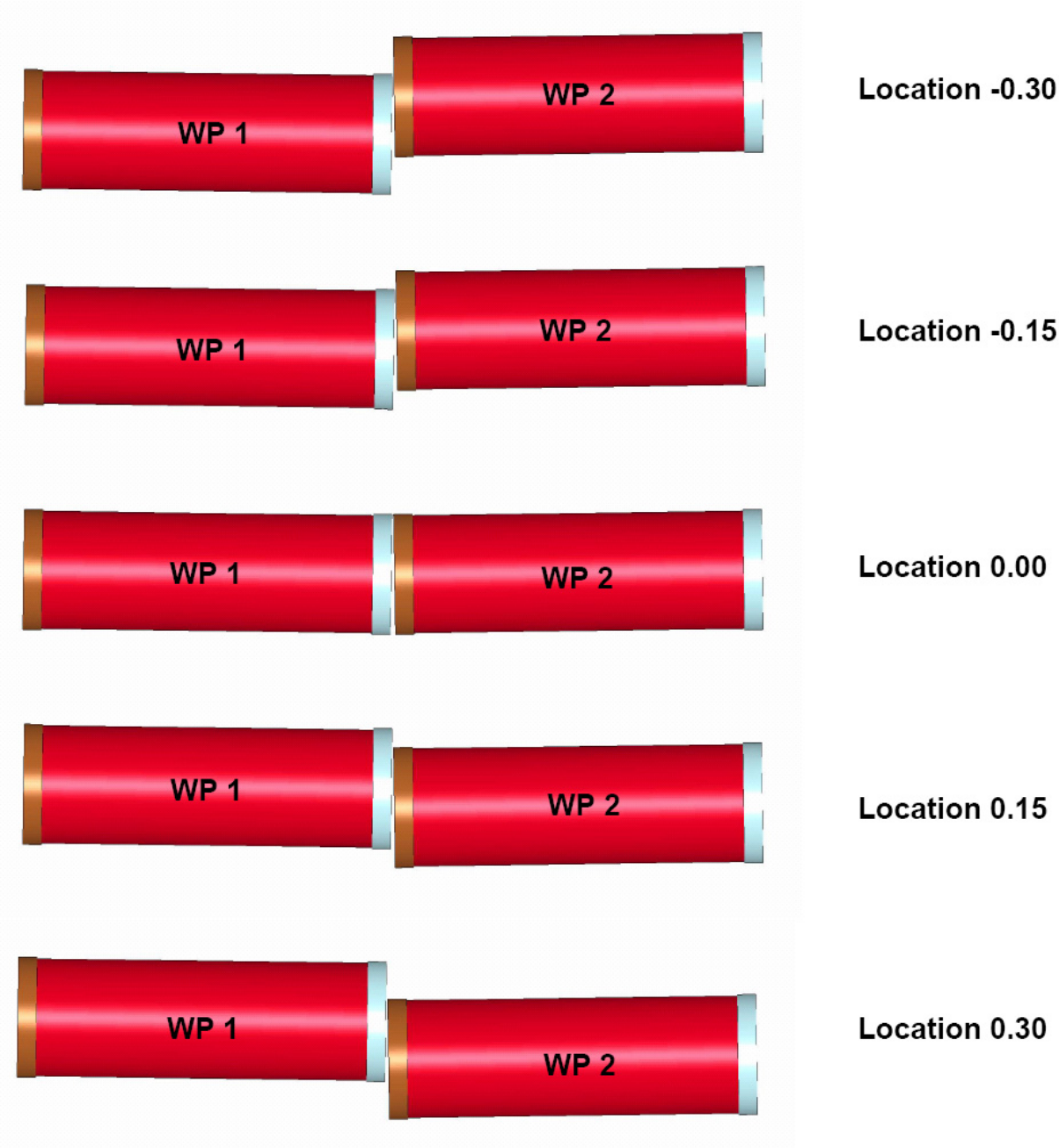

Output DTN: LL0704PA051SPC.026, file *Figures_Mech_Assessment_AMR.tar.gz.*

NOTES: All analyses were performed with an impact angle of 1.5 degrees.
WP = waste package.

Figure 6-17. Impact Location Configurations for TAD-Bearing Waste Package-to-TAD-Bearing Waste Package Damage Lookup Table Analyses

Output DTN: LL0704PA051SPC.026, file *Figures_Mech_Assessment_AMR.tar.gz.*

NOTES: All analyses were performed with an impact angle of 1.5 degrees.
CDSP = codisposal; NL/TAD = TAD-bearing; WP = waste package.

Figure 6-18. Impact Location Configurations for Codisposal Waste Package-to-TAD-Bearing Waste Package Damage Lookup Table Analyses

For waste package-to-pallet impacts, the impact velocity is defined as shown in Figure 6-19. The waste package is prescribed to have an initial velocity such that it impacts one half of the pallet cradle in the direction normal to the surface of the cradle. The impact angle is defined as the difference between the pitch angle of the waste package and the pitch angle of the pallet cradle. The pitch is the angle about the cross drift axis (Figure 6-8). The impact location is defined as the normalized distance between the impact point and the left end of the waste package. The distance is normalized by the length of the waste package.

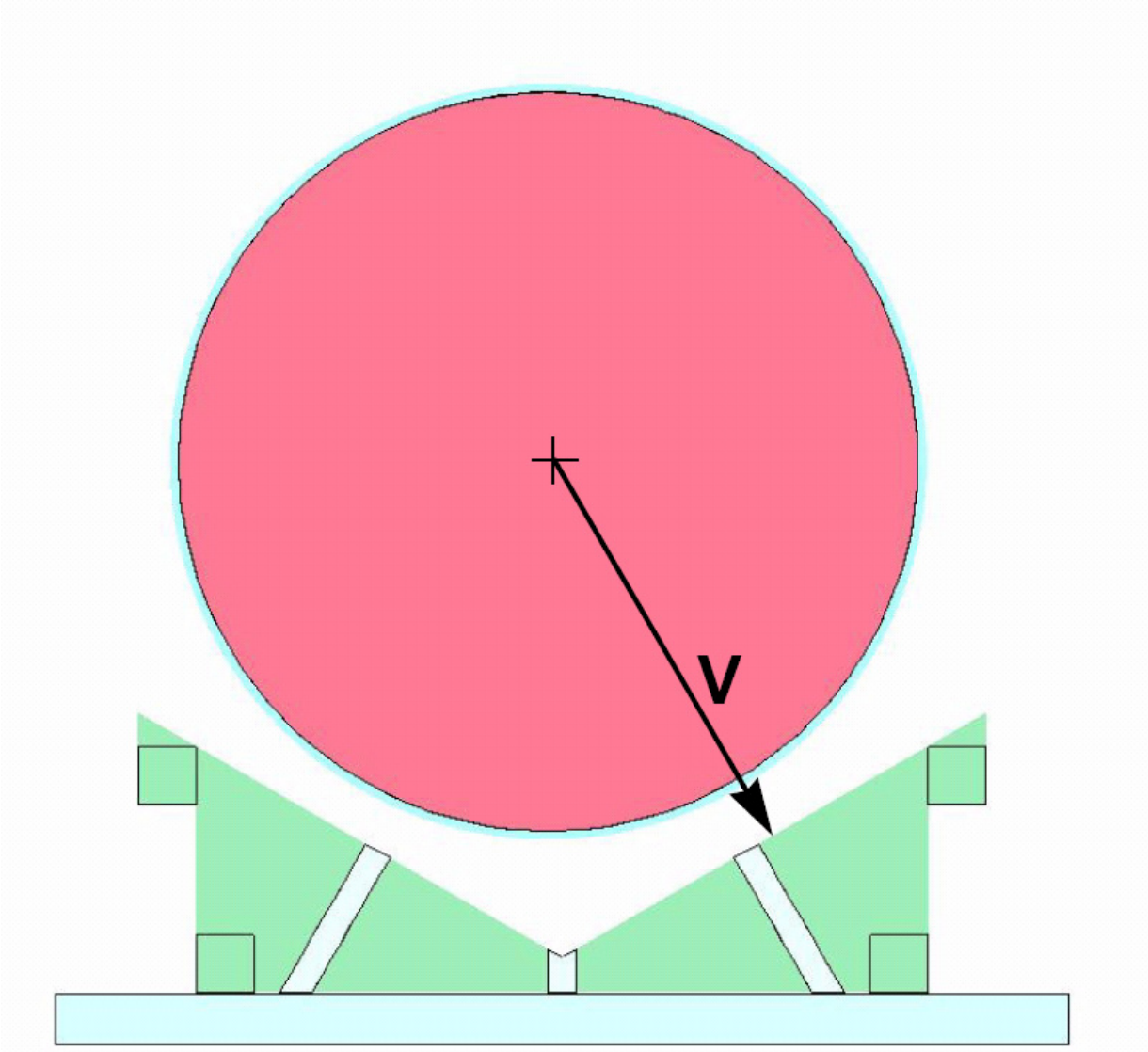

Output DTN: LL0704PA051SPC.026, file *Figures_Mech_Assessment_AMR.tar.gz.*

Figure 6-19. Impact Orientation for Waste Package-to-Pallet Analyses

For the TAD-bearing waste package-to-pallet analyses with intact internals, impact angles of 0 degrees, +0.25 degrees, and +6 degrees were chosen; and for the analyses with degraded internals, impact angles of 0 degrees, −0.25 degrees, and −6 degrees were chosen (Figure 6-20). The range of angles was chosen to encompass the impact angles observed in the kinematic

analyses. For the 0 degrees impact configuration, the waste package is centered on the pallet, and the waste package impacts both pallet cradles at the same time. This would be expected to be a configuration that reasonably represents the condition of the waste package only during a small seismic event, because the waste package can travel significant distances relative to the pallet in larger seismic events. Thus, the 0 degrees impact analyses were only performed for lower velocity impacts (up to 2.00 m/s), because the larger velocity impacts are not likely to occur in the smaller seismic events.

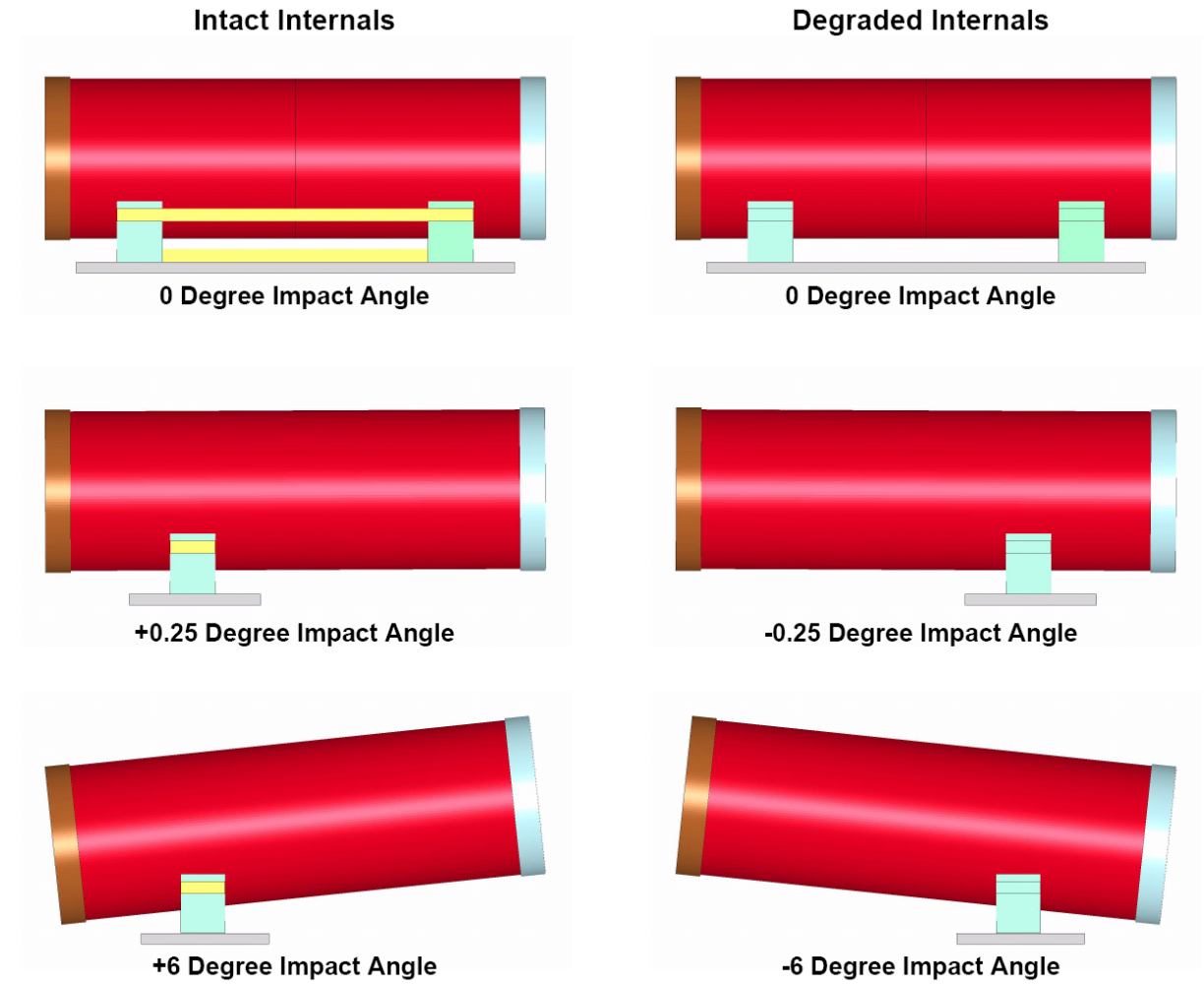

Output DTN: LL0704PA051SPC.026, file *Figures_Mech_Assessment_AMR.tar.gz.*

Figure 6-20. Representative Impact Angle Configurations for Waste Package-to-Pallet Damage Lookup Table Analyses for the TAD-Bearing (shown) and Codisposal Waste Package

Positive impact angles were used for intact internals and negative angles for degraded internals. For the positive angle impacts (intact internals), the impact locations were chosen at 1/8 point, 1/4 point, and 1/2 point; and for the negative angle impacts (degraded internals), the impact locations were chosen at 7/8 point, 3/4 point, and 1/2 point (Figure 6-21). This was done because those combinations of angles and locations tend to yield conservative results for the respective states of the waste package compared to the opposite angles and opposite locations at the other end of the waste package.

With the internals intact, the shield plug of the waste package is at the right end of the waste package (see Figure 6-20 for reference). This positions the center of gravity of the waste package toward the right end, so impacts with positive angles are more severe because the waste package has more of a tendency to roll into the pallet cradle rather than off of it. With the internals degraded, the shield plug is not present, so the severity of the impact is controlled by the distance between the impact point and the outer corrosion barrier lids. Since the sleeve overhangs the waste package on the left side, impacts on the right side of the pallet are further from the lid on the right side of the waste package than corresponding impacts on the left side of the pallet are from the lid on the left side of the waste package. This feature is also present for the intact internals waste package, but the effect that the shield plug has on the center of gravity appears to dominate.

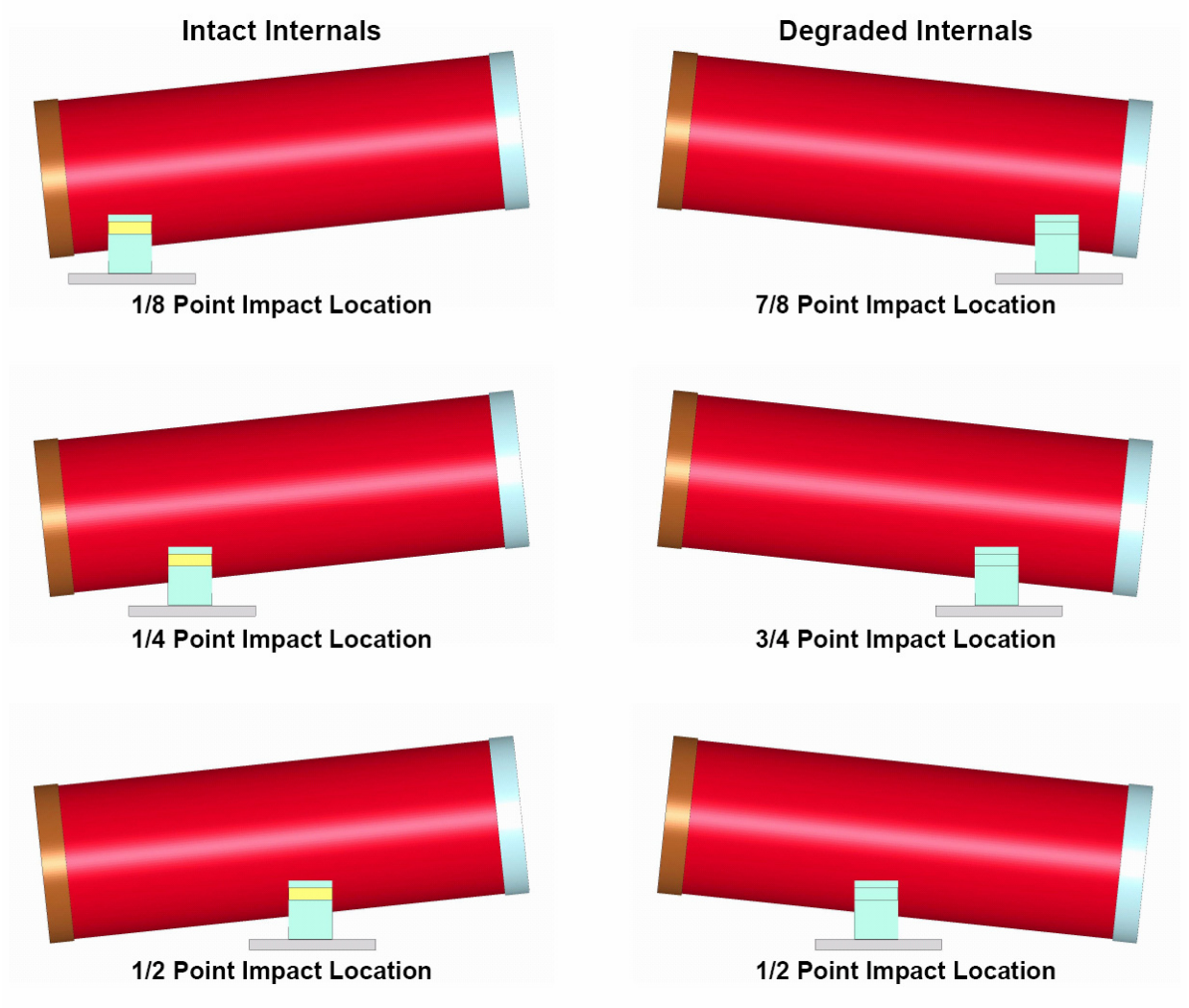

Output DTN: LL0704PA051SPC.026, file *Figures_Mech_Assessment_AMR.tar.gz.*

NOTE: The impact angles shown are 6 degrees.

Figure 6-21. Representative Impact Location Configurations for Waste Package-to-Pallet Damage Lookup Table Analyses for the TAD-Bearing (shown) and Codisposal Waste Package

For the codisposal waste package-to-pallet analyses with intact and degraded internals, the impact angle and impact location combinations were chosen identically to those of the TAD-bearing waste package (Figure 6-20 and Figure 6-21), except some additional analyses were also performed for the intact internals state. The intact internals analyses were also performed for impact angles of −0.25 degrees and −6 degrees with impact locations at the 7/8-point and 3/4-point locations. These additional analyses were done because the differences in the damaged areas between the positive and negative angles are not as clear for intact internals as they are for degraded internals, and, unlike the TAD-bearing waste package where the damaged areas for all intact internals analyses are very small (see Section 6.3.2.2.7), the codisposal waste package analyses with intact internals yield more-substantial damaged areas. The differences between positive and negative angles are less clear for intact internals than degraded internals because of the two competing factors described previously for the

TAD-bearing waste package for intact internals, only one of which is present for degraded internals.

The ranges of impact velocities for both the TAD-bearing waste package-to-pallet and codisposal waste package-to-pallet analyses can be found in Section 6.3.2.2.7. The impact velocities for each angle and location correspond to an impact force as explained in Section 6.3.2.2.4. The upper limit for the impact velocities was chosen to encompass nearly all impact forces observed in the kinematic analyses. For some very large impact forces, corresponding damage lookup table analyses were not performed. This is because, for the very high impact velocities, the deformation of the pallet is very large and could lead to numerical stability problems. For the impacts in the kinematic analyses with forces that exceed the range of the damage lookup table analyses, the damaged areas and rupture conditions for the upper limit of the lookup tables are used, and, as these occurrences are rare, the effect on the statistical distributions of damage is small. The lower limits for impact velocities are determined by observing impacts with either zero or very small damaged areas, and then the areas are interpolated to zero at an impact velocity of 0 m/s (meaning no impact).

6.3.2.2.4 Kinematic Model Force Correspondence

The waste package-to-pallet damage lookup table analyses are set up for several impact velocities, impact angles, and impact locations. In order to map these analyses to impacts that occur in the kinematic analyses, the peak impact force is utilized. However, the impact force for the kinematic representations of the waste package and pallet will be substantially different than the impact force for the detailed representations of the waste package and pallet. Thus, the impact force that is used to map a single impact in a kinematic seismic analysis to the damaged area and rupture condition from a detailed waste package-to-pallet impact analysis is determined by running a waste package-to-pallet impact analysis with the kinematic representations of the waste package and pallet.

The kinematic waste package-to-pallet impact analyses are run for every impact velocity, impact angle, and impact location used in the waste package-to-pallet damage lookup table analyses (Figure 6-22). However, unlike the damage lookup table analyses, for which only a subset of the impact angles and impact locations is performed (see Section 6.3.2.2.3), all possible combinations of impact angle and impact location (including impacts at the ends of the waste package) are performed for each impact velocity for the kinematic waste package-to-pallet analyses. This is performed so that every impact in the kinematic seismic analyses can be properly mapped to an impact velocity based on its impact angle and impact location. Thus, the damaged area and rupture condition computed from the damage lookup table analyses will be properly mapped to each impact.

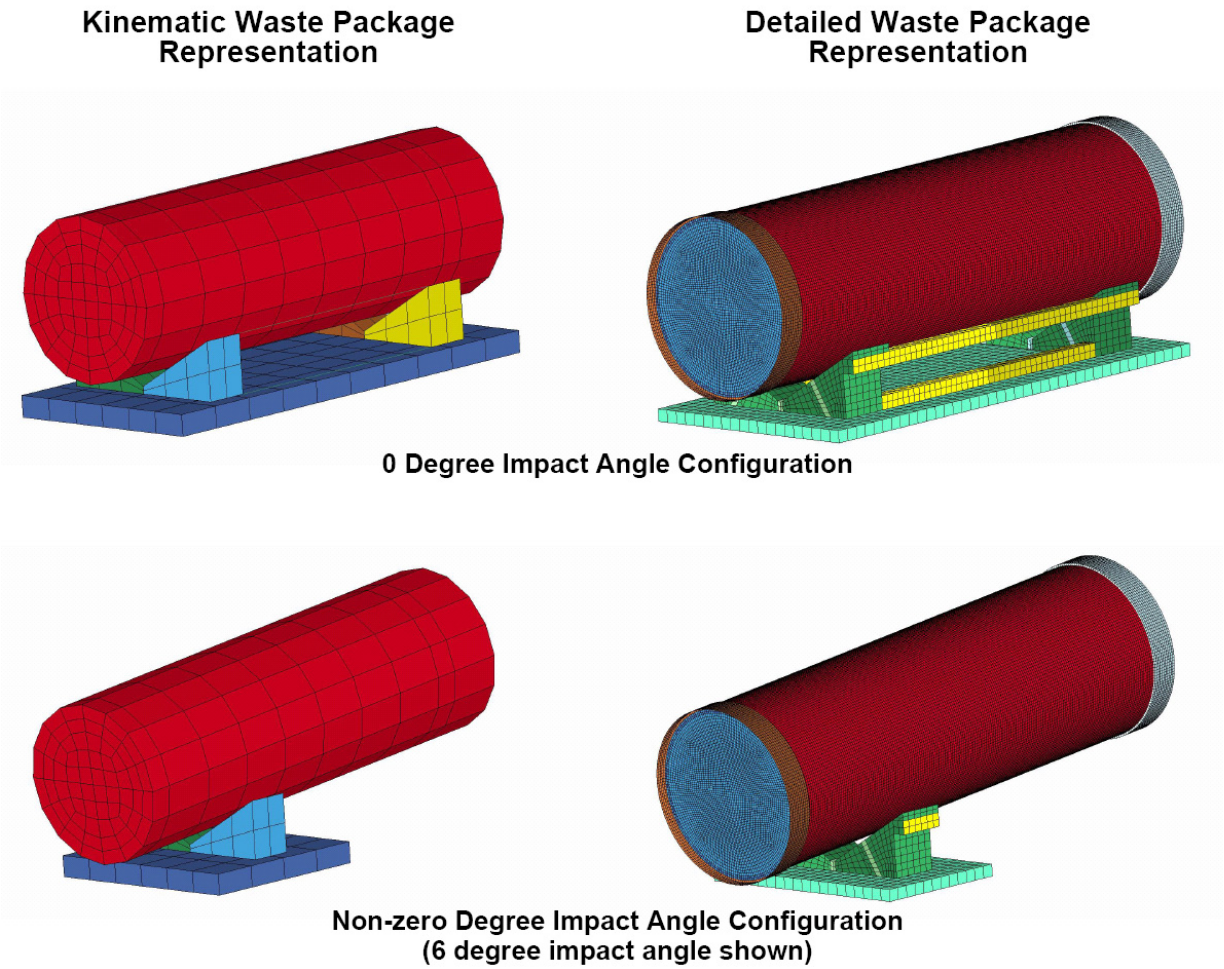

Output DTN: LL0704PA051SPC.026, file *Figures_Mech_Assessment_AMR.tar.gz.*

NOTE: The impact angles shown are 0 and 6 degrees.

Figure 6-22. Kinematic Waste Package-to-Pallet Impact Analyses Corresponding to the Detailed Waste Package-to-Pallet Damage Lookup Table Analyses

The peak impact forces determined from kinematic waste package-to-pallet impact analyses for the TAD-bearing waste package are presented in Table 6-10 to Table 6-14, and the peak impact forces for the codisposal waste package are presented in Table 6-15 to Table 6-19. For the analyses with an impact angle of 0 degrees, both pallet cradles are present, so the impact force on each half cradle (designated with locations of "< 1/2" and "> 1/2" in Table 6-10 and Table 6-15) is determined separately. This is necessary because the center-of-gravity is not at the center of the waste package, so the forces differ at the left and right ends of the package. Also, for the analyses with an impact angle of 0 degrees, the analyses are only performed for impact velocities up to 2.00 m/s as with the damage lookup table analyses (see Section 6.3.2.2.3).

Input and output files for the TAD-bearing waste package analyses can be found in output DTN: LL0704PA048SPC.023, file *NavalLong_TAD_WPP_kinematic_analyses.tar.gz*. Input

and output files for the codisposal waste package analyses can be found in output DTN: LL0704PA049SPC.024, file *CDSP_WPP_kinematic_analyses.tar.gz*.

Some of the force pulses for analyses with +/−0.25 degree impact angles are very broad, meaning that the peak force value yields an underestimation of impact momentum compared to the other impact scenarios. Using these underestimated peak values in the damage lookup tables would lead to overly conservative results, so these peak force values corresponding to the broad peaks were corrected.

For the TAD-bearing waste package, the values were corrected by substituting values obtained for analyses at the opposite end of the waste package. This is a reasonable approximation because the impact momentum should be about the same for opposite ends of the waste package. The impact configurations for which substitutions have been made are denoted in Table 6-11 and Table 6-12. For the impacts at +0.25 degrees (Table 6-11), the peak forces are substituted for impacts at the 1/8-point between 0.20 m/s and 0.50 m/s and impacts at the 1/4-point between 0.20 m/s and 1.00 m/s. For the impacts at −0.25 degrees (Table 6-12), the peak forces are substituted for impacts at the 7/8-point between 0.20 m/s and 0.50 m/s and impacts at the 3/4-point between 0.20 m/s and 1.00 m/s. In these two tables, the original values are shown in *italics*, and the corrected values are given below the original values. For the codisposal waste package, the values were corrected by scaling them by a factor of 1.75. This was necessary because, for the codisposal waste package, the broad peaks occur for both ends of the package. The factor of 1.75 is based on observations of the relative areas under the force pulses compared between various impact locations, and it is a reasonable factor that mitigates some conservatism introduced by the occurrence of broad peaks. The impact configurations for which substitutions have been made are denoted in Table 6-16 and Table 6-17. For impacts at both +0.25 degrees and −0.25 degrees, the peak forces are substituted for impacts at the 1/4-point and 3/4-point between 0.15 m/s and 1.00 m/s. In these two tables, the original values are shown in *italics* and the corrected values are given below the original values.

Table 6-10. Waste Package-to-Pallet Impact Forces (lbs) for the Kinematic Model of the TAD-Bearing Waste Package for an Impact Angle of 0 Degrees

Impact Velocity (m/s)	Location	
	< 1/2	> 1/2
0.20	134,000	141,000
0.25	167,000	176,000
0.30	200,000	211,000
0.35	233,000	245,000
0.40	265,000	280,000
0.50	330,000	348,000
1.00	659,000	692,000
2.00	1,650,000	1,770,000

Output DTN: LL0704PA048SPC.023, file *NavalLong_TAD_WPP_kinematic_analyses_force.xls,* sheet “0 degrees.”

Table 6-11. Waste Package-to-Pallet Impact Forces (lbs) for the Kinematic Model of the TAD-Bearing Waste Package for an Impact Angle of +0.25 Degrees

Impact Velocity (m/s)	Location						
	0	1/8	1/4	1/2	3/4	7/8	1
0.20	144,000	*82,000* 172,000	*133,000* 204,000	277,000	204,000	172,000	152,000
0.25	184,000	*103,000* 214,000	*166,000* 256,000	347,000	256,000	214,000	190,000
0.30	222,000	*123,000* 257,000	*198,000* 307,000	416,000	307,000	257,000	227,000
0.35	263,000	*143,000* 299,000	*231,000* 357,000	485,000	357,000	299,000	266,000
0.40	304,000	*163,000* 341,000	*263,000* 408,000	555,000	408,000	341,000	304,000
0.50	384,000	*206,000* 425,000	*332,000* 510,000	693,000	510,000	425,000	380,000
1.00	770,000	792,000	*664,000* 1,010,000	1,390,000	1,010,000	837,000	758,000
2.00	1,530,000	2,230,000	2,500,000	3,200,000	2,460,000	1,600,000	1,500,000
3.00	2,380,000	3,570,000	4,510,000	4,320,000	3,790,000	2,640,000	2,220,000
5.00	3,640,000	6,940,000	8,190,000	9,440,000	7,100,000	5,120,000	3,290,000
7.00	6,580,000	9,630,000	11,200,000	12,400,000	9,960,000	7,880,000	5,220,000
10.00	10,300,000	12,600,000	15,100,000	17,400,000	13,700,000	11,300,000	8,560,000

Output DTN: LL0704PA048SPC.023, file *NavalLong_TAD_WPP_kinematic_analyses_force.xls,* sheets “+0.25 degrees” and “+0.25 degrees (original).”

NOTE: Original values in *italics*, and corrected values given below original values.

Table 6-12. Waste Package-to-Pallet Impact Forces (lbs) for the Kinematic Model of the TAD-Bearing Waste Package for an Impact Angle of −0.25 Degrees

Impact Velocity (m/s)	Location						
	0	1/8	1/4	1/2	3/4	7/8	1
0.20	141,000	136,000	193,000	278,000	*141,000* 193,000	*87,000* 136,000	151,000
0.25	177,000	170,000	242,000	347,000	*176,000* 242,000	*108,000* 170,000	189,000
0.30	212,000	204,000	290,000	417,000	*210,000* 290,000	*130,000* 204,000	226,000
0.35	247,000	237,000	337,000	486,000	*244,000* 337,000	*151,000* 237,000	264,000
0.40	283,000	271,000	386,000	555,000	*280,000* 386,000	*173,000* 271,000	302,000
0.50	353,000	336,000	483,000	693,000	*350,000* 483,000	*216,000* 336,000	377,000
1.00	707,000	662,000	958,000	1,390,000	*774,000* 958,000	914,000	753,000
2.00	1,410,000	1,570,000	2,270,000	3,170,000	2,670,000	2,390,000	1,580,000
3.00	2,070,000	2,550,000	3,600,000	4,300,000	4,900,000	3,970,000	2,680,000
5.00	3,290,000	4,560,000	6,550,000	9,320,000	8,740,000	7,390,000	4,220,000
7.00	3,900,000	7,390,000	9,320,000	12,300,000	11,800,000	10,100,000	7,740,000
10.00	5,100,000	10,600,000	12,900,000	17,000,000	15,900,000	13,300,000	11,800,000

Output DTN: LL0704PA048SPC.023, file *NavalLong_TAD_WPP_kinematic_analyses_force.xls,* sheets "−0.25 degrees" and "−0.25 degrees (original)."

NOTE: Original values in *italics*, and corrected values given below original values.

Table 6-13. Waste Package-to-Pallet Impact Forces (lbs) for the Kinematic Model of the TAD-Bearing Waste Package for an Impact Angle of +6 Degrees

Impact Velocity (m/s)	Location						
	0	1/8	1/4	1/2	3/4	7/8	1
0.20	148,000	186,000	222,000	281,000	225,000	164,000	148,000
0.25	186,000	232,000	278,000	351,000	281,000	205,000	185,000
0.30	223,000	278,000	334,000	422,000	338,000	245,000	222,000
0.35	259,000	325,000	389,000	492,000	394,000	285,000	258,000
0.40	297,000	371,000	444,000	562,000	451,000	326,000	295,000
0.50	371,000	464,000	565,000	702,000	562,000	405,000	369,000
1.00	740,000	927,000	1,140,000	1,400,000	1,100,000	796,000	736,000
2.00	1,480,000	1,690,000	2,180,000	2,690,000	2,250,000	1,500,000	1,470,000
3.00	2,170,000	2,860,000	3,540,000	4,130,000	3,770,000	2,270,000	2,180,000
5.00	3,620,000	5,030,000	5,210,000	6,250,000	6,590,000	4,240,000	3,460,000
7.00	5,540,000	6,520,000	6,700,000	8,010,000	8,800,000	5,700,000	4,600,000
10.00	7,580,000	8,210,000	11,500,000	14,900,000	12,000,000	7,880,000	5,810,000

Output DTN: LL0704PA048SPC.023, file *NavalLong_TAD_WPP_kinematic_analyses_force.xls,* sheet "+6 degrees."

Table 6-14. Waste Package-to-Pallet Impact Forces (lbs) for the Kinematic Model of the TAD-Bearing Waste Package for an Impact Angle of −6 Degrees

Impact Velocity (m/s)	Location						
	0	1/8	1/4	1/2	3/4	7/8	1
0.20	137,000	176,000	212,000	279,000	236,000	191,000	159,000
0.25	172,000	220,000	265,000	349,000	294,000	239,000	199,000
0.30	206,000	264,000	318,000	419,000	353,000	287,000	239,000
0.35	241,000	308,000	370,000	489,000	411,000	335,000	279,000
0.40	275,000	352,000	424,000	559,000	471,000	383,000	318,000
0.50	344,000	440,000	529,000	698,000	599,000	478,000	398,000
1.00	686,000	879,000	1,040,000	1,390,000	1,190,000	949,000	796,000
2.00	1,370,000	1,590,000	2,070,000	2,670,000	2,380,000	1,810,000	1,580,000
3.00	2,030,000	2,720,000	3,510,000	4,110,000	3,760,000	3,080,000	2,330,000
5.00	3,240,000	5,040,000	6,170,000	6,240,000	5,510,000	5,190,000	3,880,000
7.00	4,350,000	7,100,000	8,340,000	8,010,000	6,980,000	6,570,000	5,810,000
10.00	5,550,000	9,760,000	11,600,000	14,500,000	12,800,000	8,530,000	7,810,000

Output DTN: LL0704PA048SPC.023, file *NavalLong_TAD_WPP_kinematic_analyses_force.xls,* sheet "−6 degrees."

Table 6-15. Waste Package-to-Pallet Impact Forces (lbs) for the Kinematic Model of the Codisposal Waste Package for an Impact Angle of 0 Degrees

Impact Velocity (m/s)	Location	
	< 1/2	> 1/2
0.15	116,000	125,000
0.25	193,000	207,000
0.35	269,000	289,000
0.50	382,000	413,000
1.00	747,000	817,000
2.00	1,420,000	1,530,000

Output DTN: LL0704PA049SPC.024, file *CDSP_WPP_kinematic_analyses_force.xls,* sheet "0 degrees."

Table 6-16. Waste Package-to-Pallet Impact Forces (lbs) for the Kinematic Model of the Codisposal Waste Package for an Impact Angle of +0.25 Degrees

Impact Velocity (m/s)	Location						
	0	1/8	1/4	1/2	3/4	7/8	1
0.15	98,900	82,500	*65,000* 114,000	190,000	*62,700* 110,000	134,000	109,000
0.25	168,000	137,000	*108,000* 189,000	316,000	*104,000* 182,000	269,000	182,000
0.35	241,000	191,000	*151,000* 264,000	442,000	*146,000* 256,000	400,000	254,000
0.50	351,000	273,000	*214,000* 375,000	632,000	*208,000* 364,000	631,000	363,000
1.00	713,000	536,000	*415,000* 726,000	1,310,000	*400,000* 700,000	1,530,000	726,000
2.00	1,400,000	1,020,000	2,650,000	2,390,000	2,190,000	3,190,000	1,430,000
3.00	2,040,000	2,340,000	4,930,000	3,780,000	4,490,000	4,710,000	2,070,000
5.00	3,140,000	5,940,000	8,320,000	8,850,000	7,730,000	7,550,000	3,240,000
7.00	4,040,000	8,590,000	11,100,000	12,100,000	10,400,000	10,000,000	3,760,000
10.00	8,120,000	12,000,000	14,500,000	15,600,000	13,700,000	13,500,000	6,870,000

Output DTN: LL0704PA049SPC.024, file *CDSP_WPP_kinematic_analyses_force.xls,* sheets "+0.25 degrees" and "+0.25 degrees (original)."

NOTE: Original values in *italics* and corrected values given below original values.

Table 6-17. Waste Package-to-Pallet Impact Forces (lbs) for the Kinematic Model of the Codisposal Waste Package for an Impact Angle of −0.25 Degrees

Impact Velocity (m/s)	Location						
	0	1/8	1/4	1/2	3/4	7/8	1
0.15	102,000	68,900	*58,200* 102,000	196,000	*69,600* 122,000	109,000	111,000
0.25	170,000	114,000	*96,700* 169,000	327,000	*116,000* 203,000	181,000	185,000
0.35	238,000	160,000	*136,000* 238,000	458,000	*161,000* 282,000	253,000	259,000
0.50	340,000	227,000	*193,000* 338,000	653,000	*227,000* 397,000	359,000	370,000
1.00	679,000	449,000	*375,000* 656,000	1,340,000	*438,000* 767,000	709,000	739,000
2.00	1,340,000	857,000	1,690,000	2,430,000	3,050,000	1,350,000	1,460,000
3.00	1,940,000	1,510,000	4,010,000	3,810,000	5,420,000	1,970,000	2,110,000
5.00	3,080,000	4,460,000	7,220,000	8,830,000	8,940,000	5,370,000	3,610,000
7.00	3,630,000	7,220,000	9,720,000	12,000,000	11,800,000	8,350,000	5,320,000
10.00	4,540,000	10,300,000	12,900,000	15,300,000	15,600,000	12,300,000	10,000,000

Output DTN: LL0704PA049SPC.024, file *CDSP_WPP_kinematic_analyses_force.xls,* sheets "−0.25 degrees" and "−0.25 degrees (original)."

NOTE: Original values in *italics* and corrected values given below original values.

Table 6-18. Waste Package-to-Pallet Impact Forces (lbs) for the Kinematic Model of the Codisposal Waste Package for an Impact Angle of +6 Degrees

Impact Velocity (m/s)	Location						
	0	1/8	1/4	1/2	3/4	7/8	1
0.15	104,000	173,000	207,000	192,000	213,000	175,000	105,000
0.25	174,000	286,000	346,000	319,000	355,000	291,000	176,000
0.35	244,000	400,000	483,000	447,000	496,000	407,000	249,000
0.50	349,000	573,000	690,000	638,000	709,000	582,000	351,000
1.00	696,000	1,150,000	1,380,000	1,280,000	1,410,000	1,160,000	702,000
2.00	1,370,000	2,270,000	2,680,000	2,440,000	2,770,000	2,300,000	1,390,000
3.00	1,990,000	3,300,000	3,810,000	3,520,000	3,970,000	3,330,000	2,020,000
5.00	3,200,000	5,230,000	5,600,000	5,790,000	5,900,000	5,320,000	3,260,000
7.00	4,670,000	6,800,000	6,820,000	7,270,000	7,080,000	7,180,000	4,820,000
10.00	6,800,000	8,450,000	9,110,000	10,900,000	8,800,000	9,540,000	6,950,000

Output DTN: LL0704PA049SPC.024, file *CDSP_WPP_kinematic_analyses_force.xls,* sheet "+6 degrees."

Table 6-19. Waste Package-to-Pallet Impact Forces (lbs) for the Kinematic Model of the Codisposal Waste Package for an Impact Angle of −6 Degrees

Impact Velocity (m/s)	Location						
	0	1/8	1/4	1/2	3/4	7/8	1
0.15	99,000	168,000	202,000	196,000	228,000	111,000	117,000
0.25	165,000	280,000	335,000	327,000	379,000	185,000	195,000
0.35	230,000	392,000	469,000	458,000	530,000	257,000	273,000
0.50	329,000	561,000	670,000	654,000	757,000	365,000	391,000
1.00	657,000	1,120,000	1,340,000	1,300,000	1,510,000	718,000	780,000
2.00	1,300,000	2,220,000	2,640,000	2,460,000	2,920,000	1,450,000	1,540,000
3.00	1,900,000	3,260,000	3,810,000	3,520,000	4,180,000	2,580,000	2,220,000
5.00	3,040,000	5,150,000	5,740,000	5,820,000	5,920,000	4,470,000	3,530,000
7.00	4,130,000	6,750,000	6,950,000	7,300,000	7,070,000	5,850,000	5,190,000
10.00	5,560,000	8,480,000	8,440,000	10,600,000	10,300,000	7,770,000	7,230,000

Output DTN: LL0704PA049SPC.024, file *CDSP_WPP_kinematic_analyses_force.xls,* sheet "−6 degrees."

6.3.2.2.5 Extracting Damaged Areas and Rupture Condition

Damaged area and rupture condition are determined for the OCB of the waste package. The OCB shell and the outer OCB lids are considered to make up the OCB for this purpose. All of these components are Alloy 22.

The damaged area is computed by determining the area of the OCB surface that has a residual maximum (first) principal stress that exceeds one of three damage levels (90%, 100%, and 105% of yield strength). The residual stresses are obtained by allowing the impact event to complete and then applying damping to the analyses for 0.05 seconds. The yield strength for Alloy 22 at 60°C is 350 MPa (51,000 psi), so the three stress levels correspond to 316 MPa, 350 MPa, and

369 MPa (45,900 psi, 51,000 psi, and 53,550 psi), respectively. An element of the finite element mesh contributes to the damaged area if any of the outer, inner, or middle surfaces has a residual stress that exceeds the damage level. The area for an element is only counted once if multiple surfaces of that element exceed the damage level.

The postprocessing for damaged area is performed using LS-PREPOST. The area fraction of a part that exceeds a residual maximum principal stress level is determined using the "volume of material failure" option in LS-PREPOST. Since the OCB is modeled with shell elements, the "volume of material failure" option produces an area of material failure. The failure levels for maximum principal stress are set at 90%, 100%, and 105% of the yield strength of Alloy 22, and the area is determined by taking the area fractions that exceed the levels at the end of the analysis and multiplying by the surface area of the part. This is accomplished by applying a scale factor to the curves. Figure 6-23 shows an example of the curves after being multiplied by the scale factor. Figure 6-24 shows the damaged area. The dark blue is below 90% of yield strength; the light blue, green, yellow, and red combined are above 90% of yield strength; the yellow and red combined are above 100% of yield strength; and the red is above 105% of yield strength. The damaged areas are determined separately for the OCB shell and the OCB lids. For waste package-to-waste package impacts, the damaged areas from the OCB shell and the OCB lids for each waste package are summed to obtain a damaged area for that waste package. The damaged areas are determined separately for both waste packages. For waste package-to-pallet impacts, the damaged areas for the OCB shells and both OCB lids are recorded separately for use in the binning feature of km_impacts_pp (V. 1.0. STN: 11235-1.0-00 [DIRS 178489]), the postprocessor for the kinematic analyses.

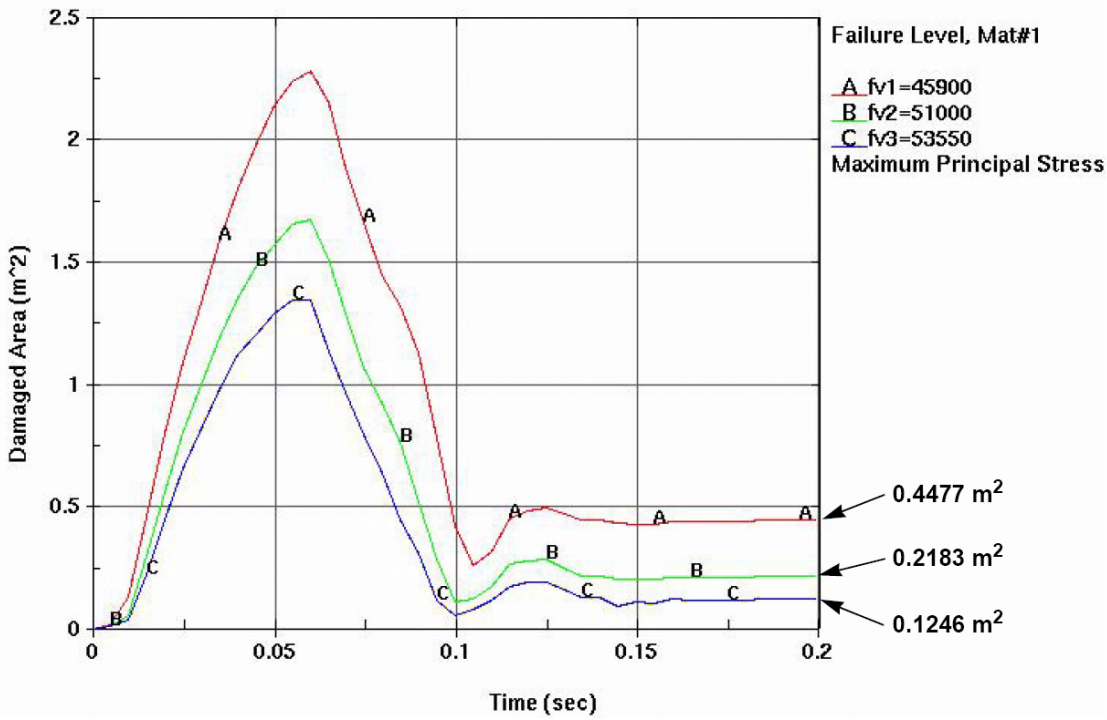

Output DTN: LL0704PA051SPC.026, file *Figures_Mech_Assessment_AMR.tar.gz.*

NOTE: The red line (A) corresponds to the 90% level, the green line (B) to 100%, the blue line (C) to 105%.

Figure 6-23. Example of Curves Used for Computing the Damaged Area of the OCB Shell at 90%, 100%, and 105% of Yield Strength

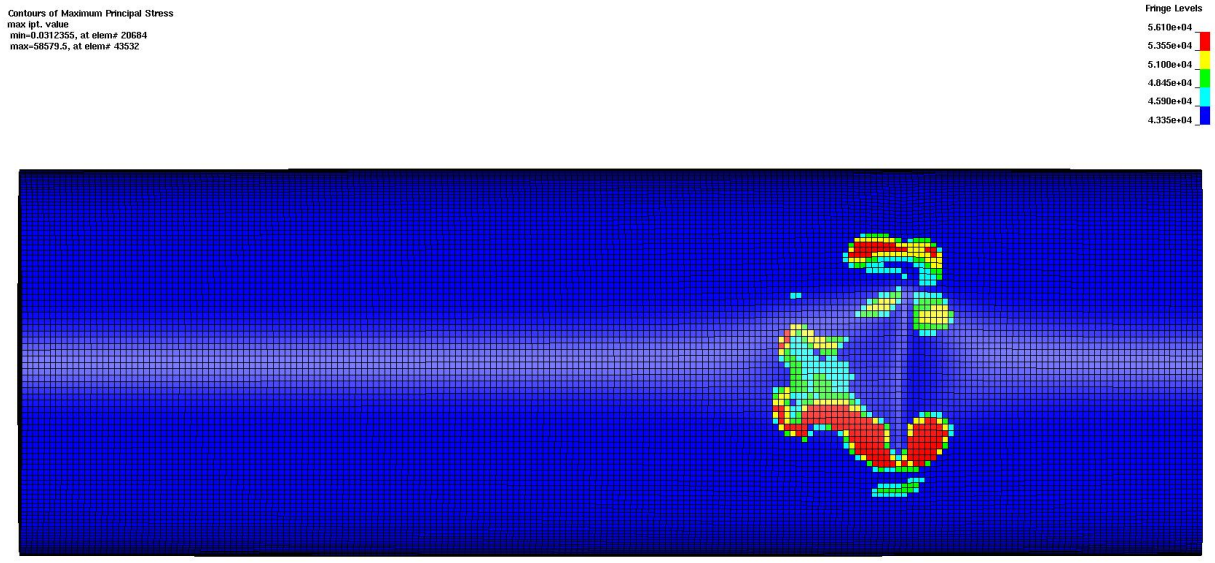

Output DTN: LL0704PA051SPC.026, file *Figures_Mech_Assessment_AMR.tar.gz.*

NOTE: Dark blue area corresponds to below 90% of yield strength; light blue, green, yellow, and red areas correspond to above 90%; yellow and red correspond to above 100%; red corresponds to above 105%.

Figure 6-24. Example of a Fringe Plot Showing the Damaged Area on the OCB Shell

The rupture condition of a waste package is determined by comparing the maximum effective strain from all elements on the outer and inner surfaces of the OCB to the ultimate tensile strain limit. The determination of the strain limit is discussed in Appendix A. For uniaxial tension, the maximum effective strain limit is 0.57; and for biaxial tension, the maximum effective strain limit can be as low as 0.285, based on a triaxiality factor of 2.0 (see Appendix A).

The OCB rupture condition is determined using LS-PREPOST to perform a multi-layer screening process as illustrated in Figure 6-25. The maximum effective strain on the OCB (on both the outer and inner surfaces) is used to identify potential rupture; an example curve is shown in Figure 6-26. If the maximum effective strain does not exceed 0.285 at any time during the analysis, rupture is screened out. If the maximum effective strain for any elements of the OCB exceeds 0.285 at any time, then the triaxiality factor (see Appendix A) is computed for the stress state of those elements on the appropriate surface. The elements that have effective strain exceeding 0.285 at some time during the analysis are determined visually (Figure 6-27). Element numbers are determined by using the mouse to select the elements. The OCB shell and OCB lids are considered simultaneously for both waste package-to-waste package impacts and waste package-to-pallet impacts to obtain the rupture condition for a package.

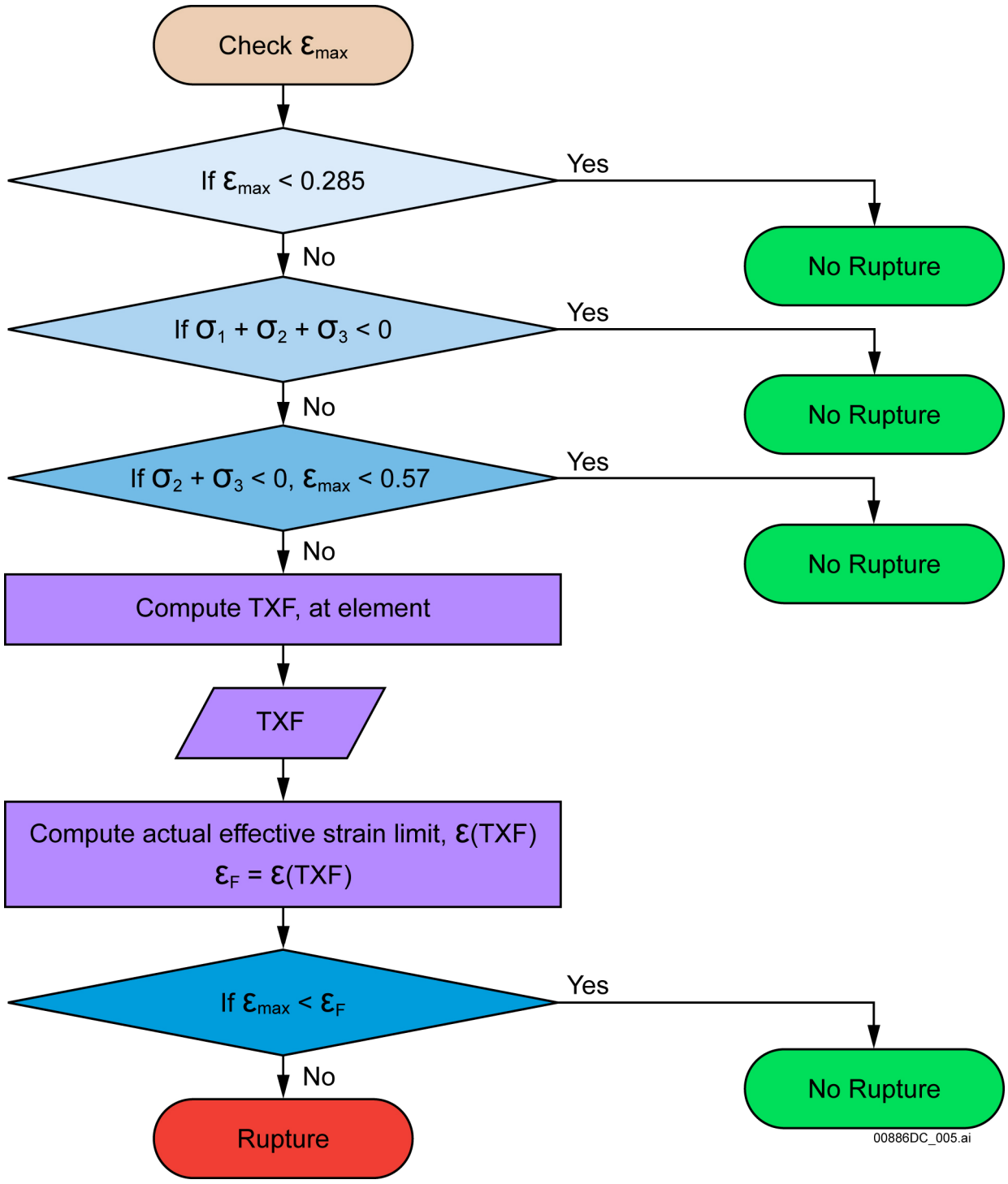

Source: Created for illustrative purposes only.

NOTE: TXF = triaxiality factor.

Figure 6-25. Flow Chart Showing Decision Process for Screening Rupture for a Specific Element, Based on the Stress-Strain State

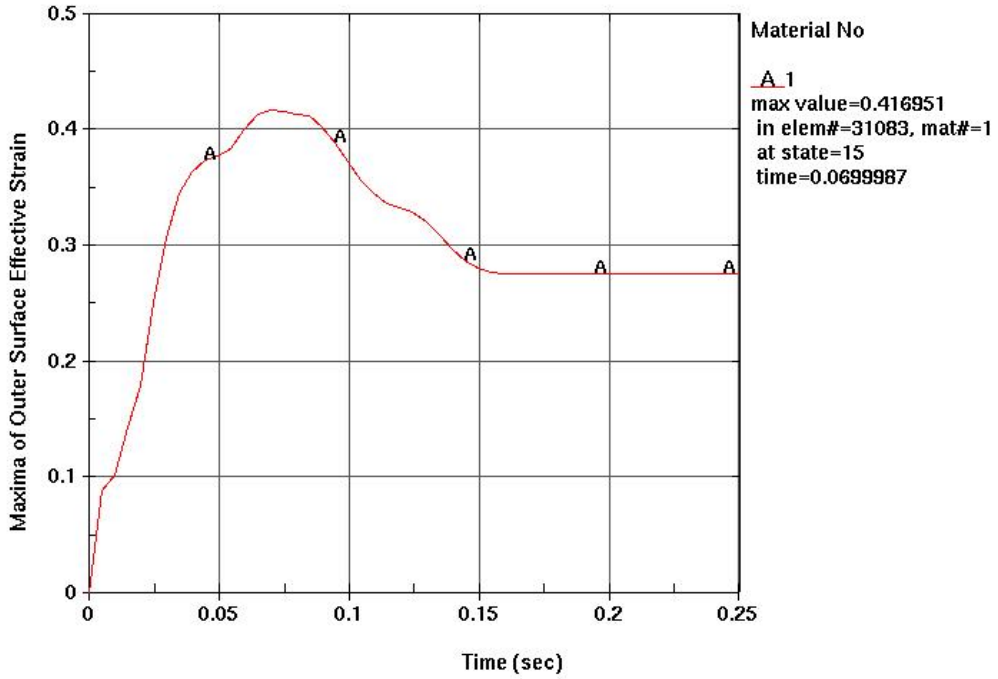

Output DTN: LL0704PA051SPC.026, file *Figures_Mech_Assessment_AMR.tar.gz.*

Figure 6-26. Example of a Maximum Effective Strain Plot for the Outer Surface of the OCB Shell

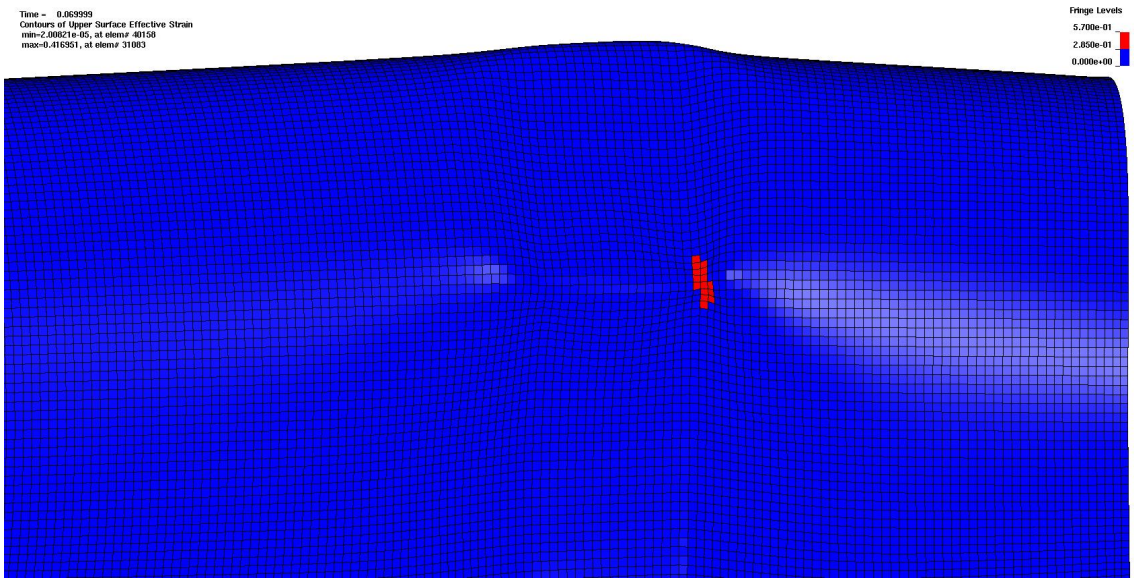

Output DTN: LL0704PA051SPC.026, file *Figures_Mech_Assessment_AMR.tar.gz.*

NOTE: Element numbers are determined by selecting the elements with the mouse in LS-PREPOST. Elements with effective strains exceeding 0.285 are shaded red.

Figure 6-27. Example of a Fringe Plot Showing the Area of the OCB Shell with Elements with Effective Strains Exceeding 0.285

The stress state is determined by plotting the time history of the three principal stresses at the appropriate surface (inner or outer) of the element. The triaxiality factor is computed as described in Appendix A. If the stress state is compressive ($\sigma_1 + \sigma_2 + \sigma_3 < 0$) for the time that the effective strain exceeds 0.285, then rupture is screened out. If the stress state is uniaxial tension or its equivalent ($\sigma_2 + \sigma_3 < 0$) and the effective strain does not exceed 0.57 during that time, then rupture is screened out. If none of these conditions is met, then the actual effective strain limit is computed using a triaxiality factor and compared to the effective strain of the element. Rupture is screened out if the effective strain does not exceed the limit at any time during the analysis. The waste package is determined to rupture if the effective strain does exceed the strain limit determined from the stress state of the element. Examples of the principal stress curves, with the corresponding effective strains are shown in Figure 6-28 to Figure 6-30. Figure 6-28 illustrates a stress state that is compressive during the time that the effective strain exceeds 0.285. Figure 6-29 illustrates a stress state that is uniaxial tension or compressive during the time that the effective strain exceeds 0.285. Figure 6-30 illustrates a situation where the triaxiality factor must be calculated to determine the strain limit for times that the stress state is biaxial tension in order to screen out rupture.

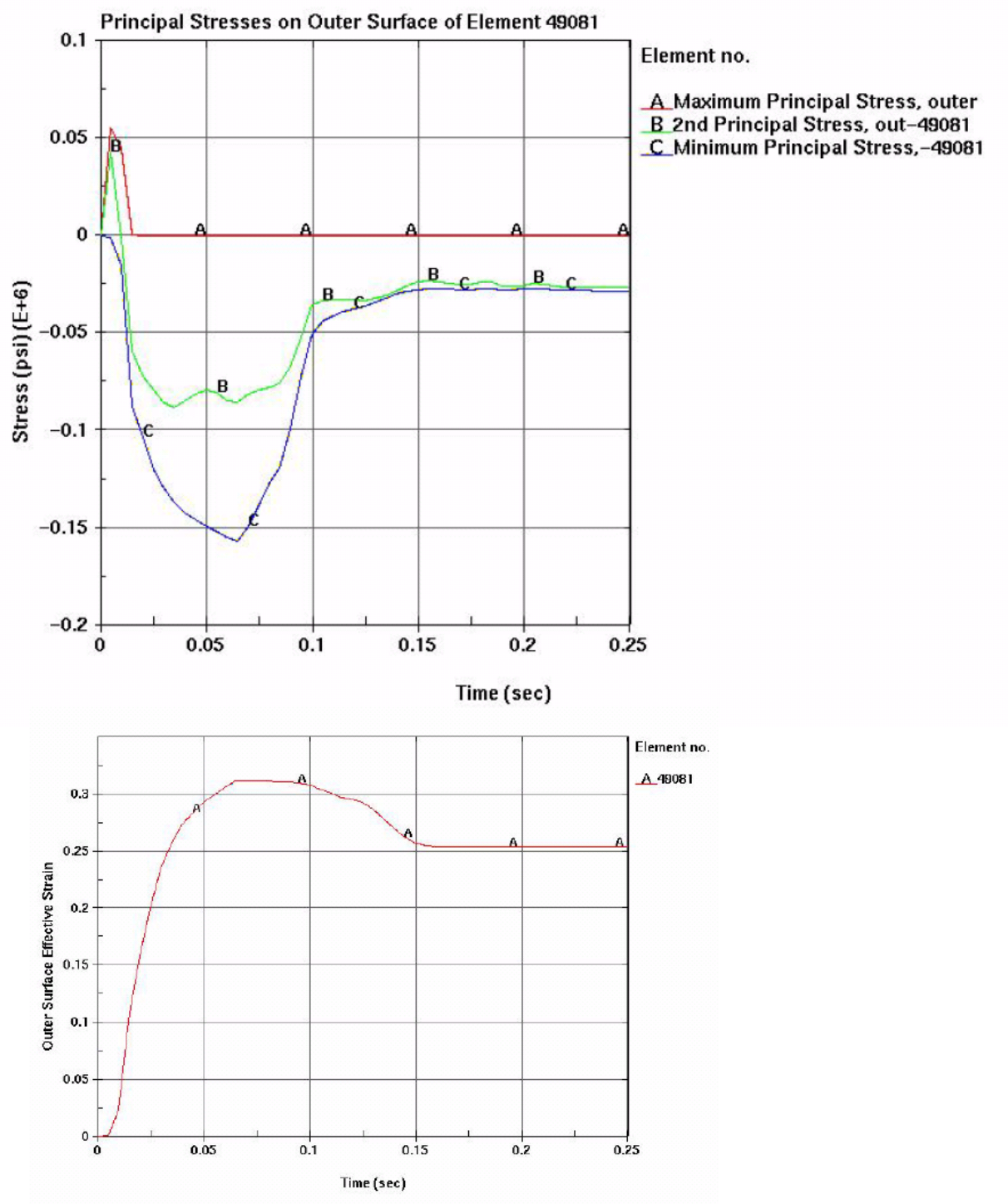

Output DTN: LL0704PA051SPC.026, file *Figures_Mech_Assessment_AMR.tar.gz.*

Figure 6-28. Example of Principal Stress Curves and the Corresponding Effective Strain Curve for a Compressive Stress State

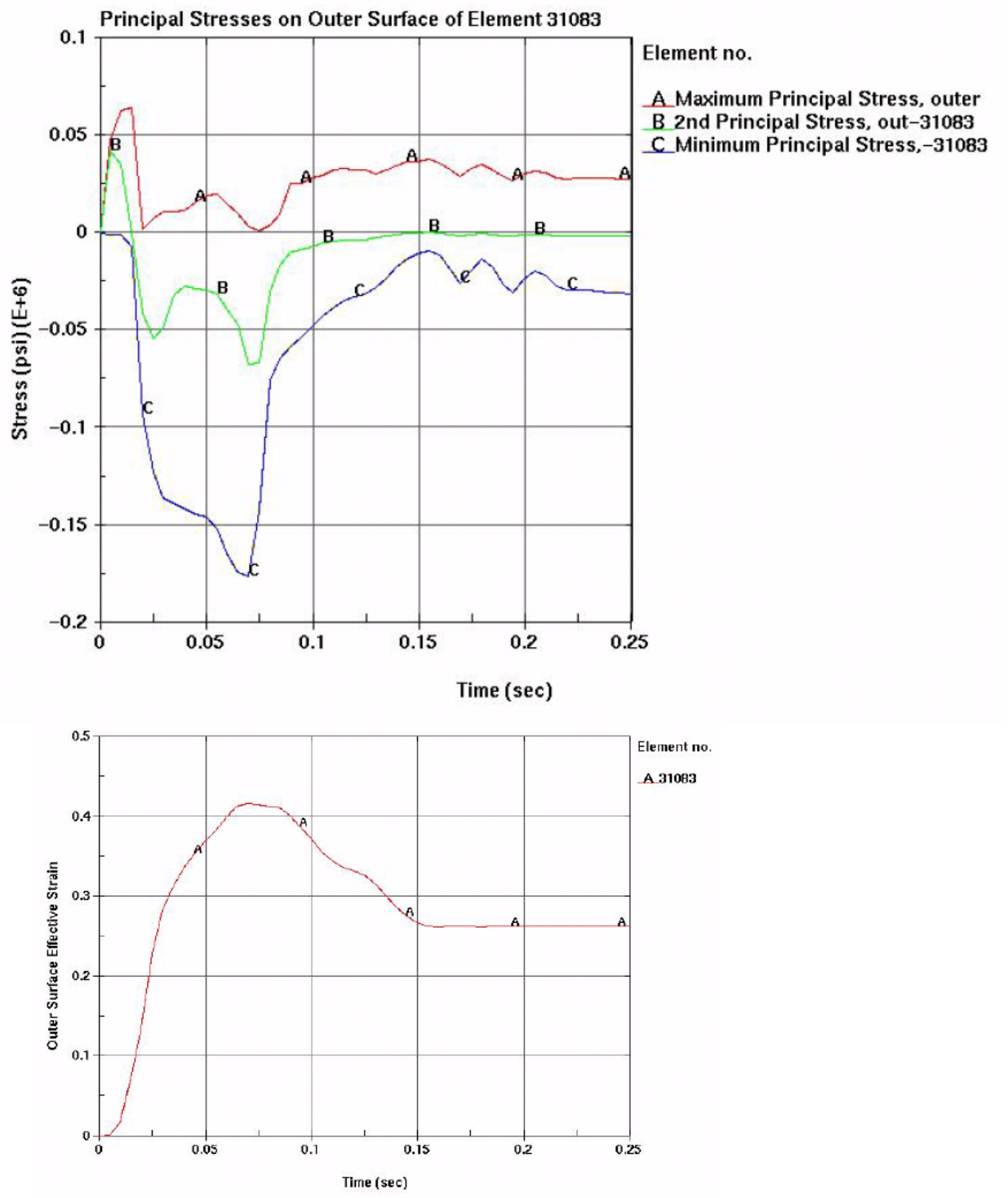

Output DTN: LL0704PA051SPC.026, file *Figures_Mech_Assessment_AMR.tar.gz.*

Figure 6-29. Example of Principal Stress Curves and the Corresponding Effective Strain Curve for a Uniaxial Tension/Compressive Stress State

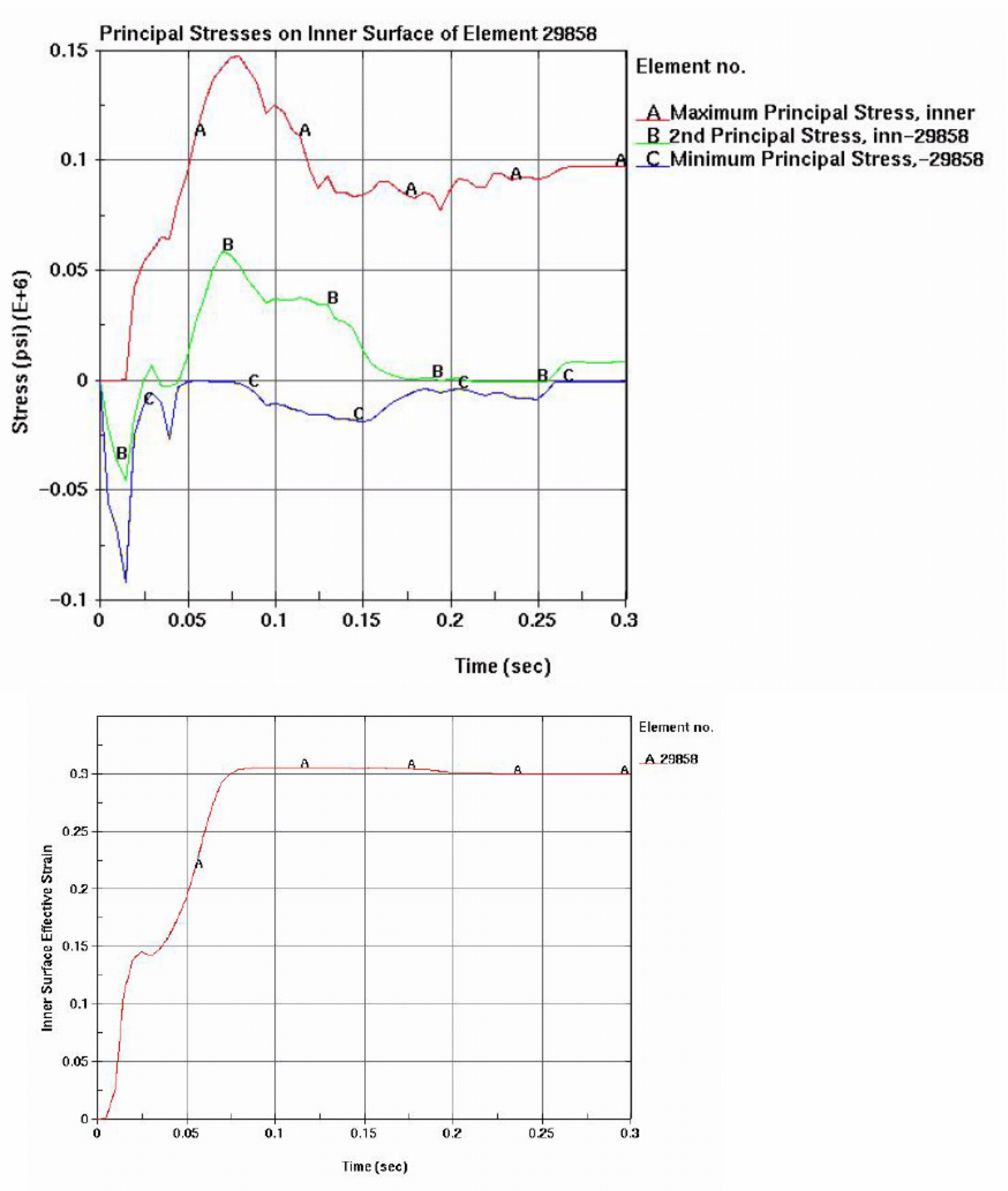

Output DTN: LL0704PA051SPC.026, file *Figures_Mech_Assessment_AMR.tar.gz.*

Figure 6-30. Example of Principal Stress Curves and the Corresponding Effective Strain Curve for a Biaxial Tension Stress State

6.3.2.2.6 Waste Package-to-Waste Package Damage Lookup Tables

Waste package-to-waste package impact analyses for determining damaged area and rupture condition for TAD-bearing packages were performed for 90 configurations. The analyses were performed for impact velocities of 0.50 m/s, 1.00 m/s, 2.00 m/s, 4.00 m/s, 6.00 m/s, and 9.00 m/s; impact locations of −0.30, −0.15, 0.00, 0.15 and 0.30; and one impact angle of 1.5 degrees (Figure 6-17, Section 6.3.2.2.3). Three configurations of the waste packages were used: 23-mm OCB with intact internals, 23-mm OCB with degraded internals and 17-mm OCB with degraded internals. Damaged area and rupture condition of the two waste packages were recorded separately. The results for damaged area (at 90%, 100%, and 105% of yield strength) are presented in Table 6-20 to Table 6-25. The results for rupture condition are presented in Table 6-26 to Table 6-31. The maximum effective strain is presented for each analysis, and a condition of "Yes" or "No" to designate whether the waste package ruptured is presented. The procedure for determining the rupture condition is described in Section 6.3.2.2.5. For the TAD-bearing waste package, a rupture condition of "No" is predicted for all impacts. Input and output files for these analyses can be found in output DTN: LL0704PA048SPC.023, file *NavalLong_TAD_WPWP_catalog_analyses.tar.gz* and *NavalLong_TAD_WPWP_catalog_crvfiles.tar.gz*.

Waste package-to-waste package impact analyses for determining damaged area and rupture condition for codisposal packages were performed for 105 configurations. The analyses were performed for impact velocities of 0.50 m/s, 1.00 m/s, 2.00 m/s, 4.00 m/s, 6.00 m/s, 9.00 m/s, and 10.00 m/s; impact locations of −0.30, −0.15, 0.00, 0.15 and 0.30; and one impact angle of 1.5 degrees (Figure 6-18, Section 6.3.2.2.3). Three configurations of the waste packages were used: 23-mm OCB with intact internals, 23-mm OCB with degraded internals, and 17-mm OCB with degraded internals. Damaged area and rupture condition were only recorded for the codisposal waste package. The results for damaged area (at 90%, 100%, and 105% of yield strength) are presented in Table 6-32 to Table 6-34. The results for rupture condition are presented in Table 6-35 to Table 6-37. The maximum effective strain is presented for each analysis, and a condition of "Yes" or "No" to designate whether the waste package ruptured is presented. The procedure for determining the rupture condition is described in Section 6.3.2.2.5. For the codisposal waste package, a rupture condition of "No" is predicted for all impacts. Input and output files for these analyses can be found in output DTN: LL0704PA049SPC.024, file *CDSP_WPWP_catalog_ analyses.tar.gz* and *CDSP_WPWP_catalog_crvfiles .tar.gz*.

Table 6-20. Damaged Areas (m^2) for TAD-Bearing Waste Packages, 23-mm OCB with Intact Internals, Waste Package-to-Waste Package Impacts, WP 1

Impact Velocity (m/s)	Percentage of Yield Strength	Location				
		−0.30	−0.15	0.00	0.15	0.30
0.50	90%	0.0000	0.0000	0.0000	0.0000	0.0000
	100%	0.0000	0.0000	0.0000	0.0000	0.0000
	105%	0.0000	0.0000	0.0000	0.0000	0.0000
1.00	90%	0.0000	0.0000	0.0000	0.0000	0.0319
	100%	0.0000	0.0000	0.0000	0.0000	0.0029
	105%	0.0000	0.0000	0.0000	0.0000	0.0000

Table 6-20. Damaged Areas (m^2) for TAD-Bearing Waste Packages, 23-mm OCB with Intact Internals, Waste Package-to-Waste Package Impacts, WP 1 (Continued)

Impact Velocity (m/s)	Percentage of Yield Strength	Location				
		−0.30	−0.15	0.00	0.15	0.30
2.00	90%	0.0000	0.0000	0.0000	0.0000	0.0062
	100%	0.0000	0.0000	0.0000	0.0000	0.0000
	105%	0.0000	0.0000	0.0000	0.0000	0.0000
4.00	90%	0.0000	0.0000	0.0000	0.0018	0.0013
	100%	0.0000	0.0000	0.0000	0.0000	0.0000
	105%	0.0000	0.0000	0.0000	0.0000	0.0000
6.00	90%	0.0000	0.0030	0.0000	0.0015	0.0000
	100%	0.0000	0.0015	0.0000	0.0000	0.0000
	105%	0.0000	0.0000	0.0000	0.0000	0.0000
9.00	90%	0.0112	0.0000	0.0000	0.0000	0.0000
	100%	0.0000	0.0000	0.0000	0.0000	0.0000
	105%	0.0000	0.0000	0.0000	0.0000	0.0000

Output DTN: LL0704PA048SPC.023, file *NavalLong_TAD_WPWP_catalog_analyses_DA.xls,* sheet "WP1 i23."

Table 6-21. Damaged Areas (m^2) for TAD-Bearing Waste Packages, 23-mm OCB with Intact Internals, Waste Package-to-Waste Package Impacts, WP 2

Impact Velocity (m/s)	Percentage of Yield Strength	Location				
		−0.30	−0.15	0.00	0.15	0.30
0.50	90%	0.0000	0.0000	0.0000	0.0000	0.0000
	100%	0.0000	0.0000	0.0000	0.0000	0.0000
	105%	0.0000	0.0000	0.0000	0.0000	0.0000
1.00	90%	0.0000	0.0000	0.0000	0.0000	0.0000
	100%	0.0000	0.0000	0.0000	0.0000	0.0000
	105%	0.0000	0.0000	0.0000	0.0000	0.0000
2.00	90%	0.0000	0.0000	0.0000	0.0000	0.0000
	100%	0.0000	0.0000	0.0000	0.0000	0.0000
	105%	0.0000	0.0000	0.0000	0.0000	0.0000
4.00	90%	0.0000	0.0000	0.0000	0.0000	0.0000
	100%	0.0000	0.0000	0.0000	0.0000	0.0000
	105%	0.0000	0.0000	0.0000	0.0000	0.0000
6.00	90%	0.0000	0.0000	0.0000	0.0000	0.0000
	100%	0.0000	0.0000	0.0000	0.0000	0.0000
	105%	0.0000	0.0000	0.0000	0.0000	0.0000
9.00	90%	0.0000	0.0000	0.0000	0.0000	0.0000
	100%	0.0000	0.0000	0.0000	0.0000	0.0000
	105%	0.0000	0.0000	0.0000	0.0000	0.0000

Output DTN: LL0704PA048SPC.023, file *NavalLong_TAD_WPWP_catalog_analyses_DA.xls,* sheet "WP2 i23."

Table 6-22. Damaged Areas (m^2) for TAD-Bearing Waste Packages, 23-mm OCB with Degraded Internals, Waste Package-to-Waste Package Impacts, WP 1

Impact Velocity (m/s)	Percentage of Yield Strength	Location				
		−0.30	−0.15	0.00	0.15	0.30
0.50	90%	0.0000	0.0000	0.0000	0.0000	0.0000
	100%	0.0000	0.0000	0.0000	0.0000	0.0000
	105%	0.0000	0.0000	0.0000	0.0000	0.0000
1.00	90%	0.0000	0.0000	0.0000	0.0000	0.0000
	100%	0.0000	0.0000	0.0000	0.0000	0.0000
	105%	0.0000	0.0000	0.0000	0.0000	0.0000
2.00	90%	0.0015	0.0000	0.0000	0.0000	0.0275
	100%	0.0000	0.0000	0.0000	0.0000	0.0055
	105%	0.0000	0.0000	0.0000	0.0000	0.0000
4.00	90%	0.0036	0.0000	0.0000	0.0000	0.0312
	100%	0.0000	0.0000	0.0000	0.0000	0.0000
	105%	0.0000	0.0000	0.0000	0.0000	0.0000
6.00	90%	0.0000	0.0000	0.0000	0.0035	0.0015
	100%	0.0000	0.0000	0.0000	0.0000	0.0000
	105%	0.0000	0.0000	0.0000	0.0000	0.0000
9.00	90%	0.0000	0.0000	0.0000	0.0014	0.0045
	100%	0.0000	0.0000	0.0000	0.0000	0.0000
	105%	0.0000	0.0000	0.0000	0.0000	0.0000

Output DTN: LL0704PA048SPC.023, file *NavalLong_TAD_WPWP_catalog_analyses_DA.xls,* sheet "WP1 d23."

Table 6-23. Damaged Areas (m^2) for TAD-Bearing Waste Packages, 23-mm OCB with Degraded Internals, Waste Package-to-Waste Package Impacts, WP 2

Impact Velocity (m/s)	Percentage of Yield Strength	Location				
		−0.30	−0.15	0.00	0.15	0.30
0.50	90%	0.0000	0.0000	0.0000	0.0000	0.0000
	100%	0.0000	0.0000	0.0000	0.0000	0.0000
	105%	0.0000	0.0000	0.0000	0.0000	0.0000
1.00	90%	0.0000	0.0000	0.0000	0.0000	0.0000
	100%	0.0000	0.0000	0.0000	0.0000	0.0000
	105%	0.0000	0.0000	0.0000	0.0000	0.0000
2.00	90%	0.0000	0.0000	0.0000	0.0000	0.0000
	100%	0.0000	0.0000	0.0000	0.0000	0.0000
	105%	0.0000	0.0000	0.0000	0.0000	0.0000
4.00	90%	0.0000	0.0000	0.0000	0.0000	0.0000
	100%	0.0000	0.0000	0.0000	0.0000	0.0000
	105%	0.0000	0.0000	0.0000	0.0000	0.0000
6.00	90%	0.0000	0.0000	0.0000	0.0000	0.0000
	100%	0.0000	0.0000	0.0000	0.0000	0.0000
	105%	0.0000	0.0000	0.0000	0.0000	0.0000

Table 6-23. Damaged Areas (m^2) for TAD-Bearing Waste Packages, 23-mm OCB with Degraded Internals, Waste Package-to-Waste Package Impacts, WP 2 (Continued)

Impact Velocity (m/s)	Percentage of Yield Strength	Location				
		−0.30	−0.15	0.00	0.15	-0.30
9.00	90%	0.0000	0.0000	0.0000	0.0000	0.0000
	100%	0.0000	0.0000	0.0000	0.0000	0.0000
	105%	0.0000	0.0000	0.0000	0.0000	0.0000

Output DTN: LL0704PA048SPC.023, file *NavalLong_TAD_WPWP_catalog_analyses_DA.xls,* sheet "WP2 d23."

Table 6-24. Damaged Areas (m^2) for TAD-Bearing Waste Packages, 17-mm OCB with Degraded Internals, Waste Package-to-Waste Package Impacts, WP 1

Impact Velocity (m/s)	Percentage of Yield Strength	Location				
		−0.30	−0.15	0.00	0.15	0.30
0.50	90%	0.0000	0.0000	0.0000	0.0000	0.0000
	100%	0.0000	0.0000	0.0000	0.0000	0.0000
	105%	0.0000	0.0000	0.0000	0.0000	0.0000
1.00	90%	0.0000	0.0000	0.0000	0.0000	0.0000
	100%	0.0000	0.0000	0.0000	0.0000	0.0000
	105%	0.0000	0.0000	0.0000	0.0000	0.0000
2.00	90%	0.0030	0.0000	0.0000	0.0000	0.0015
	100%	0.0000	0.0000	0.0000	0.0000	0.0000
	105%	0.0000	0.0000	0.0000	0.0000	0.0000
4.00	90%	0.0017	0.0000	0.0000	0.0000	0.0058
	100%	0.0000	0.0000	0.0000	0.0000	0.0000
	105%	0.0000	0.0000	0.0000	0.0000	0.0000
6.00	90%	0.0000	0.0000	0.0000	0.0000	0.0015
	100%	0.0000	0.0000	0.0000	0.0000	0.0000
	105%	0.0000	0.0000	0.0000	0.0000	0.0000
9.00	90%	0.0000	0.0000	0.0000	0.0000	0.0059
	100%	0.0000	0.0000	0.0000	0.0000	0.0000
	105%	0.0000	0.0000	0.0000	0.0000	0.0000

Output DTN: LL0704PA048SPC.023, file *NavalLong_TAD_WPWP_catalog_analyses_DA.xls,* sheet "WP1 d17."

Table 6-25. Damaged Areas (m^2) for TAD-Bearing Waste Packages, 17-mm OCB with Degraded Internals, Waste Package-to-Waste Package Impacts, WP 2

Impact Velocity (m/s)	Percentage of Yield Strength	Location				
		−0.30	−0.15	0.00	0.15	0.30
0.50	90%	0.0000	0.0000	0.0000	0.0000	0.0000
	100%	0.0000	0.0000	0.0000	0.0000	0.0000
	105%	0.0000	0.0000	0.0000	0.0000	0.0000

Table 6-25. Damaged Areas (m^2) for TAD-Bearing Waste Packages, 17-mm OCB with Degraded Internals, Waste Package-to-Waste Package Impacts, WP 2 (Continued)

Impact Velocity (m/s)	Percentage of Yield Strength	Location				
		−0.30	−0.15	0.00	0.15	0.30
1.00	90%	0.0000	0.0000	0.0000	0.0000	0.0000
	100%	0.0000	0.0000	0.0000	0.0000	0.0000
	105%	0.0000	0.0000	0.0000	0.0000	0.0000
2.00	90%	0.0000	0.0000	0.0000	0.0000	0.0000
	100%	0.0000	0.0000	0.0000	0.0000	0.0000
	105%	0.0000	0.0000	0.0000	0.0000	0.0000
4.00	90%	0.0000	0.0000	0.0000	0.0000	0.0000
	100%	0.0000	0.0000	0.0000	0.0000	0.0000
	105%	0.0000	0.0000	0.0000	0.0000	0.0000
6.00	90%	0.0000	0.0000	0.0000	0.0000	0.0000
	100%	0.0000	0.0000	0.0000	0.0000	0.0000
	105%	0.0000	0.0000	0.0000	0.0000	0.0000
9.00	90%	0.0016	0.0000	0.0000	0.0000	0.0000
	100%	0.0000	0.0000	0.0000	0.0000	0.0000
	105%	0.0000	0.0000	0.0000	0.0000	0.0000

Output DTN: LL0704PA048SPC.023, file *NavalLong_TAD_WPWP_catalog_analyses_DA.xls,* sheet "WP2 d17."

Table 6-26. Maximum Effective Strain and Rupture Condition for TAD-Bearing Waste Packages, 23-mm OCB with Intact Internals, Waste Package-to-Waste Package Impacts, WP 1

Impact Velocity (m/s)	Location									
	−0.30		−0.15		0		0.15		0.30	
	Maximum Effective Strain	Rupture	Maximum Effective Strain	Rupture	Maximum Effective Strain	Rupture	Maximum Effective Strain	Rupture	Maximum Effective Strain	Rupture
0.50	0.001	No	0.000	No	0.001	No	0.002	No	0.002	No
1.00	0.010	No	0.002	No	0.001	No	0.015	No	0.022	No
2.00	0.063	No	0.035	No	0.001	No	0.052	No	0.068	No
4.00	0.132	No	0.113	No	0.004	No	0.108	No	0.127	No
6.00	0.166	No	0.127	No	0.017	No	0.118	No	0.152	No
9.00	0.161	No	0.149	No	0.029	No	0.210	No	0.176	No

Output DTN: LL0704PA048SPC.023, file *NavalLong_TAD_WPWP_catalog_analyses_DA.xls,* sheet "WP1 i23."

Table 6-27. Maximum Effective Strain and Rupture Condition for TAD-Bearing Waste Packages, 23-mm OCB with Intact Internals, Waste Package-to-Waste Package Impacts, WP 2

Impact Velocity (m/s)	Location									
	−0.30		−0.15		0		0.15		0.30	
	Maximum Effective Strain	Rupture	Maximum Effective Strain	Rupture	Maximum Effective Strain	Rupture	Maximum Effective Strain	Rupture	Maximum Effective Strain	Rupture
0.50	0.000	No	0.000	No	0.001	No	0.000	No	0.001	No
1.00	0.001	No	0.001	No	0.001	No	0.001	No	0.001	No
2.00	0.001	No	0.001	No	0.001	No	0.001	No	0.001	No
4.00	0.002	No	0.004	No	0.002	No	0.003	No	0.002	No
6.00	0.005	No	0.005	No	0.005	No	0.003	No	0.006	No
9.00	0.121	No	0.098	No	0.006	No	0.029	No	0.014	No

Output DTN: LL0704PA048SPC.023, file *NavalLong_TAD_WPWP_catalog_analyses_DA.xls,* sheet "WP2 i23."

Table 6-28. Maximum Effective Strain and Rupture Condition for TAD-Bearing Waste Packages, 23-mm OCB with Degraded Internals, Waste Package-to-Waste Package Impacts, WP 1

Impact Velocity (m/s)	Location									
	−0.30		−0.15		0		0.15		0.30	
	Maximum Effective Strain	Rupture	Maximum Effective Strain	Rupture	Maximum Effective Strain	Rupture	Maximum Effective Strain	Rupture	Maximum Effective Strain	Rupture
0.50	0.000	No	0.000	No	0.000	No	0.001	No	0.001	No
1.00	0.001	No	0.001	No	0.001	No	0.002	No	0.002	No
2.00	0.009	No	0.001	No	0.001	No	0.012	No	0.018	No
4.00	0.054	No	0.026	No	0.001	No	0.038	No	0.066	No
6.00	0.095	No	0.069	No	0.002	No	0.073	No	0.104	No
9.00	0.143	No	0.118	No	0.009	No	0.118	No	0.137	No

Output DTN: LL0704PA048SPC.023, file *NavalLong_TAD_WPWP_catalog_analyses_DA.xls,* sheet "WP1 d23."

Table 6-29. Maximum Effective Strain and Rupture Condition for TAD-Bearing Waste Packages, 23-mm OCB with Degraded Internals, Waste Package-to-Waste Package Impacts, WP 2

Impact Velocity (m/s)	Location									
	−0.30		−0.15		0		0.15		0.30	
	Maximum Effective Strain	Rupture	Maximum Effective Strain	Rupture	Maximum Effective Strain	Rupture	Maximum Effective Strain	Rupture	Maximum Effective Strain	Rupture
0.50	0.000	No	0.000	No	0.000	No	0.000	No	0.000	No
1.00	0.001	No	0.001	No	0.001	No	0.001	No	0.001	No
2.00	0.001	No	0.001	No	0.001	No	0.001	No	0.001	No
4.00	0.002	No	0.002	No	0.002	No	0.003	No	0.003	No
6.00	0.008	No	0.008	No	0.008	No	0.010	No	0.010	No
9.00	0.023	No	0.021	No	0.021	No	0.023	No	0.025	No

Output DTN: LL0704PA048SPC.023, file *NavalLong_TAD_WPWP_catalog_analyses_DA.xls,* sheet "WP2 d23."

Table 6-30. Maximum Effective Strain and Rupture Condition for TAD-Bearing Waste Packages, 17-mm OCB with Degraded Internals, Waste Package-to-Waste Package Impacts, WP 1

Impact Velocity (m/s)	Location									
	−0.30		−0.15		0		0.15		0.30	
	Maximum Effective Strain	Rupture	Maximum Effective Strain	Rupture	Maximum Effective Strain	Rupture	Maximum Effective Strain	Rupture	Maximum Effective Strain	Rupture
0.50	0.000	No	0.000	No	0.000	No	0.001	No	0.001	No
1.00	0.001	No	0.001	No	0.001	No	0.002	No	0.003	No
2.00	0.012	No	0.002	No	0.001	No	0.011	No	0.025	No
4.00	0.047	No	0.039	No	0.021	No	0.049	No	0.061	No
6.00	0.076	No	0.066	No	0.004	No	0.078	No	0.085	No
9.00	0.096	No	0.100	No	0.009	No	0.098	No	0.113	No

Output DTN: LL0704PA048SPC.023, file *NavalLong_TAD_WPWP_catalog_analyses_DA.xls,* sheet "WP1 d17."

Table 6-31. Maximum Effective Strain and Rupture Condition for TAD-Bearing Waste Packages, 17-mm OCB with Degraded Internals, Waste Package-to-Waste Package Impacts, WP 2

Impact Velocity (m/s)	Location									
	−0.30		−0.15		0		0.15		0.30	
	Maximum Effective Strain	Rupture	Maximum Effective Strain	Rupture	Maximum Effective Strain	Rupture	Maximum Effective Strain	Rupture	Maximum Effective Strain	Rupture
0.50	0.000	No	0.000	No	0.000	No	0.000	No	0.000	No
1.00	0.001	No	0.001	No	0.001	No	0.001	No	0.001	No
2.00	0.001	No	0.001	No	0.001	No	0.001	No	0.001	No
4.00	0.004	No	0.003	No	0.003	No	0.005	No	0.006	No
6.00	0.015	No	0.012	No	0.014	No	0.014	No	0.016	No
9.00	0.027	No	0.027	No	0.027	No	0.029	No	0.030	No

Output DTN: LL0704PA048SPC.023, file *NavalLong_TAD_WPWP_catalog_analyses_DA.xls,* sheet "WP2 d17."

Table 6-32. Damaged Areas (m^2) for Codisposal Waste Packages, 23-mm OCB with Intact Internals, Waste Package-to-Waste Package Impacts

Impact Velocity (m/s)	Percentage of Yield Strength	Location				
		−0.30	−0.15	0.00	0.15	0.30
0.50	90%	0.0000	0.0000	0.0000	0.0000	0.0000
	100%	0.0000	0.0000	0.0000	0.0000	0.0000
	105%	0.0000	0.0000	0.0000	0.0000	0.0000
1.00	90%	0.0000	0.0000	0.0000	0.0000	0.0000
	100%	0.0000	0.0000	0.0000	0.0000	0.0000
	105%	0.0000	0.0000	0.0000	0.0000	0.0000
2.00	90%	0.0000	0.0000	0.0000	0.0000	0.0024
	100%	0.0000	0.0000	0.0000	0.0000	0.0000
	105%	0.0000	0.0000	0.0000	0.0000	0.0000

Table 6-32. Damaged Areas (m^2) for Codisposal Waste Packages, 23-mm OCB with Intact Internals, Waste Package-to-Waste Package Impacts (Continued)

Impact Velocity (m/s)	Percentage of Yield Strength	Location				
		−0.30	−0.15	0.00	0.15	0.30
4.00	90%	0.0060	0.0000	0.0000	0.0029	0.0025
	100%	0.0000	0.0000	0.0000	0.0000	0.0000
	105%	0.0000	0.0000	0.0000	0.0000	0.0000
6.00	90%	0.0000	0.0000	0.0000	0.0000	0.0000
	100%	0.0000	0.0000	0.0000	0.0000	0.0000
	105%	0.0000	0.0000	0.0000	0.0000	0.0000
9.00	90%	0.0000	0.0000	0.0000	0.0000	0.0013
	100%	0.0000	0.0000	0.0000	0.0000	0.0000
	105%	0.0000	0.0000	0.0000	0.0000	0.0000
10.00	90%	0.0054	0.0000	0.0000	0.0000	0.0062
	100%	0.0013	0.0000	0.0000	0.0000	0.0000
	105%	0.0000	0.0000	0.0000	0.0000	0.0000

Output DTN: LL0704PA049SPC.024, file *CDSP_WPWP_catalog_analyses_DA.xls,* sheet "i23."

Table 6-33. Damaged Areas (m^2) for Codisposal Waste Packages, 23-mm OCB with Degraded Internals, Waste Package-to-Waste Package Impacts

Impact Velocity (m/s)	Percentage of Yield Strength	Location				
		−0.30	−0.15	0.00	0.15	0.30
0.50	90%	0.0000	0.0000	0.0000	0.0000	0.0000
	100%	0.0000	0.0000	0.0000	0.0000	0.0000
	105%	0.0000	0.0000	0.0000	0.0000	0.0000
1.00	90%	0.0000	0.0000	0.0000	0.0000	0.0000
	100%	0.0000	0.0000	0.0000	0.0000	0.0000
	105%	0.0000	0.0000	0.0000	0.0000	0.0000
2.00	90%	0.0000	0.0000	0.0000	0.0000	0.0065
	100%	0.0000	0.0000	0.0000	0.0000	0.0000
	105%	0.0000	0.0000	0.0000	0.0000	0.0000
4.00	90%	0.0022	0.0000	0.0000	0.0000	0.0000
	100%	0.0000	0.0000	0.0000	0.0000	0.0000
	105%	0.0000	0.0000	0.0000	0.0000	0.0000
6.00	90%	0.0000	0.0000	0.0000	0.0064	0.0000
	100%	0.0000	0.0000	0.0000	0.0000	0.0000
	105%	0.0000	0.0000	0.0000	0.0000	0.0000
9.00	90%	0.0014	0.0000	0.0000	0.0137	0.0267
	100%	0.0000	0.0000	0.0000	0.0000	0.0014
	105%	0.0000	0.0000	0.0000	0.0000	0.0000
10.00	90%	0.0037	0.0000	0.0000	0.0155	0.0193
	100%	0.0000	0.0000	0.0000	0.0017	0.0014
	105%	0.0000	0.0000	0.0000	0.0000	0.0000

Output DTN: LL0704PA049SPC.024, file *CDSP_WPWP_catalog_analyses_DA.xls,* sheet "d23."

Table 6-34. Damaged Areas (m^2) for Codisposal Waste Packages, 17-mm OCB with Degraded Internals, Waste Package-to-Waste Package Impacts

Impact Velocity (m/s)	Percentage of Yield Strength	Location				
		−0.30	−0.15	0.00	0.15	0.30
0.50	90%	0.0000	0.0000	0.0000	0.0000	0.0000
	100%	0.0000	0.0000	0.0000	0.0000	0.0000
	105%	0.0000	0.0000	0.0000	0.0000	0.0000
1.00	90%	0.0000	0.0000	0.0000	0.0000	0.0000
	100%	0.0000	0.0000	0.0000	0.0000	0.0000
	105%	0.0000	0.0000	0.0000	0.0000	0.0000
2.00	90%	0.0000	0.0000	0.0000	0.0000	0.0000
	100%	0.0000	0.0000	0.0000	0.0000	0.0000
	105%	0.0000	0.0000	0.0000	0.0000	0.0000
4.00	90%	0.0000	0.0000	0.0000	0.0000	0.0014
	100%	0.0000	0.0000	0.0000	0.0000	0.0000
	105%	0.0000	0.0000	0.0000	0.0000	0.0000
6.00	90%	0.0000	0.0000	0.0000	0.0000	0.0000
	100%	0.0000	0.0000	0.0000	0.0000	0.0000
	105%	0.0000	0.0000	0.0000	0.0000	0.0000
9.00	90%	0.0000	0.0000	0.0000	0.0000	0.0074
	100%	0.0000	0.0000	0.0000	0.0000	0.0000
	105%	0.0000	0.0000	0.0000	0.0000	0.0000
10.00	90%	0.0000	0.0000	0.0000	0.0000	0.0052
	100%	0.0000	0.0000	0.0000	0.0000	0.0000
	105%	0.0000	0.0000	0.0000	0.0000	0.0000

Output DTN: LL0704PA049SPC.024, file *CDSP_WPWP_catalog_analyses_DA.xls,* sheet "d17."

Table 6-35. Maximum Effective Strain and Rupture Condition for Codisposal Waste Packages, 23-mm OCB with Intact Internals, Waste Package-to-Waste Package Impacts

Impact Velocity (m/s)	Location									
	−0.30		−0.15		0		0.15		0.30	
	Maximum Effective Strain	Rupture	Maximum Effective Strain	Rupture	Maximum Effective Strain	Rupture	Maximum Effective Strain	Rupture	Maximum Effective Strain	Rupture
0.50	0.001	No	0.001	No	0.001	No	0.002	No	0.007	No
1.00	0.004	No	0.004	No	0.002	No	0.007	No	0.026	No
2.00	0.029	No	0.026	No	0.012	No	0.034	No	0.081	No
4.00	0.096	No	0.063	No	0.039	No	0.068	No	0.137	No
6.00	0.188	No	0.140	No	0.066	No	0.095	No	0.146	No
9.00	0.282	No	0.279	No	0.130	No	0.172	No	0.262	No
10.00	0.301	No	0.294	No	0.167	No	0.198	No	0.274	No

Output DTN: LL0704PA049SPC.024, file *CDSP_WPWP_catalog_analyses_DA.xls,* sheet "i23."

Table 6-36. Maximum Effective Strain and Rupture Condition for Codisposal Waste Packages, 23-mm OCB with Degraded Internals, Waste Package-to-Waste Package Impacts

Impact Velocity (m/s)	Location									
	−0.30		−0.15		0		0.15		0.30	
	Maximum Effective Strain	Rupture	Maximum Effective Strain	Rupture	Maximum Effective Strain	Rupture	Maximum Effective Strain	Rupture	Maximum Effective Strain	Rupture
0.50	0.000	No	0.000	No	0.001	No	0.001	No	0.001	No
1.00	0.001	No	0.001	No	0.001	No	0.003	No	0.001	No
2.00	0.007	No	0.001	No	0.003	No	0.013	No	0.011	No
4.00	0.082	No	0.035	No	0.003	No	0.035	No	0.056	No
6.00	0.166	No	0.071	No	0.010	No	0.058	No	0.117	No
9.00	0.245	No	0.165	No	0.024	No	0.082	No	0.214	No
10.00	0.264	No	0.188	No	0.029	No	0.098	No	0.237	No

Output DTN: LL0704PA049SPC.024, file *CDSP_WPWP_catalog_analyses_DA.xls,* sheet "d23."

Table 6-37. Maximum Effective Strain and Rupture Condition for Codisposal Waste Packages, 17-mm OCB with Degraded Internals, Waste Package-to-Waste Package Impacts

Impact Velocity (m/s)	Location									
	−0.30		−0.15		0		0.15		0.30	
	Maximum Effective Strain	Rupture	Maximum Effective Strain	Rupture	Maximum Effective Strain	Rupture	Maximum Effective Strain	Rupture	Maximum Effective Strain	Rupture
0.50	0.000	No	0.000	No	0.000	No	0.001	No	0.001	No
1.00	0.001	No	0.001	No	0.001	No	0.002	No	0.002	No
2.00	0.008	No	0.001	No	0.001	No	0.011	No	0.017	No
4.00	0.086	No	0.023	No	0.003	No	0.035	No	0.057	No
6.00	0.138	No	0.068	No	0.013	No	0.055	No	0.107	No
9.00	0.207	No	0.143	No	0.025	No	0.096	No	0.199	No
10.00	0.235	No	0.158	No	0.030	No	0.112	No	0.231	No

Output DTN: LL0704PA049SPC.024, file *CDSP_WPWP_catalog_analyses_DA.xls,* sheet "d17."

6.3.2.2.7 Waste Package-to-Pallet Damage Lookup Tables

Waste package-to-pallet impact analyses for determining damaged area and rupture condition were performed for three states of the TAD-bearing and codisposal waste packages: 23-mm OCB with intact internals, 23-mm OCB with degraded internals, and 17-mm OCB with degraded internals. Analyses of the TAD-bearing and codisposal waste packages were performed for 188 and 209 configurations, respectively. Section 6.3.2.2.3 describes the various analysis configurations. Results for the TAD-bearing waste package are summarized in Table 6-38 to Table 6-63. Results for the codisposal waste package are summarized in Table 6-64 to Table 6-93.

For the TAD-bearing waste package with 23-mm OCB with intact internals, analyses were performed at impact angles of 0, +0.25, and +6 degrees. The analyses with a 0 degree impact angle were performed for impact velocities of 1.00 m/s and 2.00 m/s; with the waste package centered on the pallet. For the 0-degree impacts, the damaged area is determined separately for the left and right sides of the waste package. These locations are referred to as "< 1/2" and "> 1/2," respectively. The analyses with a +0.25- or +6-degree impact angle were performed for impact velocities of 1.00 m/s, 2.00 m/s, 3.00 m/s, 5.00 m/s, 7.00 m/s, and 10.00 m/s and impact locations of 1/8 point, 1/4 point and 1/2 point. At 1.00 m/s for all configurations with intact internals, there was zero computed damaged area. Thus, it was not necessary to perform analyses at lower impact velocities. The results for damaged area (at 90%, 100%, and 105% of yield strength) are presented in Table 6-38 to Table 6-40. No damaged area was computed on the OCB lids, so results for the lids are not presented in the tables. The results for rupture condition are presented in Table 6-55 to Table 6-57. The maximum effective strain is presented for each analysis, and a condition of "Yes" or "No" to designate whether the waste package is ruptured is presented. The procedure for determining the rupture condition is described in Section 6.3.2.2.5. For the TAD-bearing waste package with 23-mm OCB with intact internals, a rupture condition of "No" is predicted for all impacts.

For the TAD-bearing waste package with 23-mm OCB with degraded internals, analyses were performed at impact angles of 0, −0.25, and −6 degrees. The analyses with a 0-degree impact angle were performed for impact velocities of 0.30 m/s, 0.35 m/s, 0.40 m/s, 0.50 m/s, 1.00 m/s, and 2.00 m/s, with the waste package centered on the pallet. The analyses with a −0.25- or −6-degree impact angle were performed for impact velocities of 0.20 m/s, 0.25 m/s, 0.30 m/s, 0.35 m/s, 0.40 m/s, 0.50 m/s, 1.00 m/s, 2.00 m/s, 3.00 m/s, 5.00 m/s, 7.00 m/s, and 10.00 m/s and impact locations of 7/8, 3/4, and 1/2 points. At 0.30 m/s for 0 degrees and −0.25 degrees at 7/8 and 3/4 points, there was zero computed damaged area; and at 0.25 m/s for −6 degrees at 7/8 point, there was also zero computed damaged area. Thus, it was not necessary to perform analyses at lower impact velocities for these configurations. The results for damaged area (at 90%, 100%, and 105% of yield strength) are presented in Table 6-41 to Table 6-47. For the left and right OCB lids, the tables only include results for impact velocities of 7.00 m/s and 10.00 m/s because no damaged area was computed on the lids for impacts below 7.00 m/s. The results for rupture condition are presented in Table 6-58 to Table 6-60. For the TAD-bearing waste package with 23-mm OCB with degraded internals, a rupture condition of "No" is predicted for all impacts.

For the TAD-bearing waste package with 17-mm OCB with degraded internals, analyses were performed at impact angles of 0, −0.25, and −6 degrees. The analyses with a 0 degree impact angle were performed for impact velocities of 0.25 m/s, 0.30 m/s, 0.35 m/s, 0.40 m/s, 0.50 m/s, 1.00 m/s, and 2.00 m/s, with the waste package centered on the pallet. The analyses with a −0.25- or −6-degree impact angle were performed for impact velocities of 0.20 m/s, 0.25 m/s, 0.30 m/s, 0.35 m/s, 0.40 m/s, 0.50 m/s, 1.00 m/s, 2.00 m/s, 3.00 m/s, 5.00 m/s, 7.00 m/s, and 10.00 m/s and impact locations of 7/8, 3/4 and 1/2 points. At 0.25 m/s for 0 degrees and −0.25 degrees at 7/8 point, there was zero computed damaged area. Thus, it was not necessary to perform analyses at lower impact velocities for these configurations. The analysis at 10.00 m/s, −0.25 degrees at 1/2 point did not reach completion due to numerical issues. The results for damaged area (at 90%, 100%, and 105% of yield strength) are presented in Table 6-48 to Table 6-54. For the left and right OCB lids, the tables only include results for impact velocities of 7.00

m/s and 10.00 m/s because no damaged area was computed on the lids for impacts below 7.00 m/s. The results for rupture condition are presented in Table 6-61 to Table 6-63. For the TAD-bearing waste package with 17-mm OCB with degraded internals, a rupture condition of "No" is predicted for all impacts.

Input and output files for the TAD-bearing waste package analyses can be found in output DTN: LL0704PA048SPC.023, file (*NavalLong_TAD_WPP_catalog_analyses.tar.gz* and *NavalLong_ TAD_WPP_catalog_crvfiles.tar.gz*).

For the codisposal waste package with 23-mm OCB with intact internals, analyses were performed at impact angles of 0, +/-0.25, and +/-6 degrees. The analyses with a 0-degree impact angle were performed for impact velocities of 0.35 m/s, 0.50 m/s, 1.00 m/s, and 2.00 m/s; with the waste package centered on the pallet. The analyses with a +0.25- or +6-degree impact angle were performed for impact velocities of 0.15 m/s, 0.25 m/s, 0.35 m/s, 0.50 m/s, 1.00 m/s, 2.00 m/s, 3.00 m/s, 5.00 m/s, 7.00 m/s, and 10.00 m/s and impact locations of 1/8, 1/4 and 1/2 points. The analyses with a −0.25- or −6-degree impact angle were performed for impact velocities of 0.25 m/s, 0.35 m/s, 0.50 m/s, 1.00 m/s, 2.00 m/s, 3.00 m/s, 5.00 m/s, 7.00 m/s, and 10.00 m/s and impact locations of 7/8 and 3/4 points. At 0.35 m/s for 0 degrees, +0.25 degrees at 1/8 and 1/4 points, −0.25 degrees at 7/8 and 3/4 points, +6 degrees at 1/8 point, and −6 degrees at 7/8 point, there was zero computed damaged area; and at 0.25 m/s for +0.25 degrees at 1/2 point, +6 degrees at 1/4 point, and −6 degrees at 3/4, there was also zero computed damaged area. Thus, it was not necessary to perform analyses at lower impact velocities for these configurations. The results for damaged area (at 90%, 100%, and 105% of yield strength) are presented in Table 6-64 to Table 6-68. No damaged area was computed on the OCB lids, so results for the lids are not presented in the tables. The results for rupture condition are presented in Table 6-83 to Table 6-87. For the codisposal waste package with 23-mm OCB with intact internals, a rupture condition of "No" is predicted for all impacts.

For the codisposal waste package with 23-mm OCB with degraded internals, analyses were performed at impact angles of 0, −0.25, and −6 degrees. The analyses with a 0-degree impact angle were performed for impact velocities of 0.35 m/s, 0.50 m/s, 1.00 m/s, and 2.00 m/s, with the waste package centered on the pallet. The analyses with a −0.25- or −6-degree impact angle were performed for impact velocities of 0.15 m/s, 0.25 m/s, 0.35 m/s, 0.40 m/s, 0.50 m/s, 1.00 m/s, 2.00 m/s, 3.00 m/s, 5.00 m/s, 7.00 m/s, and 10.00 m/s and impact locations of 7/8, 3/4, and 1/2 points. At 0.35 m/s for 0 degrees, −0.25 degrees at 7/8 point, and −6 degrees at 7/8 point, there was zero computed damaged area; and at 0.25 m/s for −0.25 degrees at 3/4 point and −6 degrees at 3/4 point, there was also zero computed damaged area. Thus, it was not necessary to perform analyses at lower impact velocities for these configurations. The results for damaged area (at 90%, 100%, and 105% of yield strength) are presented in Table 6-69 to Table 6-75. For the left and right OCB lids, the tables only include results for impact velocities of 7.00 m/s and 10.00 m/s because no damaged area was computed on the lids for impacts below 7.00 m/s. The results for rupture condition are presented in Table 6-88 to Table 6-90. For the codisposal waste package with 23-mm OCB with degraded internals, a rupture condition of "No" is predicted for all impacts.

For the codisposal waste package with 17-mm OCB with degraded internals, analyses were performed at impact angles of 0, −0.25, and −6 degrees. The analyses with a 0-degree impact angle were performed for impact velocities of 0.25 m/s, 0.35 m/s, 0.50 m/s, 1.00 m/s, and 2.00 m/s; with the waste package centered on the pallet. The analyses with a −0.25- or −6-degree impact angle were performed for impact velocities of 0.15 m/s, 0.25 m/s, 0.35 m/s, 0.40 m/s, 0.50 m/s, 1.00 m/s, 2.00 m/s, 3.00 m/s, 5.00 m/s, 7.00 m/s, and 10.00 m/s and impact locations of 7/8, 3/4, and 1/2 points. At 0.25 m/s for 0 degrees, −0.25 degrees at 7/8 point, and −6 degrees at 7/8 point, there was zero computed damaged area. Thus, it was not necessary to perform analyses at lower impact velocities for these configurations. The analysis at 10.00 m/s, −0.25 degrees at 3/4 point did not reach completion due to numerical issues. The results for damaged area (at 90%, 100%, and 105% of yield strength) are presented in Table 6-76 to Table 6-82. For the left and right OCB lids, the tables only include results for impact velocities of 7.00 m/s and 10.00 m/s because no damaged area was computed on the lids for impacts below 7.00 m/s. The results for rupture condition are presented in Table 6-91 to Table 6-93. For the codisposal waste package with 17-mm OCB with degraded internals, a rupture condition of "No" is predicted for all impacts.

Input and output files for the codisposal waste package analyses can be found in output DTN: LL0704PA049SPC.024, file *CDSP_WPP_catalog_analyses.tar.gz* and *CDSP_WPP_catalog_ crvfiles.tar.gz*.

Table 6-38. Damaged Areas (m^2) for TAD-Bearing Waste Package Shells, 23-mm OCB with Intact Internals, Waste Package-to-Pallet Impacts, Impact Angle of 0 Degrees

Impact Velocity (m/s)	Percentage of Yield Strength	Location	
		< 1/2	> 1/2
1.00	90%	0.0000	0.0000
	100%	0.0000	0.0000
	105%	0.0000	0.0000
2.00	90%	0.0000	0.0000
	100%	0.0000	0.0000
	105%	0.0000	0.0000

Output DTN: LL0704PA048SPC.023, file *NavalLong_TAD_WPP_catalog_analyses_DA.xls,* sheet "i23 0 degrees."

Table 6-39. Damaged Areas (m^2) for TAD-Bearing Waste Package Shells, 23-mm OCB with Intact Internals, Waste Package-to-Pallet Impacts, Impact Angle of +0.25 Degrees

Impact Velocity (m/s)	Percentage of Yield Strength	Location		
		1/8	1/4	1/2
1.00	90%	0.0000	0.0000	0.0000
	100%	0.0000	0.0000	0.0000
	105%	0.0000	0.0000	0.0000
2.00	90%	0.0000	0.0009	0.0000
	100%	0.0000	0.0000	0.0000
	105%	0.0000	0.0000	0.0000

Table 6-39. Damaged Areas (m^2) for TAD-Bearing Waste Package Shells, 23-mm OCB with Intact Internals, Waste Package-to-Pallet Impacts, Impact Angle of +0.25 Degrees (Continued)

Impact Velocity (m/s)	Percentage of Yield Strength	Location		
		1/8	1/4	1/2
3.00	90%	0.0000	0.0000	0.0017
	100%	0.0000	0.0000	0.0000
	105%	0.0000	0.0000	0.0000
5.00	90%	0.0000	0.0000	0.0000
	100%	0.0000	0.0000	0.0000
	105%	0.0000	0.0000	0.0000
7.00	90%	0.0000	0.0000	0.0000
	100%	0.0000	0.0000	0.0000
	105%	0.0000	0.0000	0.0000
10.00	90%	0.0000	0.0000	0.0000
	100%	0.0000	0.0000	0.0000
	105%	0.0000	0.0000	0.0000

Output DTN: LL0704PA048SPC.023, file *NavalLong_TAD_WPP_catalog_analyses_DA.xls,* sheet "i23 +0.25 degrees."

Table 6-40. Damaged Areas (m^2) for TAD-Bearing Waste Package Shells, 23-mm OCB with Intact Internals, Waste Package-to-Pallet Impacts, Impact Angle of +6 Degrees

Impact Velocity (m/s)	Percentage of Yield Strength	Location		
		1/8	1/4	1/2
1.00	90%	0.0000	0.0000	0.0000
	100%	0.0000	0.0000	0.0000
	105%	0.0000	0.0000	0.0000
2.00	90%	0.0000	0.0052	0.0000
	100%	0.0000	0.0000	0.0000
	105%	0.0000	0.0000	0.0000
3.00	90%	0.0026	0.0000	0.0034
	100%	0.0000	0.0000	0.0000
	105%	0.0000	0.0000	0.0000
5.00	90%	0.0000	0.0000	0.0043
	100%	0.0000	0.0000	0.0000
	105%	0.0000	0.0000	0.0000
7.00	90%	0.0000	0.0009	0.0000
	100%	0.0000	0.0000	0.0000
	105%	0.0000	0.0000	0.0000
10.00	90%	0.0000	0.0000	0.0000
	100%	0.0000	0.0000	0.0000
	105%	0.0000	0.0000	0.0000

Output DTN: LL0704PA048SPC.023, file *NavalLong_TAD_WPP_catalog_analyses_DA.xls,* sheet "i23 +6 degrees."

Table 6-41. Damaged Areas (m^2) for TAD-Bearing Waste Package Shells, 23-mm OCB with Degraded Internals, Waste Package-to-Pallet Impacts, Impact Angle of 0 Degrees

Impact Velocity (m/s)	Percentage of Yield Strength	Location	
		< 1/2	> 1/2
0.30	90%	0.0000	0.0000
	100%	0.0000	0.0000
	105%	0.0000	0.0000
0.35	90%	0.0000	0.0000
	100%	0.0000	0.0000
	105%	0.0000	0.0000
0.40	90%	0.0000	0.0000
	100%	0.0000	0.0000
	105%	0.0000	0.0000
0.50	90%	0.0017	0.0017
	100%	0.0009	0.0017
	105%	0.0009	0.0009
1.00	90%	0.0696	0.0731
	100%	0.0378	0.0395
	105%	0.0180	0.0215
2.00	90%	0.1848	0.1873
	100%	0.0679	0.0602
	105%	0.0215	0.0112

Output DTN: LL0704PA048SPC.023, file *NavalLong_TAD_WPP_catalog_analyses_DA.xls,* sheet "d23 0 degrees."

Table 6-42. Damaged Areas (m^2) for TAD-Bearing Waste Package Shells, 23-mm OCB with Degraded Internals, Waste Package-to-Pallet Impacts, Impact Angle of −0.25 Degrees

Impact Velocity (m/s)	Percentage of Yield Strength	Location		
		7/8	3/4	1/2
0.20	90%	–	–	0.0000
	100%	–	–	0.0000
	105%	–	–	0.0000
0.25	90%	–	–	0.0017
	100%	–	–	0.0000
	105%	–	–	0.0000
0.30	90%	0.0000	0.0000	0.0034
	100%	0.0000	0.0000	0.0026
	105%	0.0000	0.0000	0.0009
0.35	90%	0.0000	0.0017	0.0060
	100%	0.0000	0.0000	0.0034
	105%	0.0000	0.0000	0.0000
0.40	90%	0.0000	0.0034	0.0103
	100%	0.0000	0.0026	0.0043
	105%	0.0000	0.0000	0.0017

Table 6-42. Damaged Areas (m^2) for TAD-Bearing Waste Package Shells, 23-mm OCB with Degraded Internals, Waste Package-to-Pallet Impacts, Impact Angle of −0.25 Degrees (Continued)

Impact Velocity (m/s)	Percentage of Yield Strength	Location		
		7/8	3/4	1/2
0.50	90%	0.0017	0.0095	0.0206
	100%	0.0009	0.0077	0.0155
	105%	0.0000	0.0026	0.0069
1.00	90%	0.0567	0.1392	0.1787
	100%	0.0292	0.0756	0.0962
	105%	0.0146	0.0369	0.0464
2.00	90%	0.2122	0.2852	0.3317
	100%	0.0997	0.1478	0.1779
	105%	0.0455	0.0954	0.0816
3.00	90%	0.3093	0.4030	0.4486
	100%	0.1332	0.1839	0.1556
	105%	0.0541	0.0971	0.0791
5.00	90%	0.3577	0.7010	1.3279
	100%	0.1091	0.1745	0.4220
	105%	0.0327	0.0696	0.1358
7.00	90%	0.3573	0.7069	1.4143
	100%	0.0979	0.1554	0.4629
	105%	0.0361	0.0705	0.1848
10.00	90%	0.3013	0.7887	3.0839
	100%	0.0721	0.2318	1.5312
	105%	0.0232	0.1349	0.7870

Output DTN: LL0704PA048SPC.023, file *NavalLong_TAD_WPP_catalog_analyses_DA.xls,* sheet "d23 −0.25 degrees."

Table 6-43. Damaged Areas (m^2) for TAD-Bearing Waste Package Shells, 23-mm OCB with Degraded Internals, Waste Package-to-Pallet Impacts, Impact Angle of −6 Degrees

Impact Velocity (m/s)	Percentage of Yield Strength	Location		
		7/8	3/4	1/2
0.20	90%	–	0.0000	0.0034
	100%	–	0.0000	0.0017
	105%	–	0.0000	0.0000
0.25	90%	0.0000	0.0026	0.0069
	100%	0.0000	0.0017	0.0017
	105%	0.0000	0.0000	0.0000
0.30	90%	0.0034	0.0060	0.0137
	100%	0.0000	0.0009	0.0060
	105%	0.0000	0.0000	0.0000

Table 6-43 Damaged Areas (m^2) for TAD-Bearing Waste Package Shells, 23-mm OCB with Degraded Internals, Waste Package-to-Pallet Impacts, Impact Angle of −6 Degrees (Continued)

Impact Velocity (m/s)	Percentage of Yield Strength	Location		
		7/8	3/4	1/2
0.35	90%	0.0034	0.0103	0.0163
	100%	0.0000	0.0043	0.0034
	105%	0.0000	0.0026	0.0009
0.40	90%	0.0069	0.0129	0.0241
	100%	0.0000	0.0060	0.0069
	105%	0.0000	0.0026	0.0000
0.50	90%	0.0112	0.0223	0.0395
	100%	0.0017	0.0069	0.0112
	105%	0.0000	0.0009	0.0000
1.00	90%	0.0593	0.1005	0.1538
	100%	0.0361	0.0636	0.0962
	105%	0.0103	0.0318	0.0507
2.00	90%	0.2028	0.2887	0.3618
	100%	0.0988	0.1487	0.1899
	105%	0.0464	0.0808	0.0963
3.00	90%	0.3283	0.4477	0.3945
	100%	0.1375	0.2183	0.1667
	105%	0.0765	0.1246	0.0816
5.00	90%	0.3996	0.6589	1.0039
	100%	0.1418	0.2516	0.1822
	105%	0.0258	0.0859	0.0808
7.00	90%	0.5027	0.7891	1.4802
	100%	0.1842	0.2275	0.3953
	105%	0.0691	0.1166	0.1976
10.00	90%	0.3780	0.9086	3.4183
	100%	0.1476	0.3435	1.7186
	105%	0.0859	0.2027	1.0578

Output DTN: LL0704PA048SPC.023, file *NavalLong_TAD_WPP_catalog_analyses_DA.xls,* sheet “d23 −6 degrees.”

Table 6-44. Damaged Areas (m^2) for Left Lid of TAD-Bearing Waste Packages, 23-mm OCB with Degraded Internals, Waste Package-to-Pallet Impacts, Impact Angle of −0.25 Degrees

Impact Velocity (m/s)	Percentage of Yield Strength	Location		
		7/8	3/4	1/2
7.00	90%	0.0000	0.0000	0.0000
	100%	0.0000	0.0000	0.0000
	105%	0.0000	0.0000	0.0000
10.00	90%	0.0000	0.0000	0.0044
	100%	0.0000	0.0000	0.0000
	105%	0.0000	0.0000	0.0000

Output DTN: LL0704PA048SPC.023, file *NavalLong_TAD_WPP_catalog_analyses_DA.xls,* sheet "d23 −0.25 degrees."

NOTE: Lower impact velocities that predicted zero damaged areas are not shown.

Table 6-45. Damaged Areas (m^2) for Right Lid of TAD-Bearing Waste Packages, 23-mm OCB with Degraded Internals, Waste Package-to-Pallet Impacts, Impact Angle of −0.25 Degrees

Impact Velocity (m/s)	Percentage of Yield Strength	Location		
		7/8	3/4	1/2
7.00	90%	0.0000	0.0000	0.0000
	100%	0.0000	0.0000	0.0000
	105%	0.0000	0.0000	0.0000
10.00	90%	0.0000	0.0000	0.0000
	100%	0.0000	0.0000	0.0000
	105%	0.0000	0.0000	0.0000

Output DTN: LL0704PA048SPC.023, file *NavalLong_TAD_WPP_catalog_analyses_DA.xls,* sheet "d23 −0.25 degrees."

NOTE: Lower impact velocities that predicted zero damaged areas are not shown.

Table 6-46. Damaged Areas (m^2) for Left Lid of TAD-Bearing Waste Packages, 23-mm OCB with Degraded Internals, Waste Package-to-Pallet Impacts, Impact Angle of −6 Degrees

Impact Velocity (m/s)	Percentage of Yield Strength	Location		
		7/8	3/4	1/2
7.00	90%	0.0000	0.0000	0.0000
	100%	0.0000	0.0000	0.0000
	105%	0.0000	0.0000	0.0000
10.00	90%	0.0000	0.0000	0.0603
	100%	0.0000	0.0000	0.0000
	105%	0.0000	0.0000	0.0000

Output DTN: LL0704PA048SPC.023, file *NavalLong_TAD_WPP_catalog_analyses_DA.xls,* sheet ""i23 −6 degrees."

NOTE: Lower impact velocities that predicted zero damaged areas are not shown.

Table 6-47. Damaged Areas (m^2) for Right Lid of TAD-Bearing Waste Packages, 23-mm OCB with Degraded Internals, Waste Package-to-Pallet Impacts, Impact Angle of −6 Degrees

Impact Velocity (m/s)	Percentage of Yield Strength	Location		
		7/8	3/4	1/2
7.00	90%	0.0000	0.0000	0.0000
	100%	0.0000	0.0000	0.0000
	105%	0.0000	0.0000	0.0000
10.00	90%	0.0000	0.0000	0.0000
	100%	0.0000	0.0000	0.0000
	105%	0.0000	0.0000	0.0000

Output DTN: LL0704PA048SPC.023, file *NavalLong_TAD_WPP_catalog_analyses_DA.xls,* sheet "d23 −6 degrees."

NOTE: Lower impact velocities that predicted zero damaged areas are not shown.

Table 6-48. Damaged Areas (m^2) for TAD-Bearing Waste Package Shells, 17-mm OCB with Degraded Internals, Waste Package-to-Pallet Impacts, Impact Angle of 0 Degrees

Impact Velocity (m/s)	Percentage of Yield Strength	Location	
		< 1/2	> 1/2
0.25	90%	0.0000	0.0000
	100%	0.0000	0.0000
	105%	0.0000	0.0000
0.30	90%	0.0017	0.0017
	100%	0.0000	0.0000
	105%	0.0000	0.0000
0.35	90%	0.0043	0.0043
	100%	0.0017	0.0017
	105%	0.0009	0.0017
0.40	90%	0.0069	0.0069
	100%	0.0052	0.0052
	105%	0.0026	0.0017
0.50	90%	0.0155	0.0155
	100%	0.0103	0.0112
	105%	0.0026	0.0026
1.00	90%	0.0928	0.0945
	100%	0.0387	0.0413
	105%	0.0086	0.0086
2.00	90%	0.2493	0.2527
	100%	0.0877	0.0911
	105%	0.0473	0.0481

Output DTN: LL0704PA048SPC.023, file *NavalLong_TAD_WPP_catalog_analyses_DA.xls,* sheet "d17 0 degrees."

Table 6-49. Damaged Areas (m^2) for TAD-Bearing Waste Package Shells, 17-mm OCB with Degraded Internals, Waste Package-to-Pallet Impacts, Impact Angle of −0.25 Degrees

Impact Velocity (m/s)	Percentage of Yield Strength	Location		
		7/8	3/4	1/2
0.20	90%	–	0.0000	0.0034
	100%	–	0.0000	0.0034
	105%	–	0.0000	0.0000
0.25	90%	0.0000	0.0034	0.0034
	100%	0.0000	0.0017	0.0034
	105%	0.0000	0.0000	0.0000
0.30	90%	0.0034	0.0034	0.0103
	100%	0.0009	0.0034	0.0026
	105%	0.0000	0.0017	0.0009
0.35	90%	0.0034	0.0095	0.0146
	100%	0.0034	0.0069	0.0095
	105%	0.0000	0.0000	0.0043
0.40	90%	0.0052	0.0137	0.0241
	100%	0.0043	0.0086	0.0112
	105%	0.0000	0.0009	0.0017
0.50	90%	0.0137	0.0249	0.0395
	100%	0.0077	0.0146	0.0189
	105%	0.0017	0.0069	0.0043
1.00	90%	0.0799	0.1650	0.2328
	100%	0.0318	0.0894	0.1461
	105%	0.0060	0.0215	0.0507
2.00	90%	0.2328	0.3755	0.3816
	100%	0.1100	0.1590	0.1702
	105%	0.0644	0.0756	0.0851
3.00	90%	0.3171	0.6498	0.7814
	100%	0.1280	0.1814	0.3292
	105%	0.0645	0.0954	0.1100
5.00	90%	0.2217	0.2415	0.6171
	100%	0.0636	0.0791	0.1582
	105%	0.0344	0.0473	0.0963
7.00	90%	0.1409	0.4968	2.0186
	100%	0.0610	0.2372	1.0965
	105%	0.0232	0.1349	0.7519
10.00	90%	0.4291	6.7964	–
	100%	0.2157	2.8679	–
	105%	0.1375	1.3138	–

Output DTN: LL0704PA048SPC.023, file *NavalLong_TAD_WPP_catalog_analyses_DA.xls,* sheet “d17 −0.25 degrees.”

Table 6-50. Damaged Areas (m^2) for TAD-Bearing Waste Package Shells, 17-mm OCB with Degraded Internals, Waste Package-to-Pallet Impacts, Impact Angle of −6 Degrees

Impact Velocity (m/s)	Percentage of Yield Strength	Location		
		7/8	3/4	1/2
0.20	90%	0.0009	0.0034	0.0052
	100%	0.0000	0.0017	0.0000
	105%	0.0000	0.0000	0.0000
0.25	90%	0.0034	0.0077	0.0137
	100%	0.0034	0.0034	0.0052
	105%	0.0000	0.0000	0.0000
0.30	90%	0.0052	0.0120	0.0146
	100%	0.0000	0.0060	0.0034
	105%	0.0000	0.0017	0.0000
0.35	90%	0.0103	0.0137	0.0241
	100%	0.0034	0.0034	0.0034
	105%	0.0000	0.0009	0.0000
0.40	90%	0.0137	0.0189	0.0344
	100%	0.0034	0.0043	0.0137
	105%	0.0000	0.0009	0.0017
0.50	90%	0.0189	0.0326	0.0550
	100%	0.0026	0.0103	0.0352
	105%	0.0000	0.0017	0.0129
1.00	90%	0.0790	0.1383	0.1985
	100%	0.0550	0.0851	0.1040
	105%	0.0352	0.0593	0.0756
2.00	90%	0.1787	0.3394	0.3335
	100%	0.0911	0.1916	0.1384
	105%	0.0627	0.0954	0.0636
3.00	90%	0.3204	0.5045	0.5338
	100%	0.1607	0.1960	0.1384
	105%	0.0722	0.0816	0.0619
5.00	90%	0.1926	0.2493	0.5544
	100%	0.0490	0.0954	0.1685
	105%	0.0146	0.0619	0.0791
7.00	90%	0.1667	0.5544	3.7709
	100%	0.0636	0.2518	1.2459
	105%	0.0292	0.1229	0.5852
10.00	90%	0.5624	6.0376	7.8455
	100%	0.2645	2.6471	2.8828
	105%	0.1562	0.9657	1.2696

Output DTN: LL0704PA048SPC.023, file *NavalLong_TAD_WPP_catalog_analyses_DA.xls,* sheet "d17 −6 degrees."

Table 6-51. Damaged Areas (m^2) for Left Lid of TAD-Bearing Waste Packages, 17-mm OCB with Degraded Internals, Waste Package-to-Pallet Impacts, Impact Angle of −0.25 Degrees

Impact Velocity (m/s)	Percentage of Yield Strength	Location		
		7/8	3/4	1/2
7.00	90%	0.0000	0.0000	0.0000
	100%	0.0000	0.0000	0.0000
	105%	0.0000	0.0000	0.0000
10.00	90%	0.0000	0.0100	–
	100%	0.0000	0.0000	–
	105%	0.0000	0.0000	–

Output DTN: LL0704PA048SPC.023, file *NavalLong_TAD_WPP_catalog_analyses_DA.xls,* sheet "d17 −0.25 degrees."

NOTE: Lower impact velocities that predicted zero damaged areas are not shown.

Table 6-52. Damaged Areas (m^2) for Right Lid of TAD-Bearing Waste Packages, 17-mm OCB with Degraded Internals, Waste Package-to-Pallet Impacts, Impact Angle of −0.25 Degrees

Impact Velocity (m/s)	Percentage of Yield Strength	Location		
		7/8	3/4	1/2
7.00	90%	0.0000	0.0000	0.0000
	100%	0.0000	0.0000	0.0000
	105%	0.0000	0.0000	0.0000
10.00	90%	0.0000	0.0638	–
	100%	0.0000	0.0100	–
	105%	0.0000	0.0015	–

Output DTN: LL0704PA048SPC.023, file *NavalLong_TAD_WPP_catalog_analyses_DA.xls,* sheet "d17 −0.25 degrees."

NOTE: Lower impact velocities that predicted zero damaged areas are not shown.

Table 6-53. Damaged Areas (m^2) for Left Lid of TAD-Bearing Waste Packages, 17-mm OCB with Degraded Internals, Waste Package-to-Pallet Impacts, Impact Angle of −6 Degrees

Impact Velocity (m/s)	Percentage of Yield Strength	Location		
		7/8	3/4	1/2
7.00	90%	0.0000	0.0000	0.0192
	100%	0.0000	0.0000	0.0000
	105%	0.0000	0.0000	0.0000
10.00	90%	0.0000	0.0000	0.6819
	100%	0.0000	0.0000	0.2652
	105%	0.0000	0.0000	0.1639

Output DTN: LL0704PA048SPC.023, file *NavalLong_TAD_WPP_catalog_analyses_DA.xls,* sheet "d17 −6 degrees."

NOTE: Lower impact velocities that predicted zero damaged areas are not shown.

Table 6-54. Damaged Areas (m^2) for Right Lid TAD-Bearing Waste Packages, 17-mm OCB with Degraded Internals, Waste Package-to-Pallet Impacts, Impact Angle of −6 Degrees

Impact Velocity (m/s)	Percentage of Yield Strength	Location		
		7/8	3/4	1/2
7.00	90%	0.0000	0.0000	0.0000
	100%	0.0000	0.0000	0.0000
	105%	0.0000	0.0000	0.0000
10.00	90%	0.0000	0.1443	0.1597
	100%	0.0000	0.0213	0.0087
	105%	0.0000	0.0037	0.0000

Output DTN: LL0704PA048SPC.023, file *NavalLong_TAD_WPP_catalog_analyses_DA.xls,* sheet "d17 −6 degrees."

NOTE: Lower impact velocities that predicted zero damaged areas are not shown.

Table 6-55. Maximum Effective Strain and Rupture Condition for TAD-Bearing Waste Packages, 23-mm OCB with Intact Internals, Waste Package-to-Pallet Impacts, Impact Angle of 0 Degree

Impact Velocity (m/s)	Location			
	< 1/2		> 1/2	
	Maximum Effective Strain	Rupture	Maximum Effective Strain	Rupture
1.00	0.017	No	0.017	No
2.00	0.021	No	0.022	No

Output DTN: LL0704PA048SPC.023, file *NavalLong_TAD_WPP_catalog_analyses_DA.xls,* sheet "i23 0 degrees."

Table 6-56. Maximum Effective Strain and Rupture Condition for TAD-Bearing Waste Packages, 23-mm OCB with Intact Internals, Waste Package-to-Pallet Impacts, Impact Angle of +0.25 Degrees

Impact Velocity (m/s)	Location					
	1/8		1/4		1/2	
	Maximum Effective Strain	Rupture	Maximum Effective Strain	Rupture	Maximum Effective Strain	Rupture
1.00	0.014	No	0.010	No	0.016	No
2.00	0.022	No	0.021	No	0.020	No
3.00	0.027	No	0.025	No	0.026	No
5.00	0.032	No	0.035	No	0.051	No
7.00	0.033	No	0.039	No	0.043	No
10.00	0.046	No	0.038	No	0.052	No

Output DTN: LL0704PA048SPC.023, file *NavalLong_TAD_WPP_catalog_analyses_DA.xls,* sheet "i23 +0.25 degrees."

Table 6-57. Maximum Effective Strain and Rupture Condition for TAD-Bearing Waste Packages, 23-mm OCB with Intact Internals, Waste Package-to-Pallet Impacts, Impact Angle of +6 Degrees

Impact Velocity (m/s)	Location					
	1/8		1/4		1/2	
	Maximum Effective Strain	Rupture	Maximum Effective Strain	Rupture	Maximum Effective Strain	Rupture
1.00	0.028	No	0.022	No	0.021	No
2.00	0.031	No	0.032	No	0.028	No
3.00	0.037	No	0.040	No	0.042	No
5.00	0.041	No	0.041	No	0.052	No
7.00	0.041	No	0.042	No	0.041	No
10.00	0.059	No	0.044	No	0.064	No

Output DTN: LL0704PA048SPC.023, file *NavalLong_TAD_WPP_catalog_analyses_DA.xls,* sheet "i23 +6 degrees."

Table 6-58. Maximum Effective Strain and Rupture Condition for TAD-Bearing Waste Packages, 23-mm OCB with Degraded Internals, Waste Package-to-Pallet Impacts, Impact Angle of 0 Degrees

Impact Velocity (m/s)	Location			
	< 1/2		> 1/2	
	Maximum Effective Strain	Rupture	Maximum Effective Strain	Rupture
0.30	0.002	No	0.002	No
0.35	0.003	No	0.003	No
0.40	0.005	No	0.005	No
0.50	0.008	No	0.009	No
1.00	0.031	No	0.031	No
2.00	0.045	No	0.044	No

Output DTN: LL0704PA048SPC.023, file *NavalLong_TAD_WPP_catalog_analyses_DA.xls,* sheet "d23 0 degrees."

Table 6-59. Maximum Effective Strain and Rupture Condition for TAD-Bearing Waste Packages, 23-mm OCB with Degraded Internals, Waste Package-to-Pallet Impacts, Impact Angle of −0.25 Degrees

Impact Velocity (m/s)	Location					
	7/8		3/4		1/2	
	Maximum Effective Strain	Rupture	Maximum Effective Strain	Rupture	Maximum Effective Strain	Rupture
0.20	–	–	–	–	0.005	No
0.25	–	–	–	–	0.008	No
0.30	0.003	No	0.005	No	0.010	No
0.35	0.004	No	0.007	No	0.013	No
0.40	0.005	No	0.009	No	0.015	No
0.50	0.008	No	0.013	No	0.022	No
1.00	0.027	No	0.032	No	0.037	No

Table 6-59. Maximum Effective Strain and Rupture Condition for TAD-Bearing Waste Packages, 23-mm OCB with Degraded Internals, Waste Package-to-Pallet Impacts, Impact Angle of −0.25 Degrees (Continued)

Impact Velocity (m/s)	Location					
	7/8		3/4		1/2	
	Maximum Effective Strain	Rupture	Maximum Effective Strain	Rupture	Maximum Effective Strain	Rupture
2.00	0.050	No	0.052	No	0.053	No
3.00	0.070	No	0.077	No	0.078	No
5.00	0.111	No	0.172	No	0.250	No
7.00	0.223	No	0.323	No	0.398	No
10.00	0.344	No	0.421	No	0.459	No

Output DTN: LL0704PA048SPC.023, file *NavalLong_TAD_WPP_catalog_analyses_DA.xls,* sheet "d23 −0.25 degrees."

Table 6-60. Maximum Effective Strain and Rupture Condition for TAD-Bearing Waste Packages, 23-mm OCB with Degraded Internals, Waste Package-to-Pallet Impacts, Impact Angle of −6 Degrees

Impact Velocity (m/s)	Location					
	7/8		3/4		1/2	
	Maximum Effective Strain	Rupture	Maximum Effective Strain	Rupture	Maximum Effective Strain	Rupture
0.20	–	–	0.006	No	0.010	No
0.25	0.005	No	0.011	No	0.016	No
0.30	0.008	No	0.017	No	0.023	No
0.35	0.011	No	0.024	No	0.029	No
0.40	0.015	No	0.029	No	0.034	No
0.50	0.025	No	0.038	No	0.041	No
1.00	0.052	No	0.071	No	0.070	No
2.00	0.068	No	0.081	No	0.098	No
3.00	0.093	No	0.104	No	0.128	No
5.00	0.126	No	0.241	No	0.365	No
7.00	0.216	No	0.375	No	0.501	No
10.00	0.311	No	0.446	No	0.671	No

Output DTN: LL0704PA048SPC.023, file *NavalLong_TAD_WPP_catalog_analyses_DA.xls,* sheet "d23 −6 degrees."

Table 6-61. Maximum Effective Strain and Rupture Condition for TAD-Bearing Waste Packages, 17-mm OCB with Degraded Internals, Waste Package-to-Pallet Impacts, Impact Angle of 0 Degrees

Impact Velocity (m/s)	Location			
	< 1/2		> 1/2	
	Maximum Effective Strain	Rupture	Maximum Effective Strain	Rupture
0.25	0.004	No	0.004	No
0.30	0.007	No	0.007	No
0.35	0.009	No	0.010	No
0.40	0.013	No	0.013	No
0.50	0.020	No	0.020	No
1.00	0.035	No	0.034	No
2.00	0.046	No	0.044	No

Output DTN: LL0704PA048SPC.023, file *NavalLong_TAD_WPP_catalog_analyses_DA.xls,* sheet "d217 0 degrees."

Table 6-62. Maximum Effective Strain and Rupture Condition for TAD-Bearing Waste Packages, 17-mm OCB with Degraded Internals, Waste Package-to-Pallet Impacts, Impact Angle of −0.25 Degrees

Impact Velocity (m/s)	Location					
	7/8		3/4		1/2	
	Maximum Effective Strain	Rupture	Maximum Effective Strain	Rupture	Maximum Effective Strain	Rupture
0.20	–	–	0.006	No	0.009	No
0.25	0.006	No	0.008	No	0.012	No
0.30	0.007	No	0.011	No	0.015	No
0.35	0.009	No	0.014	No	0.018	No
0.40	0.011	No	0.018	No	0.021	No
0.50	0.016	No	0.023	No	0.024	No
1.00	0.032	No	0.034	No	0.037	No
2.00	0.053	No	0.047	No	0.059	No
3.00	0.074	No	0.073	No	0.106	No
5.00	0.082	No	0.123	No	0.252	No
7.00	0.083	No	0.231	No	0.487	No
10.00	0.201	No	0.344	No	–	–

Output DTN: LL0704PA048SPC.023, file *NavalLong_TAD_WPP_catalog_analyses_DA.xls,* sheet "d17 −0.25 degrees."

Table 6-63. Maximum Effective Strain and Rupture Condition for TAD-Bearing Waste Packages, 17-mm OCB with Degraded Internals, Waste Package-to-Pallet Impacts, Impact Angle of −6 Degrees

Impact Velocity (m/s)	Location					
	7/8		3/4		1/2	
	Maximum Effective Strain	Rupture	Maximum Effective Strain	Rupture	Maximum Effective Strain	Rupture
0.20	0.006	No	0.011	No	0.015	No
0.25	0.010	No	0.020	No	0.022	No
0.30	0.014	No	0.026	No	0.026	No
0.35	0.019	No	0.031	No	0.029	No
0.40	0.023	No	0.035	No	0.032	No
0.50	0.028	No	0.043	No	0.037	No
1.00	0.049	No	0.061	No	0.070	No
2.00	0.080	No	0.085	No	0.104	No
3.00	0.111	No	0.121	No	0.232	No
5.00	0.118	No	0.269	No	0.323	No
7.00	0.140	No	0.256	No	0.523	No
10.00	0.257	No	0.489	No	0.488	No

Output DTN: LL0704PA048SPC.023, file *NavalLong_TAD_WPP_catalog_analyses_DA.xls,* sheet "d17 −6 degrees."

Table 6-64. Damaged Areas (m^2) for Codisposal Waste Package Shells, 23-mm OCB with Intact Internals, Waste Package-to-Pallet Impacts, Impact Angle of 0 Degrees

Impact Velocity (m/s)	Percentage of Yield Strength	Location	
		< 1/2	> 1/2
0.35	90%	0.0000	0.0000
	100%	0.0000	0.0000
	105%	0.0000	0.0000
0.50	90%	0.0000	0.0009
	100%	0.0000	0.0000
	105%	0.0000	0.0000
1.00	90%	0.0077	0.0086
	100%	0.0009	0.0000
	105%	0.0000	0.0000
2.00	90%	0.0137	0.0120
	100%	0.0000	0.0000
	105%	0.0000	0.0000

Output DTN: LL0704PA049SPC.024, file *CDSP_WPP_catalog_analyses_DA.xls,* sheet "i23 0 degrees."

Table 6-65. Damaged Areas (m^2) for Codisposal Waste Package Shells, 23-mm OCB with Intact Internals, Waste Package-to-Pallet Impacts, Impact Angle of +0.25 Degrees

Impact Velocity (m/s)	Percentage of Yield Strength	Location		
		1/8	1/4	1/2
0.25	90%	–	–	0.0000
	100%	–	–	0.0000
	105%	–	–	0.0000
0.35	90%	0.0000	0.0000	0.0009
	100%	0.0000	0.0000	0.0000
	105%	0.0000	0.0000	0.0000
0.50	90%	0.0009	0.0017	0.0034
	100%	0.0000	0.0009	0.0000
	105%	0.0000	0.0000	0.0000
1.00	90%	0.0103	0.0128	0.0120
	100%	0.0009	0.0000	0.0000
	105%	0.0000	0.0000	0.0000
2.00	90%	0.0231	0.0240	0.0693
	100%	0.0000	0.0009	0.0000
	105%	0.0000	0.0000	0.0000
3.00	90%	0.0488	0.1070	0.0539
	100%	0.0000	0.0009	0.0000
	105%	0.0000	0.0000	0.0000
5.00	90%	0.0402	0.0274	0.0642
	100%	0.0000	0.0000	0.0000
	105%	0.0000	0.0000	0.0000
7.00	90%	0.0137	0.0163	0.0137
	100%	0.0000	0.0000	0.0000
	105%	0.0000	0.0000	0.0000
10.00	90%	0.0308	0.0394	0.0762
	100%	0.0000	0.0000	0.0060
	105%	0.0000	0.0000	0.0000

Output DTN: LL0704PA049SPC.024, file *CDSP_WPP_catalog_analyses_DA.xls,* sheet "i23 +0.25 degrees."

Table 6-66. Damaged Areas (m^2) for Codisposal Waste Package Shells, 23-mm OCB with Intact Internals, Waste Package-to-Pallet Impacts, Impact Angle of −0.25 Degrees

Impact Velocity (m/s)	Percentage of Yield Strength	Location	
		7/8	3/4
0.35	90%	0.0000	0.0000
	100%	0.0000	0.0000
	105%	0.0000	0.0000
0.50	90%	0.0009	0.0017
	100%	0.0000	0.0009
	105%	0.0000	0.0000
1.00	90%	0.0103	0.0111
	100%	0.0000	0.0000
	105%	0.0000	0.0000
2.00	90%	0.0214	0.0360
	100%	0.0000	0.0000
	105%	0.0000	0.0000
3.00	90%	0.0462	0.1104
	100%	0.0000	0.0000
	105%	0.0000	0.0000
5.00	90%	0.0248	0.0608
	100%	0.0000	0.0000
	105%	0.0000	0.0000
7.00	90%	0.0351	0.0342
	100%	0.0000	0.0000
	105%	0.0000	0.0000
10.00	90%	0.0471	0.0642
	100%	0.0000	0.0000
	105%	0.0000	0.0000

Output DTN: LL0704PA049SPC.024, file *CDSP_WPP_catalog_analyses_DA.xls,* sheet “i23 −0.25 degrees.”

Table 6-67. Damaged Areas (m^2) for Codisposal Waste Package Shells, 23-mm OCB with Intact Internals, Waste Package-to-Pallet Impacts, Impact Angle of +6 Degrees

Impact Velocity (m/s)	Percentage of Yield Strength	Location		
		1/8	1/4	1/2
0.15	90%	–	–	0.0000
	100%	–	–	0.0000
	105%	–	–	0.0000
0.25	90%	–	0.0000	0.0009
	100%	–	0.0000	0.0000
	105%	–	0.0000	0.0000
0.35	90%	0.0000	0.0009	0.0034
	100%	0.0000	0.0000	0.0026
	105%	0.0000	0.0000	0.0000
0.50	90%	0.0000	0.0043	0.0060
	100%	0.0000	0.0000	0.0000
	105%	0.0000	0.0000	0.0000
1.00	90%	0.0086	0.0068	0.0137
	100%	0.0017	0.0000	0.0026
	105%	0.0000	0.0000	0.0009
2.00	90%	0.0385	0.0471	0.0522
	100%	0.0111	0.0043	0.0060
	105%	0.0017	0.0000	0.0009
3.00	90%	0.0497	0.0659	0.0796
	100%	0.0043	0.0128	0.0128
	105%	0.0000	0.0000	0.0051
5.00	90%	0.0676	0.0685	0.1686
	100%	0.0017	0.0051	0.0317
	105%	0.0000	0.0000	0.0060
7.00	90%	0.1002	0.0873	0.1121
	100%	0.0017	0.0026	0.0111
	105%	0.0000	0.0000	0.0000
10.00	90%	0.1053	0.1096	0.1259
	100%	0.0000	0.0043	0.0086
	105%	0.0000	0.0000	0.0000

Output DTN: LL0704PA049SPC.024, file *CDSP_WPP_catalog_analyses_DA.xls,* sheet "i23 +6 degrees."

Table 6-68. Damaged Areas (m^2) for Codisposal Waste Package Shells, 23-mm OCB with Intact Internals, Waste Package-to-Pallet Impacts, Impact Angle of −6 Degrees

Impact Velocity (m/s)	Percentage of Yield Strength	Location	
		7/8	3/4
0.25	90%	–	0.0000
	100%	–	0.0000
	105%	–	0.0000
0.35	90%	0.0000	0.0017
	100%	0.0000	0.0009
	105%	0.0000	0.0000
0.50	90%	0.0026	0.0043
	100%	0.0000	0.0000
	105%	0.0000	0.0000
1.00	90%	0.0103	0.0103
	100%	0.0017	0.0017
	105%	0.0009	0.0000
2.00	90%	0.0300	0.0445
	100%	0.0060	0.0068
	105%	0.0000	0.0000
3.00	90%	0.0402	0.0642
	100%	0.0034	0.0068
	105%	0.0000	0.0000
5.00	90%	0.0599	0.1002
	100%	0.0077	0.0060
	105%	0.0000	0.0000
7.00	90%	0.0762	0.1224
	100%	0.0009	0.0154
	105%	0.0000	0.0000
10.00	90%	0.0848	0.1387
	100%	0.0009	0.0043
	105%	0.0000	0.0000

Output DTN: LL0704PA049SPC.024, file *CDSP_WPP_catalog_analyses_DA.xls,* sheet “i23 −6 degrees.”

Table 6-69. Damaged Areas (m^2) for Codisposal Waste Package Shells, 23-mm OCB with Degraded Internals, Waste Package-to-Pallet Impacts, Impact Angle of 0 Degrees

Impact Velocity (m/s)	Percentage of Yield Strength	Location	
		< 1/2	> 1/2
0.35	90%	0.0000	0.0000
	100%	0.0000	0.0000
	105%	0.0000	0.0000
0.50	90%	0.0009	0.0026
	100%	0.0009	0.0009
	105%	0.0000	0.0000
1.00	90%	0.0376	0.0496
	100%	0.0222	0.0222
	105%	0.0060	0.0094
2.00	90%	0.1660	0.1702
	100%	0.0599	0.0667
	105%	0.0163	0.0180

Output DTN: LL0704PA049SPC.024, file *CDSP_WPP_catalog_analyses_DA.xls,* sheet "d23 0 degrees."

Table 6-70. Damaged Areas (m^2) for Codisposal Waste Package Shells, 23-mm OCB with Degraded Internals, Waste Package-to-Pallet Impacts, Impact Angle of −0.25 Degrees

Impact Velocity (m/s)	Percentage of Yield Strength	Location		
		7/8	3/4	1/2
0.15	90%	–	–	0.0000
	100%	–	–	0.0000
	105%	–	–	0.0000
0.25	90%	–	0.0000	0.0009
	100%	–	0.0000	0.0000
	105%	–	0.0000	0.0000
0.35	90%	0.0000	0.0009	0.0060
	100%	0.0000	0.0000	0.0026
	105%	0.0000	0.0000	0.0009
0.50	90%	0.0009	0.0086	0.0180
	100%	0.0009	0.0043	0.0086
	105%	0.0000	0.0009	0.0034
1.00	90%	0.0411	0.1233	0.1609
	100%	0.0214	0.0616	0.0813
	105%	0.0086	0.0248	0.0036
2.00	90%	0.2037	0.2996	0.3441
	100%	0.0993	0.1421	0.1575
	105%	0.0351	0.0796	0.0873

Table 6-70. Damaged Areas (m^2) for Codisposal Waste Package Shells, 23-mm OCB with Degraded Internals, Waste Package-to-Pallet Impacts, Impact Angle of −0.25 Degrees (Continued)

Impact Velocity (m/s)	Percentage of Yield Strength	Location		
		7/8	3/4	1/2
3.00	90%	0.2953	0.4555	0.4606
	100%	0.1318	0.2517	0.2243
	105%	0.0565	0.1139	0.1096
5.00	90%	0.3879	0.6345	1.0266
	100%	0.1387	0.1747	0.3031
	105%	0.0300	0.0959	0.1216
7.00	90%	0.3978	0.7021	1.0335
	100%	0.1070	0.1336	0.2475
	105%	0.0103	0.0557	0.0882
10.00	90%	0.2993	0.5810	1.1159
	100%	0.0715	0.1627	0.3681
	105%	0.0214	0.0950	0.2157

Output DTN: LL0704PA049SPC.024, file *CDSP_WPP_catalog_analyses_DA.xls,* sheet "d23 −0.25 degrees."

Table 6-71. Damaged Areas (m^2) for Codisposal Waste Package Shells, 23-mm OCB with Degraded Internals, Waste Package-to-Pallet Impacts, Impact Angle of −6 Degrees

Impact Velocity (m/s)	Percentage of Yield Strength	Location		
		7/8	3/4	1/2
0.15	90%	–	–	0.0000
	100%	–	–	0.0000
	105%	–	–	0.0000
0.25	90%	–	0.0000	0.0051
	100%	–	0.0000	0.0000
	105%	–	0.0000	0.0000
0.35	90%	0.0000	0.0068	0.0137
	100%	0.0000	0.0009	0.0017
	105%	0.0000	0.0000	0.0000
0.50	90%	0.0103	0.0197	0.0360
	100%	0.0017	0.0034	0.0077
	105%	0.0000	0.0000	0.0009
1.00	90%	0.0479	0.0873	0.1335
	100%	0.0231	0.0505	0.0796
	105%	0.0017	0.0283	0.0385
2.00	90%	0.1729	0.2654	0.3382
	100%	0.0805	0.1378	0.1849
	105%	0.0291	0.0711	0.0762

Table 6-71. Damaged Areas (m^2) for Codisposal Waste Package Shells, 23-mm OCB with Degraded Internals, Waste Package-to-Pallet Impacts, Impact Angle of −6 Degrees (Continued)

Impact Velocity (m/s)	Percentage of Yield Strength	Location		
		7/8	3/4	1/2
3.00	90%	0.2560	0.4640	0.3878
	100%	0.1361	0.2269	0.2038
	105%	0.0676	0.1070	0.0839
5.00	90%	0.3776	0.5959	0.9213
	100%	0.1635	0.1695	0.1738
	105%	0.0557	0.1027	0.0967
7.00	90%	0.4396	0.6861	1.0565
	100%	0.1797	0.1824	0.2329
	105%	0.0873	0.1105	0.0899
10.00	90%	0.4402	0.6704	1.3188
	100%	0.1506	0.1943	0.5393
	105%	0.0728	0.1259	0.2970

Output DTN: LL0704PA049SPC.024, file *CDSP_WPP_catalog_analyses_DA.xls,* sheet "d23 −6 degrees."

Table 6-72. Damaged Areas (m^2) for Left Lid of Codisposal Waste Packages, 23-mm OCB with Degraded Internals, Waste Package-to-Pallet Impacts, Impact Angle of −0.25 Degrees

Impact Velocity (m/s)	Percentage of Yield Strength	Location		
		7/8	3/4	1/2
7.00	90%	0.0000	0.0000	0.0000
	100%	0.0000	0.0000	0.0000
	105%	0.0000	0.0000	0.0000
10.00	90%	0.0000	0.0000	0.0114
	100%	0.0000	0.0000	0.0000
	105%	0.0000	0.0000	0.0000

Output DTN: LL0704PA049SPC.024, file *CDSP_WPP_catalog_analyses_DA.xls,* sheet "d23 −0.25 degrees."

NOTE: Lower impact velocities that predicted zero damaged areas are not shown.

Table 6-73. Damaged Areas (m^2) for Right Lid of Codisposal Waste Packages, 23-mm OCB with Degraded Internals, Waste Package-to-Pallet Impacts, Impact Angle of −0.25 Degrees

Impact Velocity (m/s)	Percentage of Yield Strength	Location		
		7/8	3/4	1/2
7.00	90%	0.0000	0.0000	0.0000
	100%	0.0000	0.0000	0.0000
	105%	0.0000	0.0000	0.0000
10.00	90%	0.0544	0.0000	0.0000
	100%	0.0030	0.0000	0.0000
	105%	0.0000	0.0000	0.0000

Output DTN: LL0704PA049SPC.024, file *CDSP_WPP_catalog_analyses_DA.xls,* sheet "d23 −0.25 degrees."

NOTE: Lower impact velocities that predicted zero damaged areas are not shown.

Table 6-74. Damaged Areas (m^2) for Left Lid of Codisposal Waste Packages, 23-mm OCB with Degraded Internals, Waste Package-to-Pallet Impacts, Impact Angle of −6 Degrees

Impact Velocity (m/s)	Percentage of Yield Strength	Location		
		7/8	3/4	1/2
7.00	90%	0.0000	0.0000	0.0000
	100%	0.0000	0.0000	0.0000
	105%	0.0000	0.0000	0.0000
10.00	90%	0.0000	0.0000	0.0000
	100%	0.0000	0.0000	0.0000
	105%	0.0000	0.0000	0.0000

Output DTN: LL0704PA049SPC.024, file *CDSP_WPP_catalog_analyses_DA.xls,* sheet "d23 −6 degrees."

NOTE: Lower impact velocities that predicted zero damaged areas are not shown.

Table 6-75. Damaged Areas (m^2) for Right Lid of Codisposal Waste Packages, 23-mm OCB with Degraded Internals, Waste Package-to-Pallet Impacts, Impact Angle of −6 Degrees

Impact Velocity (m/s)	Percentage of Yield Strength	Location		
		7/8	3/4	1/2
7.00	90%	0.0000	0.0000	0.0000
	100%	0.0000	0.0000	0.0000
	105%	0.0000	0.0000	0.0000
10.00	90%	0.0774	0.0095	0.0000
	100%	0.0034	0.0000	0.0000
	105%	0.0000	0.0000	0.0000

Output DTN: LL0704PA049SPC.024, file *CDSP_WPP_catalog_analyses_DA.xls,* sheet "d23 −6 degrees."

NOTE: Lower impact velocities that predicted zero damaged areas are not shown.

Table 6-76. Damaged Areas (m^2) for Codisposal Waste Package Shells, 17-mm OCB with Degraded Internals, Waste Package-to-Pallet Impacts, Impact Angle of 0 Degrees

Impact Velocity (m/s)	Percentage of Yield Strength	Location	
		< 1/2	> 1/2
0.25	90%	0.0000	0.0000
	100%	0.0000	0.0000
	105%	0.0000	0.0000
0.35	90%	0.0017	0.0026
	100%	0.0009	0.0017
	105%	0.0000	0.0000
0.50	90%	0.0103	0.0111
	100%	0.0068	0.0077
	105%	0.0009	0.0009
1.00	90%	0.0607	0.0650
	100%	0.0111	0.0128
	105%	0.0026	0.0009
2.00	90%	0.1754	0.1976
	100%	0.0727	0.0804
	105%	0.0274	0.0342

Output DTN: LL0704PA049SPC.024, file *CDSP_WPP_catalog_analyses_DA.xls,* sheet "d17 0 degrees."

Table 6-77. Damaged Areas (m^2) for Codisposal Waste Package Shells, 17-mm OCB with Degraded Internals, Waste Package-to-Pallet Impacts, Impact Angle of −0.25 Degrees

Impact Velocity (m/s)	Percentage of Yield Strength	Location		
		7/8	3/4	1/2
0.15	90%	–	0.0000	0.0000
	100%	–	0.0000	0.0000
	105%	–	0.0000	0.0000
0.25	90%	0.0000	0.0017	0.0043
	100%	0.0000	0.0009	0.0034
	105%	0.0000	0.0000	0.0000
0.35	90%	0.0017	0.0060	0.0128
	100%	0.0017	0.0034	0.0051
	105%	0.0000	0.0000	0.0000
0.50	90%	0.0094	0.0214	0.0351
	100%	0.0060	0.0120	0.0188
	105%	0.0009	0.0034	0.0034
1.00	90%	0.0711	0.1438	0.2123
	100%	0.0094	0.0462	0.1130
	105%	0.0009	0.0034	0.0300
2.00	90%	0.2046	0.3904	0.4298
	100%	0.0899	0.1319	0.2098
	105%	0.0420	0.0685	0.0985
3.00	90%	0.2791	0.5360	0.7400
	100%	0.1096	0.2106	0.2286
	105%	0.0497	0.1293	0.1087
5.00	90%	0.3733	0.2244	0.5378
	100%	0.1730	0.0505	0.1901
	105%	0.0856	0.0205	0.0642
7.00	90%	0.1242	0.2971	1.4562
	100%	0.0325	0.1379	0.3579
	105%	0.0120	0.0839	0.1515
10.00	90%	0.2962	–	8.2512
	100%	0.1661	–	4.3122
	105%	0.1036	–	2.4829

Output DTN: LL0704PA049SPC.024, file *CDSP_WPP_catalog_analyses_DA.xls,* sheet "d17 −0.25 degrees."

Table 6-78. Damaged Areas (m^2) for Codisposal Waste Package Shells, 17-mm OCB with Degraded Internals, Waste Package-to-Pallet Impacts, Impact Angle of −6 Degrees

Impact Velocity (m/s)	Percentage of Yield Strength	Location		
		7/8	3/4	1/2
0.15	90%	–	0.0000	0.0017
	100%	–	0.0000	0.0000
	105%	–	0.0000	0.0000
0.25	90%	0.0000	0.0034	0.0103
	100%	0.0000	0.0017	0.0034
	105%	0.0000	0.0000	0.0000
0.35	90%	0.0060	0.0146	0.0205
	100%	0.0026	0.0026	0.0017
	105%	0.0000	0.0000	0.0000
0.50	90%	0.0188	0.0283	0.0479
	100%	0.0051	0.0060	0.0308
	105%	0.0000	0.0000	0.0077
1.00	90%	0.0719	0.1199	0.1704
	100%	0.0402	0.0736	0.1010
	105%	0.0240	0.0479	0.0642
2.00	90%	0.1413	0.3203	0.3151
	100%	0.0873	0.1687	0.1901
	105%	0.0548	0.0728	0.0993
3.00	90%	0.3048	0.4144	0.5437
	100%	0.1165	0.1841	0.1533
	105%	0.0659	0.0933	0.0676
5.00	90%	0.3074	0.2749	0.3665
	100%	0.0993	0.0916	0.1139
	105%	0.0300	0.0531	0.0317
7.00	90%	0.1901	0.3579	1.1155
	100%	0.0497	0.1473	0.1498
	105%	0.0146	0.0839	0.0702
10.00	90%	0.4324	2.1899	8.5502
	100%	0.1841	0.5059	4.3412
	105%	0.1045	0.2864	2.8237

Output DTN: LL0704PA049SPC.024, file *CDSP_WPP_catalog_analyses_DA.xls,* sheet “d17 −6 degrees.”

Table 6-79. Damaged Areas (m^2) for Left Lid of Codisposal Waste Packages, 17-mm OCB with Degraded Internals, Waste Package-to-Pallet Impacts, Impact Angle of −0.25 Degrees

Impact Velocity (m/s)	Percentage of Yield Strength	Location		
		7/8	3/4	1/2
7.00	90%	0.0000	0.0000	0.0000
	100%	0.0000	0.0000	0.0000
	105%	0.0000	0.0000	0.0000
10.00	90%	0.0000	_	0.4273
	100%	0.0000	_	0.0236
	105%	0.0000	_	0.0000

Output DTN: LL0704PA049SPC.024, file *CDSP_WPP_catalog_analyses_DA.xls,* sheet "d17 −0.25 degrees."

NOTE: Lower impact velocities that predicted zero damaged areas are not shown.

Table 6-80. Damaged Areas (m^2) for Right Lid of Codisposal Waste Packages, 17-mm OCB with Degraded Internals, Waste Package-to-Pallet Impacts, Impact Angle of −0.25 Degrees

Impact Velocity (m/s)	Percentage of Yield Strength	Location		
		7/8	3/4	1/2
7.00	90%	0.0000	0.0000	0.0000
	100%	0.0000	0.0000	0.0000
	105%	0.0000	0.0000	0.0000
10.00	90%	0.0000	_	0.0000
	100%	0.0000	_	0.0000
	105%	0.0000	_	0.0000

Output DTN: LL0704PA049SPC.024, file *CDSP_WPP_catalog_analyses_DA.xls,* sheet "d17 −0.25 degrees."

NOTE: Lower impact velocities that predicted zero damaged areas are not shown.

Table 6-81. Damaged Areas (m^2) for Left Lid of Codisposal Waste Packages, 17-mm OCB with Degraded Internals, Waste Package-to-Pallet Impacts, Impact Angle of −6 Degrees

Impact Velocity (m/s)	Percentage of Yield Strength	Location		
		7/8	3/4	1/2
7.00	90%	0.0000	0.0000	0.0000
	100%	0.0000	0.0000	0.0000
	105%	0.0000	0.0000	0.0000
10.00	90%	0.0000	0.0000	0.4270
	100%	0.0000	0.0000	0.0246
	105%	0.0000	0.0000	0.0000

Output DTN: LL0704PA049SPC.024, file *CDSP_WPP_catalog_analyses_DA.xls,* sheet "d17 −6 degrees."

NOTE: Lower impact velocities that predicted zero damaged areas are not shown.

Table 6-82. Damaged Areas (m^2) for Right Lid Codisposal Waste Packages, 17-mm OCB with Degraded Internals, Waste Package-to-Pallet Impacts, Impact Angle of −6 Degrees

Impact Velocity (m/s)	Percentage of Yield Strength	Location		
		7/8	3/4	1/2
7.00	90%	0.0000	0.0000	0.0000
	100%	0.0000	0.0000	0.0000
	105%	0.0000	0.0000	0.0000
10.00	90%	0.0000	0.0187	0.0000
	100%	0.0000	0.0062	0.0000
	105%	0.0000	0.0028	0.0000

Output DTN: LL0704PA049SPC.024, file *CDSP_WPP_catalog_analyses_DA.xls,* sheet "d17 −6 degrees."

NOTE: Lower impact velocities that predicted zero damaged areas are not shown.

Table 6-83. Maximum Effective Strain and Rupture Condition for Codisposal Waste Packages, 23-mm OCB with Intact Internals, Waste Package-to-Pallet Impacts, Impact Angle of 0 Degrees

Impact Velocity (m/s)	Location			
	< 1/2		> 1/2	
	Maximum Effective Strain	Rupture	Maximum Effective Strain	Rupture
0.35	0.003	No	0.004	No
0.50	0.006	No	0.008	No
1.00	0.013	No	0.016	No
2.00	0.027	No	0.024	No

Output DTN: LL0704PA049SPC.024, file *CDSP_WPP_catalog_analyses_DA.xls,* sheet "i23 0 degrees."

Table 6-84. Maximum Effective Strain and Rupture Condition for Codisposal Waste Packages, 23-mm OCB with Intact Internals, Waste Package-to-Pallet Impacts, Impact Angle of +0.25 Degrees

Impact Velocity (m/s)	Location					
	1/8		1/4		1/2	
	Maximum Effective Strain	Rupture	Maximum Effective Strain	Rupture	Maximum Effective Strain	Rupture
0.25	–	–	–	–	0.007	No
0.35	0.005	No	0.006	No	0.010	No
0.50	0.008	No	0.009	No	0.014	No
1.00	0.015	No	0.018	No	0.020	No
2.00	0.025	No	0.026	No	0.034	No
3.00	0.037	No	0.037	No	0.047	No
5.00	0.052	No	0.052	No	0.058	No
7.00	0.057	No	0.053	No	0.057	No
10.00	0.060	No	0.056	No	0.064	No

Output DTN: LL0704PA049SPC.024, file *CDSP_WPP_catalog_analyses_DA.xls,* sheet "i23 +0.25 degrees."

Table 6-85. Maximum Effective Strain and Rupture Condition for Codisposal Waste Packages, 23-mm OCB with Intact Internals, Waste Package-to-Pallet Impacts, Impact Angle of −0.25 Degrees

Impact Velocity (m/s)	Location			
	7/8		3/4	
	Maximum Effective Strain	Rupture	Maximum Effective Strain	Rupture
0.35	0.005	No	0.007	No
0.50	0.009	No	0.011	No
1.00	0.015	No	0.018	No
2.00	0.025	No	0.031	No
3.00	0.038	No	0.045	No
5.00	0.047	No	0.060	No
7.00	0.050	No	0.061	No
10.00	0.055	No	0.063	No

Output DTN: LL0704PA049SPC.024, file *CDSP_WPP_catalog_analyses_DA.xls,* sheet "i23 −0.25 degrees."

Table 6-86. Maximum Effective Strain and Rupture Condition for Codisposal Waste Packages, 23-mm OCB with Intact Internals, Waste Package-to-Pallet Impacts, Impact Angle of +6 Degrees

Impact Velocity (m/s)	Location					
	1/8		1/4		1/2	
	Maximum Effective Strain	Rupture	Maximum Effective Strain	Rupture	Maximum Effective Strain	Rupture
0.15	–	–	–	–	0.005	No
0.25	–	–	0.004	No	0.009	No
0.35	0.004	No	0.008	No	0.012	No
0.50	0.009	No	0.013	No	0.015	No
1.00	0.020	No	0.021	No	0.025	No
2.00	0.039	No	0.038	No	0.044	No
3.00	0.054	No	0.052	No	0.050	No
5.00	0.063	No	0.058	No	0.053	No
7.00	0.068	No	0.063	No	0.059	No
10.00	0.072	No	0.067	No	0.076	No

Output DTN: LL0704PA049SPC.024, file *CDSP_WPP_catalog_analyses_DA.xls,* sheet "i23 +6 degrees."

Table 6-87. Maximum Effective Strain and Rupture Condition for Codisposal Waste Packages, 23-mm OCB with Intact Internals, Waste Package-to-Pallet Impacts, Impact Angle of −6 Degrees

Impact Velocity (m/s)	Location			
	7/8		3/4	
	Maximum Effective Strain	Rupture	Maximum Effective Strain	Rupture
0.25	–	–	0.005	No
0.35	0.006	No	0.010	No
0.50	0.013	No	0.014	No
1.00	0.020	No	0.021	No
2.00	0.033	No	0.038	No
3.00	0.042	No	0.051	No
5.00	0.048	No	0.054	No
7.00	0.052	No	0.059	No
10.00	0.057	No	0.063	No

Output DTN: LL0704PA049SPC.024, file *CDSP_WPP_catalog_analyses_DA.xls,* sheet "i23 −6 degrees."

Table 6-88. Maximum Effective Strain and Rupture Condition for Codisposal Waste Packages, 23-mm OCB with Degraded Internals, Waste Package-to-Pallet Impacts, Impact Angle of 0 Degrees

Impact Velocity (m/s)	Location			
	< 1/2		> 1/2	
	Maximum Effective Strain	Rupture	Maximum Effective Strain	Rupture
0.35	0.003	No	0.004	No
0.50	0.008	No	0.009	No
1.00	0.024	No	0.025	No
2.00	0.049	No	0.048	No

Output DTN: LL0704PA049SPC.024, file *CDSP_WPP_catalog_analyses_DA.xls,* sheet "d23 0 degrees."

Table 6-89. Maximum Effective Strain and Rupture Condition for Codisposal Waste Packages, 23-mm OCB with Degraded Internals, Waste Package-to-Pallet Impacts, Impact Angle of −0.25 Degrees

Impact Velocity (m/s)	Location					
	7/8		3/4		1/2	
	Maximum Effective Strain	Rupture	Maximum Effective Strain	Rupture	Maximum Effective Strain	Rupture
0.15	–	–	–	–	0.003	No
0.25	–	–	0.004	No	0.008	No
0.35	0.004	No	0.007	No	0.013	No
0.50	0.009	No	0.014	No	0.021	No
1.00	0.023	No	0.031	No	0.037	No
2.00	0.040	No	0.048	No	0.046	No
3.00	0.064	No	0.061	No	0.061	No
5.00	0.100	No	0.117	No	0.180	No
7.00	0.145	No	0.274	No	0.347	No
10.00	0.307	No	0.433	No	0.453	No

Output DTN: LL0704PA049SPC.024, file *CDSP_WPP_catalog_analyses_DA.xls,* sheet "d23 −0.25 degrees."

Table 6-90. Maximum Effective Strain and Rupture Condition for Codisposal Waste Packages, 23-mm OCB with Degraded Internals, Waste Package-to-Pallet Impacts, Impact Angle of −6 Degrees

Impact Velocity (m/s)	Location					
	7/8		3/4		1/2	
	Maximum Effective Strain	Rupture	Maximum Effective Strain	Rupture	Maximum Effective Strain	Rupture
0.15	–	–	–	–	0.005	No
0.25	–	–	0.006	No	0.014	No
0.35	0.006	No	0.013	No	0.024	No
0.50	0.015	No	0.027	No	0.037	No
1.00	0.060	No	0.056	No	0.060	No
2.00	0.075	No	0.075	No	0.093	No
3.00	0.081	No	0.090	No	0.111	No
5.00	0.122	No	0.165	No	0.316	No
7.00	0.142	No	0.337	No	0.483	No
10.00	0.306	No	0.440	No	0.681	No

Output DTN: LL0704PA049SPC.024, file *CDSP_WPP_catalog_analyses_DA.xls,* sheet “d23 −6 degrees.”

Table 6-91. Maximum Effective Strain and Rupture Condition for Codisposal Waste Packages, 17-mm OCB with Degraded Internals, Waste Package-to-Pallet Impacts, Impact Angle of 0 Degrees

Impact Velocity (m/s)	Location			
	< 1/2		> 1/2	
	Maximum Effective Strain	Rupture	Maximum Effective Strain	Rupture
0.25	0.005	No	0.005	No
0.35	0.009	No	0.009	No
0.50	0.013	No	0.013	No
1.00	0.037	No	0.037	No
2.00	0.052	No	0.051	No

Output DTN: LL0704PA049SPC.024, file *CDSP_WPP_catalog_analyses_DA.xls,* sheet “d17 0 degrees.”

Table 6-92. Maximum Effective Strain and Rupture Condition for Codisposal Waste Packages, 17-mm OCB with Degraded Internals, Waste Package-to-Pallet Impacts, Impact Angle of −0.25 Degrees

Impact Velocity (m/s)	Location					
	7/8		3/4		1/2	
	Maximum Effective Strain	Rupture	Maximum Effective Strain	Rupture	Maximum Effective Strain	Rupture
0.15	–	–	0.003	No	0.006	No
0.25	0.006	No	0.009	No	0.012	No
0.35	0.010	No	0.013	No	0.017	No
0.50	0.013	No	0.018	No	0.023	No
1.00	0.030	No	0.033	No	0.035	No
2.00	0.045	No	0.046	No	0.047	No
3.00	0.058	No	0.057	No	0.089	No
5.00	0.097	No	0.100	No	0.238	No
7.00	0.085	No	0.183	No	0.443	No
10.00	0.218	No	–	–	0.594	No

Output DTN: LL0704PA049SPC.024, file *CDSP_WPP_catalog_analyses_DA.xls,* sheet "d17 −0.25 degrees."

Table 6-93. Maximum Effective Strain and Rupture Condition for Codisposal Waste Packages, 17-mm OCB with Degraded Internals, Waste Package-to-Pallet Impacts, Impact Angle of −6 Degrees

Impact Velocity (m/s)	Location					
	7/8		3/4		1/2	
	Maximum Effective Strain	Rupture	Maximum Effective Strain	Rupture	Maximum Effective Strain	Rupture
0.15	–	–	0.003	No	0.008	No
0.25	0.005	No	0.010	No	0.018	No
0.35	0.012	No	0.020	No	0.026	No
0.50	0.028	No	0.031	No	0.034	No
1.00	0.056	No	0.052	No	0.062	No
2.00	0.072	No	0.083	No	0.095	No
3.00	0.081	No	0.095	No	0.158	No
5.00	0.089	No	0.203	No	0.313	No
7.00	0.109	No	0.250	No	0.475	No
10.00	0.193	No	0.506	No	0.554	No

Output DTN: LL0704PA049SPC.024, file *CDSP_WPP_catalog_analyses_DA.xls,* sheet "d17 −6 degrees."

6.3.3 Estimates of Waste Package Damage and Rupture Condition

The damaged area lookup tables are compiled from the waste package-to-waste package and waste package-to-pallet impact analyses and are used as input to km_impacts_pp (V. 1.0. STN: 11235-1.0-00 [DIRS 178489]), which postprocesses these results to determine damaged areas and rupture conditions for the waste packages subjected to seismic ground motion. Since

the rupture condition is "No" for all impact analyses for the TAD-bearing and codisposal waste packages, it is not necessary to include the rupture condition lookup tables as input to km_impacts_pp. Although no lookup table analysis predicts that the waste package has a rupture condition of "Yes" after a single impact, inspection of the results shows that the deformation of the OCB induced by the larger waste package-to-pallet impacts for waste packages with degraded internals is significant. Thus, an approach that accounts for the effect of multiple large impacts is also used to assess the rupture condition of the waste packages.

6.3.3.1 Damaged Area Postprocessing

For waste package-to-waste package impacts, the damaged area for each impact is linearly interpolated based on the impact velocity and location. For TAD-bearing waste packages, the damaged area prescribed to a waste package depends on whether the package is on the left or right side of the impact. For codisposal waste packages, the damaged area from lookup table analyses with the codisposal package on the left is prescribed to the waste package whether it is on the left or the right in the kinematic analysis. This is a conservative estimate (see Section 6.3.2.2.3). The damaged area is cumulatively summed for every impact on a waste package.

For waste package-to-pallet impacts, the damaged area from each impact is applied separately to the OCB shell and to both OCB lids. The damaged area for each impact is linearly interpolated based on the impact force, the impact location, and the impact angle. To prevent multiple impacts at the same location from accumulating excessive damage, the area of the OCB shell was divided into small rectangular bins (approximately 100,000 bins), and the area of each OCB lid was divided into small wedge-shaped bins (approximately 10,000 bins). The interpolated damaged area on the OCB shell was accumulated into bins based on impact location and the roll angle of the waste package. The interpolated damaged area on the OCB lids was accumulated into bins based on the roll angle of the waste package. The accumulated damaged area in a bin was not allowed to exceed the area of the bin. The damaged area for a waste package was determined by summing the binned areas from the OCB shell and the OCB lids. This is only necessary for waste package-to-pallet impacts, which are more frequent and produce larger damaged areas, compared to waste package-to-waste package impacts.

For nonzero impact angles, the waste package-to-pallet damage lookup table analyses were performed for either a positive or a negative angle at a specific location. In the lookup tables, the damaged area for both positive and negative impact angles was prescribed based on the single analysis performed. Damage lookup table analyses were performed for impact locations of 1/8, 1/4, 1/2, 3/4, and 7/8 points, but in most cases only locations sets of 1/8, 1/4, and 1/2 points or 7/8, 3/4, and 1/2 points were performed. In the cases where the analyses were performed for locations of 1/8, 1/4, and 1/2 points, the damaged area from the 1/8-point location analysis is also prescribed in the lookup tables for locations of 0, 7/8, and 1 points; and the damaged area from the 1/4-point location analysis is also prescribed in the lookup tables for the 3/4-point location. Similarly, in the cases where analyses were performed for 7/8, 3/4, and 1/2 points, the damaged area from the 7/8-point location analysis is also prescribed in the lookup tables for locations of 0, 1/8, and 1 points; and the damaged area from the 3/4-point location analysis is also prescribed in the lookup tables for the 1/4-point location.

The waste package-to-pallet damage lookup table analyses with a 0 degree impact angle are only performed with impact velocities up to 2.00 m/s. For the lookup tables above 2.00 m/s, the damaged areas from the analyses at +/−0.25 degrees are assumed for the 0-degree impacts. Below 2.00 m/s, the damaged areas from the +/−0.25-degree impacts are still assumed at the 0-, 1/2-, and 1-point locations, and the lookup tables analyses at 0 degrees provide the damaged area for the 1/8-, 1/4-, 3/4-, and 7/8-point locations at 0 degrees. The damaged area associated with the "< 1/2" location (see Section 6.3.2.2.7) is prescribed for the 1/8- and 1/4-point locations, and the damaged area associated with the "> 1/2" location is prescribed for the 3/4- and 7/8-point locations.

For both waste package-to-waste package and waste package-to-pallet impacts, a damaged area tolerance is utilized in the postprocessing of the kinematic analyses. For any single impact that has an interpolated damaged area of less than 0.0024 m^2, the damaged area for that impact is set to zero. This area corresponds to less than the area of three typical elements of the OCB shell. This limit on the minimum size for damaged area is used in order to mitigate some conservatism present in the approach for determining total damaged area. In any single lookup table analysis, an area that exceeds a residual stress threshold that is less than four elements can reasonably be assumed to overestimate the damaged area due to the finite nature of the model discretization. Thus, while this area is not very significant by itself, multiple very small impacts in the kinematic analyses would lead to overestimation of damaged area because many small impacts can sum together.

6.3.3.2 Rupture Postprocessing

The rupture condition for all single impact analyses is "No," so no postprocessing is performed for the kinematic analyses to determine rupture condition in this manner. However, the probability of rupture is assessed based on a criterion that accounts for multiple large waste package-to-pallet impacts in the kinematic analyses. Waste package-to-waste package impacts are not considered here, because the large waste package-to-pallet impacts cause much more severe deformation of the OCB.

For the lookup table analyses with very large strains, the largest strains typically occur in elements for which the stress state is compressive or similar to uniaxial tension. In some elements, the stress state can be biaxial, but not such that the rupture strain is below the effective strain in the element. However, if the deformation is large enough, then it can be reasoned that another large impact has the potential to cause rupture of the waste package. Table 6-94 and Table 6-95 provide the maximum effective strains computed for a location of 1/2 point with an impact velocity of 3.00 m/s or greater for TAD-bearing waste package-to-pallet analyses and codisposal waste package-to-pallet analyses, respectively. The 1/2-point location is considered because these impacts typically impart these largest deformations on the waste package.

Table 6-94. Maximum Effective Strains Computed from TAD-Bearing Waste Package-to-Pallet Lookup Table Analyses with a 1/2-Point Impact Location

	Intact Internals 23-mm-Thick OCB		Degraded Internals 23-mm-Thick OCB		Degraded Internals 17-mm-Thick OCB	
Impact Velocity	+0.25 Degrees[a]	+6 Degrees[b]	−0.25 Degrees[c]	−6 Degrees[d]	−0.25 Degrees[e]	−6 Degrees[f]
3 m/s	0.026	0.042	0.078	0.128	0.106	0.232
5 m/s	0.051	0.052	0.250	0.365	0.252	0.323
7 m/s	0.043	0.041	0.398	0.501	0.487	0.523
10 m/s	0.052	0.064	0.459	0.671	—	0.488

Sources: [a] From Table 6-56.
[b] From Table 6-57.
[c] From Table 6-59.
[d] From Table 6-60.
[e] From Table 6-62.
[f] From Table 6-63.

Table 6-95. Maximum Effective Strains Computed from Codisposal Waste Package-to-Pallet Lookup Table Analyses with a 1/2-Point Impact Location

	Intact Internals 23-mm-Thick OCB		Degraded Internals 23-mm-Thick OCB		Degraded Internals 17-mm-Thick OCB	
Impact Velocity	+0.25 Degrees[a]	+6 Degrees[b]	−0.25 Degrees[c]	−6 Degrees[d]	−0.25 Degrees[e]	−6 Degrees[f]
3 m/s	0.047	0.050	0.061	0.111	0.089	0.158
5 m/s	0.058	0.053	0.180	0.316	0.238	0.313
7 m/s	0.057	0.059	0.347	0.483	0.443	0.475
10 m/s	0.064	0.076	0.453	0.681	0.594	0.554

Sources: [a] From Table 6-84.
[b] From Table 6-86.
[c] From Table 6-89.
[d] From Table 6-90.
[e] From Table 6-92.
[f] From Table 6-93.

Typically, the deformation of the OCB is more severe for analyses with impacts angles of +/−6 degrees compared to +/−0.25 degrees. Figure 6-31 shows deformation of a 23-mm-thick OCB of a TAD-bearing waste package with intact internals for impact velocities 3.00 m/s, 5.00 m/s, 7.00 m/s, and 10.00 m/s with an impact angle of +6 degrees and an impact location of 1/2 point. Figure 6-32 shows the deformation of a 23-mm-thick OCB of a TAD-bearing waste package with degraded internals for the same impact velocities with an impact angle of −6 degrees and an impact location of 1/2 point. Figure 6-33 shows the deformation of a 17-mm-thick OCB of a TAD-bearing waste package with degraded internals for the same impact velocities with an impact angle of −6 degrees and an impact location of 1/2 point. Figure 6-34 shows the deformation of a 23-mm-thick OCB of a codisposal waste package with intact internals for the same impact velocities with an impact angle of +6 degrees and an impact location of 1/2 point. Figure 6-35 shows the deformation of a 23-mm-thick OCB of a codisposal waste package with degraded internals for the same impact velocities with an impact angle of −6 degrees and an impact location of 1/2 point. Figure 6-36 shows the deformation of a 17-mm-thick OCB of a codisposal waste package with degraded internals for the same impact velocities with an impact

angle of −6 degrees and an impact location of 1/2 point. In order to provide perspective for the previous figures, Figure 6-37 shows another view of the deformation of a 17-mm-thick OCB of a TAD-bearing waste package with degraded internals for an impact velocity of 10.00 m/s.

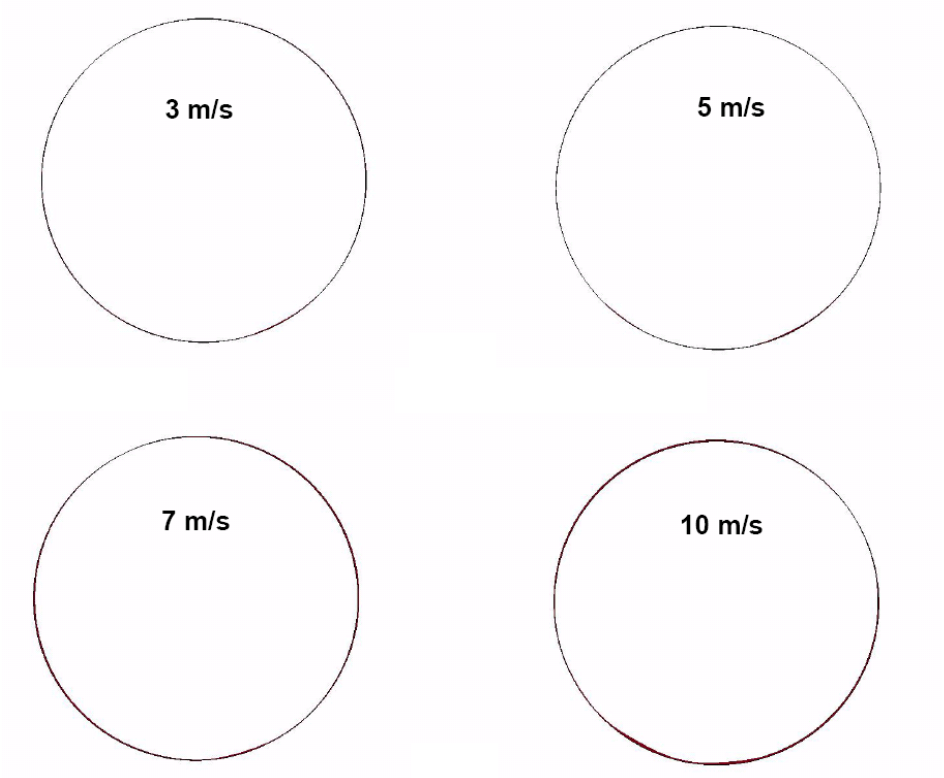

Output DTN: LL0704PA051SPC.026, file *Figures_Mech_Assessment_AMR.tar.gz.*

Figure 6-31. Deformation of a 23-mm-Thick OCB of a TAD-Bearing Waste Package with Intact Internals (+6 Degrees, 1/2 Point)

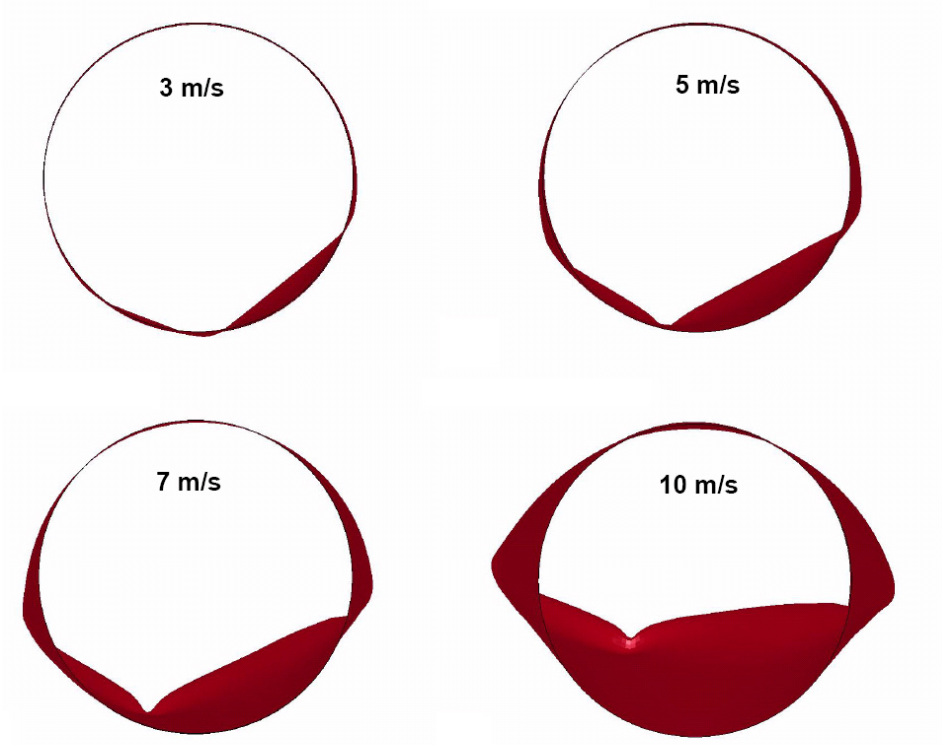

Output DTN: LL0704PA051SPC.026, file *Figures_Mech_Assessment_AMR.tar.gz.*

Figure 6-32. Deformation of a 23-mm-Thick OCB of a TAD-Bearing Waste Package with Degraded Internals (−6 Degrees, 1/2 Point)

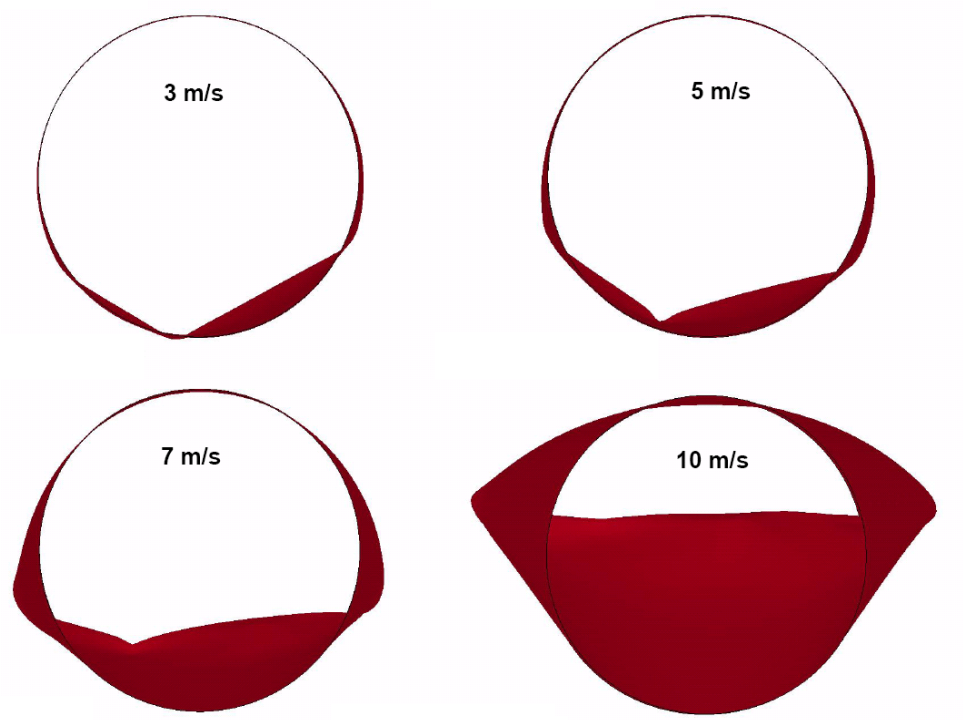

Output DTN: LL0704PA051SPC.026, file *Figures_Mech_Assessment_AMR.tar.gz*.

Figure 6-33. Deformation of a 17-mm-Thick OCB of a TAD-Bearing Waste Package with Degraded Internals (−6 Degrees, 1/2 Point)

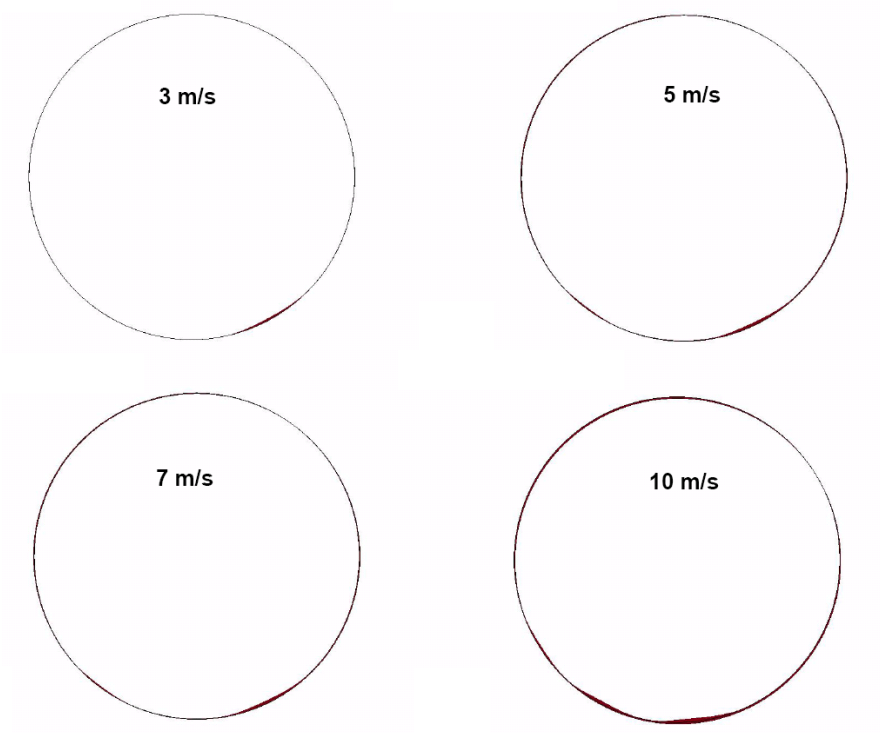

Output DTN: LL0704PA051SPC.026, file *Figures_Mech_Assessment_AMR.tar.gz.*

Figure 6-34. Deformation of a 23-mm-Thick OCB of a Codisposal Waste Package with Intact Internals (+6 Degrees, 1/2 Point)

Output DTN: LL0704PA051SPC.026, file *Figures_Mech_Assessment_AMR.tar.gz.*

Figure 6-35. Deformation of a 23-mm-Thick OCB of a Codisposal Waste Package with Degraded Internals (−6 Degrees, 1/2 Point)

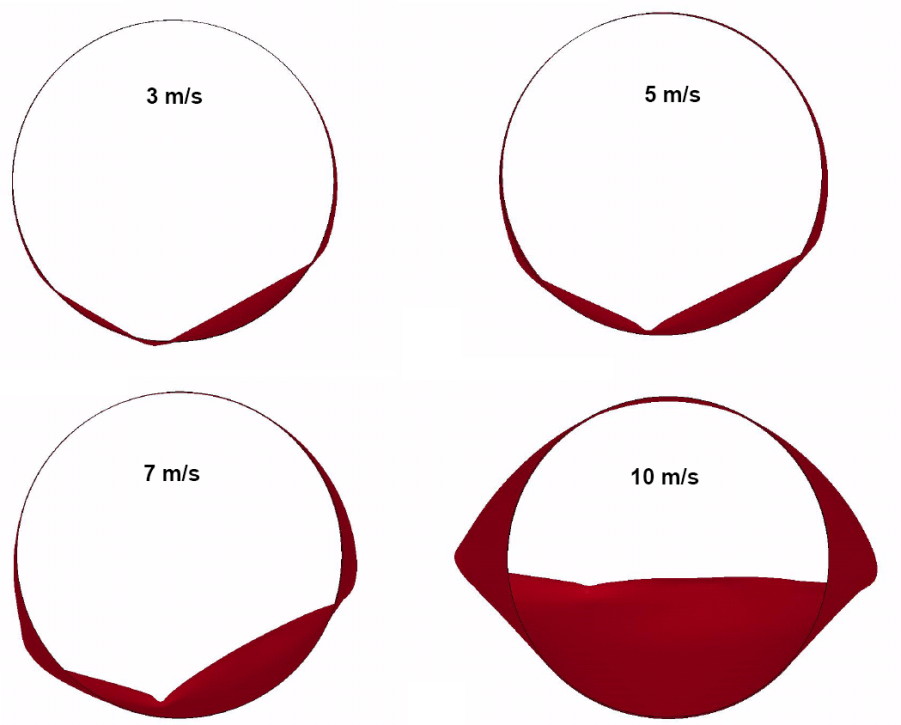

Output DTN: LL0704PA051SPC.026, file *Figures_Mech_Assessment_AMR.tar.gz.*

Figure 6-36. Deformation of a 17-mm-Thick OCB of a Codisposal Waste Package with Degraded Internals (−6 Degrees, 1/2 Point)

Output DTN: LL0704PA051SPC.026, file *Figures_Mech_Assessment_AMR.tar.gz.*

Figure 6-37. Deformation of a 17-mm-Thick OCB of a TAD-Bearing Waste Package with Degraded Internals (10.00 m/s, −6 Degrees, 1/2 Point)

For both TAD-bearing and codisposal waste packages, it is apparent that the deformation is insignificant for intact internals, even at the largest impact velocities. Thus, there is no rupture of waste packages with intact internals. For both states of degraded internals for the TAD-bearing and codisposal waste packages, the deformation at an impact velocity of 3.00 m/s is not estimated to be severe enough to lead to rupture after multiple impacts at that level. However, for both states of degraded internals for the TAD-bearing and codisposal waste packages, the deformation becomes very large as impact velocity increases. The deformed shapes are very similar for both types of waste packages and for both OCB thicknesses when the impact velocity is 5.00 m/s. The OCB shell starts to bulge noticeably at both sides of the deformed section, and the shell starts to have a noticeable kink where the waste package deforms into the center of the pallet cradle. It is estimated that the deformation from a 5.00 m/s impact is a reasonable lower bound such that another impact above 5.00 m/s would cause a rupture of the OCB. For both types of packages and both OCB thicknesses, the deformation caused by impacts of 10.00 m/s is so severe that multiple impacts of that level are certainly expected to cause rupture of the waste package.

For impacts of 7.00 m/s, the degree of certainty as to whether multiple impacts at that velocity would cause rupture varies with the waste package type and OCB thickness. The deformation of the TAD-bearing waste package with 17-mm-thick OCB is severe enough that multiple impacts are judged to cause rupture. However, the TAD-bearing waste package with 23-mm-thick OCB and the codisposal waste package with 23-mm- and 17-mm-thick OCBs are estimated to have

varying probabilities (that are less than 1) associated with how likely multiple impacts at a 7.00 m/s impact velocity are to cause rupture. The probabilities for the TAD-bearing waste package with 23-mm-thick OCB and the codisposal waste package with 17-mm-thick OCB are estimated at 0.750 (3-in-4 chance), and the probability for the codisposal waste package with 23-mm-thick OCB is estimated at 0.667 (2-in-3 chance). These are qualitative estimates based on judgment.

While impact at the 1/8 and 7/8 points cannot cause as much deformation for the same impact velocities due to the proximity to the lids, the deformation for impacts at the 1/4 and 3/4 points can be comparatively large. Thus, impacts at the 1/4-, 1/2-, and 3/4–point locations are considered for determining impact force thresholds associated with the probabilities of rupture from multiple impacts. Only impacts at +/−6 degrees are considered for determining the impact force thresholds because the impact forces at +/−0.25 degrees are generally higher than those at +/−6 degrees for the higher impact velocities (see Table 6-11 and Table 6-12 for impact forces at +/−0.25 degrees for the TAD-bearing waste package, Table 6-13 and Table 6-14 for impact forces at +/−6 degrees for the TAD-bearing waste package, Table 6-16 and Table 6-17 for impact forces at +/−0.25 degrees for the codisposal package, Table 6-18 and Table 6-19 for impact forces at +/−6 degrees for the codisposal package). The averages of the six impact forces at +/−6 degrees and the 1/4-, 1/2-, and 3/4–point locations for the TAD-bearing waste package at 5.00 m/s and 7.00 m/s are 6,000,000 lbs and 7,800,000 lbs, respectively (see Table 6-13 and Table 6-14). The averages of the six impact forces at +/−6 degrees and the 1/4-, 1/2-, and 3/4–point locations for the codisposal waste package at 5.00 m/s and 7.00 m/s are 5,800,000 lbs and 7,100,000 lbs, respectively (see Table 6-18 and Table 6-19). The probability that an impact causes deformation such that another impact can cause rupture of the waste package is interpolated between the impact force thresholds associated with each type of waste package for states of degradation. The probabilities are extrapolated above the 7.00 m/s thresholds up to a probability of 1.

Incipient rupture is defined as a state in which a waste package has been subjected to one impact during a seismic event that causes deformation such that another large impact during a later seismic event will cause rupture of the waste package. A waste package is in a state of incipient rupture at the end of a kinematic seismic analysis if one and only one impact causing deformation associated with this state occurs during that analysis. If two or more such impacts occur for a waste package during a kinematic seismic analysis, then the waste package is in a state of rupture. The probabilities of the waste packages being in either of these states are computed by statistically combining the probabilities for each impact over the corresponding force thresholds. The details of this statistical combination can be found in output DTN: LL0703PA029SPC.014, file *kinematic_analyses_rupture_summary.xls*.

6.3.4 Damaged Area and Rupture Results

The results for damaged area and rupture from the kinematic analyses are summarized in tables contained in the following sections.

6.3.4.1 Damaged Area Results

Damaged area for waste packages due to vibratory ground motion was determined at four different levels of PGV for two waste package configurations. At each PGV level, all 17 ground motion time histories were applied to the 11-waste-package configuration (TAD-bearing waste package analyses), and to the 13-waste-package configuration (codisposal analyses). The number of impacts, the angles of impact, impact locations, relative impact velocities, and impact forces for each of the 68 11-waste-package analyses can be found in output DTN: LL0704PA048SPC.023, file *NavalLong_TAD_kinematic_analyses.tar.gz*. The number of impacts, the angles of impact, impact locations, relative impact velocities, and impact forces for each of the 68 13-waste-package analyses can be found in output DTN: LL0704PA049SPC.024, file *CDSP_kinematic_analyses.tar.gz*.

Damaged areas for 90%, 100%, and 105% of yield strength, were obtained for the three central TAD-bearing waste packages (I, J, and K) for the 11-waste-package configuration analyses, and for the two central codisposal waste packages (H and L) for the 13-waste-package configuration analyses. The damaged areas were obtained for six waste package configurations, TAD-bearing waste packages with 23-mm OCB and intact internals, TAD-bearing waste packages with 23-mm OCB and degraded internals, TAD-bearing waste packages with 17-mm OCB and degraded internals, codisposal waste packages with 23-mm OCB and intact internals, codisposal waste packages with 23-mm OCB and degraded internals, and codisposal waste packages with 17-mm OCB and degraded internals.

The analyses for the TAD-bearing and codisposal waste packages are summarized in Table 6-96 and Table 6-97, respectively. Damaged area results for the TAD-bearing waste packages are presented in Table 6-98 to Table 6-108 and for the codisposal waste packages are presented in Table 6-109 to Table 6-121. Each table lists the waste package identifier (I, J, and K for TAD-bearing waste packages and H and L for codisposal waste packages) and the damaged areas for 90%, 100%, and 105% of yield strength, as a function of realization number (1 to 17). Many of the realizations at low PGV have zero predicted damage, and these have been removed from the tables to improve readability. The tables are organized by waste-package type (TAD-bearing and codisposal), ground motion level (0.40 m/s PGV, 1.05 m/s PGV, 2.44 m/s PGV, and 4.07 m/s PGV), waste package configuration (23-mm OCB with intact internals, 23-mm OCB with degraded internals, and 17-mm OCB with degraded internals), and finally by impact type (waste package-to-waste package impacts and waste package-to-pallet impacts). The sets of analyses where all realizations predicted zero damaged areas are indicated with a dash in the "Table" column of Table 6-96 and Table 6-97. There are no damaged area tables reported for these sets of analyses.

Table 6-96. Analyses Conducted for TAD-Bearing Damaged Areas using 11-Waste-Package Configuration

Ground Motion Level	Waste Package Configuration	Impact Type	Table
0.40 m/s PGV	23-mm OCB, intact internals	WP-WP	–
		WP-Pallet	–
	23-mm OCB, degraded internals	WP-WP	–
		WP-Pallet	Table 6-98
	17-mm OCB, degraded internals	WP-WP	–
		WP-Pallet	Table 6-99
1.05 m/s PGV	23-mm OCB, intact internals	WP-WP	–
		WP-Pallet	–
	23-mm OCB, degraded internals	WP-WP	–
		WP-Pallet	Table 6-100
	17-mm OCB, degraded internals	WP-WP	–
		WP-Pallet	Table 6-101
2.44 m/s PGV	23-mm OCB, intact internals	WP-WP	–
		WP-Pallet	–
	23-mm OCB, degraded internals	WP-WP	–
		WP-Pallet	Table 6-102
	17-mm OCB, degraded internals	WP-WP	–
		WP-Pallet	Table 6-103
4.07 m/s PGV	23-mm OCB, intact internals	WP-WP	Table 6-104
		WP-Pallet	Table 6-105
	23-mm OCB, degraded internals	WP-WP	Table 6-106
		WP-Pallet	Table 6-107
	17-mm OCB, degraded internals	WP-WP	–
		WP-Pallet	Table 6-108

Source: Created to enhance readability only.

NOTES: Column labeled “Table” provides location of results of analyses.
“–“ indicates no damage predicted.
OCB = outer corrosion barrier; PGV = peak ground velocity;
WP = waste package.

Table 6-97. Analyses Conducted for Codisposal Damaged Areas using 13-Waste Package Configuration

Ground Motion Level	Waste Package Configuration	Impact Type	Table
0.40 m/s PGV	23-mm OCB, intact Internals	WP-WP	–
		WP-Pallet	Table 6-109
	23-mm OCB, degraded Internals	WP-WP	–
		WP-Pallet	Table 6-110
	17-mm OCB, degraded Internals	WP-WP	–
		WP-Pallet	Table 6-111
1.05 m/s PGV	23-mm OCB, intact Internals	WP-WP	–
		WP-Pallet	Table 6-112
	23-mm OCB, degraded Internals	WP-WP	–
		WP-Pallet	Table 6-113
	17-mm OCB, degraded Internals	WP-WP	–
		WP-Pallet	Table 6-114
2.44 m/s PGV	23-mm OCB, intact Internals	WP-WP	–
		WP-Pallet	Table 6-115
	23-mm OCB, degraded Internals	WP-WP	–
		WP-Pallet	Table 6-116
	17-mm OCB, degraded Internals	WP-WP	–
		WP-Pallet	Table 6-117
4.07 m/s PGV	23-mm OCB, intact Internals	WP-WP	–
		WP-Pallet	Table 6-118
	23-mm OCB, degraded Internals	WP-WP	Table 6-119
		WP-Pallet	Table 6-120
	17-mm OCB, degraded Internals	WP-WP	–
		WP-Pallet	Table 6-121

Source: Created to enhance readability only.

NOTES: Column labeled “Table” provides location of results of analyses.
“–“ indicates no damage predicted.
OCB = outer corrosion barrier; PGV = peak ground velocity;
WP = waste package.

Table 6-98. Damaged Areas for TAD-Bearing Waste Packages for 0.40 m/s PGV, 23-mm OCB with Degraded Internals, Waste Package-to-Pallet Impacts

Realization	Waste Package	Damaged Area at 90% Yield Strength (m^2)	Damaged Area at 100% Yield Strength (m^2)	Damaged Area at 105% Yield Strength (m^2)
3	WP I	0.1947	0.1058	0.0552
	WP J	0.2526	0.1287	0.0655
	WP K	0.1365	0.0753	0.0361
4	WP I	0.2702	0.1529	0.0790
	WP J	0.3548	0.1987	0.1027
	WP K	0.3321	0.1829	0.0925
8	WP I	0.0000	0.0000	0.0000
	WP J	0.0000	0.0000	0.0000
	WP K	0.0025	0.0000	0.0000
10	WP I	0.7692	0.3743	0.1789
	WP J	0.6281	0.3222	0.1626
	WP K	0.8962	0.4447	0.2123
11	WP I	0.0526	0.0281	0.0144
	WP J	0.0558	0.0316	0.0150
	WP K	0.0374	0.0214	0.0098
14	WP I	0.0000	0.0000	0.0000
	WP J	0.0000	0.0000	0.0000
	WP K	0.1040	0.0579	0.0310

Output DTN: LL0704PA048SPC.023, file *NavalLong_TAD_Kinematic_Analyses_DA_Summary.xls,* sheet "WP-Pallet."

NOTES: Realizations that predicted zero damaged areas are not shown.
WP = waste package.

Table 6-99. Damaged Areas for TAD-Bearing Waste Packages for 0.40 m/s PGV, 17-mm OCB with Degraded Internals, Waste Package-to-Pallet Impacts

Realization	Waste Package	Damaged Area at 90% Yield Strength (m^2)	Damaged Area at 100% Yield Strength (m^2)	Damaged Area at 105% Yield Strength (m^2)
3	WP I	0.2944	0.1416	0.0363
	WP J	0.3634	0.1692	0.0536
	WP K	0.2285	0.1118	0.0293
4	WP I	0.3873	0.1829	0.0483
	WP J	0.5083	0.2358	0.0619
	WP K	0.4791	0.2246	0.0600
6	WP I	0.0103	0.0057	0.0000
	WP J	0.0138	0.0036	0.0000
	WP K	0.0000	0.0000	0.0000
8	WP I	0.0000	0.0000	0.0000
	WP J	0.0424	0.0301	0.0025
	WP K	0.0607	0.0410	0.0078

Table 6-99. Damaged Areas for TAD-Bearing Waste Packages for 0.40 m/s PGV, 17-mm OCB with Degraded Internals, Waste Package-to-Pallet Impacts (Continued)

Realization	Waste Package	Damaged Area at 90% Yield Strength (m^2)	Damaged Area at 100% Yield Strength (m^2)	Damaged Area at 105% Yield Strength (m^2)
10	WP I	1.0102	0.4199	0.1380
	WP J	0.8283	0.3619	0.1212
	WP K	1.1836	0.5434	0.2081
11	WP I	0.1299	0.0725	0.0198
	WP J	0.1380	0.0813	0.0238
	WP K	0.1138	0.0661	0.0174
13	WP I	0.0000	0.0000	0.0000
	WP J	0.0025	0.0000	0.0000
	WP K	0.0000	0.0000	0.0000
14	WP I	0.0000	0.0000	0.0000
	WP J	0.0124	0.0082	0.0000
	WP K	0.1987	0.1081	0.0283
17	WP I	0.0284	0.0133	0.0025
	WP J	0.0000	0.0000	0.0000
	WP K	0.0343	0.0219	0.0051

Output DTN: LL0704PA048SPC.023, file *NavalLong_TAD_Kinematic_Analyses_DA_Summary.xls,* sheet "WP-Pallet."

NOTES: Realizations that predicted zero damaged areas are not shown.
WP = waste package.

Table 6-100. Damaged Areas for TAD-Bearing Waste Packages for 1.05 m/s PGV, 23-mm OCB with Degraded Internals, Waste Package-to-Pallet Impacts

Realization	Waste Package	Damaged Area at 90% Yield Strength (m^2)	Damaged Area at 100% Yield Strength (m^2)	Damaged Area at 105% Yield Strength (m^2)
2	WP I	0.0145	0.0087	0.0040
	WP J	0.0387	0.0200	0.0105
	WP K	0.0096	0.0059	0.0000
3	WP I	1.1927	0.6390	0.3512
	WP J	0.5416	0.2652	0.1290
	WP K	1.2705	0.6924	0.3947
4	WP I	1.6466	0.9734	0.5759
	WP J	1.9592	1.0608	0.6350
	WP K	1.9780	1.0859	0.6311
5	WP I	0.6072	0.3387	0.1764
	WP J	0.2812	0.1474	0.0742
	WP K	1.0124	0.5781	0.3151
6	WP I	0.4042	0.2299	0.1280
	WP J	0.5148	0.2916	0.1613
	WP K	0.3195	0.1767	0.0941

Table 6-100. Damaged Areas for TAD-Bearing Waste Packages for 1.05 m/s PGV, 23-mm OCB with Degraded Internals, Waste Package-to-Pallet Impacts (Continued)

Realization	Waste Package	Damaged Area at 90% Yield Strength (m^2)	Damaged Area at 100% Yield Strength (m^2)	Damaged Area at 105% Yield Strength (m^2)
7	WP I	0.0801	0.0456	0.0239
	WP J	0.0000	0.0000	0.0000
	WP K	0.0318	0.0184	0.0040
8	WP I	0.2896	0.1463	0.0639
	WP J	0.5966	0.3044	0.1464
	WP K	0.3473	0.1713	0.0796
10	WP I	2.5474	1.3167	0.7032
	WP J	3.1465	1.6565	0.8653
	WP K	2.8180	1.4149	0.6977
11	WP I	0.5298	0.3079	0.1625
	WP J	0.9739	0.5025	0.2788
	WP K	0.8772	0.4813	0.2717
12	WP I	0.4064	0.2174	0.1105
	WP J	0.4615	0.2340	0.1120
	WP K	0.3394	0.1776	0.0897
13	WP I	0.0285	0.0141	0.0074
	WP J	0.1918	0.1095	0.0540
	WP K	0.1091	0.0638	0.0338
14	WP I	0.5570	0.2912	0.1502
	WP J	0.4751	0.2302	0.1117
	WP K	0.9900	0.4856	0.2434
15	WP I	0.7622	0.3712	0.1838
	WP J	0.6167	0.3363	0.1793
	WP K	0.2390	0.1341	0.0724
17	WP I	0.3446	0.1961	0.1028
	WP J	0.4939	0.2575	0.1288
	WP K	0.3633	0.1918	0.0965

Output DTN: LL0704PA048SPC.023, file *NavalLong_TAD_Kinematic_Analyses_DA_Summary.xls,* sheet "WP-Pallet."

NOTES: Realizations that predicted zero damaged areas are not shown.
WP = waste package.

Table 6-101. Damaged Areas for TAD-Bearing Waste Packages for 1.05 m/s PGV, 17-mm OCB with Degraded Internals, Waste Package-to-Pallet Impacts

Realization	Waste Package	Damaged Area at 90% Yield Strength (m^2)	Damaged Area at 100% Yield Strength (m^2)	Damaged Area at 105% Yield Strength (m^2)
1	WP I	0.0000	0.0000	0.0000
	WP J	0.0197	0.0079	0.0000
	WP K	0.0000	0.0000	0.0000
2	WP I	0.0971	0.0683	0.0194
	WP J	0.1329	0.0898	0.0266
	WP K	0.0933	0.0651	0.0147
3	WP I	1.5614	0.7507	0.3576
	WP J	0.7250	0.3189	0.1139
	WP K	1.6148	0.7570	0.3916
4	WP I	1.9518	1.0771	0.5099
	WP J	2.2193	1.1601	0.5945
	WP K	2.3661	1.1997	0.6352
5	WP I	0.8065	0.3917	0.1225
	WP J	0.4189	0.1978	0.0547
	WP K	1.2848	0.6752	0.2511
6	WP I	0.5700	0.2769	0.0791
	WP J	0.6973	0.3472	0.1175
	WP K	0.4631	0.2281	0.0624
7	WP I	0.1846	0.1077	0.0261
	WP J	0.0051	0.0000	0.0000
	WP K	0.1060	0.0657	0.0155
8	WP I	0.4574	0.2251	0.0667
	WP J	0.7978	0.3771	0.1289
	WP K	0.5072	0.2421	0.0800
10	WP I	2.7607	1.3710	0.7136
	WP J	3.6345	1.7507	0.8628
	WP K	3.4470	1.5864	0.8112
11	WP I	0.7084	0.3895	0.1358
	WP J	1.2908	0.6084	0.2630
	WP K	1.1022	0.5626	0.2539
12	WP I	0.5471	0.2477	0.0775
	WP J	0.6266	0.2740	0.0879
	WP K	0.4714	0.2104	0.0560
13	WP I	0.1054	0.0649	0.0149
	WP J	0.3583	0.2052	0.0537
	WP K	0.2357	0.1381	0.0401

Table 6-101. Damaged Areas for TAD-Bearing Waste Packages for 1.05 m/s PGV, 17-mm OCB with Degraded Internals, Waste Package-to-Pallet Impacts (Continued)

Realization	Waste Package	Damaged Area at 90% Yield Strength (m^2)	Damaged Area at 100% Yield Strength (m^2)	Damaged Area at 105% Yield Strength (m^2)
14	WP I	0.7242	0.3376	0.1147
	WP J	0.6611	0.3006	0.1152
	WP K	1.2430	0.5555	0.2298
15	WP I	0.9971	0.4359	0.1669
	WP J	0.8216	0.3891	0.1330
	WP K	0.3859	0.1983	0.0594
16	WP I	0.0072	0.0000	0.0000
	WP J	0.0101	0.0053	0.0000
	WP K	0.0000	0.0000	0.0000
17	WP I	0.5329	0.2903	0.0940
	WP J	0.6732	0.2996	0.0853
	WP K	0.5198	0.2349	0.0605

Output DTN: LL0704PA048SPC.023, file *NavalLong_TAD_Kinematic_Analyses_DA_Summary.xls,* sheet "WP-Pallet."

NOTES: Realizations that predicted zero damaged areas are not shown.
WP = waste package.

Table 6-102. Damaged Areas for TAD-Bearing Waste Packages for 2.44m/s PGV, 23-mm OCB with Degraded Internals, Waste Package-to-Pallet Impacts

Realization	Waste Package	Damaged Area at 90% Yield Strength (m^2)	Damaged Area at 100% Yield Strength (m^2)	Damaged Area at 105% Yield Strength (m^2)
1	WP I	0.9384	0.5296	0.3041
	WP J	0.5333	0.3101	0.1773
	WP K	0.6735	0.3754	0.2078
2	WP I	1.3811	0.7741	0.4422
	WP J	0.7399	0.4276	0.2472
	WP K	1.2354	0.6770	0.3828
3	WP I	2.8355	1.4079	0.7223
	WP J	1.8926	0.9169	0.4722
	WP K	1.9549	1.0106	0.5125
4	WP I	3.0813	1.7581	1.0086
	WP J	4.3207	2.4721	1.3360
	WP K	3.5838	2.1418	1.2152
5	WP I	2.2476	1.2349	0.6568
	WP J	1.6729	1.0050	0.5917
	WP K	2.2123	1.2794	0.6945
6	WP I	2.9980	1.8179	1.1016
	WP J	1.9898	1.2060	0.7634
	WP K	3.0404	1.7937	1.0237

Table 6-102. Damaged Areas for TAD-Bearing Waste Packages for 2.44m/s PGV, 23-mm OCB with Degraded Internals, Waste Package-to-Pallet Impacts (Continued)

Realization	Waste Package	Damaged Area at 90% Yield Strength (m^2)	Damaged Area at 100% Yield Strength (m^2)	Damaged Area at 105% Yield Strength (m^2)
7	WP I	1.8054	1.0946	0.6267
	WP J	1.6289	0.9300	0.5436
	WP K	2.0148	1.1959	0.6848
8	WP I	0.7837	0.4188	0.2063
	WP J	0.9373	0.4935	0.2536
	WP K	1.8291	1.0287	0.5766
9	WP I	0.1709	0.0972	0.0526
	WP J	0.1403	0.0803	0.0436
	WP K	0.1486	0.0828	0.0419
10	WP I	4.8587	2.7256	1.5089
	WP J	3.8279	2.2977	1.3343
	WP K	3.9657	2.2966	1.3213
11	WP I	1.5603	0.8919	0.5236
	WP J	2.4211	1.4794	0.8570
	WP K	2.3135	1.3651	0.7660
12	WP I	1.4465	0.7617	0.4188
	WP J	2.4835	1.4203	0.8089
	WP K	1.3816	0.7536	0.3967
13	WP I	1.4841	0.7637	0.4324
	WP J	1.4082	0.8249	0.4534
	WP K	1.1557	0.6431	0.3583
14	WP I	0.9296	0.5496	0.3119
	WP J	1.5363	0.8876	0.5009
	WP K	2.4826	1.4769	0.8122
15	WP I	2.6331	1.6011	0.9887
	WP J	2.9772	1.6960	0.9657
	WP K	3.0163	1.5564	0.8688
16	WP I	1.0481	0.5791	0.3310
	WP J	1.1523	0.7441	0.4566
	WP K	0.8253	0.4708	0.2649
17	WP I	4.0230	2.2855	1.2348
	WP J	3.7642	2.2076	1.1950
	WP K	2.9530	1.7940	1.0641

Output DTN: LL0704PA048SPC.023, file *NavalLong_TAD_Kinematic_Analyses_DA_Summary.xls,* sheet "WP-Pallet."

NOTE: WP = waste package.

Table 6-103. Damaged Areas for TAD-Bearing Waste Packages for 2.44 m/s PGV, 17-mm OCB with Degraded Internals, Waste Package-to-Pallet Impacts

Realization	Waste Package	Damaged Area at 90% Yield Strength (m2)	Damaged Area at 100% Yield Strength (m2)	Damaged Area at 105% Yield Strength (m2)
1	WP I	1.1898	0.5962	0.2425
	WP J	0.7055	0.3672	0.1331
	WP K	0.8638	0.4233	0.1519
2	WP I	1.6573	0.8902	0.4296
	WP J	0.9755	0.5212	0.1995
	WP K	1.5523	0.7956	0.3638
3	WP I	3.3858	1.5689	0.7369
	WP J	1.9134	0.8899	0.4566
	WP K	2.4293	1.1830	0.5259
4	WP I	3.5475	1.9144	1.0293
	WP J	4.8825	2.6797	1.3929
	WP K	4.1537	2.3567	1.2244
5	WP I	2.7383	1.4241	0.6214
	WP J	2.0227	1.1650	0.6021
	WP K	2.7130	1.5399	0.6576
6	WP I	3.3861	1.9505	1.0998
	WP J	2.3553	1.3314	0.7160
	WP K	3.5650	1.9960	0.9312
7	WP I	2.2280	1.2816	0.4963
	WP J	2.0802	1.0642	0.4897
	WP K	2.4168	1.3583	0.6418
8	WP I	1.0796	0.5618	0.1985
	WP J	1.2818	0.6093	0.2261
	WP K	2.2107	1.1897	0.5100
9	WP I	0.2873	0.1490	0.0389
	WP J	0.2704	0.1582	0.0495
	WP K	0.2836	0.1533	0.0453
10	WP I	5.0735	2.8431	1.5359
	WP J	4.1702	2.4243	1.2794
	WP K	4.2764	2.4389	1.2851
11	WP I	1.9081	1.0325	0.5017
	WP J	2.8425	1.6671	0.7948
	WP K	2.7696	1.5359	0.7249
12	WP I	1.8088	0.8761	0.4022
	WP J	3.0464	1.6331	0.7884
	WP K	1.6879	0.9126	0.4163
13	WP I	1.9037	0.8500	0.4044
	WP J	1.7383	0.9731	0.4108
	WP K	1.4607	0.7551	0.3525

Table 6-103. Damaged Areas for TAD-Bearing Waste Packages for 2.44 m/s PGV, 17-mm OCB with Degraded Internals, Waste Package-to-Pallet Impacts (Continued)

Realization	Waste Package	Damaged Area at 90% Yield Strength (m^2)	Damaged Area at 100% Yield Strength (m^2)	Damaged Area at 105% Yield Strength (m^2)
14	WP I	1.1739	0.6232	0.2460
	WP J	1.8554	1.0219	0.4848
	WP K	2.9880	1.6608	0.6453
15	WP I	2.8541	1.7057	0.9730
	WP J	3.4361	1.8503	0.8985
	WP K	3.4514	1.6469	0.8630
16	WP I	1.3235	0.6468	0.2596
	WP J	1.4215	0.8529	0.3533
	WP K	1.0728	0.5402	0.2016
17	WP I	4.6223	2.5091	1.2745
	WP J	4.3691	2.4656	1.2711
	WP K	3.4393	1.9526	1.0258

Output DTN: LL0704PA048SPC.023, file *NavalLong_TAD_Kinematic_Analyses_DA_Summary.xls,* sheet "WP-Pallet."

NOTE: WP = waste package.

Table 6-104. Damaged Areas for TAD-Bearing Waste Packages for 4.07 m/s PGV, 23-mm OCB with Intact Internals, Waste Package-to-Waste Package Impacts

Realization	Waste Package	Damaged Area at 90% Yield Strength (m^2)	Damaged Area at 100% Yield Strength (m^2)	Damaged Area at 105% Yield Strength (m^2)
4	WP I	0.0000	0.0000	0.0000
	WP J	0.0055	0.0000	0.0000
	WP K	0.0000	0.0000	0.0000
5	WP I	0.0039	0.0000	0.0000
	WP J	0.0000	0.0000	0.0000
	WP K	0.0000	0.0000	0.0000
6	WP I	0.0032	0.0000	0.0000
	WP J	0.0000	0.0000	0.0000
	WP K	0.0000	0.0000	0.0000
14	WP I	0.0000	0.0000	0.0000
	WP J	0.0030	0.0000	0.0000
	WP K	0.0000	0.0000	0.0000
15	WP I	0.0000	0.0000	0.0000
	WP J	0.0037	0.0000	0.0000
	WP K	0.0000	0.0000	0.0000

Output DTN: LL0704PA048SPC.023, file *NavalLong_TAD_Kinematic_Analyses_DA_Summary.xls,* sheet "WP-WP."

NOTES: Realizations that predicted zero damaged areas are not shown.
WP = waste package.

Table 6-105. Damaged Areas for TAD-Bearing Waste Packages for 4.07 m/s PGV, 23-mm OCB with Intact Internals, Waste Package-to-Pallet Impacts

Realization	Waste Package	Damaged Area at 90% Yield Strength (m^2)	Damaged Area at 100% Yield Strength (m^2)	Damaged Area at 105% Yield Strength (m^2)
4	WP I	0.0026	0.0000	0.0000
	WP J	0.0000	0.0000	0.0000
	WP K	0.0000	0.0000	0.0000
6	WP I	0.0026	0.0000	0.0000
	WP J	0.0000	0.0000	0.0000
	WP K	0.0000	0.0000	0.0000

Output DTN: LL0704PA048SPC.023, file *NavalLong_TAD_Kinematic_Analyses_DA_Summary.xls,* sheet "WP-Pallet."

NOTES: Realizations that predicted zero damaged areas are not shown.
WP = waste package.

Table 6-106. Damaged Areas for TAD-Bearing Waste Packages for 4.07 m/s PGV, 23-mm OCB with Degraded Internals, Waste Package-to-Waste Package Impacts

Realization	Waste Package	Damaged Area at 90% Yield Strength (m^2)	Damaged Area at 100% Yield Strength (m^2)	Damaged Area at 105% Yield Strength (m^2)
4	WP I	0.0028	0.0000	0.0000
	WP J	0.0034	0.0000	0.0000
	WP K	0.0000	0.0000	0.0000
10	WP I	0.0000	0.0000	0.0000
	WP J	0.0033	0.0000	0.0000
	WP K	0.0000	0.0000	0.0000
13	WP I	0.0030	0.0000	0.0000
	WP J	0.0000	0.0000	0.0000
	WP K	0.0000	0.0000	0.0000
15	WP I	0.0030	0.0000	0.0000
	WP J	0.0000	0.0000	0.0000
	WP K	0.0000	0.0000	0.0000

Output DTN: LL0704PA048SPC.023, file *NavalLong_TAD_Kinematic_Analyses_DA_Summary.xls,* sheet "WP-WP."

NOTES: Realizations that predicted zero damaged areas are not shown.
WP = waste package.

Table 6-107. Damaged Areas for TAD-Bearing Waste Packages for 4.07 m/s PGV, 23-mm OCB with Degraded Internals, Waste Package-to-Pallet Impacts

Realization	Waste Package	Damaged Area at 90% Yield Strength (m^2)	Damaged Area at 100% Yield Strength (m^2)	Damaged Area at 105% Yield Strength (m^2)
1	WP I	2.0052	1.3024	0.8150
	WP J	3.3685	1.9859	1.1034
	WP K	2.1863	1.3138	0.7675
2	WP I	2.9819	1.6683	0.8797
	WP J	3.2336	1.8728	1.0677
	WP K	3.5954	1.8998	1.0114
3	WP I	4.3639	2.2922	1.2204
	WP J	3.3456	1.9357	1.0840
	WP K	4.3321	2.2878	1.2405
4	WP I	4.8700	2.8857	1.7057
	WP J	7.1812	4.0668	2.3040
	WP K	7.0200	3.8409	2.1208
5	WP I	2.8368	1.6262	0.9351
	WP J	2.4767	1.4639	0.8233
	WP K	6.3018	3.4870	1.8611
6	WP I	7.0733	4.7374	2.9634
	WP J	6.4261	4.4342	2.7618
	WP K	6.9231	4.3750	2.6957
7	WP I	3.4845	2.1925	1.3452
	WP J	3.4187	2.1808	1.3289
	WP K	5.0829	3.1163	1.8474
8	WP I	3.0125	1.6928	0.9407
	WP J	2.9566	1.5720	0.8323
	WP K	4.0666	2.2700	1.2809
9	WP I	1.7047	0.9894	0.5650
	WP J	1.8208	1.0651	0.6177
	WP K	1.9645	1.1580	0.6582
10	WP I	8.1963	4.3181	2.4794
	WP J	8.9684	5.1216	2.9479
	WP K	9.2554	4.8737	2.6610
11	WP I	3.8471	2.1165	1.1308
	WP J	3.9537	2.0699	1.0467
	WP K	3.7880	2.1375	1.1476
12	WP I	4.2244	2.3177	1.1867
	WP J	5.0011	2.7366	1.5030
	WP K	4.7389	2.7085	1.4716
13	WP I	2.1516	1.3050	0.7610
	WP J	3.2576	1.9163	1.0613
	WP K	3.3913	2.0237	1.0843
14	WP I	3.6246	2.2431	1.3068
	WP J	3.7169	2.3514	1.4121
	WP K	4.1086	2.5291	1.5355

Table 6-107. Damaged Areas for TAD-Bearing Waste Packages for 4.07 m/s PGV, 23-mm OCB with Degraded Internals, Waste Package-to-Pallet Impacts (Continued)

Realization	Waste Package	Damaged Area at 90% Yield Strength (m^2)	Damaged Area at 100% Yield Strength (m^2)	Damaged Area at 105% Yield Strength (m^2)
15	WP I	7.0677	3.6326	2.0082
	WP J	6.3144	3.5972	2.0586
	WP K	4.6226	2.8817	1.7081
16	WP I	2.1962	1.3061	0.7555
	WP J	2.6679	1.6844	1.0341
	WP K	2.4542	1.3933	0.7909
17	WP I	10.2011	6.1036	3.4403
	WP J	6.1478	3.8511	2.3035
	WP K	5.6741	3.7452	2.2291

Output DTN: LL0704PA048SPC.023, file *NavalLong_TAD_Kinematic_Analyses_DA_Summary.xls,* sheet "WP-Pallet."

NOTE: WP = waste package.

Table 6-108. Damaged Areas for TAD-Bearing Waste Packages for 4.07 m/s PGV, 17-mm OCB with Degraded Internals, Waste Package-to-Pallet Impacts

Realization	Waste Package	Damaged Area at 90% Yield Strength (m^2)	Damaged Area at 100% Yield Strength (m^2)	Damaged Area at 105% Yield Strength (m^2)
1	WP I	2.3274	1.4357	0.7387
	WP J	4.0136	2.2553	1.0803
	WP K	2.6076	1.4941	0.6496
2	WP I	3.4875	1.8513	0.8955
	WP J	3.9088	2.1158	1.0565
	WP K	4.1612	2.1465	1.0279
3	WP I	4.9199	2.4851	1.2164
	WP J	3.7708	2.1111	1.0781
	WP K	4.7280	2.4040	1.2077
4	WP I	6.2323	3.3795	2.0030
	WP J	7.2318	3.9343	2.2709
	WP K	7.2760	3.9979	2.1077
5	WP I	3.0676	1.7326	0.8553
	WP J	3.0569	1.7361	0.8504
	WP K	6.5384	3.6542	1.7572
6	WP I	7.6282	4.9901	3.0401
	WP J	6.8415	4.6803	2.7105
	WP K	7.8467	4.8127	2.5979
7	WP I	3.9120	2.3490	1.2601
	WP J	3.8642	2.4228	1.2239
	WP K	5.7764	3.4009	1.8246

Table 6-108. Damaged Areas for TAD-Bearing Waste Packages for 4.07 m/s PGV, 17-mm OCB with Degraded Internals, Waste Package-to-Pallet Impacts (Continued)

Realization	Waste Package	Damaged Area at 90% Yield Strength (m^2)	Damaged Area at 100% Yield Strength (m^2)	Damaged Area at 105% Yield Strength (m^2)
8	WP I	3.4577	1.9022	0.9357
	WP J	3.4724	1.7233	0.8025
	WP K	4.2753	2.4195	1.1683
9	WP I	2.0803	1.1433	0.5336
	WP J	2.2085	1.2337	0.5240
	WP K	2.3701	1.3202	0.6158
10	WP I	14.6905	7.8485	4.2912
	WP J	12.3387	7.1671	4.1586
	WP K	18.3112	9.7697	5.2184
11	WP I	4.4228	2.3553	1.1677
	WP J	4.6184	2.2419	1.0921
	WP K	4.5077	2.4639	1.1186
12	WP I	4.7672	2.5968	1.3118
	WP J	5.7913	3.0515	1.5653
	WP K	5.3882	2.9529	1.5727
13	WP I	2.6232	1.4763	0.6987
	WP J	3.9684	2.2108	1.0799
	WP K	3.9827	2.2653	1.0604
14	WP I	4.1680	2.4566	1.2748
	WP J	4.0596	2.5086	1.4687
	WP K	4.6426	2.7347	1.5271
15	WP I	9.0824	4.8545	2.6585
	WP J	8.6261	4.6798	2.5960
	WP K	6.6032	3.8065	2.1897
16	WP I	2.6922	1.5273	0.6199
	WP J	3.1645	1.9158	1.0279
	WP K	3.0354	1.6029	0.6948
17	WP I	11.2613	6.4579	3.4517
	WP J	6.6536	4.1468	2.3467
	WP K	6.1602	3.9988	2.2923

Output DTN: LL0704PA048SPC.023, file *NavalLong_TAD_Kinematic_Analyses_DA_Summary.xls,* sheet "WP-Pallet."

NOTE: WP = waste package.

Table 6-109. Damaged Areas for Codisposal Waste Packages for 0.40 m/s PGV, 23-mm OCB with Intact Internals, Waste Package-to-Pallet Impacts

Realization	Waste Package	Damaged Area at 90% Yield Strength (m^2)	Damaged Area at 100% Yield Strength (m^2)	Damaged Area at 105% Yield Strength (m^2)
3	WP H	0.0028	0.0000	0.0000
	WP L	0.0053	0.0000	0.0000
4	WP H	0.0223	0.0000	0.0000
	WP L	0.0072	0.0000	0.0000
10	WP H	0.0376	0.0000	0.0000
	WP L	0.1088	0.0000	0.0000

Output DTN: LL0704PA049SPC.024, file *CDSP_kinematic_analyses_DA_summary.xls,* sheet "WP-Pallet."

NOTES: Realizations that predicted zero damaged areas are not shown.
WP = waste package.

Table 6-110. Damaged Areas for Codisposal Waste Packages for 0.40 m/s PGV, 23-mm OCB with Degraded Internals, Waste Package-to-Pallet Impacts

Realization	Waste Package	Damaged Area at 90% Yield Strength (m^2)	Damaged Area at 100% Yield Strength (m^2)	Damaged Area at 105% Yield Strength (m^2)
3	WP H	0.0193	0.0078	0.0000
	WP L	0.0298	0.0161	0.0041
4	WP H	0.1080	0.0577	0.0194
	WP L	0.0403	0.0203	0.0031
8	WP H	0.0070	0.0042	0.0000
	WP L	0.0000	0.0000	0.0000
10	WP H	0.1494	0.0794	0.0326
	WP L	0.5255	0.2818	0.1061

Output DTN: LL0704PA049SPC.024, file *CDSP_kinematic_analyses_DA_summary.xls,* sheet "WP-Pallet."

NOTES: Realizations that predicted zero damaged areas are not shown.
WP = waste package.

Table 6-111. Damaged Areas for Codisposal Waste Packages for 0.40 m/s PGV, 17-mm OCB with Degraded Internals, Waste Package-to-Pallet Impacts

Realization	Waste Package	Damaged Area at 90% Yield Strength (m^2)	Damaged Area at 100% Yield Strength (m^2)	Damaged Area at 105% Yield Strength (m^2)
3	WP H	0.0588	0.0299	0.0000
	WP L	0.0612	0.0177	0.0000
4	WP H	0.1923	0.0569	0.0025
	WP L	0.0986	0.0379	0.0000
8	WP H	0.0216	0.0069	0.0000
	WP L	0.0126	0.0063	0.0000
10	WP H	0.2506	0.0639	0.0074
	WP L	0.7000	0.2504	0.0589

Output DTN: LL0704PA049SPC.024, file *CDSP_kinematic_analyses_DA_summary.xls,* sheet WP-Pallet.

NOTES: Realizations that predicted zero damaged areas are not shown.
WP = waste package.

Table 6-112. Damaged Areas for Codisposal Waste Packages for 1.05 m/s PGV, 23-mm OCB with Intact Internals, Waste Package-to-Pallet Impacts

Realization	Waste Package	Damaged Area at 90% Yield Strength (m^2)	Damaged Area at 100% Yield Strength (m^2)	Damaged Area at 105% Yield Strength (m^2)
3	WP H	0.1836	0.0000	0.0000
	WP L	0.2319	0.0000	0.0000
4	WP H	0.3515	0.0000	0.0000
	WP L	0.3025	0.0000	0.0000
5	WP H	0.0000	0.0000	0.0000
	WP L	0.0235	0.0000	0.0000
6	WP H	0.0070	0.0000	0.0000
	WP L	0.0246	0.0000	0.0000
8	WP H	0.0146	0.0000	0.0000
	WP L	0.0096	0.0000	0.0000
10	WP H	0.2948	0.0000	0.0000
	WP L	0.4778	0.0000	0.0000
12	WP H	0.0414	0.0000	0.0000
	WP L	0.0091	0.0000	0.0000
14	WP H	0.1310	0.0000	0.0000
	WP L	0.0692	0.0000	0.0000
15	WP H	0.0402	0.0000	0.0000
	WP L	0.0464	0.0000	0.0000
17	WP H	0.0058	0.0000	0.0000
	WP L	0.0081	0.0000	0.0000

Output DTN: LL0704PA049SPC.024, file *CDSP_kinematic_analyses_DA_summary.xls,* sheet "WP-Pallet."

NOTES: Realizations that predicted zero damaged areas are not shown.
WP = waste package.

Table 6-113. Damaged Areas for Codisposal Waste Packages for 1.05 m/s PGV, 23-mm OCB with Degraded Internals, Waste Package-to-Pallet Impacts

Realization	Waste Package	Damaged Area at 90% Yield Strength (m^2)	Damaged Area at 100% Yield Strength (m^2)	Damaged Area at 105% Yield Strength (m^2)
3	WP H	1.1654	0.5458	0.2221
	WP L	1.4145	0.6878	0.2966
4	WP H	1.7491	0.9401	0.4478
	WP L	1.7118	0.8432	0.3963
5	WP H	0.0000	0.0000	0.0000
	WP L	0.1679	0.0791	0.0264
6	WP H	0.0346	0.0165	0.0034
	WP L	0.1186	0.0648	0.0212
7	WP H	0.0131	0.0054	0.0000
	WP L	0.0000	0.0000	0.0000
8	WP H	0.0684	0.0342	0.0106
	WP L	0.0456	0.0239	0.0082
10	WP H	1.4556	0.7705	0.3730
	WP L	3.0346	1.5099	0.6339
12	WP H	0.2552	0.1267	0.0481
	WP L	0.0449	0.0238	0.0047
14	WP H	0.7478	0.3898	0.1397
	WP L	0.4686	0.2281	0.0847
15	WP H	0.2766	0.1350	0.0506
	WP L	0.2946	0.1419	0.0524
17	WP H	0.0361	0.0187	0.0045
	WP L	0.0375	0.0200	0.0043

Output DTN: LL0704PA049SPC.024, file *CDSP_kinematic_analyses_DA_summary.xls,* sheet "WP-Pallet."

NOTES: Realizations that predicted zero damaged areas are not shown.
WP = waste package.

Table 6-114. Damaged Areas for Codisposal Waste Packages for 1.05 m/s PGV, 17-mm OCB with Degraded Internals, Waste Package-to-Pallet Impacts

Realization	Waste Package	Damaged Area at 90% Yield Strength (m^2)	Damaged Area at 100% Yield Strength (m^2)	Damaged Area at 105% Yield Strength (m^2)
3	WP H	1.2531	0.4596	0.1820
	WP L	1.5272	0.6185	0.2835
4	WP H	1.8385	0.8604	0.4240
	WP L	1.8524	0.7543	0.3548
5	WP H	0.0193	0.0127	0.0000
	WP L	0.2141	0.0855	0.0267
6	WP H	0.0958	0.0458	0.0000
	WP L	0.1976	0.0611	0.0084
7	WP H	0.0448	0.0252	0.0000
	WP L	0.0000	0.0000	0.0000
8	WP H	0.1272	0.0378	0.0000
	WP L	0.0987	0.0346	0.0000
10	WP H	1.5463	0.7282	0.3560
	WP L	3.1325	1.3987	0.6312
11	WP H	0.0103	0.0055	0.0000
	WP L	0.0247	0.0129	0.0000
12	WP H	0.3133	0.1025	0.0357
	WP L	0.0905	0.0268	0.0000
14	WP H	0.9514	0.3664	0.1066
	WP L	0.5950	0.2226	0.0625
15	WP H	0.3365	0.1318	0.0426
	WP L	0.3828	0.1188	0.0307
17	WP H	0.0662	0.0180	0.0000
	WP L	0.0801	0.0251	0.0000

Output DTN: LL0704PA049SPC.024, file *CDSP_kinematic_analyses_DA_summary.xls,* sheet "WP-Pallet."

NOTES: Realizations that predicted zero damaged areas are not shown.
WP = waste package.

Table 6-115. Damaged Areas for Codisposal Waste Packages for 2.44 m/s PGV, 23-mm OCB with Intact Internals, Waste Package-to-Pallet Impacts

Realization	Waste Package	Damaged Area at 90% Yield Strength (m^2)	Damaged Area at 100% Yield Strength (m^2)	Damaged Area at 105% Yield Strength (m^2)
1	WP H	0.0127	0.0000	0.0000
	WP L	0.0164	0.0000	0.0000
2	WP H	0.0402	0.0000	0.0000
	WP L	0.1097	0.0000	0.0000
3	WP H	0.3197	0.0000	0.0000
	WP L	0.2958	0.0000	0.0000
4	WP H	1.0292	0.0036	0.0000
	WP L	0.7796	0.0029	0.0000
5	WP H	0.1219	0.0000	0.0000
	WP L	0.1270	0.0000	0.0000
6	WP H	0.7340	0.0028	0.0000
	WP L	0.6569	0.0000	0.0000
7	WP H	0.3221	0.0000	0.0000
	WP L	0.0296	0.0000	0.0000
8	WP H	0.1173	0.0000	0.0000
	WP L	0.1334	0.0000	0.0000
10	WP H	0.8694	0.0128	0.0000
	WP L	1.0330	0.0041	0.0000
11	WP H	0.0804	0.0000	0.0000
	WP L	0.1640	0.0000	0.0000
12	WP H	0.3335	0.0000	0.0000
	WP L	0.1331	0.0000	0.0000
13	WP H	0.1724	0.0000	0.0000
	WP L	0.1780	0.0000	0.0000
14	WP H	0.2692	0.0000	0.0000
	WP L	0.2648	0.0000	0.0000
15	WP H	0.7337	0.0000	0.0000
	WP L	0.8210	0.0000	0.0000
16	WP H	0.0521	0.0000	0.0000
	WP L	0.0943	0.0000	0.0000
17	WP H	0.3790	0.0000	0.0000
	WP L	0.3934	0.0000	0.0000

Output DTN: LL0704PA049SPC.024, file *CDSP_kinematic_analyses_DA_summary.xls,* sheet "WP-Pallet."

NOTES: Realizations that predicted zero damaged areas are not shown.
WP = waste package.

Table 6-116. Damaged Areas for Codisposal Waste Packages for 2.44 m/s PGV, 23-mm OCB with Degraded Internals, Waste Package-to-Pallet Impacts

Realization	Waste Package	Damaged Area at 90% Yield Strength (m^2)	Damaged Area at 100% Yield Strength (m^2)	Damaged Area at 105% Yield Strength (m^2)
1	WP H	0.0741	0.0392	0.0115
	WP L	0.0523	0.0295	0.0127
2	WP H	0.2096	0.1088	0.0376
	WP L	0.5453	0.2798	0.1137
3	WP H	1.4937	0.7974	0.3776
	WP L	1.7043	0.8631	0.4237
4	WP H	4.3391	2.5693	1.2690
	WP L	3.4272	1.9567	1.0144
5	WP H	0.7315	0.3613	0.1664
	WP L	0.6441	0.3499	0.1510
6	WP H	3.3670	1.9482	0.9853
	WP L	2.9028	1.6681	0.7816
7	WP H	1.6173	0.9038	0.4218
	WP L	0.1751	0.0884	0.0274
8	WP H	0.6439	0.3413	0.1424
	WP L	0.6598	0.3591	0.1646
10	WP H	4.2619	2.4264	1.1029
	WP L	4.7782	2.6869	1.2225
11	WP H	0.4156	0.2100	0.0794
	WP L	0.7906	0.4264	0.1883
12	WP H	1.7149	0.9325	0.4466
	WP L	0.7974	0.3792	0.1414
13	WP H	0.9127	0.4906	0.2124
	WP L	0.8304	0.4594	0.2059
14	WP H	1.2167	0.6902	0.3219
	WP L	1.2687	0.7004	0.3255
15	WP H	3.6112	1.9667	0.8890
	WP L	3.6910	2.1776	1.0125
16	WP H	0.2465	0.1286	0.0528
	WP L	0.4600	0.2389	0.0972
17	WP H	2.0582	1.0898	0.5194
	WP L	2.0413	1.0924	0.5157

Output DTN: LL0704PA049SPC.024, file *CDSP_kinematic_analyses_DA_summary.xls,* sheet "WP-Pallet."

NOTES: Realizations that predicted zero damaged areas are not shown.
WP = waste package.

Table 6-117. Damaged Areas for Codisposal Waste Packages for 2.44 m/s PGV, 17-mm OCB with Degraded Internals, Waste Package-to-Pallet Impacts

Realization	Waste Package	Damaged Area at 90% Yield Strength (m^2)	Damaged Area at 100% Yield Strength (m^2)	Damaged Area at 105% Yield Strength (m^2)
1	WP H	0.1421	0.0462	0.0000
	WP L	0.1156	0.0445	0.0000
2	WP H	0.3153	0.1024	0.0201
	WP L	0.6767	0.2476	0.0686
3	WP H	1.6688	0.7221	0.3621
	WP L	1.9953	0.7793	0.3446
4	WP H	4.5839	2.3859	1.2871
	WP L	3.4904	1.7961	1.0053
5	WP H	0.8131	0.3336	0.1478
	WP L	0.8128	0.3244	0.0927
6	WP H	3.7479	1.8501	0.8549
	WP L	3.1749	1.5130	0.7072
7	WP H	1.8165	0.8468	0.3794
	WP L	0.2633	0.0989	0.0190
8	WP H	0.7669	0.2789	0.0699
	WP L	0.7855	0.3210	0.0999
10	WP H	4.4478	2.2342	1.1076
	WP L	5.0003	2.5119	1.2916
11	WP H	0.5441	0.2252	0.0526
	WP L	0.9560	0.4116	0.1429
12	WP H	1.9520	0.8250	0.3603
	WP L	0.9977	0.3536	0.1130
13	WP H	1.0338	0.4609	0.1813
	WP L	0.9701	0.4413	0.1568
14	WP H	1.4319	0.6397	0.2519
	WP L	1.4186	0.6212	0.2683
15	WP H	3.7202	1.7698	0.8033
	WP L	3.7774	2.0043	1.0100
16	WP H	0.3509	0.1339	0.0289
	WP L	0.5833	0.2292	0.0657
17	WP H	2.2461	1.0079	0.4637
	WP L	2.2131	0.9881	0.4442

Output DTN: LL0704PA049SPC.024, file *CDSP_kinematic_analyses_DA_summary.xls,* sheet "WP-Pallet."

NOTES: Realizations that predicted zero damaged areas are not shown.
WP = waste package.

Table 6-118. Damaged Areas for Codisposal Waste Packages for 4.07 m/s PGV, 23-mm OCB with Intact Internals, Waste Package-to-Pallet Impacts

Realization	Waste Package	Damaged Area at 90% Yield Strength (m^2)	Damaged Area at 100% Yield Strength (m^2)	Damaged Area at 105% Yield Strength (m^2)
1	WP H	0.2027	0.0000	0.0000
	WP L	0.2384	0.0000	0.0000
2	WP H	0.2719	0.0000	0.0000
	WP L	0.2606	0.0000	0.0000
3	WP H	0.6471	0.0000	0.0000
	WP L	0.5915	0.0000	0.0000
4	WP H	1.7446	0.0091	0.0000
	WP L	1.5070	0.0083	0.0000
5	WP H	0.5415	0.0027	0.0000
	WP L	0.6150	0.0028	0.0000
6	WP H	1.4748	0.0000	0.0000
	WP L	1.2658	0.0147	0.0000
7	WP H	0.5631	0.0000	0.0000
	WP L	0.3369	0.0000	0.0000
8	WP H	0.4640	0.0024	0.0000
	WP L	0.5754	0.0000	0.0000
9	WP H	0.0809	0.0000	0.0000
	WP L	0.1346	0.0000	0.0000
10	WP H	1.9766	0.0000	0.0000
	WP L	1.7356	0.0090	0.0000
11	WP H	0.4843	0.0000	0.0000
	WP L	0.4184	0.0000	0.0000
12	WP H	0.5476	0.0000	0.0000
	WP L	0.6208	0.0000	0.0000
13	WP H	0.6824	0.0000	0.0000
	WP L	0.4557	0.0060	0.0000
14	WP H	1.4130	0.0070	0.0000
	WP L	1.1513	0.0031	0.0000
15	WP H	1.3185	0.0000	0.0000
	WP L	1.3560	0.0054	0.0000
16	WP H	0.2817	0.0000	0.0000
	WP L	0.5380	0.0030	0.0000
17	WP H	1.1603	0.0091	0.0000
	WP L	1.2746	0.0030	0.0000

Output DTN: LL0704PA049SPC.024, file *CDSP_kinematic_analyses_DA_summary.xls,* sheet "WP-Pallet."

NOTE: WP = waste package.

Table 6-119. Damaged Areas for Codisposal Waste Packages for 4.07 m/s PGV, 23-mm OCB with Degraded Internals, Waste Package-to-Waste Package Impacts

Realization	Waste Package	Damaged Area at 90% Yield Strength (m^2)	Damaged Area at 100% Yield Strength (m^2)	Damaged Area at 105% Yield Strength (m^2)
4	WP H	0.0000	0.0000	0.0000
	WP L	0.0042	0.0000	0.0000
6	WP H	0.0027	0.0000	0.0000
	WP L	0.0000	0.0000	0.0000

Output DTN: LL0704PA049SPC.024, file *CDSP_kinematic_analyses_DA_summary.xls,* sheet "WP-WP."

NOTES: Realizations that predicted zero damaged areas are not shown.
WP = waste package.

Table 6-120. Damaged Areas for Codisposal Waste Packages for 4.07 m/s PGV, 23-mm OCB with Degraded Internals, Waste Package-to-Pallet Impacts

Realization	Waste Package	Damaged Area at 90% Yield Strength (m^2)	Damaged Area at 100% Yield Strength (m^2)	Damaged Area at 105% Yield Strength (m^2)
1	WP H	1.0213	0.5262	0.2435
	WP L	1.0539	0.6059	0.2911
2	WP H	1.3386	0.6989	0.3236
	WP L	1.3686	0.7246	0.3073
3	WP H	3.2031	1.7117	0.7632
	WP L	3.2886	1.6898	0.7251
4	WP H	6.9478	4.0460	2.0062
	WP L	5.9964	3.5561	1.8110
5	WP H	2.3202	1.3239	0.6631
	WP L	3.2359	1.8321	0.8263
6	WP H	5.4754	3.5684	1.9732
	WP L	4.8013	3.0433	1.6904
7	WP H	2.7908	1.6039	0.7445
	WP L	1.6337	0.9358	0.4203
8	WP H	2.4062	1.3014	0.5935
	WP L	2.8384	1.5602	0.7188
9	WP H	0.4311	0.2218	0.0852
	WP L	0.9222	0.4489	0.1806
10	WP H	8.1315	4.7886	2.4062
	WP L	6.1231	3.5097	1.9989
11	WP H	2.1978	1.2433	0.6141
	WP L	2.1878	1.1789	0.5283
12	WP H	1.9398	1.1713	0.6494
	WP L	3.1865	1.7985	0.8190
13	WP H	3.3507	1.9697	0.8902
	WP L	2.5226	1.3831	0.6501
14	WP H	4.8246	3.3506	1.7977
	WP L	4.5709	2.9371	1.5509
15	WP H	4.8711	2.9831	1.5400
	WP L	5.6665	3.4837	1.6266

Table 6-120. Damaged Areas for Codisposal Waste Packages for 4.07 m/s PGV, 23-mm OCB with Degraded Internals, Waste Package-to-Pallet Impacts (Continued)

Realization	Waste Package	Damaged Area at 90% Yield Strength (m^2)	Damaged Area at 100% Yield Strength (m^2)	Damaged Area at 105% Yield Strength (m^2)
16	WP H	1.5722	0.8253	0.3353
	WP L	2.6455	1.5153	0.7333
17	WP H	4.0161	2.5385	1.4358
	WP L	4.8784	2.9678	1.5351

Output DTN: LL0704PA049SPC.024, file *CDSP_kinematic_analyses_DA_summary.xls,* sheet "WP-Pallet."

NOTE: WP = waste package.

Table 6-121. Damaged Areas for Codisposal Waste Packages for 4.07 m/s PGV, 17-mm OCB with Degraded Internals, Waste Package-to-Pallet Impacts

Realization	Waste Package	Damaged Area at 90% Yield Strength (m^2)	Damaged Area at 100% Yield Strength (m^2)	Damaged Area at 105% Yield Strength (m^2)
1	WP H	1.1743	0.4660	0.1815
	WP L	1.2188	0.5665	0.2436
2	WP H	1.5033	0.6226	0.2659
	WP L	1.5199	0.6725	0.2721
3	WP H	3.3876	1.6255	0.7641
	WP L	3.5307	1.5506	0.6800
4	WP H	6.8571	3.8618	2.2152
	WP L	5.6056	3.2162	1.8481
5	WP H	2.4972	1.2506	0.6114
	WP L	3.5790	1.7055	0.8006
6	WP H	5.8554	3.4367	1.8313
	WP L	5.1502	2.9803	1.6783
7	WP H	3.0144	1.4668	0.6411
	WP L	1.9532	0.8664	0.2822
8	WP H	2.6385	1.2559	0.5780
	WP L	3.1257	1.4127	0.6183
9	WP H	0.5138	0.2126	0.0930
	WP L	1.0582	0.3904	0.1616
10	WP H	8.3286	4.7319	2.7850
	WP L	6.1728	3.6068	2.2461
11	WP H	2.3920	1.1170	0.5006
	WP L	2.4438	1.0892	0.4992
12	WP H	2.1394	1.0578	0.5859
	WP L	3.5290	1.6798	0.7393
13	WP H	3.6841	1.7977	0.8369
	WP L	2.8621	1.3605	0.6778
14	WP H	5.0826	3.1557	1.8290
	WP L	4.7650	2.7378	1.5130
15	WP H	4.9461	2.7763	1.5489
	WP L	5.7125	3.2010	1.6485

Table 6-121. Damaged Areas for Codisposal Waste Packages for 4.07 m/s PGV, 17-mm OCB with Degraded Internals, Waste Package-to-Pallet Impacts (Continued)

Realization	Waste Package	Damaged Area at 90% Yield Strength (m^2)	Damaged Area at 100% Yield Strength (m^2)	Damaged Area at 105% Yield Strength (m^2)
16	WP H	1.8890	0.7203	0.2396
	WP L	2.8808	1.4063	0.6546
17	WP H	4.1043	2.3961	1.4477
	WP L	5.0701	2.7716	1.5516

Output DTN: LL0704PA049SPC.024, file *CDSP_kinematic_analyses_DA_summary.xls,* sheet "WP-Pallet."

NOTE: WP = waste package.

6.3.4.2 Rupture Results

No waste packages (TAD-bearing or codisposal) are determined to have a rupture condition of "Yes" based on single impacts, so no results are presented for that assessment.

The calculations to determine the probability of whether a waste package is in a state of incipient rupture or rupture based on multiple impacts are performed for all of the same kinematic analyses for which damaged area was computed. The probabilities were computed for the same waste packages in the kinematic analyses and for the same waste package states. The calculations for the TAD-bearing and codisposal waste packages are summarized in Table 6-122 and Table 6-123, respectively. The probability results for the TAD-bearing waste package are presented in Table 6-124 to Table 6-129, and the probability results are presented in Table 6-130 to Table 6-133. As with the tables of damaged area, each table lists the waste package identifier (I, J, and K for TAD-bearing waste packages and H and L for codisposal waste packages) and the probabilities of incipient rupture and rupture, as a function of realization number. Also similar to the damaged area tables, many of the realizations at low PGV have zero predicted probabilities, and these have been removed from the tables to improve readability. The tables are organized by waste package type (TAD-bearing and codisposal), ground motion level (0.40 m/s PGV, 1.05 m/s PGV, 2.44 m/s PGV, and 4.07 m/s PGV), and finally by waste package configuration (23-mm OCB with intact internals, 23-mm OCB with degraded internals, and 17-mm OCB with degraded internals). The sets of analyses where all realizations predicted zero for all probabilities are indicated with a dash in the "Table" column of Table 6-122 and Table 6-123. There are no rupture probability tables reported for these sets of analyses.

Table 6-122. Analyses Conducted for TAD-Bearing Rupture Probabilities for 11-Waste-Package Configuration

Ground Motion Level	Waste Package Configuration	Table
0.40 m/s PGV	23-mm OCB, intact Internals	–
	23-mm OCB, degraded Internals	–
	17-mm OCB, degraded Internals	–
1.05 m/s PGV	23-mm OCB, intact Internals	–
	23-mm OCB, degraded Internals	Table 6-124
	17-mm OCB, degraded Internals	Table 6-125
2.44 m/s PGV	23-mm OCB, intact Internals	–
	23-mm OCB, degraded Internals	Table 6-126
	17-mm OCB, degraded Internals	Table 6-127
4.07 m/s PGV	23-mm OCB, intact Internals	–
	23-mm OCB, degraded Internals	Table 6-128
	17-mm OCB, degraded Internals	Table 6-129

Source: Created to enhance readability only.

NOTES: Column labeled “Table” provides location of results of analyses.
“–“ indicates no rupture probabilities predicted.
OCB = outer corrosion barrier; PGV = peak ground velocity.

Table 6-123. Analyses Conducted for Codisposal Rupture Probabilities for 13-Waste-Package Configuration

Ground Motion Level	Waste Package Configuration	Table
0.40 m/s PGV	23-mm OCB, intact Internals	–
	23-mm OCB, degraded Internals	–
	17-mm OCB, degraded Internals	–
1.05 m/s PGV	23-mm OCB, intact Internals	–
	23-mm OCB, degraded Internals	–
	17-mm OCB, degraded Internals	–
2.44 m/s PGV	23-mm OCB, intact Internals	–
	23-mm OCB, degraded Internals	Table 6-130
	17-mm OCB, degraded Internals	Table 6-131
4.07 m/s PGV	23-mm OCB, intact Internals	–
	23-mm OCB, degraded Internals	Table 6-132
	17-mm OCB, degraded Internals	Table 6-133

Source: Created to enhance readability only.

NOTE: Column labeled “Table” provides location of results of analyses.
“–“ indicates no rupture probabilities predicted.
OCB = outer corrosion barrier; PGV = peak ground velocity.

Table 6-124. Rupture Probabilities for TAD-Bearing Waste Packages for 1.05 m/s PGV, 23-mm OCB with Degraded Internals

Realization Number	Waste Package	Incipient Rupture	Rupture
10	WP I	0.258	0.000
	WP J	0.000	0.000
	WP K	0.000	0.000
	Average	**0.005**	**0.000**

Output DTN: LL0703PA029SPC.014,
file *kinematic_analyses_rupture_summary.xls,*
sheet "Naval Long TAD summary."

NOTES: Realizations that predicted zero rupture probabilities are not shown. However, the average includes all realizations.
WP = waste package

Table 6-125. Rupture Probabilities for TAD-Bearing Waste Packages for 1.05 m/s PGV, 17-mm OCB with Degraded Internals

Realization Number	Waste Package	Incipient Rupture	Rupture
10	WP I	0.343	0.000
	WP J	0.000	0.000
	WP K	0.000	0.000
	Average	**0.007**	**0.000**

Output DTN: LL0703PA029SPC.014,
file *kinematic_analyses_rupture_summary.xls,*
sheet "Naval Long TAD summary."

NOTES: Realizations that predicted zero rupture probabilities are not shown. However, the average includes all realizations.
WP = waste package.

Table 6-126. Rupture Probabilities for TAD-Bearing Waste Packages for 2.44 m/s PGV, 23-mm OCB with Degraded Internals

Realization Number	Waste Package	Incipient Rupture	Rupture
4	WP I	0.422	0.000
	WP J	0.000	0.000
	WP K	0.000	0.000
10	WP I	0.177	0.000
	WP J	0.176	0.000
	WP K	0.000	0.000

Table 6-126. Rupture Probabilities for TAD-Bearing Waste Packages for 2.44 m/s PGV, 23-mm OCB with Degraded Internals (Continued)

Realization Number	Waste Package	Incipient Rupture	Rupture
15	WP I	0.000	0.000
	WP J	0.000	0.000
	WP K	1.000	0.000
	Average	**0.035**	**0.000**

Output DTN: LL0703PA029SPC.014,
file *kinematic_analyses_rupture_summary.xls,*
sheet "Naval Long TAD summary."

NOTES: Realizations that predicted zero rupture probabilities are not shown. However, the average includes all realizations.
WP = waste package.

Table 6-127. Rupture Probabilities for TAD-Bearing Waste Packages for 2.44 m/s PGV, 17-mm OCB with Degraded Internals

Realization Number	Waste Package	Incipient Rupture	Rupture
4	WP I	0.562	0.000
	WP J	0.000	0.000
	WP K	0.000	0.000
10	WP I	0.237	0.000
	WP J	0.234	0.000
	WP K	0.000	0.000
15	WP I	0.000	0.000
	WP J	0.000	0.000
	WP K	1.000	0.000
	Average	**0.040**	**0.000**

Output DTN: LL0703PA029SPC.014,
file *kinematic_analyses_rupture_summary.xls,*
sheet "Naval Long TAD summary."

NOTE: Realizations that predicted zero rupture probabilities are not shown. However, the average includes all realizations.
WP = waste package.

Table 6-128. Rupture Probabilities for TAD-Bearing Waste Packages for 4.07 m/s PGV, 23-mm OCB with Degraded Internals

Realization Number	Waste Package	Incipient Rupture	Rupture
3	WP I	0.158	0.000
	WP J	1.000	0.000
	WP K	0.390	0.000
4	WP I	0.271	0.729
	WP J	0.472	0.528
	WP K	0.000	1.000
5	WP I	0.319	0.000
	WP J	0.000	0.000
	WP K	0.371	0.061
6	WP I	0.000	0.000
	WP J	0.525	0.003
	WP K	0.000	0.000
7	WP I	0.240	0.000
	WP J	0.000	0.000
	WP K	0.000	0.000
8	WP I	0.000	0.000
	WP J	0.000	0.000
	WP K	1.000	0.000
10	WP I	0.000	1.000
	WP J	0.000	1.000
	WP K	0.000	1.000
12	WP I	0.000	0.000
	WP J	0.266	0.000
	WP K	0.000	0.000
15	WP I	0.000	1.000
	WP J	0.000	1.000
	WP K	0.000	1.000
17	WP I	0.802	0.109
	WP J	0.454	0.458
	WP K	0.000	0.000
	Average	**0.123**	**0.174**

Output DTN: LL0703PA029SPC.014,
file *kinematic_analyses_rupture_summary.xls,*
sheet “Naval Long TAD summary.”

NOTES: Realizations that predicted zero rupture probabilities are not shown. However, the average includes all realizations.
WP = waste package.

Table 6-129. Rupture Probabilities for TAD-Bearing Waste Packages for 4.07 m/s PGV, 17-mm OCB with Degraded Internals

Realization Number	Waste Package	Incipient Rupture	Rupture
3	WP I	0.210	0.000
	WP J	1.000	0.000
	WP K	0.520	0.000
4	WP I	0.121	0.879
	WP J	0.345	0.655
	WP K	0.000	1.000
5	WP I	0.425	0.000
	WP J	0.000	0.000
	WP K	0.441	0.108
6	WP I	0.000	0.000
	WP J	0.697	0.006
	WP K	0.000	0.000
7	WP I	0.320	0.000
	WP J	0.000	0.000
	WP K	0.000	0.000
8	WP I	0.000	0.000
	WP J	0.000	0.000
	WP K	1.000	0.000
10	WP I	0.000	1.000
	WP J	0.000	1.000
	WP K	0.000	1.000
12	WP I	0.000	0.000
	WP J	0.355	0.000
	WP K	0.000	0.000
15	WP I	0.000	1.000
	WP J	0.000	1.000
	WP K	0.000	1.000
17	WP I	0.839	0.161
	WP J	0.228	0.772
	WP K	0.000	0.000
	Average	**0.127**	**0.188**

Output DTN: LL0703PA029SPC.014,
file *kinematic_analyses_rupture_summary.xls,*
sheet “Naval Long TAD summary.”

NOTES: Realizations that predicted zero rupture probabilities are not shown. However, the average includes all realizations.
WP = waste package.

Table 6-130. Rupture Probabilities for Codisposal Waste Packages for 2.44 m/s PGV, 23-mm OCB with Degraded Internals

Realization #	Waste Package	Incipient Rupture	Rupture
10	WP H	0.012	0.000
	WP L	0.000	0.000
15	WP H	0.950	0.000
	WP L	0.000	0.000
	Average	**0.028**	**0.000**

Output DTN: LL0703PA029SPC.014,
file *kinematic_analyses_rupture_summary.xls,* sheet "CDSP summary."

NOTES: Realizations that predicted zero rupture probabilities are not shown. However, the average includes all realizations.
WP = waste package.

Table 6-131. Rupture Probabilities for Codisposal Waste Packages for 2.44 m/s PGV, 17-mm OCB with Degraded Internals

Realization #	Waste Package	Incipient Rupture	Rupture
10	WP H	0.013	0.000
	WP L	0.000	0.000
15	WP H	1.000	0.000
	WP L	0.000	0.000
	Average	**0.030**	**0.000**

Output DTN: LL0703PA029SPC.014,
file *kinematic_analyses_rupture_summary.xls,* sheet "CDSP summary."

NOTES: Realizations that predicted zero rupture probabilities are not shown. However, the average includes all realizations.
WP = waste package.

Table 6-132. Rupture Probabilities for Codisposal Waste Packages for 4.07 m/s PGV, 23-mm OCB with Degraded Internals

Realization #	Waste Package	Incipient Rupture	Rupture
3	WP H	0.000	0.000
	WP L	0.919	0.000
4	WP H	0.846	0.154
	WP L	0.000	1.000
10	WP H	0.000	1.000
	WP L	0.000	1.000
14	WP H	0.987	0.000
	WP L	0.685	0.104
15	WP H	0.316	0.639
	WP L	0.378	0.019
	Average	**0.122**	**0.115**

Output DTN: LL0703PA029SPC.014,
file *kinematic_analyses_rupture_summary.xls,* sheet "CDSP summary."

NOTES: Realizations that predicted zero rupture probabilities are not shown. However, the average includes all realizations.
WP = waste package.

Table 6-133. Rupture Probabilities for Codisposal Waste Packages for 4.07 m/s PGV, 17-mm OCB with Degraded Internals

Realization #	Waste Package	Incipient Rupture	Rupture
3	WP H	0.000	0.000
	WP L	1.000	0.000
4	WP H	0.827	0.173
	WP L	0.000	1.000
10	WP H	0.000	1.000
	WP L	0.000	1.000
14	WP H	1.000	0.000
	WP L	0.742	0.132
15	WP H	0.234	0.754
	WP L	0.421	0.024
	Average	**0.124**	**0.120**

Output DTN: LL0703PA029SPC.014,
file *kinematic_analyses_rupture_summary.xls,* sheet "CDSP summary."

NOTES: Realizations that predicted zero rupture probabilities are not shown. However, the average includes all realizations.
WP = waste package.

6.4 EFFECT OF VIBRATORY GROUND MOTION AND ROCK LOADS ON THE DRIP SHIELD

6.4.1 Overview of Drip Shield Damage Analyses

This section presents a series of analyses designed to evaluate the performance of the drip shield subjected to vibratory ground motion during the postclosure period. The drip shield is a titanium structure designed to be placed over the waste package and pallet when the repository is closed. The drip shield is constructed by covering a structural framework of bulkheads and beams with a layer of welded plates as shown schematically in Figure 6-38. The purpose of the drip shield is to protect the waste packages from: (a) water dripping directly from the drift crown and walls, and (b) direct impacts of loose, falling rock blocks. The drip shield will be assembled in overlapping sections to provide continuous shielding of the waste packages.

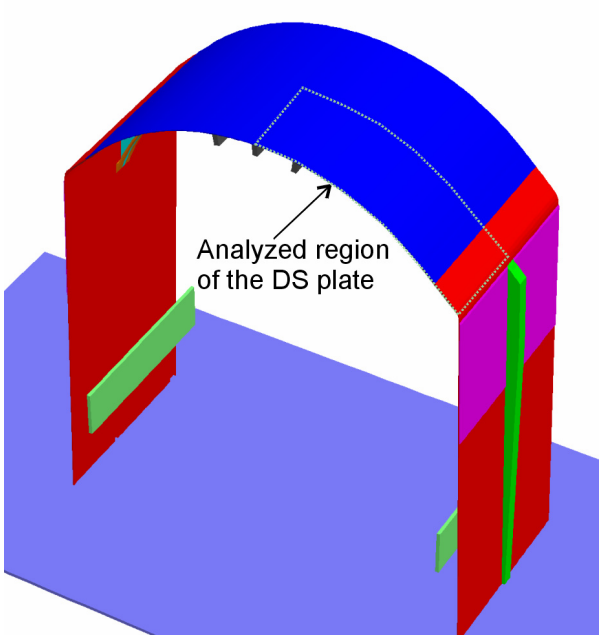

Source: Created for illustrative purposes only, from FLAC3D save file in output DTN: MO0701DRIPSHLD.000, file *drip shield framework fragility/average load/15mm/grid3.sav*, by plotting block group geometry.

NOTE: The green plates inside the drip shield represent the emplacement pallet.

Figure 6-38. Drip Shield Geometry Showing the Outline of the Analyzed Region of the Crown Plate

The functionality of the drip shield can be affected adversely if:

- The rigid body motion of the drip shield sections relative to one another creates one or more gaps between them, exposing the waste package(s) to direct water seepage or to impacts from loose blocks
- The drip shield loses structural integrity as a result of mechanical collapse or buckling
- An impact damages the drip shield plates and provides the necessary condition for rupture or stress corrosion.

With the exception of stress corrosion, these mechanical failures are important within TSPA because they eliminate the drip shield as a component of the EBS barrier to seepage and advective flow. Drip shield failure causes advective flow through the drip shield and changes the waste package damage abstractions from those for the kinematic representation to those for a waste package surrounded by rubble or another appropriate configuration in TSPA.

The mechanical loadings expected during the regulatory period that can affect the functionality of the drip shield are (a) vibratory ground motion, and (b) dynamic and static loads of loose blocks dislodged from the roof and walls of the emplacement drift.

Once rubble has accumulated on the drip shield, subsequent seismic ground shaking can potentially amplify the static load. Moreover, continuous thinning of the drip shield structural components is also expected to occur over the long postclosure period due to corrosion. This will weaken the drip shield components. The waste package may also impact the drip shield during seismic ground motion, and these impacts may damage or weaken the drip shield framework. Dynamic amplification during seismic ground motions and weakening of the structural components may cause the drip shield to fail by fracturing the plates at locations between the bulkheads, stiffeners and support beams, by fracturing the support beams or the bulkheads, or by the instability of the support beams or the bulkheads.

The crushed tuff filling the drift invert may settle and deform during the postclosure period. One cause of settling may be corrosion of the steel components built into the crushed tuff in the invert. If nonuniform settling occurs, the drip shield may tilt and become unstable during episodes of seismic ground motion.

Finally, damage to waste packages due to large rock blocks dislodged from the drift walls and roof during vibratory ground motion must be considered. This section presents a series of analyses designed to address the above issues. These analyses include:

- Damage and fragility analysis of the drip shield plates and framework under conditions of amplified rockfall loads caused by vibratory ground motion
- Analysis of the drip shield failure modes under conditions of amplified rockfall loads caused by vibratory ground motion
- Kinematic analysis of drip shield damage area caused by drip shield–waste package impacts during vibratory ground motion
- Analysis of the effects of uneven invert settlement on drip shield stability during vibratory ground motion
- Analysis of damage and fragility of the drip shield plates and framework under conditions of large block impacts (expected in nonlithophysal units) into the drip shield.

This section first describes the design of the drip shield and the material properties of titanium, which will be used to construct the drip shield (Section 6.4.2).

The fragility and damage of the drip shield plates under amplified uniform rockfall rubble loads (expected in lithophysal units) is analyzed in Section 6.4.3.1. This analysis provides information on damage area as a function of the load and the load at which the plates fail as a function of thickness; it is important because fracturing (or tearing) of the plates between the bulkheads and support beams would allow rubble to pass easily through gaps created by fractures and accumulate around the waste packages. The damage areas and critical loads are determined in a quasi-static three-dimensional analysis, assuming that amplification of the vertical static load is proportional to vertical PGA plus the acceleration of gravity (Assumption 5.16, Section 5). Results are correlated to the intensity of the ground motions (and PGV levels) in *Seismic Consequence Abstraction* (SNL 2007 [DIRS 176828]).

Analysis of the drip shield framework under amplified and relatively uniform rockfall rubble loads (expected in lithophysal units) is presented in Section 6.4.3.2. As was done for the drip shield plates, fragility of the drip shield framework was investigated using quasi-static analyses. The critical loads at which the framework fails are correlated to the vertical PGA assuming dynamic amplification of the static rubble loads. However, for understanding of consequences of drip shield collapse, it is important to know the failure mode in addition to the magnitude of the failure load. Possible modes of drip shield framework failure include buckling of the support beams in the drip shield legs and snap-through of the bulkhead in the crown. Snap-through is a form of nonlinear buckling. Curved plates or flat plates with initial imperfections can exhibit this behavior when a large change in deflection takes place with a small change in load increment. This "snap-through" jump in deflection occurs from the side of initial curvature to the other side of the supports. When small increments of load are applied to the plate, the middle surface compressive stress builds up and then suddenly releases the internal strain energy in the form of external work done, causing the snap-through jump.

The consequences of drip shield instability or failure will depend on the failure mode. If the legs of the drip shield buckle, the drip shield will collapse (sit) onto the waste package and the static rubble load will be transferred to the OCB of the waste package through the bulkhead. In this case, the contact surface will be the manufactured surface of the bulkhead flange. If the drip shield framework snaps through in the middle of the crown, the bulkhead will fracture and deform until it contacts the waste package with, most likely, sharp edges formed by irregular fracturing.

The initial contact between the failed bulkhead and the waste package will be dynamic. In this case, the static rubble load causing drip shield failure will be transferred to the waste package through the irregular, fractured surface of the bulkhead, representing a much more severe loading condition for rupturing the drip shield plates than the loading conditions when the drip shield legs buckle. Drip shield failure modes are analyzed in a two-dimensional dynamic simulation of the interaction between the drip shield structure and the surrounding rubble. This analysis is also used as a validation of the quasi-static approach for drip shield framework fragility calculations (Section 6.4.3.2). The results of the drip shield failure mode analyses are discussed in Section 6.4.4.

Section 6.4.5 presents analyses of drip shield-waste package impacts that may occur due to seismic ground motion. Such impacts could weaken the drip shield framework beyond that due

to corrosion. The three-dimensional kinematic model described in Section 6.3 is used in this analysis.

The effects of uneven settling on drip shield stability are investigated in Section 6.4.6. Over the postclosure time period, the crushed tuff filling the drift invert may settle and deform causing the drip shield to tilt. One cause of settling will be corrosion of the carbon steel components built into the crushed tuff in the invert. Tilting of the drip shield may affect its response to vibratory ground motion. This is investigated using a three-dimensional model with dead loads on the drip shield. Results presented in Section 6.4.6 respond to an AIN from the NRC (Key Technical Issue Agreement: Total System Performance Assessment and Integration 2.02, Comment J-2, Additional Information Need (Kokajko 2005 [DIRS 177025], pp. 5 and 6 of enclosure)).

Damage and fragility of the drip shield plates and framework are analyzed for impact of individual large blocks expected to form in nonlithophysal units during strong seismic ground motions. The results of analyses are presented in Section 6.4.7. Three-dimensional, dynamic simulations of impact of seven blocks with impact energies (i.e., mass and velocity) that span the expected range of impact energy are carried out for three drip shield configurations to generate damage and fragility look-up tables.

These calculations are performed with qualified versions of the finite-difference program FLAC3D (V. 2.1. Sub Release 2.10.196. STN: 10502-2.1-00 [DIRS 161947]).

The static rockfall load will increase as rubble accumulates on the crown of the drip shield from multiple seismic events. A series of two-dimensional distinct-element calculations is used to examine rubble accumulation in the lithophysal zones as a function of lithophysal rock strength and the PGV level of the ground motions. Calculations for the 1.05 m/sec PGV level and 2.44 m/sec PGV level have already been reported in *Drift Degradation Analysis* (BSC 2004 [DIRS 166107], Section 6.4.2.2.2) for all five rock categories in the lithophysal zones. However, additional calculations are needed at the 0.4 m/sec PGV level to complete development of an abstraction for rubble accumulation. Seismically induced rockfall in the lithophysal units and stable drift profiles for 0.4 m/s, 1.05 m/s, and 2.44 m/s PGV levels are discussed in Appendix C.

The uncertainty in the ground motions and in rock strength is propagated into the rockfall calculations through sampled values for these input parameters. GoldSim (V. 8.02.500. STN: 10344-8.02-05 [DIRS 174650]) provides a Latin Hypercube sampling of the rock strength and the ground motion number. The rock strength is represented by five rock categories, numbered 1 through 5, that represent the range of porosity and unconfined compressive strength observed in lithophysal rock. The rock category is sampled from a discrete distribution between 1 and 5, and the ground motion number is sampled from a discrete distribution from 1 to 15, with equal probability for each integer. This sampling provides a list of input data in which a given time history is randomly paired with a rock category at each PGV level.

The rockfall calculations were performed by a qualified version of the distinct-element program UDEC (V. 3.1 Sub-Release 3.10.109. 2002. STN: 10173-3.1-00 [DIRS 161949]).

The output from the damage calculations provides the basis for new fragility curves that will be documented in *Seismic Consequence Abstraction* (SNL 2007 [DIRS 176828]).

6.4.2 Mechanical Properties of Titanium

The main structural (load-bearing) elements of the drip shield, the bulkheads, and the support beams will be fabricated of Titanium Grade 29. The support frames will be spaced at 1,071.6 mm intervals along the drip shield (Table 4-1). However, calculations for the drip shield fragility were carried out using material properties of Titanium Grade 24 because Titanium Grade 29 was selected after completion of these calculations. The impact assessment for the difference between Titanium Grades 24 and 29 is provided in Section 4.1.5. The drip shield plates that will cover the bulkheads and support beams will be fabricated of Titanium Grade 7.

Bi-linear idealizations of the uniaxial stress-strain relations for titanium plate and frame members were used in the drip shield analyses. The initial slope of the stress-strain curve is characterized by Young's modulus (E). The material yields when the stress reaches the yield strength, σ_y, and the postyield slope of the stress-strain curve is characterized by its tangent stiffness, E_t. The material fails (ruptures) when the stress reaches the ultimate strength, σ_u, and the strain reaches the ultimate elongation, ε_u. The material properties of Titanium Grades 7 and 24 used in the calculations are listed in Table 4-3 and Appendix A. The actual FLAC3D input parameters that represent the mechanical behavior of titanium plate and frame members, as used in the calculations, are listed in Table 6-134. Detailed discussion of the titanium plate and frame members stress-strain curves, their idealization, engineering, and true stresses and strains can be found in *Mechanical Assessment of the Drip Shield Subject to Vibratory Motion and Dynamic and Static Rock Loading* (BSC 2004 [DIRS 169753], Section 5.2.3.1).

Titanium plate and frame members are represented in the FLAC3D calculations as strain-hardening Tresca materials. The Tresca constitutive relation is a degenerate case of the Mohr-Coulomb relation; it is achieved by setting the friction angle to zero and precluding tension cutoff. The latter is achieved by setting the "tensile strength" of the material to a very large number. However, that does not mean that the material cannot fail in tension. It can fail in tension, as governed by the Tresca yield surface, but the additional yield surface introduced by the tension cutoff is removed.

Table 6-134. Mechanical Properties of Titanium Grades 7 and 24 Used as Input in FLAC3D Calculation

Property	Titanium Grade 7	Titanium Grade 24	Relation
Bulk modulus K (GPa)	97.22	117.06	$K = \frac{E}{3(1-2\nu)}$
Shear modulus G (GPa)	39.77	41.93	$G = \frac{E}{2(1+\nu)}$
Cohesion c (MPa)	158	431	$c = \frac{\sigma_y}{2}$
Ultimate cohesion c_u (MPa)	198	560.5[a]	$c_u = \frac{\sigma_u}{2}$
Ultimate plastic strain ε_{up}	0.217	0.152	$\varepsilon_{up} = \varepsilon_u - \frac{\sigma_y}{E}$
Cohesion corresponding to 100% of plastic shear strain c_{p1}[b]	342	1,281	$c_{p1} = c + \frac{c_u - c}{\varepsilon_{up}}$

[a] Due to a rounding error, the value of 561 MPa is used in the calculations. The difference is small and has an inconsequential effect on the results of the calculation.

[b] Cohesion at a strain larger than any strain that will be achieved during simulation is specified to define a hardening modulus. The actual value of that large strain is irrelevant, because the hardening modulus is the only relevant parameter. The formula in Table 6-138 provides cohesion corresponding to 100% of the plastic strain. The general form of the formula is $c_{p1} = c + \varepsilon_{\max} \frac{c_u - c}{\varepsilon_{up}}$, where $\varepsilon_{\max}$ is a large strain that defines the hardening slope. In the input data for some of the calculations, $\varepsilon_{\max}$ is not equal to 1. For example, in the calculations discussed in Section 6.4.3.1, $\varepsilon_{\max}$ = 21,700.

Source: Appendix A, Tables A-1 and A-2

NOTE: E is the Young's modulus; ν is the Poisson's ratio; σ_y is the yield strength; and σ_u is the ultimate strength at 60°C. ε_u is the ultimate strain at 60°C. The formulas for K and G are taken from *Itasca Software–Cutting Edge Tools for Computational Mechanics* (Itasca Consulting Group 2002 [DIRS 160331], UDEC User's Guide, p. 2-34). The formulas for c and c_u are taken from *Itasca Software–Cutting Edge Tools for Computational Mechanics* (Itasca Consulting Group 2002 [DIRS 160331], UDEC Theory and Background, Equation 2.37 for friction angle equal to zero). The plastic strain is calculated by subtracting elastic strain from the total strain. Cohesion for 100% of plastic shear strain is calculated by extrapolation.

Strain-hardening response, after yield strength is exceeded, is formulated in FLAC3D in terms of the dependence of cohesion on plastic shear strain (Itasca 2002 [DIRS 160331], theory and background volume of the FLAC3D manual). This dependence is specified in tabular form, starting with zero plastic shear strain and cohesion corresponding to the yield strength. The other point, which defines the slope of the post yield stress-strain curve, is selected to be 100% plastic shear strain, and the value of cohesion that gives the specified tangent modulus. Therefore, ultimate strength and ultimate elongation (or strain) are not inputs in the FLAC3D calculations. The calculation is elastic–plastic, but the material rupture or failure is not simulated. Instead, the

rupture potential is assessed at the end of the simulations by inspecting the maximum tensile stresses and strains.

6.4.3 Drip Shield Plate and Drip Shield Framework Fragility

The mechanical failure mechanisms for the drip shield plates and drip shield framework are represented as a set of fragility curves that are functions of drip shield thickness, seismic intensity, and the static rockfall load on the drip shield. Within this context, mechanical failure refers to rupture of the drip shield plates or collapse/buckling of the drip shield framework. The fragility curves are based on detailed two-dimensional and three-dimensional numerical calculations of the plastic load capacity of the drip shield plates and drip shield framework. The potential for rupture from waste package-drip shield impact on an interior bulkhead will be based on kinematic calculations for the interaction of the waste package and drip shield in collapsed emplacement drifts.

A series of two- and three-dimensional finite-element calculations is used to examine the load-bearing capacity of the drip shield plates and/or drip shield framework when plastically loaded to the point of ultimate tensile failure (i.e., rupture). The plastic load-bearing capacity of the plate or framework is compared to the average static load from lithophysal rockfall combined with the peak vertical acceleration from vibratory ground motion. If the combined static load from rockfall plus the dynamic load from ground motion is greater than the load-bearing capacity, then the structure has failed. The vertical PGA of the ground motion at which the drip shield framework or plates collapses is related to the limit (ultimate) load, p_{ult}, and the vertical static load of the rubble in the collapsed drift, p, by the simple formula of Equation 6-1:

$$p_{\text{ult}} = (1 + \text{PGA})\, p \qquad \text{(Eq. 6-1)}$$

where PGA is expressed in terms of a multiple of g.[1] Since the peak vertical load varies among the ground motions at each PGV level, the results are represented as a probability of failure that is a function of plate thickness and static load at each PGV level. The curves for probability of mechanical failure define the fragility curves for the drip shield plates or drip shield framework.

In the case of drip shield plates, evolution of damage area, defined based on the maximum principal stress threshold, is monitored as a function of the load.

A quasi-static approach with a three-dimensional geometrical representation, which is used to determine fragility of the drip shield framework, is also used to examine the failure modes of the drip shield framework, such as buckling of the drip shield "legs" (sides) or buckling of the drip shield crown. Furthermore, a limited number of two-dimensional, dynamic simulations that simulate full interaction between the drip shield and surrounding rubble is used to investigate modes of framework collapse and to demonstrate that a quasi-static approach predicts failure occurring at a load that is less than that predicted with a fully dynamic approach. A quasi-static three-dimensional approach will also be used to determine the potential for a collapsed drip

[1] Under the action of gravity, only the mass of rubble results in pressure p. Vertical acceleration amplifies the pressure proportionally.

shield that settles down onto the waste package to produce damaged area on the waste package (Section 6.4.4).

The input data for the finite-element calculations include the elastic and plastic properties of the drip shield plates and/or drip shield framework, the design configuration of the drip shield, and the boundary conditions on the ends of the plates. The finite-element calculations are quasi-static, in the sense that each calculation determines the final state of strain in the plate for a given load and does not use the 17 sets of ground motions as input. Rubble in the lithophysal zone is most relevant here because the lithophysal zones encompass approximately 85% of the emplacement drifts in the repository; the effect of large rock blocks falling on the drip shield in the nonlithophysal zones is discussed in Section 6.4.7. The plates will be uniformly loaded because the typical size of the drip shield plates, approximately 1 meter on a side, or the drip shield itself, is significantly larger than the size of rubble particles in the lithophysal zones. Average joint spacing in the lithophysal zones is less than 1 meter, and at certain locations this spacing is much smaller, on the order of 0.1 meters (BSC 2004 [DIRS 166107], Section 6.1.4.1). The drifts in the lithophysal zone are predicted to collapse into small fragments with particle sizes of centimeters to decimeters (BSC 2004 [DIRS 166107], Section 8.1) under the loads imposed by vibratory ground motions. However, in the framework fragility analysis, uneven rubble pressure (i.e., due to more rubble on one side than on the other), which can affect drip shield framework ultimate strength, is taken into consideration.

Elastic and plastic material properties for the drip shield are set to constant values at 60°C (Assumption 5.7, Section 5), based on data from handbooks or manufacturers' catalogs.

6.4.3.1 Analyses for Drip Shield Plate Damage and Fragility

6.4.3.1.1 Purpose

The fragility of the drip shield plates is analyzed to determine conditions of rubble load in the lithophysal units due to rockfall and vibratory ground motion associated with their damage and failure. The drip shield plates form the outer surface of the drip shield and are attached to the drip shield framework. Rockfall in these units is expected to be relatively uniform over a single drip shield segment. The drip shield plate failure defines the state at which the drip shield does not perform the function of shielding the waste package from water seepage or direct contact with surrounding rubble. If the drip shield plates fail, the state inside the emplacement drift is idealized as a waste package surrounded by rubble (i.e., it is modeled as though the drip shield does not exist); this is discussed in Section 6.5.1. The drip shield plate fragility (failure load) is determined for uniformly distributed static loading. This failure load is correlated to the ground motion PGA using the relation in Equation 6-1 in order to determine the ground motion intensity or the PGV level at which the plates collapse.[2]

[2] In Seismic Consequence Abstraction (SNL 2007 [DIRS 176828]) fragility is defined as probability of collapse.

The plate failure is defined in terms of maximum strain and stress (or stress difference) and state of degradation. When the failure state is identified at any point of the drip shield representation, the plate is considered to have failed. Neither the mode of failure nor the evolution of failure is analyzed as a function of time or load.

6.4.3.1.2 Numerical Representation

The analysis was carried out using FLAC3D V. 2.14 numerical code. Only the drip shield plate in the crown is analyzed. One-quarter of the plate within one segment between two bulkheads is included in the calculation. Such a reduction in the size of the analyzed domain was done using symmetries of drip shield geometry and rockfall load. The possible asymmetry of the load is addressed by modifying the boundary conditions. The analyzed region of the drip shield crown plate, outlined in Figure 6-38, is bounded by (a) the vertical symmetry plane along the center of the middle stiffener, (b) the vertical plane along the contact between the crown and the legs, (c) the vertical plane perpendicular to the drip shield axis between two bulkheads, and (d) the vertical plane perpendicular to the drip shield axis along the bulkhead. (One drip shield segment is shown in Figure 6-38.) The y-axis is vertical upward; the z-axis is along the drip shield; and the x-axis is in the cross-sectional plane. In the vertical cross section, the drip shield plate is bent, conforming to a radius of 1,300 mm (Table 4-1). The initial plate thickness is 15 mm (Table 4-1). Center-to-center spacing of the bulkheads is 1,071.6 mm (Table 4-1). The spacing of the longitudinal stiffeners is 225 mm (Table 4-1).

The drip shield plate model geometry was developed from the mesh used for the drip shield creep analysis (BSC 2005 [DIRS 174715], Section 5.4.1.1). Three drip shield plate thicknesses were analyzed: 15 mm (the initial thickness), 10 mm (accounting for 5 mm of uniform thinning), and 5 mm (accounting for 10 mm of uniform thinning). In the region connecting the crown and legs, two drip shield plates overlap. This overlap was not taken into account in the calculations, and only a single plate was analyzed. For all three cases, the thickness of the plate was discretized with five elements. The geometry and the mesh of the analyzed region of the drip shield plate are shown in Figure 6-39.

Two sets of boundary conditions were used to address uncertainty in the load distribution (Figure 6-39). Case 1 boundary conditions are appropriate for uniform (or approximately uniform) rubble load over a large region of the drip shield. In this case, the middle stiffener and the bulkhead are in the planes of symmetry for both the drip shield geometry and the load. Consequently, due to the symmetry conditions, both lateral displacement and rotation should be prevented at the supports. However, if there is a nonuniform distribution of the load in the neighboring drip shield segments, the vertical planes along the axes of the middle stiffener and the bulkhead are not strictly symmetry planes.

Case 2 boundary conditions are representative of the situation in which neighboring segments are not loaded uniformly. These boundary conditions do not restrain lateral displacements at the supports above the bulkhead and the middle stiffener, but they do prevent rotation. In this case, the effect of membrane forces between the panels on ultimate load is neglected. The torsional stiffness of the bulkhead and the stiffener will prevent plate rotation above the bulkhead or the stiffener, even though the load is not symmetrical. This boundary condition, in which the gridpoints are allowed to move laterally while rotation is prevented, is achieved by attaching

together (slaving) all points on the boundary aligned along the same vertical line. (Attaching the points together means that, although the points are at different locations, their translational displacements are forced to be identical.) Consequently, the boundary points can move laterally (because none of them is fixed in the lateral direction); however, because they move identically (as a result of having been slaved together), the rotation of the section is zero.

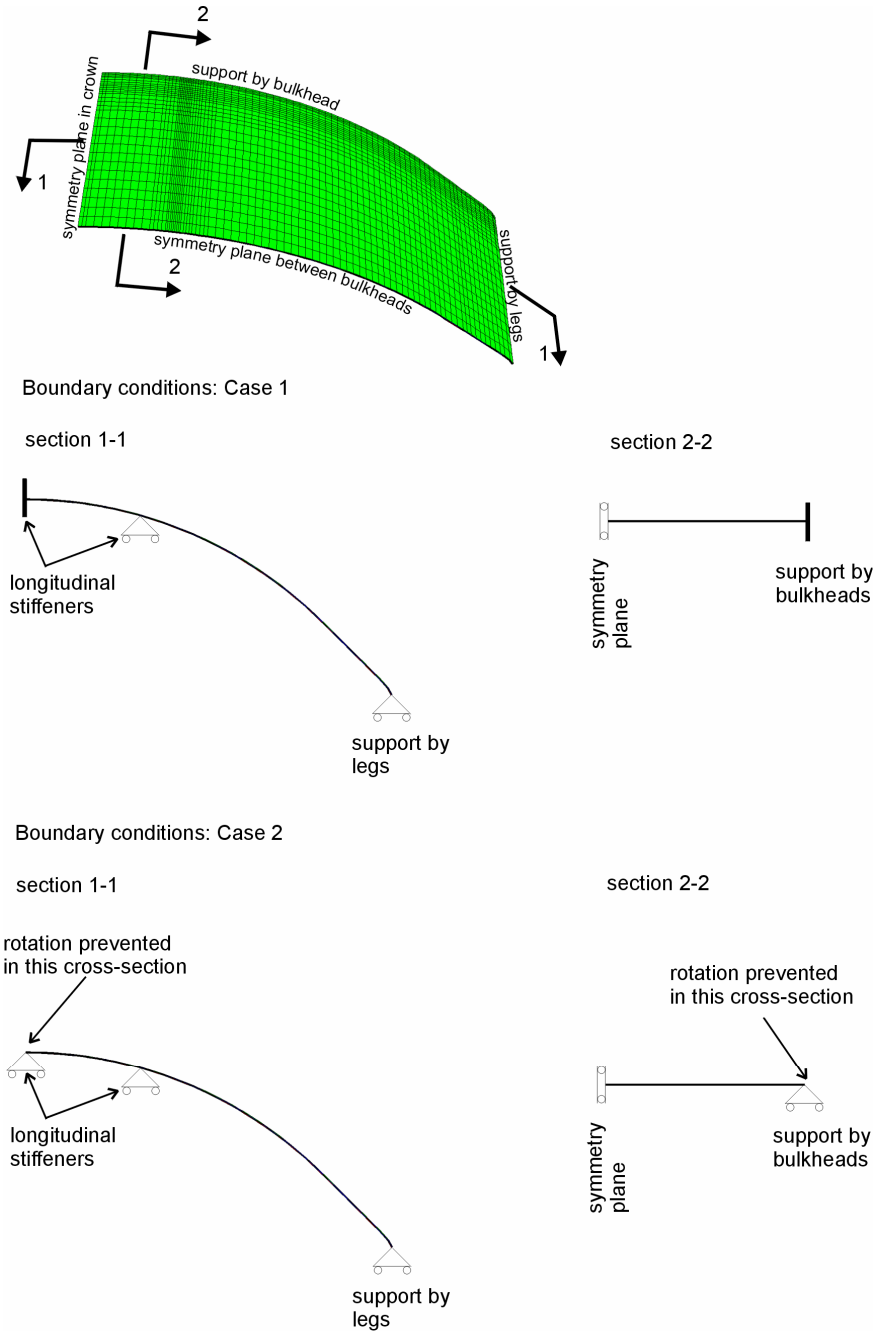

Source: Created for illustrative purposes only, from FLAC3D save file in output DTN: MO0701DRIPSHLD.000, file *drip shield plate fragility/case1-2/2_015/sav*, by plotting block group geometry.

Figure 6-39. Geometrical Representation and Boundary Conditions Used in Analysis of Drip-Shield Plate Fragility